Petrogenesis of the peralkaline granite (and associated syenite) dykes of the Straumsvola Complex, Western Dronning Maud Land, Antarctica

Tanya Dreyer

Dissertation presented for the degree of Master of Science in the Department of Geological Sciences University of Cape Town

July 2015

Supervisors: Professor Chris Harris and Dr Petrus Le Roux

University of Cape Town

The copyright of this thesis vests in the author. No quotation from it or information derived from it is to be published without full acknowledgement of the source. The thesis is to be used for private study or non-commercial research purposes only.

Published by the University of Cape Town (UCT) in terms of the non-exclusive license granted to UCT by the author.

University of Cape Town

Plagiarism declaration

I know the meaning of plagiarism and declare that all of the work in this dissertation, save for that which is properly acknowledged, is my own.

Signed:

Date:

Abstract

The Straumsvola nepheline syenite complex in Western Dronning Maud Land, Antarctica consists of an outer massive and inner layered nepheline syenite that is itself intruded by ijolite. The complex and its immediate country rock was intruded by numerous dykes. A small proportion of these dykes are peralkaline syenite and microgranite, and these are found only to intrude the nepheline syenite and not the country rock. The presence of peralkaline granite dykes intruding a silica-undersaturated complex is unexpected, given the thermal divide that exists at low pressures between silica-under and -oversaturated phases.

Major and trace element variations in the dykes are found to be consistent with fractional crystallisation of a parental peralkaline magma of trachyte composition. The dykes give an age of 171±4.4 Ma (Rb-Sr isochron) and have an initial $^{87}Sr/^{86}Sr$ ratio =0.707500 and average initial $^{143}Nd/^{144}Nd$ = 0.51190. The $\delta^{18}O$ values of quartz and aegirine give temperatures around 500°C somewhat lower than expected for felsic magmas that are consistent with the rock textures that imply subsolidus growth of aegirine. Quartz $\delta^{18}O$ values of 8.4 to 9.2‰ indicate peralkaline granite magma with an average $\delta^{18}O$ value of 8.6‰.

A number of unusual silicates are present in the granite dykes e.g. the Zr-silicates: eudialyte, dalyite and vlasovite, and a Na-Ti silicate, narsarsukite. The presence of Na-bearing accessory minerals is likely related to the peralkalinity of the dyke magmas that inhibits zircon formation.

Strongly negative ε_{Nd} (<-10), high initial $^{87}Sr/^{86}Sr$ and high $\delta^{18}O$ (average 8.6‰) compared to the expected value for a felsic magma produced entirely by fractional crystallization of a mantle-derived magma (~6.5 ‰) is consistent with a substantial crustal component in the dyke magmas. Because the country rock does not have high $\delta^{18}O$ values (average 7.7 ‰), it is suggested that the peralkaline granite dykes formed by partial melting of an alkali-metasomatised gneiss followed by fractional crystallisation.

Table of Contents

Plagiarism declaration

Abstract

1. Introduction 3

1.1 Previous work in Western Dronning Maud Land, Antarctica 3

1.2 Regional geology 4

1.3 A review on the origin of A-type granites 8

1.4 Previous studies on the felsic dykes of the Straumsvola Complex 9

1.5 Aims of this study 11

2 Major rock types of the Straumsvola Complex 12

2.1 Field relations 12

2.2 Dykes in Hand Specimen 15

2.3 Petrography 18

2.3.1 Dykes of the Straumsvola Complex 18

2.3.2 Country rock gneisses 33

2.3.4 Nepheline syenites 37

3. Methods 39

Analytical techniques 39

3.1. Electron Microprobe 39

3.2. XRF 39

3.3. Trace elements 40

3.4. Radiogenic Isotopes 42

3.4.1. Pb 42

3.4.2. Sr and Nd 42

3.5. Stable Isotopes 46

3.5.1. Oxygen Isotopes 46

4. Results 47

4.1. Mineral Chemistry 47

Pyroxene 47

Unusual Minerals 48

4.2 Major element geochemistry 55

4.3 Trace elements 57

4.3.1 Rare Earth Elements 68

4.4 Isotopes ... 71
4.4.1 Oxygen Isotopes ... 71
4.5 Radiogenic Isotopes ... 73
4.5.1 Comparison with other elements: ... 75
4.5.2 Comparison with other isotopes: Pb ... 79
5. Discussion ... 81
5.1. Major element variation ... 82
5.2. Trace elements ... 87
5.2.1. Trace element variation in the dykes ... 87
5.2.2. The effect of the unusual silicates on the composition of the dyke magma ... 88
5.3. The REE ... 92
5.3.1. The significance of eudialyte ... 93
5.4. Oxygen Isotope constraints on magmatic evolution at Straumsvola ... 94
5.5. Radiogenic Isotopes ... 97
5.5.1. Pb Isotopes ... 107
5.6. Towards a final synthesis ... 111
5.7. Comparison with other Mesozoic plutons ... 112
6. Summary of Key Findings ... 115
6.1. Petrography ... 116
6.2. Major and trace element geochemistry ... 116
6.2.1. REE ... 116
6.3. Oxygen isotopes ... 117
6.4. Radiogenic isotopes ... 117
6.4.1. Comparison with the Sistefjell Syenite ... 118
7. Model for the petrogenesis of the Straumsvola dykes ... 119
7.1. Proposed model ... 121
8. Concluding remarks ... 122
References ... 124

Appendix ... I

1. Introduction

1.1 Previous work in Western Dronning Maud Land, Antarctica

The Straumsvola igneous complex in Western Dronning Maud Land (WDML), Antarctica consists of a nepheline syenite complex intruded by numerous Mesozoic dykes of varying composition including granite.

A regional map of WDML is shown in Figure 1. Much work has been done in this region of Antarctica since the late 1960's (Ravich & Solov'ev 1969; Wolmarans & Kent 1982; Harris et al. 1991; Grantham et al. 1995; Luttinen et al. 1998; Riley et al. 2005; Curtis et al. 2008). A detailed petrologic study of the region of Central Dronning Maud Land was initially undertaken by Ravich & Solovev (1969) as part of the Russian Antarctic Survey in the early 1960's. This was followed by a detailed investigation into the geology of the mountains of western Dronning Maud Land as part of the South African National Antarctic Program (Wolmarans & Kent 1982). From these studies the major rock units and their relation to one another were identified by field mapping and detailed petrography. Subsequent mapping and geochemical investigation in the largely ice covered region of Dronning Maud Land lent support to the reconstructions of Martin & Hartnady (1986) and de Wit et al (1988) that placed Western Dronning Maud Land closest to southern Africa pre-Gondwana breakup. Similarities in age, composition and tectonic setting of the regional flood basalt sequences; the Karoo sequence in Southern Africa and the Kirwan in Dronning Maud Land; provided the physical evidence for these linkages (Harris et al. 1991; Luttinen et al. 1998). The lavas of Western Dronning Maud Land are thus particularly well-studied given its Mesozoic lavas are coeval with Karoo magmatism. In addition it remains a site of active research as the mechanism responsible for generating such large volumes of magma ($>10^6 km^2$) remains highly controversial (Heinonen et al. 2010 and references therein).

The predominantly tholeiite dykes of WDML form a regional dyke swarm that has in previous studies been related to Karoo-age volcanism in Southern Africa (Harris et al. 1991; Groenewald et al. 1991; Luttinen et al. 1998). While the majority of these dykes are mafic dolerites associated with the Karoo Large Igneous Province (LIP), a small proportion (11%) are peralkaline granites that only cut the nepheline syenite within the Straumsvola complex. The association of silica-oversaturated and –undersaturated magmas is unexpected given the thermal divide that exists at low pressures in the Qtz-Alb-Ne-Ks system (Bowen 1937). The granite dykes, their peralkalinity and petrogenesis in a silica-undersaturated complex are thus the main focus of this study.

1.2 Regional geology

A map of Western Dronning Maud Land is shown in Figure 2. It is underlain by two distinct geologic provinces separated by the Pencksökket and Jutulstraumen Glaciers (Groenewald et al. 1991). The Grunehogna Province to the West includes the Borgmassivet, Ahlmannryggen and Straumsnutane areas. The Ritscherflya Supergroup outcrops here as a weakly metamorphosed sequence of sedimentary and volcanic rocks (Wolmarans & Kent 1982). It is intruded by tholeiitic sills and dykes of the Borgmassivet Intrusion dated at between 900 and 1100Ma. The basement to the Ritscherflya Supergroup is thought to be Archean age granitoids as seen at Annandagstoppan in the south-west (Barton et al. 1987; Marschall et al. 2013).

To the east of the Penck-Jutul Glacier lies the Mesoproterozoic Maud Province. The Kirwanveggen and H.U. Sverdrupfjella regions that together form the Maud province are underlain by calc-alkaline metavolcanics and metamorphosed (amphibolite to granulite facies) gneisses of the Jutulrøra Formation (Sverdrupfjella Group). These gneisses are postulated to represent the extension of the Kibaran (1.2Ga) Namaqua-Natal Metamorphic Province of Southern Africa into Antarctica (Jacobs et al. 1993; Groenewald et al. 1995). The 50km wide Penck-Jutul Glacier overlies the crustal boundary between these two provinces and is inferred to represent a continental rift margin that was likely reactivated during the Mesozoic (Ferraccioli et al. 2005).

Three Mesozoic alkaline plutons centred on the nunataks, Sistefjell, Straumsvola and Tvora flank the eastern and southern edge of the Jutulstraumen. Worldwide, continental rifting is associated with alkaline plutonism and the presence of these plutons at the edge of the glacier lends support to the crust underlying the Jutulstraumen Glacier representing an inactive rift (Harris & Grantham 1993). Some authors have proposed that this inactive rift represents the extension of the East African rift into Antarctica (Grantham & Hunter 1991; Riedel et al. 2013). The alkaline plutons in the region of Straumsvola comprise the Straumsvola nepheline syenite that crops out at Straumsvola and Storjeon, and the nearby Tvora quartz syenite (Figure 3). The 7-10 km wide Straumsvola nepheline syenite is made up of a massive outer and layered inner zone intruded at a high angle by ijolite (Figure 4). Best estimates for the age of the Straumsvola pluton ranges from 170 Ma to180 Ma. The lower age of 170±4 Ma was calculated from a whole rock Rb-Sr isochron by Grantham et al. (1988) and the upper age of 179 Ma by Ar-Ar dating of two mafic dykes that cut the pluton and thereby provide a minimum age of pluton emplacement (Curtis et al. 2008). The complex is intruded by numerous other dykes that range in composition from ultramafic to evolved silica under- and oversaturated varieties (Harris & Grantham 1993; Riley et al. 2009).

Dyke emplacement is known to both precede and postdate intrusion of the nepheline syenite (Grantham et al. 1995). The dyke swarms of the Straumsvola complex are generally composed of dolerite but can be subdivided into two mafic suites: An older, tholeiitic flood basalt swarm and a younger, alkaline swarm (Curtis et al. 2008). The dykes are all Mesozoic in age and in addition to their temporal relation to Karoo-age magmatism, the mafic dykes have geochemical affinities

similar to the Karoo LIP (Harris et al. 1991; Curtis et al. 2008). This has led most authors to conclude that the dykes represent a minor intrusive phase of the Karoo LIP in Antarctica. Flood basalt sequences associated with the Karoo LIP are not found around the study area but do appear further to the South and West at Vestfjella, Ahlmannrygen, Heimefrontfjella and Kirwanveggen. The strikes of these dykes are centred near the present day continental margin of WDML on a proposed plume head (Curtis et al. 2008). This postulated radial dyke swarm coeval with Karoo magmatism at 175-178Ma supports the interpretation that the Karoo LIP was related to a mantle plume.

The older, 206-204 Ma, tholeiitic flood basalt is a low- Ti and low-Zr tholeiite intrusive into the country rock gneisses of the Jutulrøra Formation in H.U. Sverdrupfjella. The younger, 178-175 Ma, dolerite swarm is predominantly basanite/tephrite in composition and only intrudes the nepheline syenite and the surrounding country rock at Straumsvola and Tvora. It was hence named the Straumsvola Swarm by Curtis et al. (2008). This swarm also includes a group of felsic extrusives and phonolites that represent the final intrusive stages of the suite (Grantham et al. 1998). Peralkaline granites account for 7% of the alkaline dyke swarm at Straumsvola and 4% at Tvora (Curtis et al. 2008) (Figure 5). The felsic subgroup of dykes crosscuts all the other dykes, the nepheline syenites and pegmatites around Straumsvola and hence is the youngest phase of dyke intrusion. One felsic dyke sample gave a whole rock Ar-Ar age of 170.93±1.67 Ma (Curtis et al. 2008), the youngest age recorded for any of the dykes in this region of WDML.

In addition to the geochronology presented above, a structural study of these dykes was also undertaken by Curtis et al (2008). Their results are summarised here. The inserts of Figure 3 show rose diagrams and frequency plots of the dykes measured around and within the Straumsvola Complex. It can be seen that the dykes near Straumsvola show variable orientations while the regional dykes show a clear NNW-SSE trend. These authors concluded on the basis of geochronology and other structural controls on dyke emplacement including Anisotropy of Magnetic Susceptibility (AMS) that the Straumsvola dyke swarm and the regional dyke swarm were not produced by the same igneous event. They suggested that the Straumsvola dyke swarm, being in close proximity to the pluton, was likely locally sourced and that magma transport was mostly vertical. This was unlike the older, regional tholeiite that shows evidence for vertical magma flow near the Straumsvola pluton and lateral flow in outcrops near the Jutulstraumen Rift. Aeromagnetic data suggest several intrusive features underlie the Straumsvola Complex (Ferraccioli et al. 2005). It appears to have been a particularly active magmatic area over the period 175-178 Ma producing both the Straumsvola dolerites and post tectonic phonolite suite mentioned above. At Straumsvola and Tvora, felsic dykes of phonolitic and granitic composition exist that are rare elsewhere in WDML except in the Sistefjell group of nunataks to the south (Fig. 2). Here a variety of silica-saturated dykes, microsyenites and quartz porphyries intrude the Sistefjell syenite and country rock (Harris et al. 2002). It is notable, however, that microgranite dykes observed at Sistefjell appear to only intrude the country rock gneisses and not the syenite unlike at Straumsvola where the reverse is observed (Harris et al. 2002).

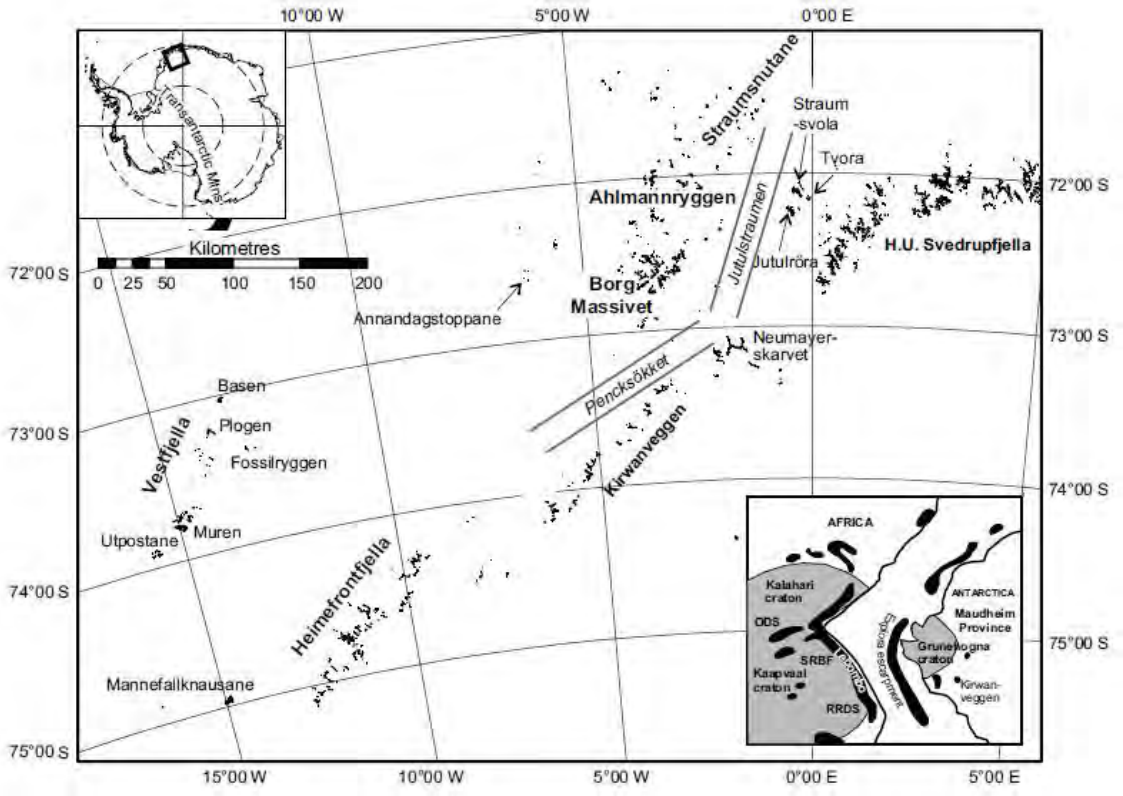

Figure 1: Regional map of Western Dronning Maud Land after Curtis et al. (2008) with an inset of the paleo-positions of WDML and Southern Africa pre-Gondwana break up.

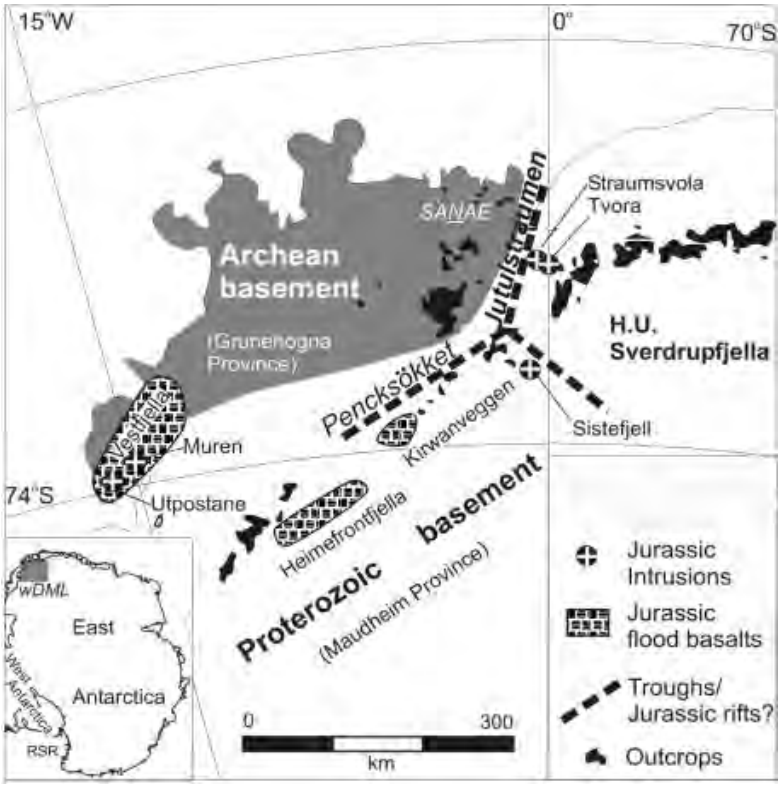

Figure 2: Geologic map of Western Dronning Maud Land outlining the Jutulstraumen-Pencksokket Glacier, separating the Grunehogna and Maudheim Provinces. Jurassic flood basalt provinces can be seen at Vestfjella, Heimefrontfjella and Kirwanveggen. The alkaline intrusions of Straumsvola and Sistjefjell are shown as white crosses alongside the Jutulstraumen Glacier. Figure after Ferraccioli et al. (2005).

Based on incompatible trace element ratios that are similar to rift related magmas of the East African Rift, the tectonic setting was presumed to have once been an active rift (Harris et al. 2002). Given the similarities between the Straumsvola and Sistefjell complexes in age (170-180 Ma), position(flanks of the Jutulstraumen Glacier), basement rock (Sverdrupfjella gneisses) and overlap in incompatible element ratios (Harris et al. 2002), it seems reasonable that they formed in the same tectonic environment i.e. within an active rift. The suite of oversaturated sills and dykes of the Sistefjell syenite was suggested by Harris et al. (2002) to have formed through extensive (87%) fractional crystallisation of a mantle derived magma (Harris et al. 2002). These processes are thus likely to have affected the Straumsvola Complex and will be investigated in this study.

Whereas silica-oversaturated dykes formed by fractional crystallisation are known from the Sistefjell syenite (Harris et al. 2002), their presence in the nepheline syenite-dominated Straumsvola Complex is unexpected. Experiments on phase equilibria predict that at low pressures a thermal divide exists that prevents a silica- oversaturated phase being produced from an undersaturated parental magma by fractional crystallisation (Tuttle & Bowen 1958). Previous studies have identified vugs within the nepheline syenite (Harris & Rickard 1987) suggesting a low depth of intrusion for the complex and therefore low magma pressures, which would suggest that a thermal divide did exist.

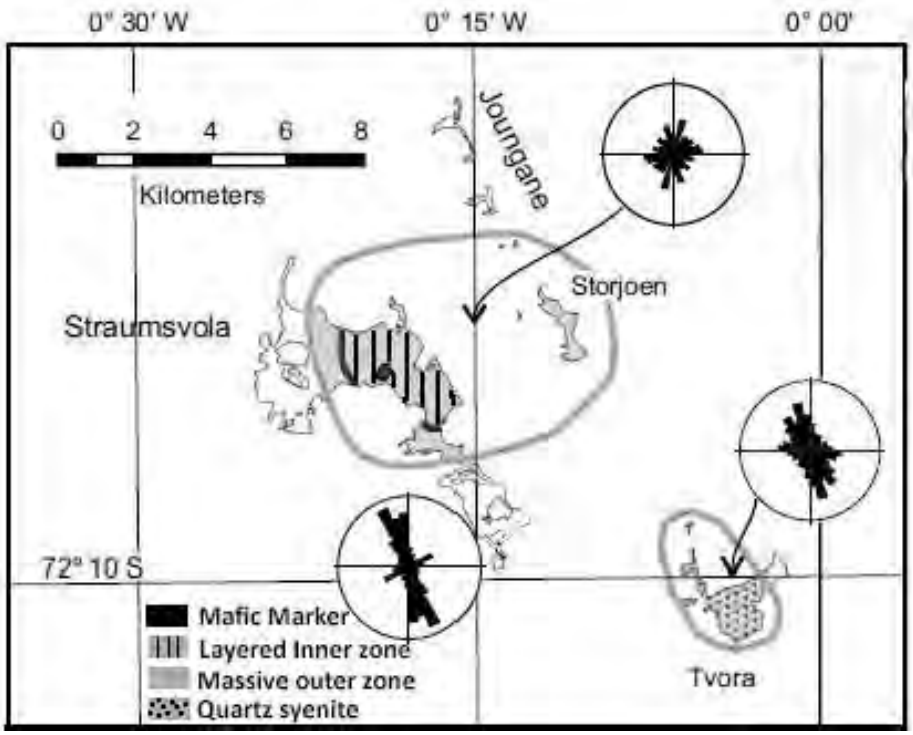

Figure 3: The Straumsvola complex includes 2 alkaline plutons, the nepheline syenite at Straumsvola and Storjeon. While a quartz syenite outcrops to the SE at Tvora, it is not sure if/how it is related to the nepheline syenite pluton. The nepheline syenite at Straumsvola can be divided into a layered inner and outer massive zone, itself cut by a mafic ijolite. Also shown are rose diagrams for the dykes of Straumsvola and Tvora that are highly variable in orientation, versus the regional dolerite suite (bottom left) that shows a pronounced NNW-SSE trend. The grey outline delineates the outcrop of the alkaline plutons. Figure adapted from Curtis et al. (2008).

Mechanisms that could produce silica over- and undersaturated magmas in the same complex include:

1) High and low pressure melting of the same mantle.
2) Melting of different parts of the mantle at the same pressure
3) Assimilation of felsic crust by an undersaturated magma OR contamination of an undersaturated magma by partial melting of felsic crust.

The association of silica under- and -oversaturated rocks in alkaline igneous provinces is not uncommon. Examples include the Puklen Complex of the Gardar Province, South Greenland; the Marangudzi in Zimbabwe; Mt. Brome in Canada and the Ambohimirahavy Complex, Madagascar (Marks et al. 2003; Foland et al. 1993; Estrade et al. 2014). The source of undersaturated alkaline magmas is generally considered to be in the upper mantle e.g. Marks et al. (2003). Syenites can be generated from these parental magmas by extensive fractional crystallisation. However, the close spatial association of some under- and oversaturated alkaline complexes has led most authors to attribute the generation of alkaline and peralkaline oversaturated magmas to crustal contamination of the alkaline syenite by the surrounding felsic upper or lower crust e.g. Marks et al. (2003), Marks et al. (2011). The effect of the surrounding country rock gneiss in the genesis of the peralkaline granites at Straumsvola must therefore also be examined.

1.3 A review on the origin of A-type granites

The granite dykes of the Straumsvola Complex display so-called 'A-type' affinities as first described by Loiselle and Wones (1979) based on their setting in an anorogenic environment, iron enriched compositions and enrichment in incompatible elements. There remains much controversy over the definition of A-type and indeed even the classic S- and I-type granite classification of Chappell & White (1974). The main argument being that the so-called 'alphabet soup' classification scheme of granites assumes an à priori knowledge of the source of the granite magma, i.e. a meta(S)edimentary source for all S-type and a meta(I)gneous source for all I-type granites (Chappell & White 1974). An additional complexity added by the A-type granites is that the 'A' is rather poorly defined. 'A' has been variably understood to represent anorogenic, alkaline or anhydrous but is also problematic because there is no consensus on the origin of these magmas, making it impractical to include it in an alphabet-type classification scheme (Bonin 2007). A-type magmas have been found in a variety of environments, i.e. are not linked to a single tectonic setting and can be formed syn-orogenically or millions of years after the main orogenic event. They are also commonly found associated with continental rift zones and this suggests some petrogenetic link with the mantle(Bonin 2007). However, there are some distinctive features of A-type granites that warrant them having their own classification (Loiselle & Wones 1979). They are enriched in incompatible elements including the LILE and HFSE but have trace element abundances common in mafic silicates and feldspars (Bonin 2007). They also

tend to have mantle signatures, which has resulted in most workers suggesting that they are fractionated products of mantle-derived alkali basalt. However, there is also evidence to suggest that A-type magmas can be produced entirely within the crust (e.g. Spitzkoppe, Namibia) with most models requiring a heat source (e.g. the mantle) to induce melting (Frindt et al. 2004; Bonin 2007). The data presented in this study therefore will add to the geological literature available on the genesis of A-type magmas and their characteristics. The general consensus seems to be that the term A-type should be removed altogether (see Frost & Frost (2010)) but as yet there is no consensus on a new/revised term.

1.4 Previous studies on the felsic dykes of the Straumsvola Complex

Fieldwork in the Straumsvola Complex was undertaken over several field seasons from 1985-1989 by Chris Harris, Geoff Grantham and others. In addition to sampling of the basement gneisses, nepheline syenites and dykes (both mafic and felsic), mapping of the dyke suites and the nature of the layered vs. non-layered nepheline syenites was investigated further. A large number of samples was collected but only a subset was subsequently analysed by Harris & Grantham (1993). For this study granitic samples that weren't previously analysed were selected while those previously identified as being the most representative of the granite dykes, those least affected by alteration or unusual and of special interest were also added to be fully analysed.

Earlier bulk geochemistry on the felsic dykes showed compositions that range from syenite to granite with a few of the granite samples displaying a strongly peralkaline (molecular $(Na_2O + K_2O) /Al_2O_3 >1$) character (Harris & Grantham 1993). Some of the dykes also have unusual accessory minerals. These include REE-enriched eudialyte ($Na_4(Ca,Ce)_2(Fe^{2+},Mn,Y)ZrSi_8O_{22}(OH,Cl)_2$), dalyite ($K_2ZrSi_6O_{15}$), vlasovite ($Na_2ZrSi_4O_{11}$) and narsarsukite ($Na_2(Ti,Fe^{3+})[Si_8O_{20}](O,OH,F)$. These minerals are unexpected but not uncommon phases in alkaline/ syenite provinces globally such as at Illimassauq, Greenland and Lovozero, Russia but are rare in peralkaline granites (Harris 1982). Eudialyte in particular is a characteristic mineral of peralkaline rocks and has been shown to crystallise from mantle derived magmas (Schilling et al. 2011) but is very rare in peralkaline granites.

The only other known locality where eudialyte, dalyite and vlasovite have been found in peralkaline granites is as xenoliths in lavas at Ascension Island in the Atlantic Ocean (Harris 1982). A detailed mineralogical investigation of the relationship between eudialyte and dalyite at Straumsvola was undertaken and described in Harris & Rickard (1987). They observed that dalyite formed first as it was commonly seen as inclusions in eudialyte. The authors suggested that at high Zr concentration, dalyite was the stable phase but once the melt was sufficiently reduced in Zr, that eudialyte became the stable Zr-bearing phase. In addition, the eudialyte from Straumsvola was found to be extremely enriched in the REE. This was attributed to REE substitution for Ca in Ca-poor magmas.

Figure 4: The Straumsvola nepheline syenite looking SE. The unconformable mafic zone nepheline syenite is clearly visible overlying the lighter-coloured nepheline syenite at a high angle. Photo by R.T. Watkins (1987). Vertical height is 250 m from the base of the figure to the highest point (Straumsvola summit).

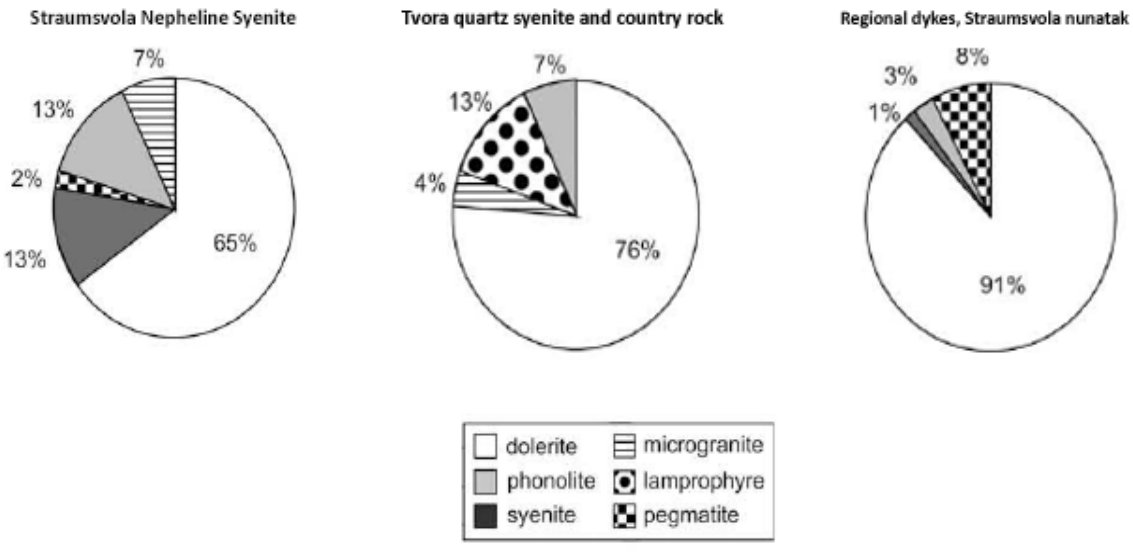

Figure 5: Dyke lithologies of the Straumsvola Complex. Dolerite dykes are the most common extrusive phase in the nepheline syenite at Straumsvola, Tvora and the surrounding country rocks. Microgranite dykes are only found intruding the nepheline syenite at Straumsvola and Tvora (7% and 4% respectively) while they are not seen intruding the surrounding country rock of the Straumsvola nunatak. Figure adapted after Curtis et al. (2008).

At Straumsvola the Ca-deficient magma is likely a consequence of the plagioclase effect (Bowen 1945) whereby plagioclase fractionation preferentially removes Ca and Al over Na resulting in a Ca-poor melt that evolves to peralkaline. The presence of these unusual accessory phases in the peralkaline granites of Straumsvola was not fully explained in the paper by Harris and Rickard (1987) nor in the subsequent work on the petrogenesis of the Straumsvola Complex (Harris & Grantham 1993) and so will be investigated here.

1.5 Aims of this study

The main aims of this study are to:

I. Provide a comprehensive assessment of the petrography of the Straumsvola peralkaline granites on a much larger sample set than previously analysed by Harris & Grantham (1993)
   - → Determine if the dykes have common petrographic features that may allow them to be grouped
   - → Describe any unusual features or minerals identified

II. Expand the geochemical database to include:
   - → More bulk rock analyses of major elements
   - → A Greater range of bulk rock and trace elements including Rare Earth Elements (REE)
   - → Oxygen isotopes of mineral separates from peralkaline granite
   - → Radiogenic isotopes (Rb-Sr, Sm-Nd and Pb) on a subset of peralkaline dykes

III. Use the results from (II) to constrain the petrogenesis of the peralkaline granites at Straumsvola

IV. Consider the generation of so-called A-type granites in general and the relationship between under- and over-saturated magmas in the same complex.

2 Major rock types of the Straumsvola Complex

In this chapter the petrography of the dykes and representative units of the nepheline syenite in the Straumsvola complex will be examined. Gneisses from the contact zone with the nepheline syenite at Straumsvola and several kilometres from the contact will also be described.

2.1 Field relations

The dykes of the Straumsvola Complex range from ultramafic to evolved silica-undersaturated and silica-oversaturated types (Harris & Grantham 1993). They form a separate suite to the regional tholeiites (Figure 3) as seen in the highly variable dyke orientations of the Straumsvola dykes when compared to the strongly NNW-SSE trend of the regional dykes. At Straumsvola, the mafic dykes are the most voluminous and are alkali- basalts that pre-and postdate intrusion of the nepheline syenite. As discussed in Chapter 1, the oversaturated peralkaline dykes of this study form a minor intrusive component of the complex and are known from field relations and Ar-Ar dating (Curtis et al. 2008) to be the youngest intrusive phase. Only these peralkaline syenitic to granitic dykes will be discussed further.

The samples were collected from the nunataks around Straumsvola and Storjeon in Western Dronning Maud Land (WDML), Antarctica between 1985 and 1989. All of the dykes are fresh with very little alteration or signs of extensive weathering. Sample localities for the 30 dyke samples chosen for the study are shown in Figure 6. Examples of Straumsvola Complex rocks in the field are shown in Figures 7 and 8. A peralkaline granite dyke (ST38) is seen intruding the nepheline syenite in Figure 8a. Figure 8b shows the sharp contact between the country rock gneiss and the nepheline syenite. Extensive fenitization of the gneisses of the contact area was identified by Harris and Grantham (1993) and was attributed to an alteration fluid caused by the intrusion of the nepheline syenite. The extent of this alteration, as seen in the textural features of the gneisses, from the contact zone to a few kilometres from the contact will be examined in this chapter.

A summary of the main features of the dykes in hand specimen is shown in Figure 9 and discussed below. Petrographically the peralkaline dykes can be subdivided into two petrographic groups, Group 1 and Group 2. Group 1 dykes generally have coarse grained-euhedral aegirines in a fine-grained mostly granitic matrix while Group 2 dykes contain mostly interstitial aegirine/alkali amphibole in a fine-grained granite/syenite matrix.

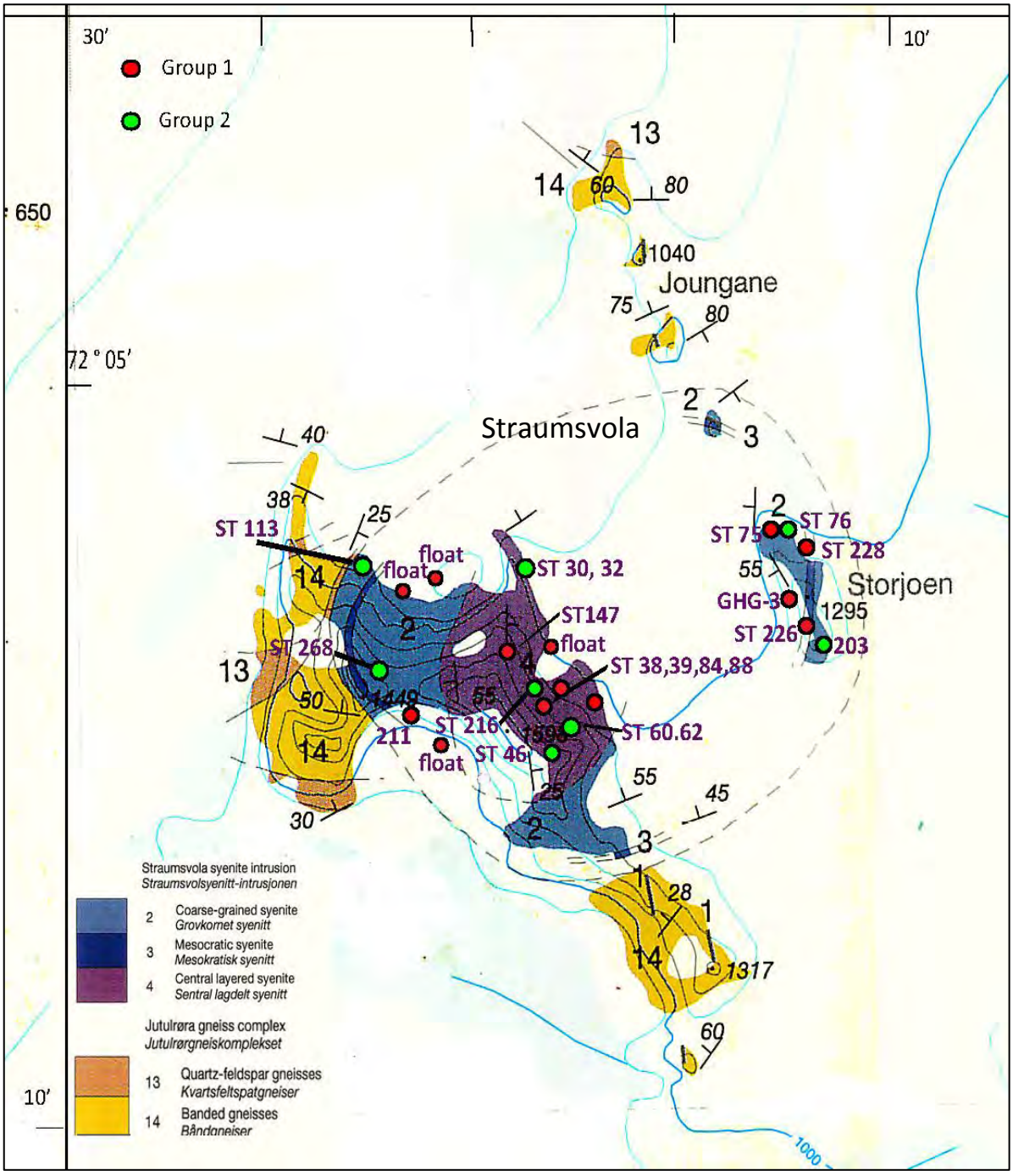

Figure 6: Map of Straumsvola and surrounding nunataks, Storjeon and Joungane indicating where the dyke samples were collected. The grouping refers to petrographic groups that are defined in detail in the next section on petrography. Float refers to samples that were not collected in situ but were picked up in that approximate location. Geological map adapted from the map of H.U.Sverdrupfjella of the Norwegian Polar Institute (2006).

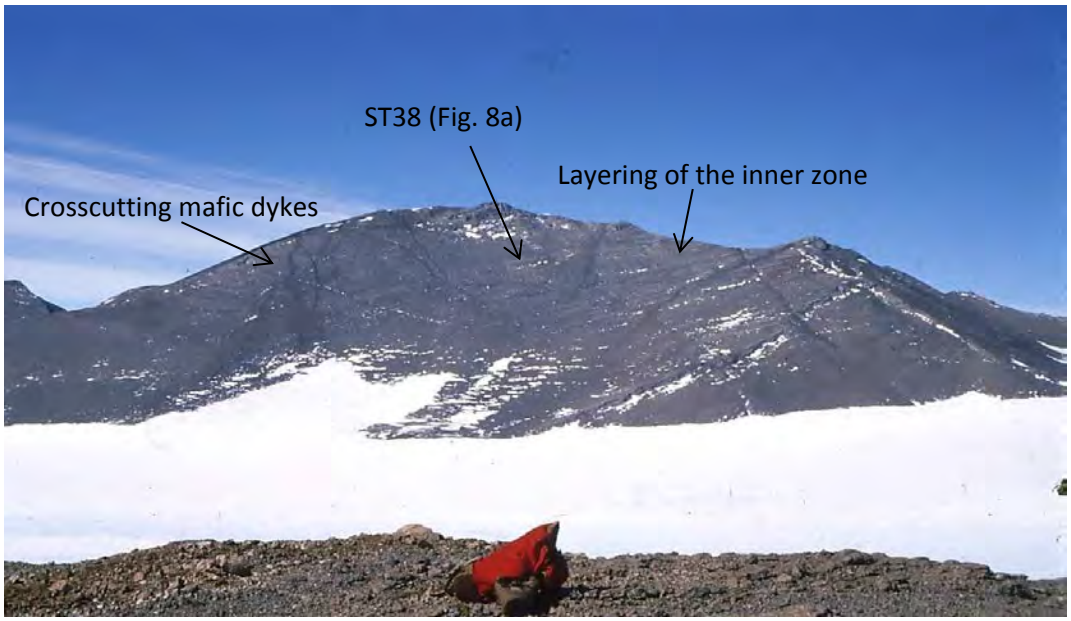

Figure 7: View towards the layered zone of the Straumsvola nepheline syenite looking North. Nearly horizontal Layering of the inner zone is just visible as well as a series of crosscutting, steeply dipping basaltic dykes. Also shown is the location of a peralkaline granite, ST38, shown in Figure 8a. Photo courtesy of C.Harris.

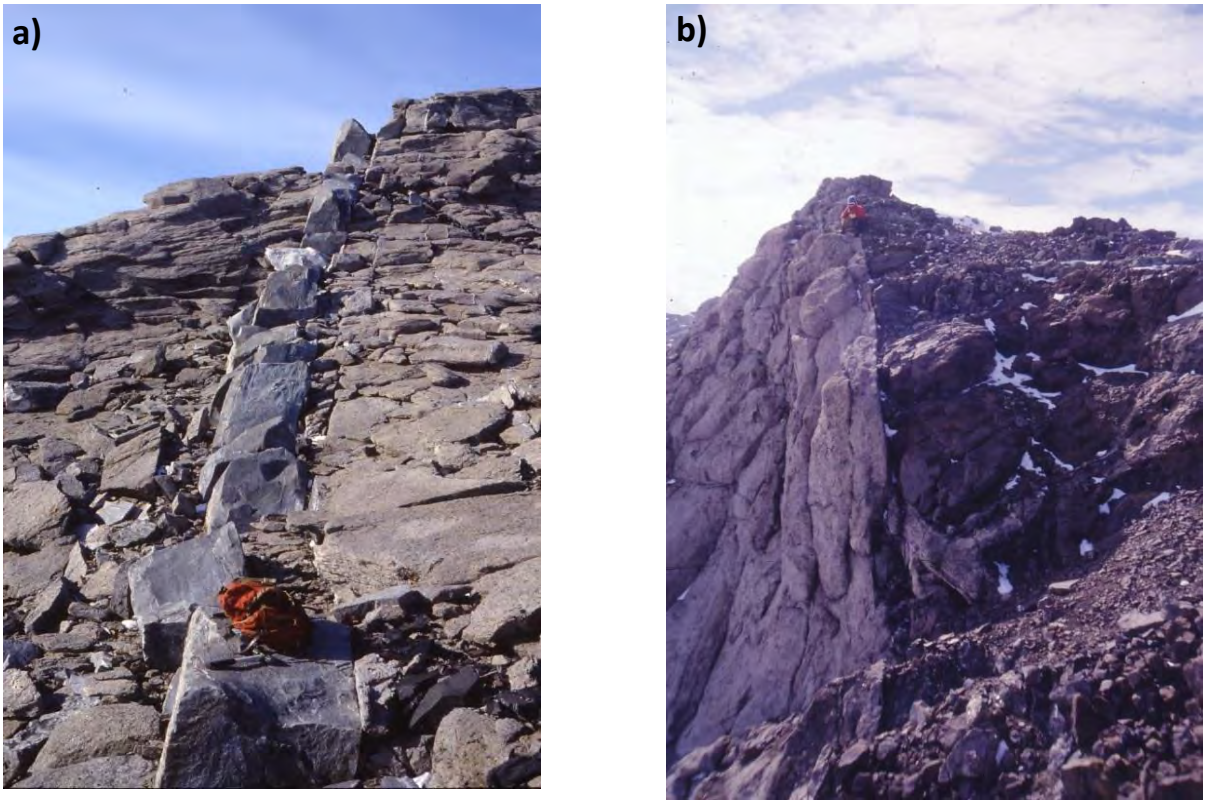

Figure 8: a) Granite dyke (ST38) intruding nepheline syenite at Straumsvola. b) A sharp contact is observed between the lighter, nepheline syenite and gneisses of the Sverdrupfjella Group. Fenitization of the gneisses at the contact zone is common. Photographs courtesy of C. Harris.

2.2 Dykes in Hand Specimen

Most of the dykes are white or light in colour with large dark-green, needle-like aegirine crystals (Figure 9a-c). One sample is particularly aplitic and contains pyroxene that is blocky in shape but is poikilitic on closer inspection (Figure 9d). In some samples the aegirines are finer-grained and tend to cluster together as in Figure 9e. These samples also contain eudialyte, a rare Zr-silicate with irregular crystal shapes as seen in Figure 11. A few of the samples are darker grey or tan and are generally finer grained (Figure 9f-g).

A few of the samples show layering/banding (Figure 10). From field observations the layering in most cases is parallel to the dyke walls. The layering generally alternates between feldspar-rich units with coarse-grained aegirines that are generally layer parallel, and darker grey layers where the mineralogy is not obvious from the hand specimen.

A number of dykes also contain visible eudialyte and narsarsukite (Harris & Grantham 1993). Eudialyte: $(Na_4(Ca,Ce)_2(Fe^{2+},Mn,Y)ZrSi_8O_{22}(OH,Cl)_2)$ is visible as dark red/maroon, blocky, irregular masses in Figure 11a and narsarsukite $((Na_2(Ti,Fe^{3+})Si_4(O,,F)_{11})$ in Figure 11b forms yellow, tabular phenocrysts. Eudialyte was identified by Harris & Rickard (1987) in a granite dyke that cropped out at two locations at Straumsvola while narsarsukite was sampled at Storjeon.

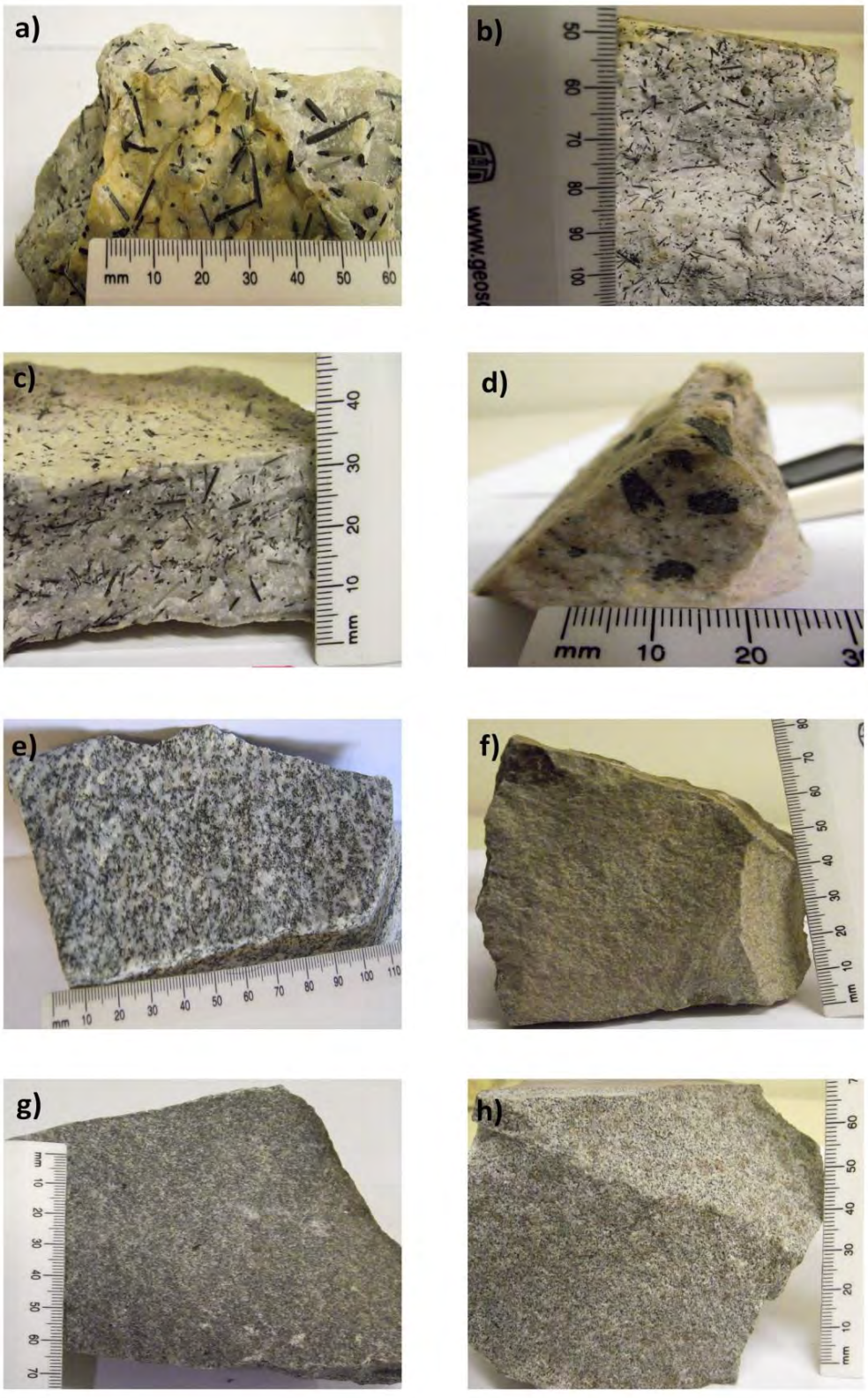

Figure 9: Dyke samples range from white with coarse grained aegirine phenocrysts in (a-e) to fine-grained grey and brown in (f-h).

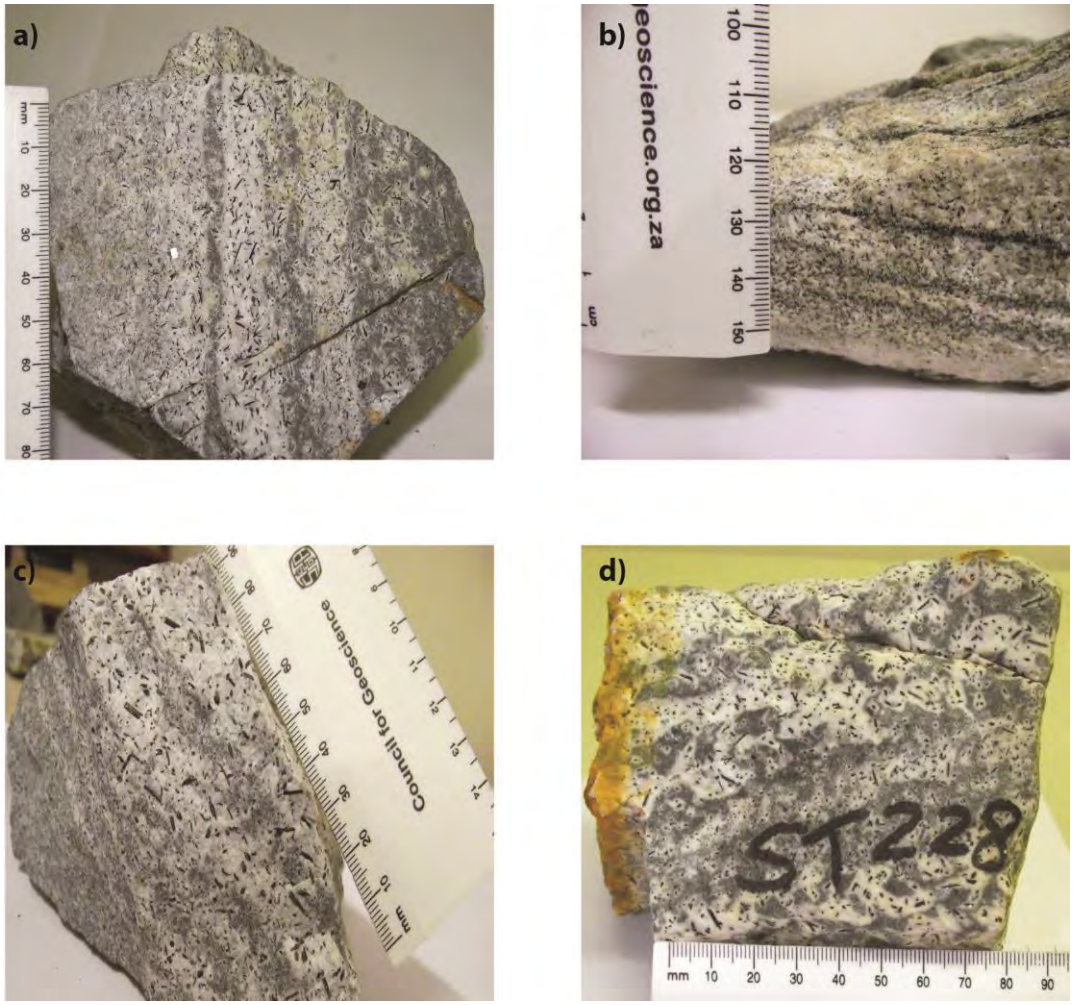

Figure 10: Layering is observed in some dyke samples and is parallel to the dyke walls.

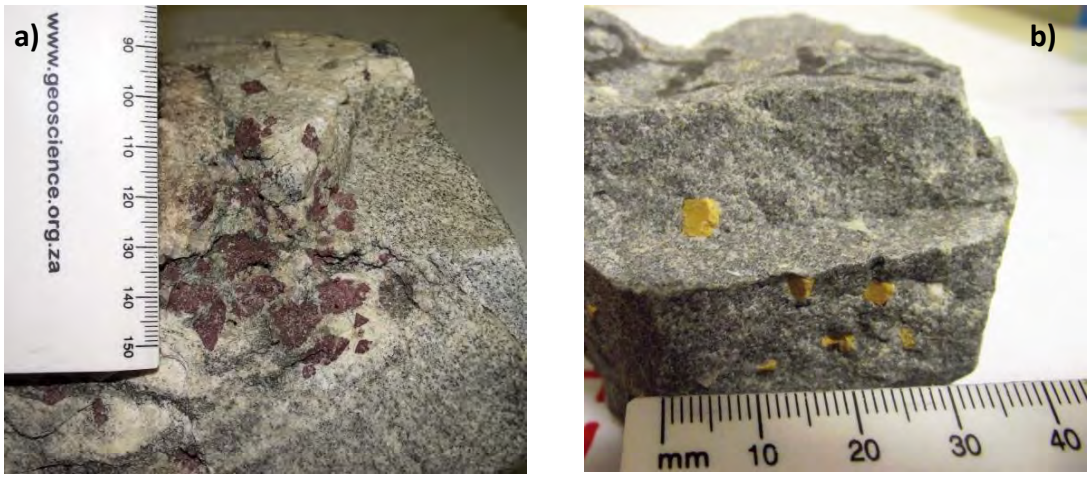

Figure 11: Unusual accessory minerals are visible in some of the dykes. These minerals have been previously identified as eudialyte- red mineral in (a) and narsarsukite- yellow mineral in (b).

2.3 Petrography

2.3.1 Dykes of the Straumsvola Complex

The dykes generally fall into two petrographic groups. Group 1 dykes contain large phenocrysts of aegirine and feldspar while Group 2 dykes lack the phenocrystic aegirines observed in Group 1. A summary of the main features of the Group 1 and 2 dykes, their subgroups and sample numbers are shown in Table 1.

Group 1:

In thin section coarse-grained (1mm-7mm), euhedral aegirines are clearly visible in a fine-grained microgranite/microsyenite matrix. Poikilitic cores of matrix feldspar and quartz are observed in all the aegirines. Alkali feldspar phenocrysts almost always show exsolution. Group 1 can be subdivided into five subgroups:

The first subgroup represents the most pristine of the granitic dyke samples and includes Samples: STFL1A and STFL1B, FL1 and FL2. Coarse-grained (2-7mm) euhedral, aegirine phenocrysts are observed in a very fine-grained undeformed microgranite matrix, Figure 12(a, b). Samples within this group were not collected in situ so their relationship to the surrounding rocks is not known but they were all collected on the slopes of the nunatak, Straumsvola.

The groundmass in these dykes consists of very fine-grained <<1mm, anhedral quartz and feldspars that define the granitic mineralogy. Within the matrix, coarse (1-7mm) perfectly fresh and euhedral aegirines are visible. The aegirines are all poikilitic in their cores (Figure 12b). Point counting confirms that aegirine is the dominant phenocryst accounting for 30% of the sample as seen in Figure 13. Aegirine is not visible in the groundmass suggesting it was entrained from elsewhere possibly a deeper source. The lack of resorption or reaction rims on aegirine suggest they were brought up in a magma that was in chemical equilibrium with the dyke magma. Phenocrysts of quartz and feldspar account for 5-10% of the sample with quartz phenocrysts more abundant in STFL1A and perthitic feldspar the dominant phenocryst in STFL1B (Figure 12c, d). There seems to be no preferred orientation in the distribution of the phenocrysts.

Samples FL1 and FL2, while mineralogically similar, differ from the aforementioned samples in having more and finer-grained aegirines (1-4mm) in a slightly coarser-grained granite matrix of quartz and feldspar. In hand sample, FL1 is layered with a more felsic unit in contact with an aegirine-rich unit. In thin section this layering is seen as a sharp boundary that contains coarse, acicular aegirines flow aligned with quartz and feldspar phenocrysts. The matrix retains a relatively uniform grain size below the contact. Sample FL2 is also layered; the layering here defined by a higher proportion of aegirine crystals and a coarser-grained granitic matrix than FL1. The layering is likely related to magma flow as it is generally a linear feature shown by the alignment of the long axes of aegirine grains.

An unusual feature of these samples is they contain the rare minerals narsarsukite ($Na_2(Ti,Fe^{3+})Si_4(O, F)_{11}$ and vlasovite ($Na_2ZrSi_4O_{11}$). Narsarsukite is seen in samples STFL1A and STFL1B where they form acicular, clear laths (in plane-polarised light) visible in the cores of some aegirines i.e. predating aegirine formation or as elongate, bladed phenocrysts forming just prior to and synchronous with aegirine crystallisation (Figure 12e). Vlasovite is only seen in two areas of the section in FL1 as very anhedral, altered masses growing in the matrix near aegirine phenocrysts.

Subgroup 2:

This group contains samples ST75, ST147, ST211, ST217 and ST228 has aegirine phenocrysts that tend to clump together forming discrete aegirine phenocryst-rich zones surrounded by a granite matrix. Surrounding these zones, a finer-grained granite matrix that contains interstitial, anhedral aegirine/alkali amphibole is visible (Figure 15a, b, d). The matrix around the pods is almost indistinguishable from the groundmass of the rest of the sample (Figure 15e). Although feldspar phenocrysts are visible, only the aegirine phenocrysts form these zones (Figure 15c). These aegirines may thus be entrained from elsewhere. Samples ST75A and ST211 show these aegirine phenocryst zones quite well. ST211 also contains a very coarse grained phenocryst of euhedral narsarsukite (confirmed by electron microprobe) that is poikilitic in its core like the aegirine phenocrysts. ST75B is from the same sample as ST75A but is texturally slightly different (Figure 14). It has no aegirine-rich zones or amphibole in the granitic matrix and is layered. The layering is defined by an increase in grain size in the aegirines and other phenocrysts as you get closer to the contact with ST75A. That these textures are so different suggests that they represent magma pulses. However, their composition is broadly similar and there are no reaction rims suggesting the magmas are in chemical equilibrium and most likely originate from the same source. Sample ST75A, from field observations is from the central portion of a sill that intrudes the nepheline syenite at Storjeon, which might imply that ST75B is the quenched, uncontaminated margin of this sill.

A few of the samples that have an amphibole-granite matrix also show layering. The layering is clearly visible in hand specimen (Figure 10) and plane-polarised light but very difficult to distinguish under cross-polarised light. In sample ST228, the layering alternates between aegirine phenocryst-rich and phenocryst-poor (Figure 16). The aegirine-rich layers are very similar to the pods described above and are also surrounded by a fine-grained granitic matrix. The aegirine phenocryst-poor layers consist only of the fine-grained granitic matrix with interstitial, anhedral aegirine. Feldspar phenocrysts (2-4mm) are common but lack the rim/mantle of matrix material seen around aegirine. Sample ST147, although appearing equivalent to ST228 in plane polarised light, has a granitic groundmass very different to all the other samples (Figure 16d).

Group 1	Subgroup	Sample	Brief description
	1	STFL1A STFL1B FL1 FL2	Most pristine of granite dyke samples. Typically contain coarse-grained, poikilitic and euhedral aegirines in a fine-grained granite matrix. Phenocrysts of quartz and feldspar are common as well as unusual minerals, narsarsukite and vlasovite.
	2	ST75A ST211 ST228 ST147 ST217	Aegirine phenocrysts tend to form zones surrounded by a granite matrix. Surrounding the pods is a fine-grained granite matrix with aegirines growing interstitially. Some of these show layering characterised by aegirine phenocryst-rich and -poor layers
	3	ST75B GHG-3	Similar matrix to subgroup 2 but has no aegirine phenocryst zones or amphibole growing interstitially in the granite matrix. Quartz and feldspar phenocrysts are larger than in other samples
	4	ST38 ST39 ST84 ST226	Host to unusual minerals eudialyte, dalyite, vlasovite and narsarsukite. Aegirines mostly form interstitially to the granite matrix and are sub- to euhedral.
	5	ST88 ST248	Replacement by amphibole of the original aegirine suggesting disequilibrium conditions and possible involvement of an alteration fluid.
Group 2	1	ST46 ST76 ST144	All have similarities with Group 1 samples. ST46 and ST144 similar to Group 1 subgroup 4 but have no aegirine phenocrysts or unusual minerals. ST76 is very similar to subgroup2 of Group 1
	2	ST203 ST216	Granite with no aegirine phenocrysts. Interstitial aegirine/amphibole
	3	ST113 ST246 ST268	Quartz syenites (15-20% Quartz). Alteration of feldspars possibly by a fluid phase that crystallised aegirine on grain boundaries. Trachtyic textures.
	4	ST60 ST62	Dyke with section through the quenched margin. Riebeckite in quenched margin and some replacement of aegirine to amphibole in core section. Preferred orientation visible in quenched margin parallel to dyke edges
	5	ST32 ST33 ST249	Syenite. No visible quartz. Aegirines tend to clump together and show various degrees of alteration. Aegirine and biotite form interstitially. Extensive alteration of alkali feldspars. ST249 has 5% eudalyite

Table 1: Summary of the main petrographic features of the felsic dykes of the Straumsvola Complex

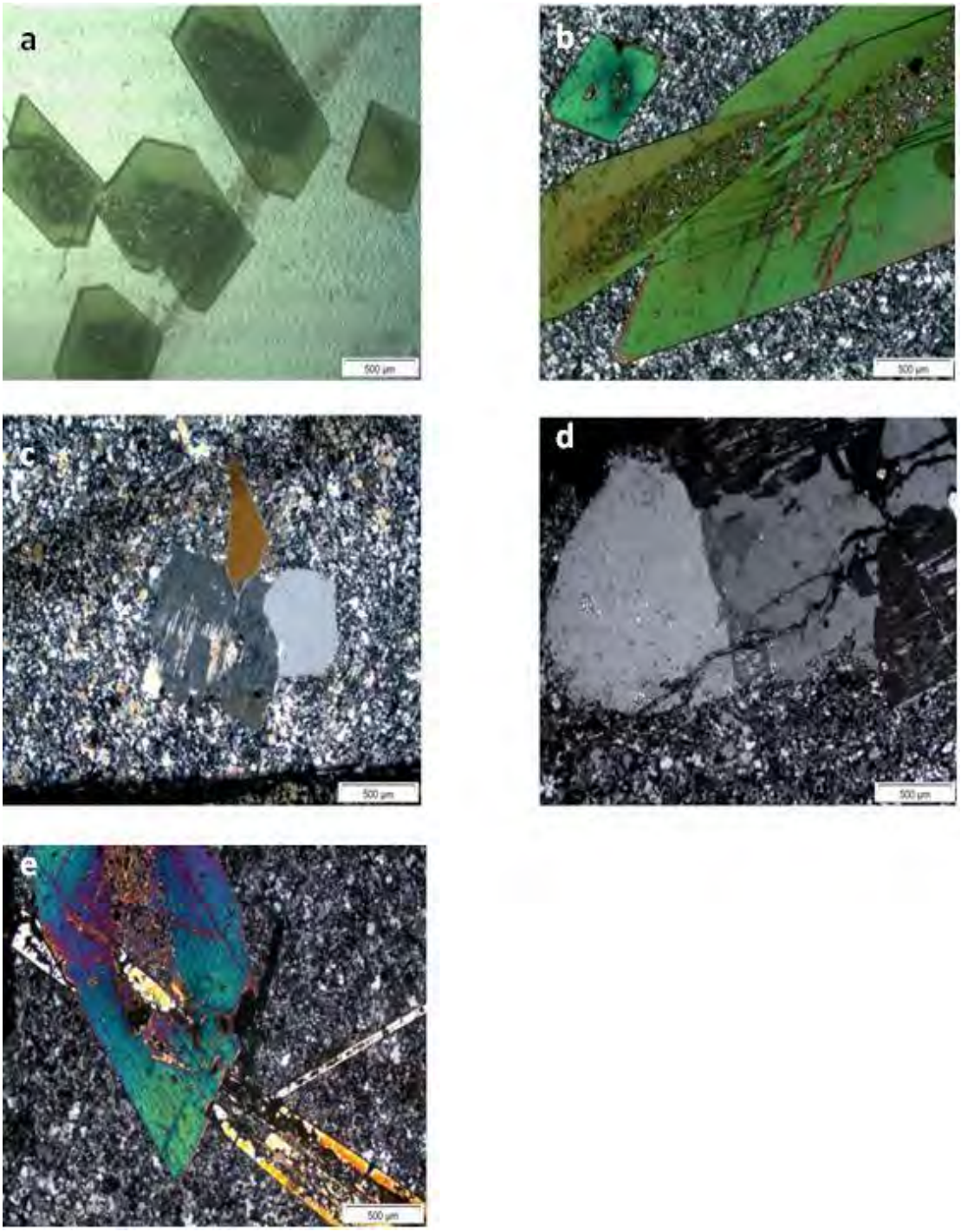

Figure 12: Group 1, subgroup 1: a) Euhedral aegirines with poikilitic cores under plane polarised light (PPL). b) Poikilitic aegirine as seen under crossed-polars (XPL) . c) Typical phenocryst phases; quartz and feldspar; within the granite matrix. d) Quartz and feldspar phenocrysts show myrmekitic intergrowths. e) An unusual mineral, narsarsukite (yellow), forms euhedral, acicular crystals in FL1 that is synchronous with aegirine formation.

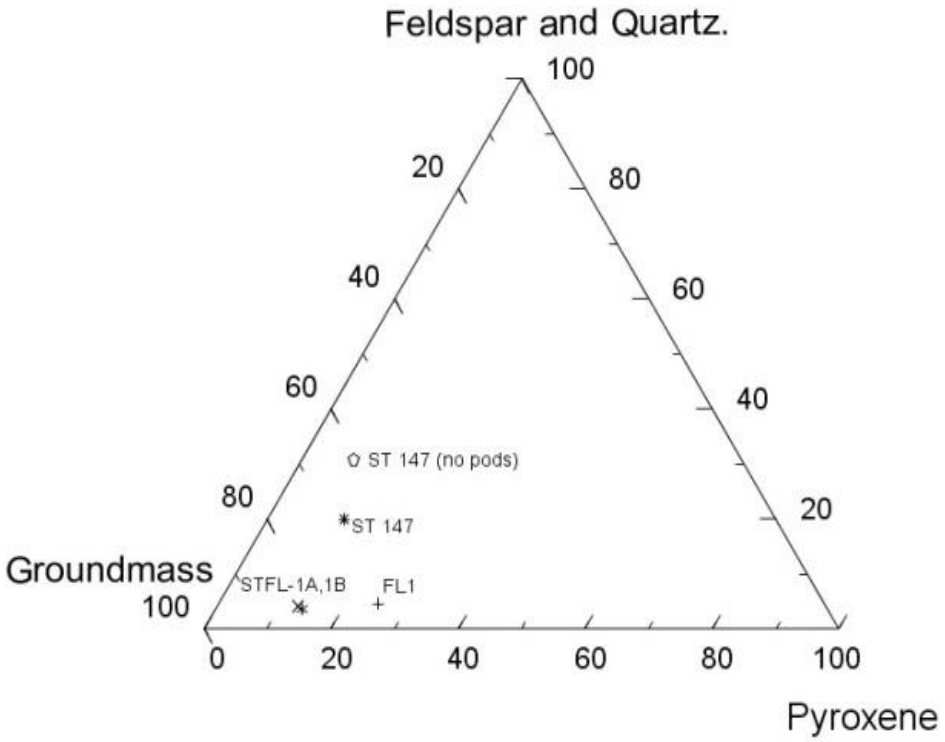

Figure 13: The four Group 1, subgroup 1 samples were point counted to determine the relative amounts of groundmass vs phenocryst phases (aegirine, feldspar and quartz). From the diagram it is clear the samples are dominated by the granite groundmass. Aegirine phenocrysts account for up to 30% whole rock while the proportion of quartz and feldspar phenocrysts is highly variable.

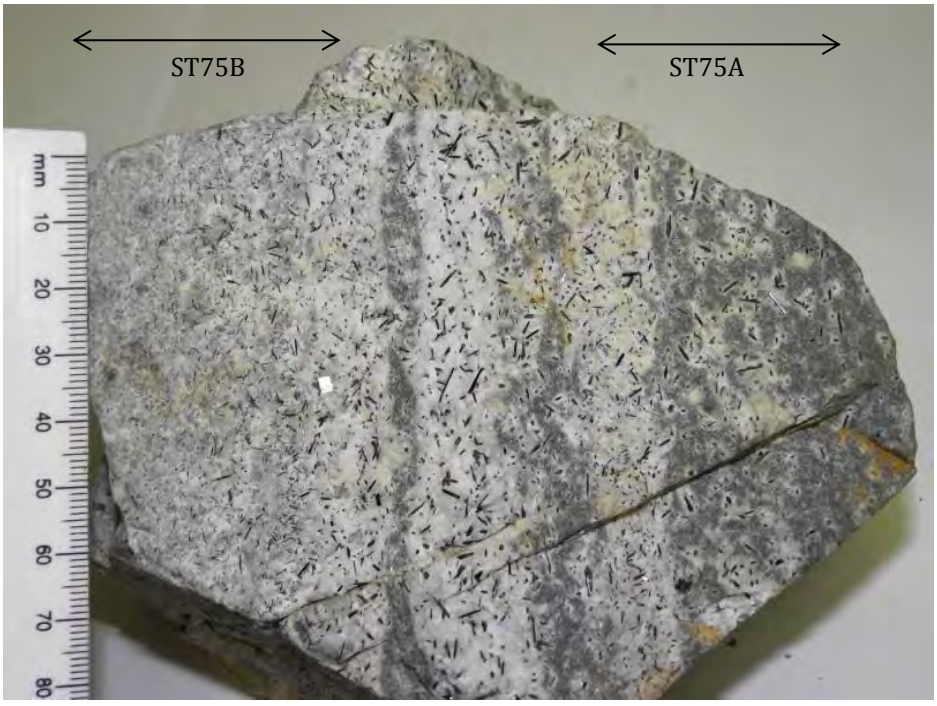

Figure 14: Hand sample of ST75. ST75A is the non- layered, massive section on the right while ST75B is from the layered unit to the left and may represent the quenched margin of sill ST75A.

Its groundmass is coarser grained with anhedral to subhedral grains of mostly exsolved feldspar (microcline) and quartz. Quartz (and to a lesser extent, feldspar) has very irregular grain boundaries and the grain size of the groundmass is inequigranular. Most of the aegirines have euhedral outline, but few are fully formed crystals indicating disequilibrium conditions in the host magma (Figure 16).

Subgroup 3:

Sample GHG-3 is very similar to ST75B and together they form a third subgroup. ST75B shows layering from coarse (2-5mm) euhedral aegirines in a fine-grained granite matrix to very fine (<1mm) euhedral aegirines in the same matrix. Quartz and feldspar phenocrysts also tend to decrease in size as the grain size of the aegirines decreases. GHG-3 has the same mineralogy and its phenocrysts are also surrounded by a fine-grained granitic matrix. The aegirines in this sample are euhedral with poikilitic coress as in previous samples but are generally finer grained (<2mm) with the exception of acicular aegirines that can be as long as 4mm. In these samples feldspar phenocrysts show signs of alteration (seritization and exsolution) while quartz shows undulose extinction, which is not really seen in any of the other sections.

Subgroup 4:

The fourth subtype contains a granite matrix consisting of fine to medium grained feldspar and quartz with aegirines of similar size. The aegirines in this group of samples are sub- to euhedral and appear to be interstitial to the granite matrix but comprise about 40% of the sample. These samples all contain at least 1 unusual mineral: eudialyte in ST38, ST39 and ST84 and narsarsukite in ST226. Sample ST38 has been described in detail by Harris &Rickard (1987) but is identical to ST84 that was collected at the same sample site. ST84 shows layering parallel to the plane of the thin section defined by aegirine laths (0.2mm-2mm) flow banded around quartz and feldspar (Figure 18a). Quartz and feldspar in the groundmass show preferred orientation in the same orientation as the aegirines. Ribbon quartz/feldspar is also present and is flow banded around the aegirines and within the groundmass (Figure 18a). ST84 also contains the mineral eudialyte which in plane-polarised light tends to form in discrete pink-orange, poikilitic patches (Figure 18b).

Two sections were cut of ST39 to show the layered (L) and massive zones (M) of this sample (Figure 17). The layering in ST39B is not well defined other than having a higher abundance of finer-grained (0.5-2mm) euhedral aegirines that tend to have a preferred orientation. The groundmass is granitic with medium-grained quartz and feldspars (1-3mm). There are no phenocrysts in these samples due to the larger grain size of the groundmass. The groundmass however is not the same everywhere with large parts of the sample exhibiting ribbon quartz similar to ST147.

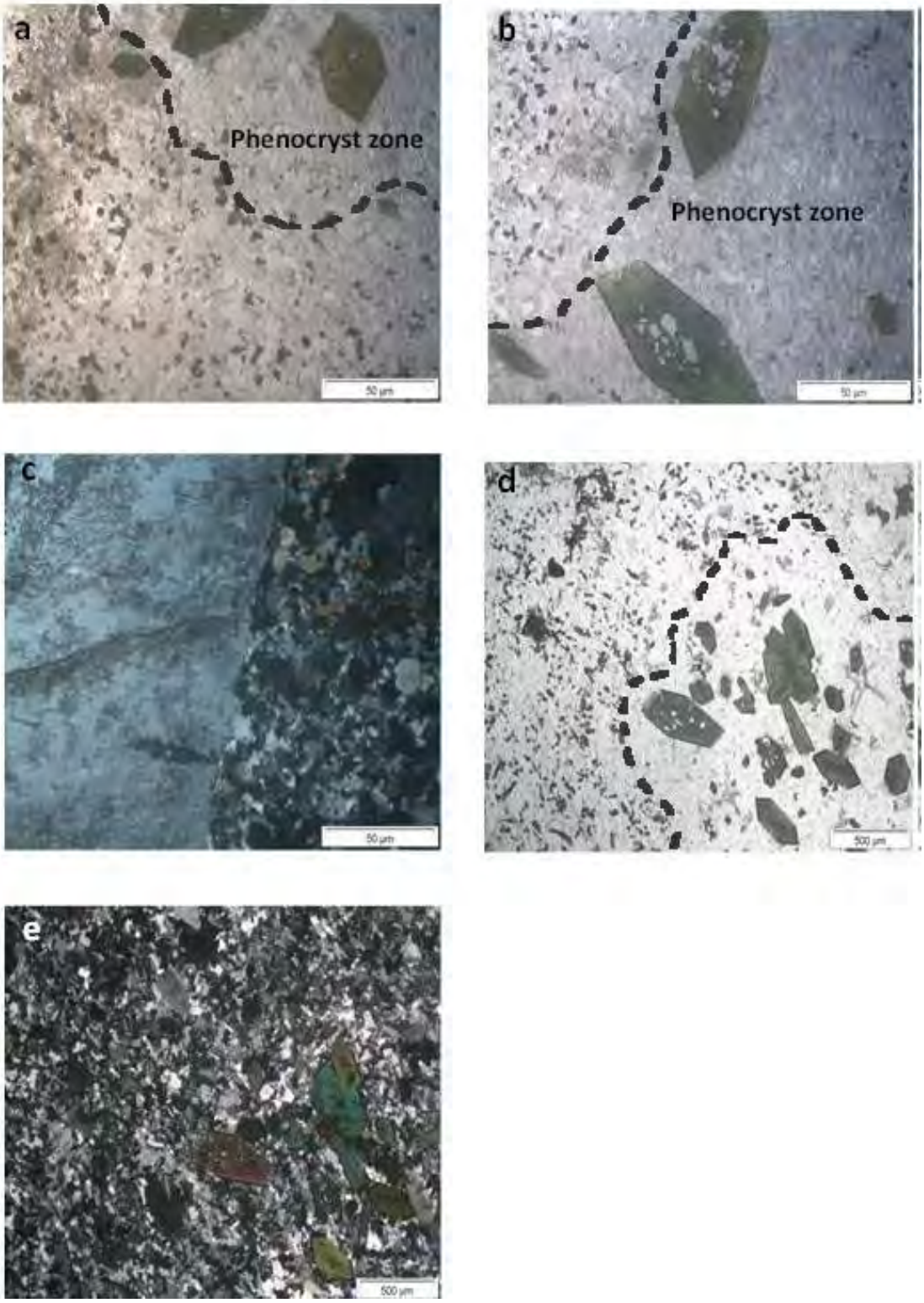

Figure 15: a and b) Aegirine phenocryst zones are separated from the groundmas (grey line) in ST75A. c) Feldspar phenocryst don't form zones. d) Aegirine phenocryst zones are separated from the matrix in ST211. e) XPL view of (d).The groundmass surrounding the phenocryst-rich zones show no major textural difference to the rest of the granitic groundmass other than having a higher proportion of groundmass aegirine.

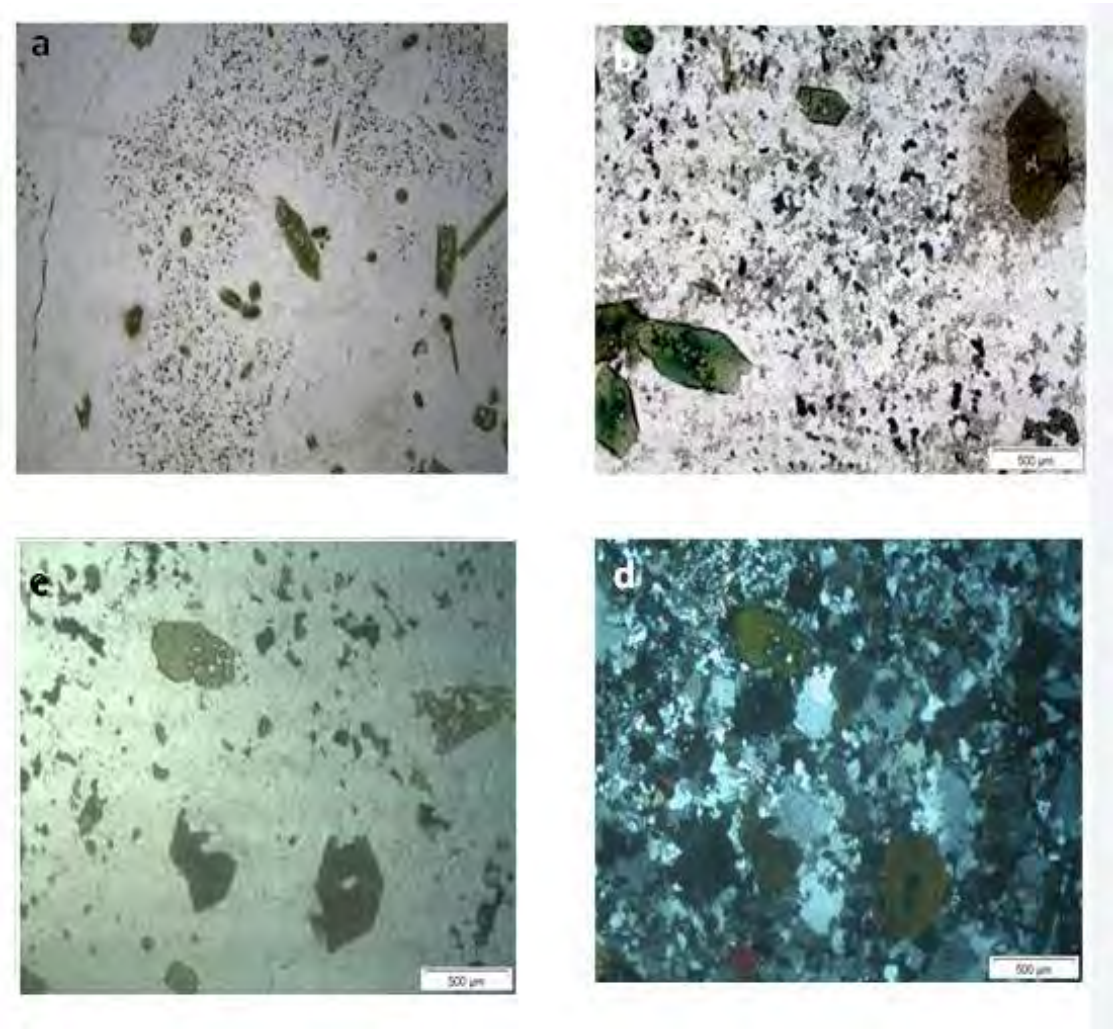

Figure 16: ST228 (a) 4x magnification under a stereo microscope clearly showing the aegirine phenocryst-rich zones that are not as easily visible under a petrographic microscope. b) ST228 under a petrographic microscope at 5x magnification. Two types of aegirine are visible; blue/green matrix aegirines and green phenocrysts c) PPL view of ST147 showing the separation of aegirine pods and aegirine/amphibole that form interstitially in the groundmass. When compared with the XPL view in d) the layering is not so easily distinguished. d) Coarser-grained granite matrix in ST147 and the finer-grained aegirine phenocrysts

As in ST38, eudialyte forms as discrete, poikilitic masses with low interference colours (dark grey) (Figure 17d). Massive zone ST39 has a very different texture to the layered zone in that the aegirines are interstitial to the granite groundmass and the groundmass consists of interlocking quartz and feldspar grains (Figure 17a). An anhedral, high birefringence (blue) mineral that is clear in plane-polarised light is observed within the matrix (<1 wt%)(Figure 17c). This mineral is dalyite. In ST38 dalyite was often observed as an inclusion in eudialyte (Harris & Rickard 1987) but here it forms as an anhedral, interstitial grain growing around aegirine.

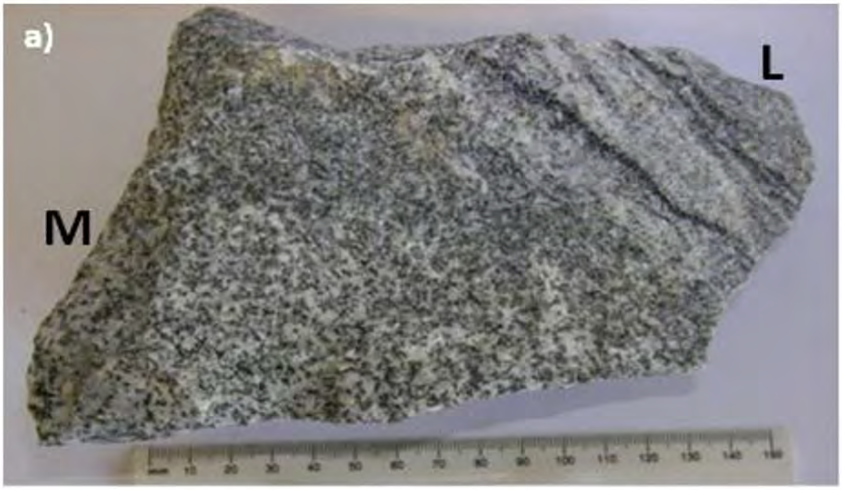

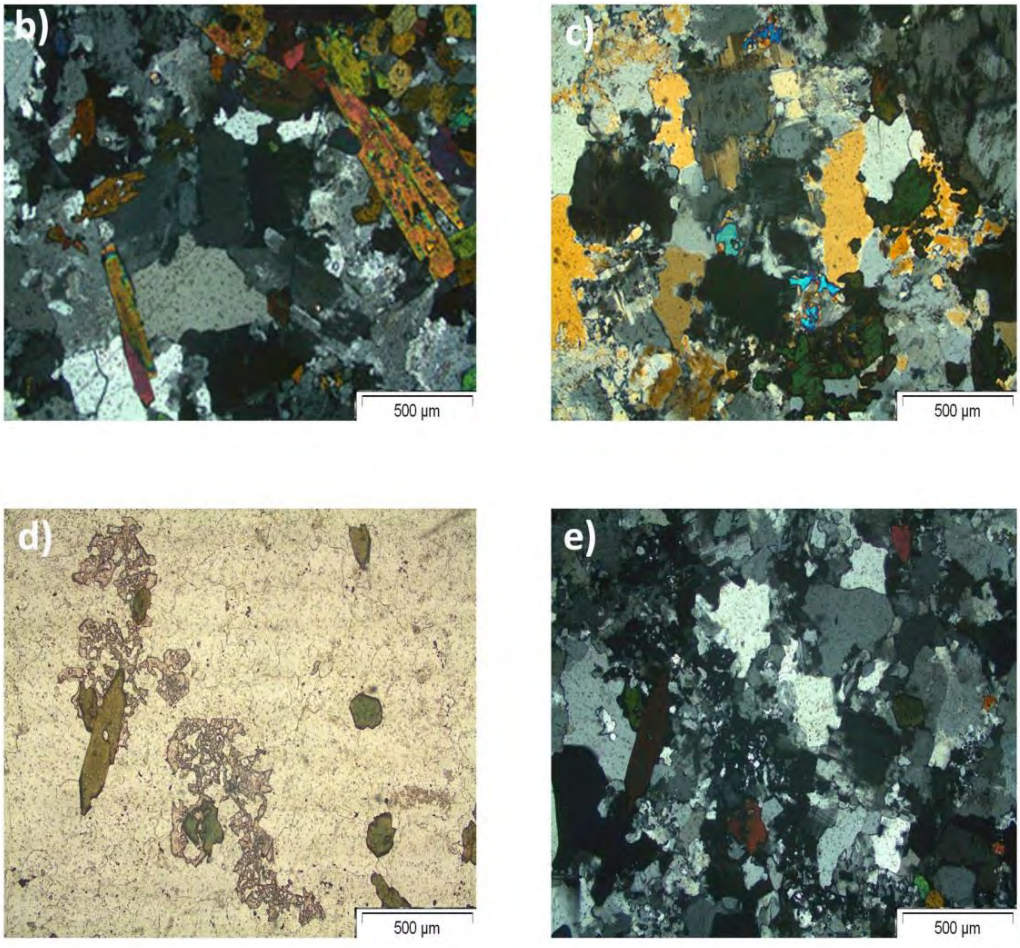

Figure 17: a) ST39- layered (L) and massive (M) zones. b) Layered zone granite with coarse grained aegirine. c) Massive zone in ST39 showing interstitial aegirine. The blue high birefringence mineral is an unusual Zr-silicate, dalyite. d) In PPL eudialyte is very distinctive as a pink, poikilitic mineral growing around aegirine phenocrysts. e) XPL view of (d) highlighting the low birefringence of eudialyte.

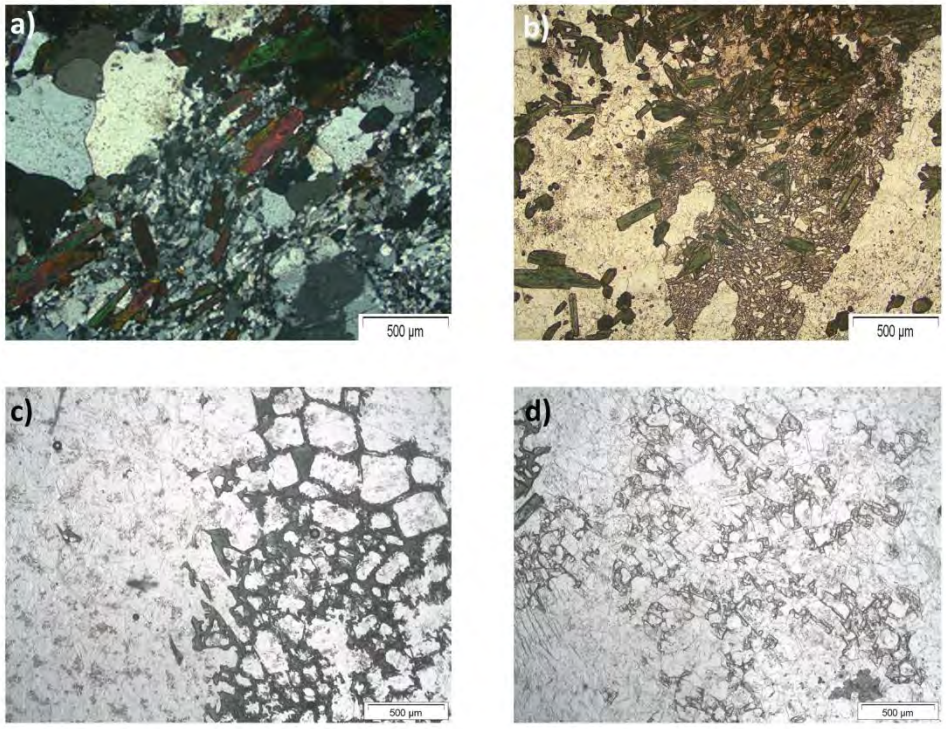

Figure 18: a) Flow alignment of the granitic matrix and aegirine phenocrysts in ST84. b) Orange/Pink poikilitic eudialyte growing around a cluster of aegirine phenocrysts. c) Skeletal outline of aegirine-augite in ST226. d) High relief pale mineral in ST226 is narsarsukite (PPL).

Sample ST226 has a much higher proportion of feldspar than the previous samples and is hence a quartz syenite. It is also from Storjoen unlike the rest of the samples in this subgroup that are from Straumsvola. Quartz and feldspar (microcline and albite) in the groundmass tend to be <1mm and anhedral to subhedral. Phenocrysts of quartz and feldspar are almost absent. Aegirine phenocrysts account for 10-20% of the slide, a much lower proportion than all the other samples, and they exist as skeletal masses (Figure 18c). The aegirine in this sample is darker green and was confirmed by electron microprobe to be aegirine-augite (Ca, Na)(Fe^{2+},Fe^{3+})Si_2O_6 . Narsarsukite forms as an interstitial mass, with a euhedral but inclusion filled appearance similar to the aegirine-augites (Figure 18d).

Subgroup 5:

A fifth subgroup of samples, ST88 and ST248 shows evidence for replacement/overgrowth of the original aegirines by amphibole (Figure 19). ST88 has the granitic matrix seen in eudialyte samples ST38 and ST84 and based on field observations may be a continuation of this dyke. As in ST38 and ST84, ribbon quartz and feldspars are observed around larger quartz and feldspar grains in the groundmass. Phenocrysts of microcline make up about 5% of the slide with the remaining phenocrysts all richterite/pargasite (15%) presumably after aegirine (Figure 19a).

Sample ST248 shows similar amphibole replacement features but displays a trachytic texture between the quartz and feldspars (Figure 19b). In this sample, there are few feldspar/quartz

phenocrysts but the majority are aegirine/hornblende phenocrysts that account for 30-40% of the total sample.

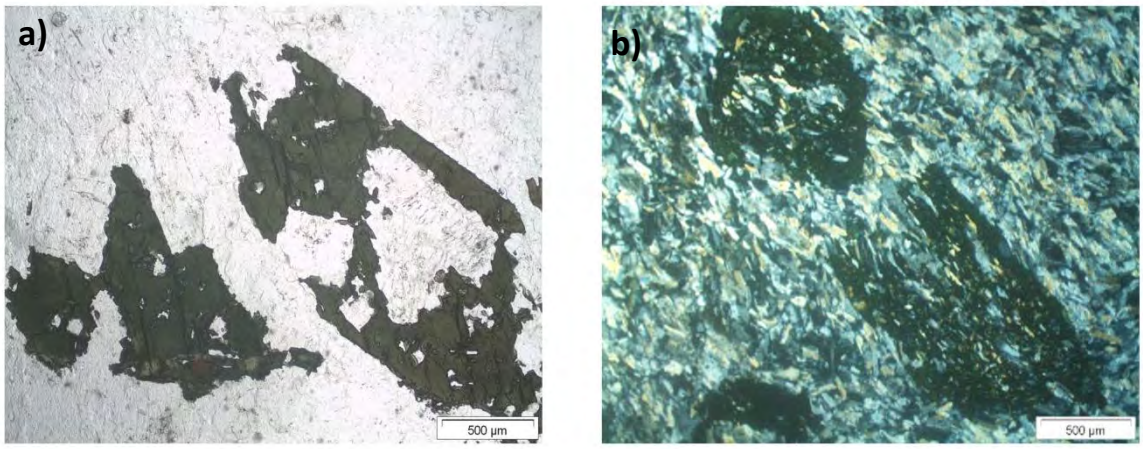

Figure 19: Deformed/altered phenocryst phases in ST88 (a) and ST248 (b) showing total replacement to amphibole after aegirine. Trachytic texture is observed in the groundmass of ST248.

Group 2:

Group 2 dykes can be defined by their lack of euhedral aegirine and abundance generally syenitic composition (modal analysis). A few samples are granitic in composition but all lack the phenocrystic aegirine that define Group 1.

The first of these share similarities with Group 1 samples and form the first subgroup of Group 2. Samples ST144 and ST46 in plane-polarised light appear equivalent to Group 1, subgroup 4 (granite matrix consisting of fine to medium grained feldspar and quartz with aegirines of similar size) lacking only the phenocrystic aegirine and unusual mineralogy. The samples are finer-grained than the Group 1 equivalents and show preferred orientation of the matrix minerals. This is seen in the alignment of the long axes of matrix aegirines and alkali feldspars (Figure 20a, b). In ST144, quartz (<<1mm) appears as rounded, interstitial blobs between alkali feldspar and aegirine. Phenocrysts of alkali feldspar are common but all display various degrees of exsolution possibly indicating disequilibrium conditions. Fine grained, interstitial fluorite is common as an accessory phase. ST46 is composed of medium-grained feldspar and fine-grained interstitial, acicular aegirines. The sample shows trachytic texture and appears flow banded (Figure 20a). Medium-grained aegirine phenocrysts are visible in thin section but they are not euhedral and appear to be reacting to form amphibole. The aegirine/amphiboles that appear to be phenocrysts are actually formed from nucleation of smaller aegirines.

Sample ST76 is a granite dyke made up of fine to medium-grained subhedral quartz, fine-grained anhedral feldspar and interstitial, anhedral riebeckite-arvedsonite (Figure 22d). Texturally it is very similar to Group 1 subgroup 2. Phenocryst phases include feldspars showing exsolution to

perthite as well as quartz and narsarsukite. The narsarsukite is yellow in hand sample, blocky, euhedral and slightly poikilitic in thin section (Figure 20c). It appears to grow around the matrix and is hence a late crystallisation product.

The remainder of the Group 2 samples have very similar textures in thin section but can be compositionally divided into 3 other subgroups: granites, quartz syenites and syenites.

Subgroup 2 consists of granites dykes, ST203 and ST216. ST203 shows anhedral, clear, medium-grained quartz and feldspars exsolving to perthite and sodic plagioclase (Figure 22a, b). Fine grained, blue-green riebeckite is seen to grow in the interstices of the quartz and feldspar and makes up of 35% of the rock. Replacement of acicular aegirine by riebeckite is visible in some areas under cross polarised light. Slightly coarser-grained but anhedral biotite is visible replacing some of the riebeckite, ultimately becoming a Fe-rich oxide. Phenocrysts are totally absent. ST216 is a fine-grained equivalent of ST203. It shows the same anhedral, interstitial amphiboles but lacks the interlocking granitic texture of ST203 and has a higher proportion of unaltered aegirine. Phenocrysts of simply twinned feldspar showing exsolution to perthite are common as well as trace high relief, fluorite.

Subgroup 3 are the quartz syenites, ST268, ST246 and ST113 that contain 15-20% quartz. ST268 shows perthitic, tabular feldspars that tend to form a trachytic texture. The feldspars are impeded by medium-grained, interstitial growth of quartz (15-20%) and finer-grained, anhedral aegirine (Figure 22c). Sample ST113 is a very altered quartz syenite and is generally finer-grained than ST268. The feldspars are all affected by alteration possibly by the fluid that formed the aegirine along grain boundaries. These aegirines are in various stages of replacement to an iron rich oxide phase as can be seen in Figure 22d. Sample ST246 (Figure 22e, f) is very similar to sample ST113. Phenocrysts are present in the form of coarse-grained, subhedral quartz and perthitic feldspar. Matrix feldspars form an interlocking texture. This sample is unique however, as it contains about 5% interstitial eudialyte. The eudialyte is variably replaced to an Fe-oxide indicating disequilibrium conditions.

Subgroup 4 is very different texturally from the other samples in that it has fine-grained acicular laths of blue riebeckite in a granite matrix of fine-grained, anhedral quartz and feldspar. The amphiboles show preferred orientation parallel to the dyke edge and flow around the phenocrystic perthitic feldspars. These textures are observed in ST60, Figure 21, which is the quenched margin of sill, ST62 in Figure 21. The main dyke in this sample is coarser-grained than ST60 and shows some preferred orientation in the feldspars but not as well defined as in ST60. Sill, ST62's feldspars are generally fine-grained and tabular while the quartz grains are mostly interstitial to the interlocking feldspar. Anhedral aegirine is common, accounting for 20% of the sample, and appears to have crystallised last as it forms on the boundaries of both quartz and feldspar. In some areas the aegirine is replaced by amphibole. Phenocrysts in this section are perthitic feldspars that show thick alteration rims.

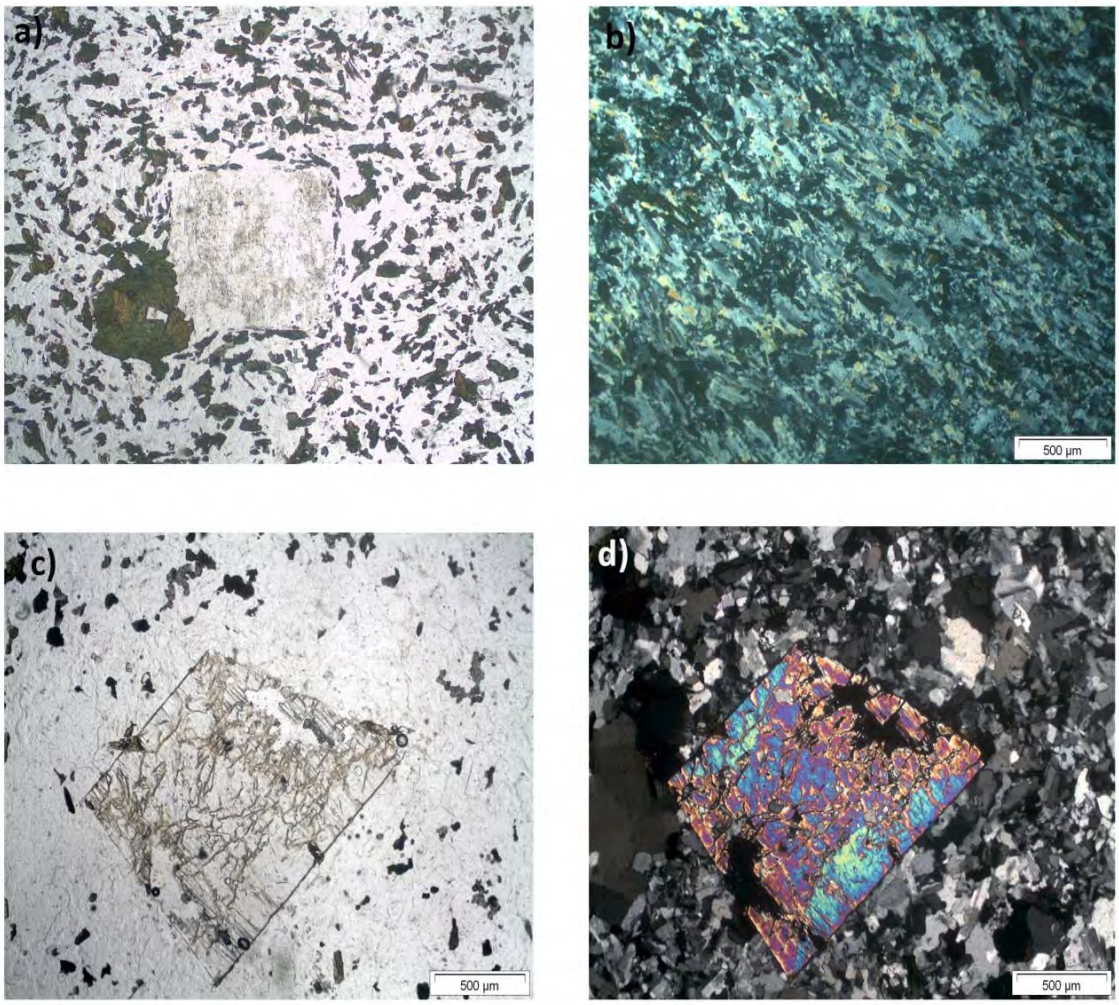

Figure 20: Group 2 subgroup 1: ST46, ST144 and ST76. Aegirines are all darker and none are present as phenocrysts. a) Flow banding around a feldspar phenocryst in ST46 in PPL. b) Trachytic texture in ST144 in XPL. c) PPL view of ST76 showing the very felsic nature of the sample and the aegirine/amphibole growing interstitially in the granitic groundmass. Also shown is a euhedral, poikilitic crystal of narsarsukite in PPL and XPL (d).

Figure 21: Contact zone between the quenched dyke margin, ST60 and sill, ST62. ST60 (top) in PPL shows blue riebeckite and flow banding. The main sill (bottom) has interstitial aegirines that are very fine-grained and appear to have crystallised last. It also has a coarser grain size than the outer, quenched margin.

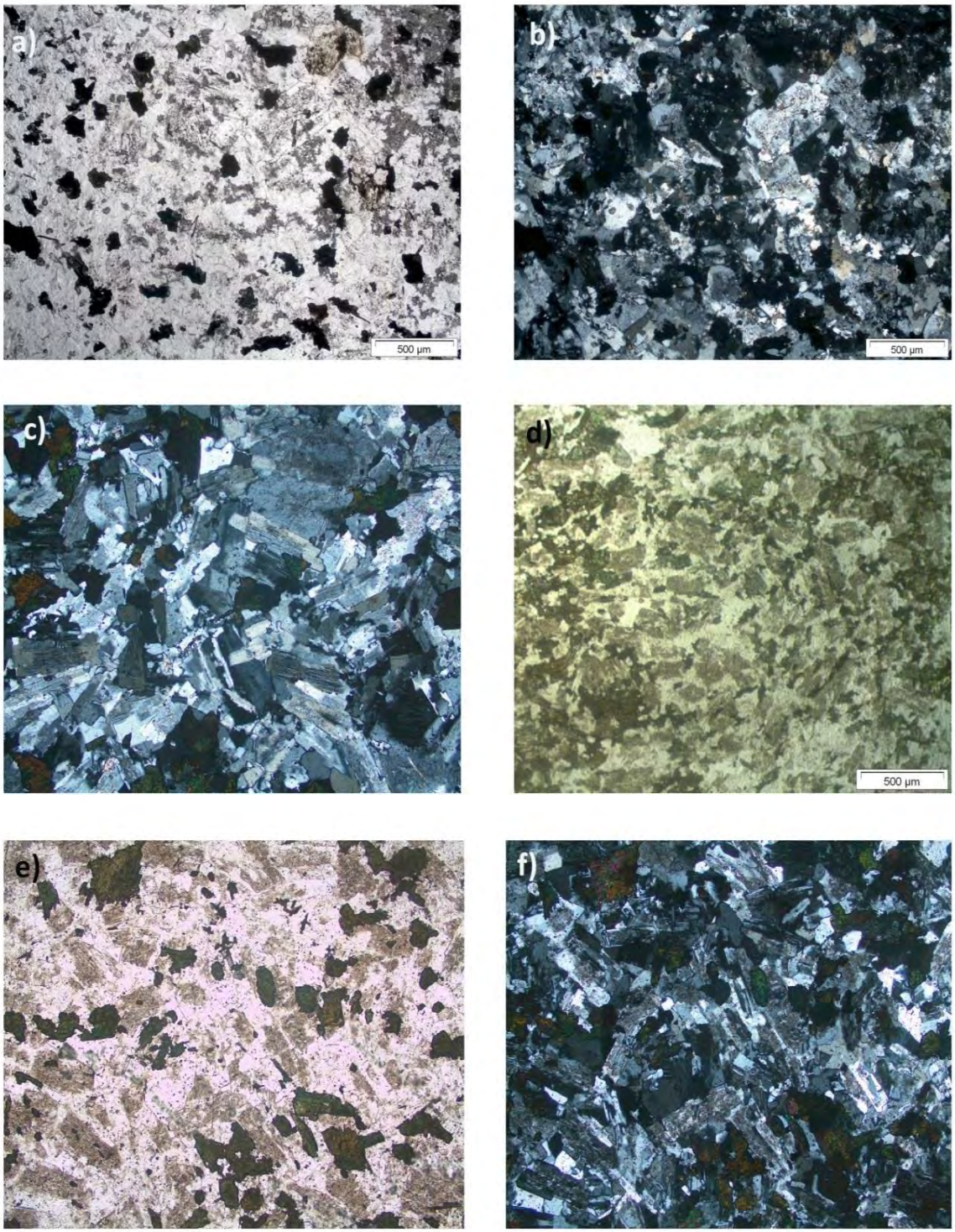

Figure 22: Subgroup 2- Granite: a) PPL and b) XPL view of ST203: coarser-grained groundmass with aegirines growing interstitially. Some alteration of the feldspars visible.

Subgroup 3- Quartz Syenites: c) XPL view of ST268 showing interlocking feldspar grains with very little quartz. Aegirine also forms interstitially. d) PPl view of ST113. Proportion of aegirine is quite high relative to feldspar (brown masses) and quartz (white) but the aegirines are anhedral and showing replacement to an oxide phase. e and f) PPL and XPL view of ST246, respectively. Grains show interlocking feldspars that are variably affected by seritisation. Aegirines are anhedral and showing signs of replacement to an oxide phase as well (brown grains in and around dark green aegirine).

The fifth and final subgroup is the syenite dykes, ST33, ST32 and ST249. Texturally ST33 resembles ST216 but it has no visible quartz. The feldspars show definite preferred orientation presumably parallel to the dyke edge with interstitial, anhedral aegirine/amphibole forming along grain boundaries (Figure 23a, b). Simply-twinned alkali feldspar phenocrysts range in size from 2-6mm while aegirine phenocrysts are found in small clusters. These 2mm clusters generally show reaction rims or complete replacement to a red-brown phyllosilicate, most likely biotite. Sample ST32 contains feldspars that form an interlocking texture of fine to medium-grained, euhedral (tabular) crystals generally exhibiting simple twins (Figure 23c). Alteration of the feldspars is visible in plane-polarised light as well as under crossed polars where minor exsolution to sodic plagioclase is observed. Biotite and aegirine in various stages of alteration are commonly seen as clumps of aegirine/hornblende and biotite/altered biotite/oxide between interlocking feldspars. They are generally anhedral, but coarser grained, than in other samples and hence probably crystallised quite soon after the feldspars. In syenite dyke, ST249, the feldspars all show alteration and exsolution textures. The very coarse-grained (3-6mm), subhedral alkali feldspars show alteration along the grain boundaries and exsolution to perthite is very common. The feldspars are interlocking with anhedral aegirine growing interstitially (Figure 23d). The aegirine is a mottled green and similar to other Group 2 aegirines that are undergoing replacement. An accessory carbonate is also present (identified by the high 3rd order colours under crossed polars) and forms interstitially in the groundmass (Figure 23f).

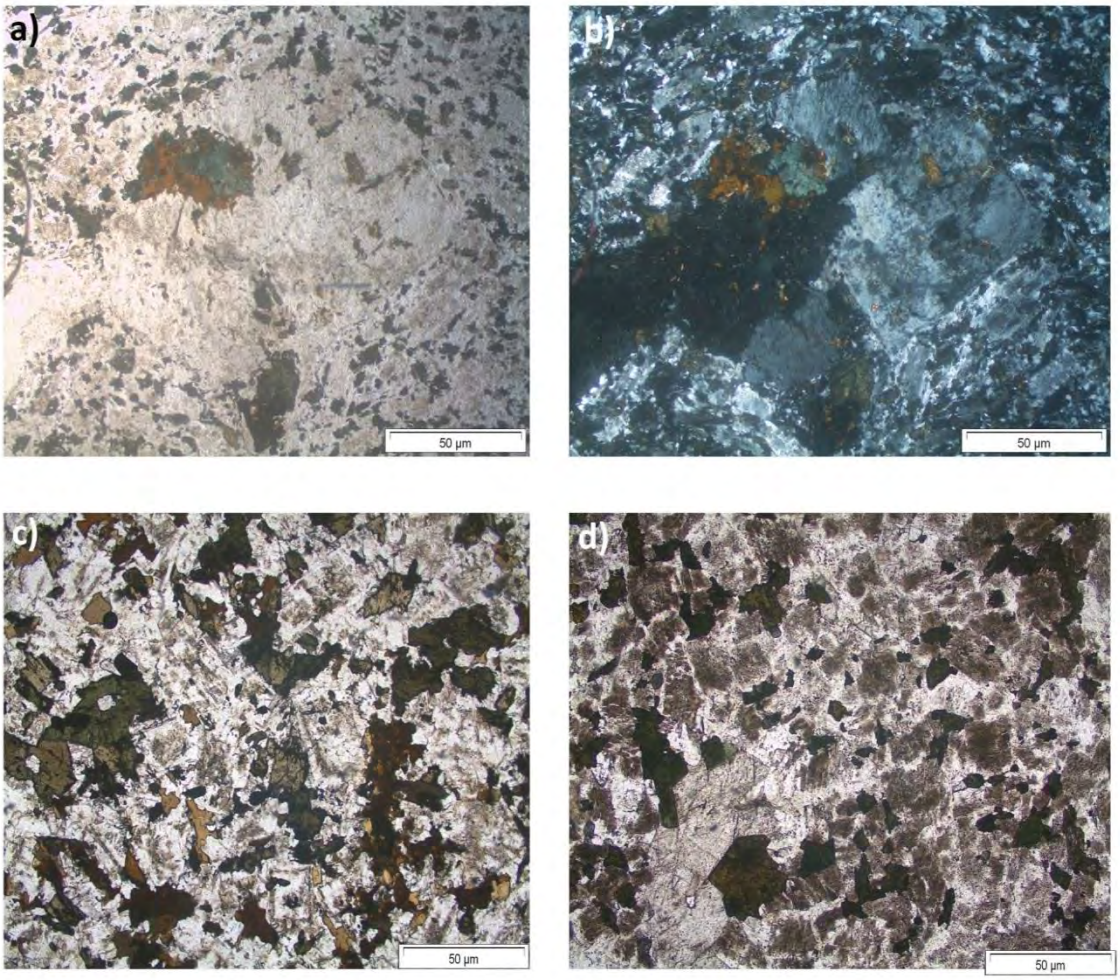

Figure 23: Syenite dykes: a) PPL view of ST33 showing preferred orientation and flow banding of the groundmass and interstitial aegirines. Aegirine clusters show replacement to biotite. b) XPL view of ST33 showing the feldspar phenocrysts and the quartz poor groundmass. c) Fe-rich syenites shown by the presence of biotite in ST32. Aegirine/amphiboles here are coarser-grained than in other samples. d) Alteration of the feldspars in ST249 is visible in PPL as a brown staining of the grains. Grains show an interlocking texture and have no visible quartz. A carbonate mineral is shown in the bottom left of the section and is an accessory phase.

2.3.2 Country rock gneisses

The country rock gneisses of the Straumsvola Complex were initially described by Harris & Grantham (1993). A detailed petrographic and fluid inclusion study by K. Maisela was subsequently undertaken in 2012 as part of an honours thesis (unpublished). The gneisses are predominantly orthogneisses and subordinate paragneiss with minor carbonate. They tend to have calc-alkaline affinities and are thus likely volcanic in origin (Groenewald et al. 1995). These Jutulrøra Formation gneisses experienced amphibolite facies metamorphism at around 1Ga as part of the regional Sverdrupfjella Group (Groenewald et al. 1995). The contact between the gneisses and the intruding nepheline syenite at Straumsvola is sharp (Figure 8b). Fenitisation, seen as green rims on orthopyroxene, is likely a result of the intrusion and is a common feature of the gneisses of the contact zone (Harris & Grantham 1993). The extent of this alteration will be

investigated below in addition to a brief petrographic description based on the observations of Maisela (2012) and my own. Important/interesting features are shown in Figures 25 and 26:

ST241: This gneiss is located <1m from the contact between the nepheline syenite pluton and the country rock gneiss. ST241 being close to the contact should therefore show the most evidence of fenitisation/sodic metasomatism. It is composed of anhedral to subhedral grains of alkali feldspar and albite that have well developed triple junctions. The feldspars are the most abundant mineral followed by anhedral clinopyroxene after orthopyroxene, biotite and quartz. An accessory oxide phase is also seen. There seems to be evidence for alteration that is pervasive across the section giving a green tinge to the pyroxenes in plane polarised light and resorbing the pyroxenes along grain boundaries (Figure 24a). Biotite grows as a late stage mineral, possibly resorbing feldspar but only where evidence of alteration is also visible. One area of the thin section shows pyroxenes mantled by green rims i.e. sodic alteration that reacts to form aegirine-augite (Figure 24b). This sample therefore agrees with the findings of Harris & Grantham (1993) that the contact zone samples are fenitised.

ST242: This sample was collected 7m from the contact zone and is from a leucocratic portion of the gneiss. It is less affected by alteration but nonetheless alteration is still visible in some areas. Mineralogically it is the same as ST241 but the biotites are coarser grained and the oxide phase is much more abundant (7-10%) (Figure 24c,d). Feldspar accounts for 60% of the gneiss and has good interlocking textures. Fenitisation of pyroxene rims is common as well as seritization of the feldspars.

ST264: This gneiss is 400m from the contact. It is a typical gneiss exhibiting preferred orientation and compositional layering of quartz, feldspar and biotites (Figure 25a). Quartz crystals are coarse-grained and subhedral while feldspars are rounded and finer-grained. Biotite forms interstitially with the long axis perpendicular to the inferred plane of maximum stress. Pyroxene is an accessory phase (<5%) and forms as interstitial, fine grained anhedral masses associated with biotite. A fenitising fluid may have been present as seen in biotite that may be pseudomorphed to chlorite (Figure 25b).

ST181: >500m from the contact. This sample was not described by K, Maisela in 2012 so a description is given here. Coarse grained (>4mm), anhedral, alkali feldspars with interlocking grain boundaries comprise the section. Exsolution to both microcline and perthite is common. Subrounded, finer-grained quartz is present with feldspar. Orthopyroxene and clinopyroxene grow interstitially ranging in size from 2mm-6mm. Most of the pyroxenes show partial replacement to aegirine augite on grain boundaries and are evidence for sodic alteration caused by an alteration fluid n(Figure 25c). The feldspars are also slightly seritised. Biotite only forms where the feldspars are the most altered.

ST254: This gneiss was collected 2000m from the contact and is a leucocratic layer within its host gneiss. It is the most pristine of the gneiss samples (Figure 25d). No evidence of an

alteration fluid or any fenitisation is visible. Quartz and feldspars are subhedral but interlocking and show preferred orientation. Biotites are also aligned in this orientation. Pyroxene is absent.

Preliminary results from the petrography of the gneisses shows that the pyroxene and feldspar content decreases from the contact to the outer zones while the quartz content overall increases. An alteration fluid was responsible for sodic metasomatism/alteration of the country rock gneisses and agrees with the results of Harris & Grantham (1993). Given that the effect of this alteration decreases away from the contact zone, it can be deduced that the source of the alteration fluid is related to the intrusion of the nepheline syenite at Straumsvola.

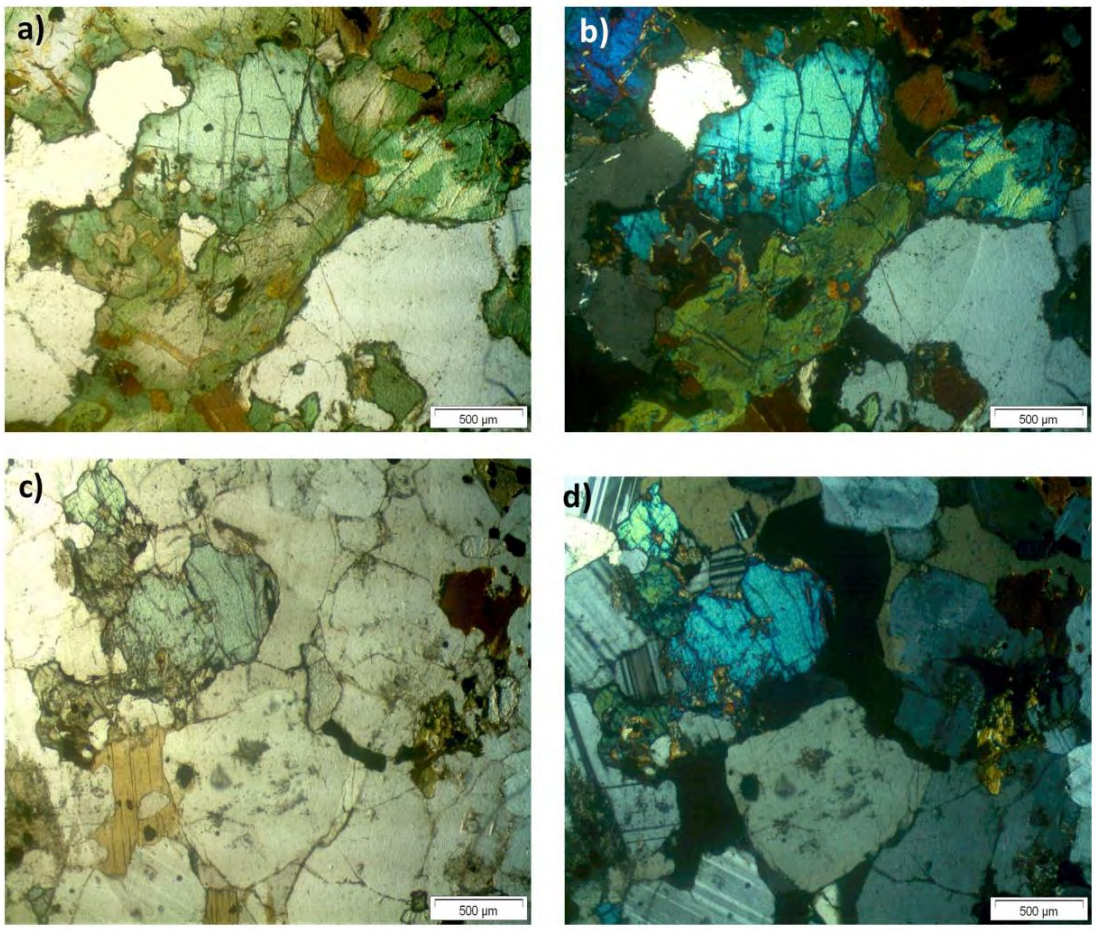

Figure 24: Gneisses of the contact zone. a) Sodic alteration on the rims of pyroxenes results in a green discolouration and growth of biotite on grain boundaries. Increased alteration on the rims vs. the core is evidence that the alteration is the result of an alteration fluid. b) XPL view of (a) showing the highly birefringent clinopyroxene and aegirine-augite rims. ST242 (c.d) shows similar textures to ST241 but less evidence of sodic alteration in PPL and XPL shown by the presence of both clinopyroxene and orthopyroxene with no reaction rims.

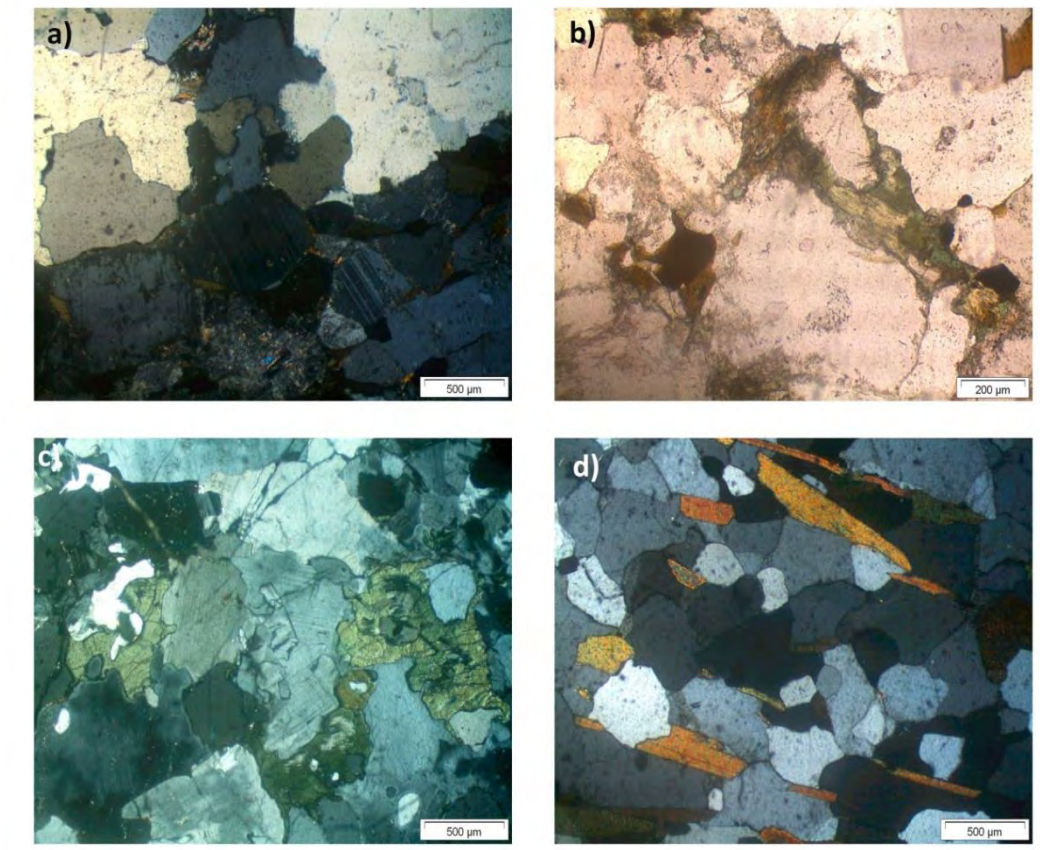

Figure 25: Country rock gneisses. a) ST264- 400m from the contact zone. Compositional layering of quartz (top) and feldspar (bottom). b) Alteration is only visible on biotite grains where they replaced to chlorite. c) ST 181- 500m from the contact. Orthopyroxene shows partial replacement to clinopyroxene by an alteration fluid. (d) ST254- 2000m from contact. Granoblastic texture of the gneiss with no alteration by a sodic fluid and no pyroxene. Biotite defines a weak lineation.

2.3.4 Nepheline syenites

The nepheline syenites that comprise the Straumsvola Complex are intrusive into the country rock gneisses. Three samples that characterise the major units are described below and shown in Figure 26a-f. The first is from the massive, outer zone (ST71), followed by ST133 from the layered zone and ST138 from the mafic marker (as described in Harris& Grantham, 1993).

Sample ST71 was collected at Storjeon and is an amphibole, biotite, nepheline syenite from the massive outer zone. Coarse grained (>4mm) alkali feldspars exsolving to antiperthite form a cumulate texture with coarse (2-5mm), low relief nepheline. Hornblende and biotite form interstitially to the cumulate syenite and are seen to replace aegirine in some areas. Oxides account for 5% of the sample and are associated with the amphibole and biotite.

Sample ST133 is from the layered zone of the nunatak Straumsvola. Layering is defined by mafic-rich and mafic-poor layers with alkali feldspars and blocks of coarse grained (2-4mm) nepheline syenite rounded and rotated into the foliation or bounded by elongated alkali feldspars. Aegirine and hornblende grow interstitially and could thus be forming synchronously with the crystal settling proposed by Harris & Grantham(1993) to cause the layering.

Ijolite, ST138 forms at the base of the mafic unit, unconformably overlying the layered zone at Straumsvola. Nepheline is the most abundant mineral forming as subhedral grains (1-4mm) long that define a poor lineation. Mafic minerals aegirine and amphibole account for 40% of the rock but are generally anhedral and interstitial to nepheline. The crystallisation order of the aegirine and amphibole is hard to distinguish as both are observed overgrowing the other. Biotite, however, forms last as evidenced by the reaction rims around aegirines, amphiboles and oxides. Accessory sphene is also present as an anhedral grain.

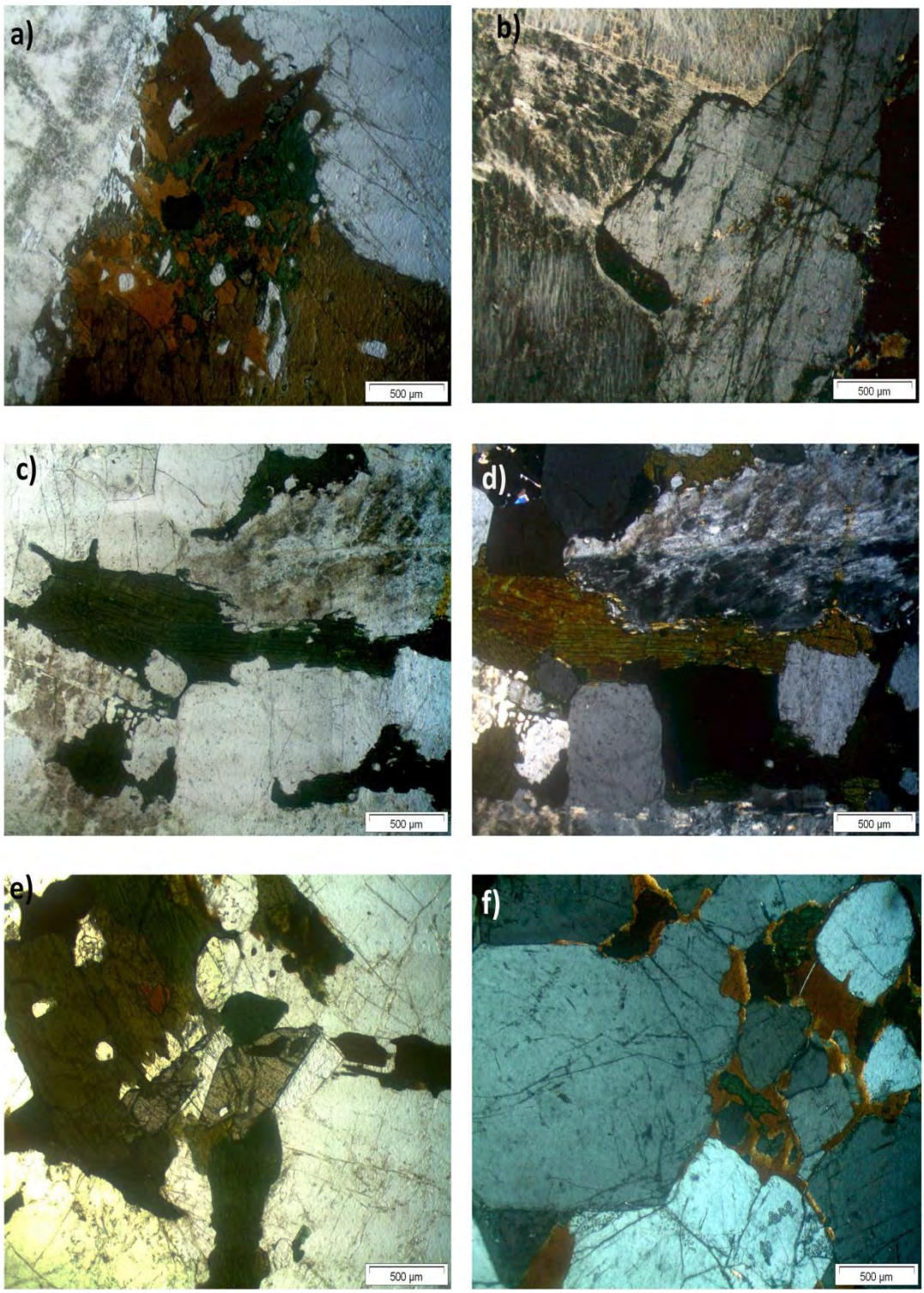

Figure 26: Nepheline syenites. (a) ST71- outer zone, massive nepheline syenite. Nepheline exhibiting low birefringence on the right. Aegirine can also be seen to be replaced by biotite and amphibole. b) XPL view of feldspar and nepheline triple junctions suggesting the syenite is a cumulate. c) ST133- layered inner zone syenite. Aegirine/amphibole grow synchronously with development of the layering. d) XPL view of (c). ST 138- Ijolite. (e) Mafic minerals: aegirine, biotite and amphibole, make up 40% of the slide. Sphene is also present as the cream/brown subhedral grain in the centre of the view. f) Cumulate texture defined by the nephelines and feldspars with biotite crystallising on grain boundaries.

3. Methods

All sample preparation and analyses were conducted in the Department of Geological Sciences at the University of Cape Town, except where otherwise noted.

Whole rock powders were prepared from samples weighing roughly around 500g-1kg. The samples were split and fed into a Sturtevant Laboratory jaw crusher. The coarsely crushed material was placed in a SeibTechnik carbon steel swing mill and ground to a fine powder. This powder was used in all subsequent analytical analyses.

Analytical techniques

3.1. Electron Microprobe

Of the 32 granite dyke samples available, 10 were chosen for electron microprobe analysis. Mineral compositions were obtained using a Jeol JXA-8100 Electron Probe Microanalyser run at 15kV and 50nA. The electron microprobe is equipped with four wavelength dispersive spectrometers and a range of crystals (LDE1, LDE2, PETJ, PETH, TAP, LIF, LIFH) for x-ray detection. A thin carbon coat was applied to each sample prior to analysis to prevent charge build up during the analysis. An inhouse diopside was used as a standard to analyse aegirine and the unknown minerals. The standard was run at the beginning of each probe session. The unknown minerals are known to be unusual Zr- and Ti-silicates but appropriate in-house standards did not exist that the electron microprobe could be calibrated against. However, the aim of analysing the unknowns under the microprobe was to confirm which Zr- and Ti- silicates were present and not their exact chemical formulas. For this reason mica's and amphiboles were used as standards.

3.2. XRF

Whole rock major-element compositions were analysed on 18 samples in 2013 by X-Ray Fluorescence (XRF) using a Philips PW1480 wavelength dispersive XRF spectrometer with a dual target Mo/Sc X-ray tube. Following the method of (Willis & Duncan (2008), approximately 2g of powdered sample was accurately weighed, dried at 110°C and then ashed at 950°C overnight to determine loss on ignition (LOI) and ensure all Fe was oxidised to Fe^{3+}.

The ashed sample was mixed with a lithium tetraborate/metaborate flux (in the proportion 57:43) with LiBr as releasing agent and fused in a Claisse gas burner to create fusion disks. Calibration standards used were a combination of natural standards from the USGS and SARMS (South African producers of Metallurgical and Geological Certified Reference Materials). Matrix corrections made use of the Fundamental Parameter method as described in Willis & Duncan (2008) and Rousseau et al. (1996).

In addition to the 18 samples measured in 2013 for this study, data for 10 other samples from Harris & Grantham (1993) were also included in the final dataset. These analyses were also conducted in the Department of Geological Science at the University of Cape Town following the method of Le Roex (1985).

3.3. Trace elements

Trace element compositions were determined for 28 samples, along with BHVO-2 and JG-2 certified reference materials (CRM), via solution inductively coupled mass spectrometry (ICP-MS) on a Thermo-Fisher X-Series II Quadrupole ICP-MS. 50mg of each powdered sample was dissolved in a 4:1 concentrated HF-HNO_3 acid mixture in sealed teflon beakers. After digestion on a hotplate at ±140ºC for 48 hours and evaporation to dryness, 2ml of concentrated HNO_3 was added to the samples in two stages. The final dried product was then taken up in 5% HNO_3 solution containing 10ppb Re, Rh, In and Bi as internal standards. Standardisation was against artificial multi-element standard solutions. Errors throughout the concentration range were better than 3%. Accuracy and procedural blank levels were similar to values reported by le Roex et al. (2001). The results for CRM BHVO-2 and JG-2 are shown against the recommended values from GeoReM in Table 2. The elements V, Co, Ni, Zn and Ba do not show good agreement with GeoRem but are not typically well resolved by ICP-MS and are also not elements of concern for this study. Sr and Zr, however, are. Differences in observed and calculated Zr concentrations may reflect incomplete dissolution of zircon in the digestion process. However, zircon is rare in both the nepheline syenites and granites of this study and so will not have an effect on the Zr concentration of the samples. To show that our Sr data is valid, the Sr values obtained via ICP-MS were compared with the elemental analysis obtained by XRF on the same samples. The results are shown in Table 3. Good agreement exists between the two datasets especially at low Sr concentration, which is important as most of the dykes in the study have a low Sr content. Therefore the Sr data obtained by ICP-MS can be used for further interpretation.

	BHVO-2 GeoReM	BHVO-2 UCT	JG-2 GeoReM	JG-2 UCT	JG-2 UCT
Li	4.8	4.228	35.9 - 43.9	39.64	38.77
Sc	32	28.67	1.4 - 2.8	1.45	1.377
V	317	307.0	n/a	0.58	0.59
Cr	280	271.7	4.5 - 8.9	1.868	1.817
Co	45	36.01	3.4 - 4.55	3.523	3.508
Ni	119	87.88	2.01 - 2.6	0.372	0.433
Cu	127	131.9	0.38 - 0.6	0.91	1.137
Zn	103	117.3	11.9 - 15	10.26	10.43
Rb	9.11	8.279	273 - 306.22	278.6	279.3
Sr	396	379.1	16 - 18.21	15.00	15.18
Y	26	23.51	77.986	61.72	63.97
Zr	172	161.9	82.6 - 125.3	85.42	85.37
Nb	18.1	17.47	12 - 18.6	12.87	13.07
Ba	131	122.1	54.9 - 77	54.83	54.89
La	15.2	14.36	15.9 - 25	16.85	16.83
Ce	37.5	35.22	44.6 - 54	41.27	41.59
Pr	5.35	5.051	5.82 - 7	5.270	5.437
Nd	24.5	23.47	23.5 - 29.6	21.78	22.20
Sm	6.07	5.885	6.3 - 9.73	6.827	6.987
Eu	2.07	1.952	0.08 - 0.11	0.085	0.079
Tb	0.92	0.869	1.45 - 2.2	1.394	1.450
Gd	6.24	5.980	7.07 - 10.5	7.747	7.898
Dy	5.31	5.090	10 - 14.7	9.901	10.18
Ho	0.98	0.952	1.47 - 3.22	2.071	2.146
Er	2.54	2.395	4.88 - 9.54	6.483	6.706
Tm	0.33	0.333	0.65 - 1.5	0.968	1.014
Yb	2	1.894	6.7 - 11.4	6.661	6.864
Lu	0.274	0.273	0.92 - 1.96	0.969	1.020
Hf	4.36	4.384	2.51 - 5.885	4.158	4.199
Ta	1.14	1.933	1.9 - 2.63	1.897	2.113
Pb	1.6	1.571	25 - 33.76	28.97	29.03
Th	1.22	1.188	25.8 - 38.41	30.76	30.88
U	0.403	0.429	9.49 - 13.01	10.20	10.15

Table 2: Analyses of the standard BHVO-2 and JG-2 against the internationally accepted values from GeoRem. Analyses that differ from the accepted values of GeoReM are highlighted in yellow. These elements, with the exception of Sr and Zr are not of particular interest in this study and so will not be considered further.

3.4. Radiogenic Isotopes

Radiogenic isotope analysis of the 28 samples selected for trace element analysis was performed using the solutions remaining after final sample dilutions for ICP-MS analysis.

3.4.1. Pb

Pb separation:

The sample solutions remaining after ICP-MS analysis were dried down and 4ml 6.2M HCl added. After drying down, the samples were converted to bromide in 1M HBr. The anion resin used for Pb chemistry is a Bio-Rad anion resin made up from AG1-XB in 6.2M HCl. The columns were initially cleaned with 6M HCl, followed by 1 wash in MilliQ water. Approximately 0.75ml of resin was then added to the columns before preconditioning with 1M HBr and the samples loaded.

The wash solutions were collected in 15ml Teflon beakers for further Sr and Nd chemistry. The columns were washed with 4ml 1M HBr, 0.5ml 2M HCl. The Pb fractions eluted in 4ml 6.2M HCl and collected in clean 7m Teflon beakers. The Pb fractions were dried down on a hotplate at 130°C and converted to nitrate by adding a few drops of concentrated HNO_3. After drying down and cooling, 1ml 2% HNO_3 was pipetted into the beaker and the solution placed in an ultrasonic bath for 30mins, after which it was ready for MC-ICP-MS analysis.

Pb isotope analysis:

Pb isotopes were analysed as 50ppb 2% HNO_3 solutions using a Nu Instruments NuPlasma HR multi-collector inductively coupled plasma mass spectrometer (MC-ICP-MS) and DSN-100 desolvating nebuliser. NIST SRM997 Tl standard was added to all samples and standards to give a ±10:1 Pb: Tl ratio. NIST SRM981 was used as the reference standard with normalising values of 36.7219, 15.4963 and 16.9405 for $^{208}Pb/^{204}Pb$, $^{207}Pb/^{204}Pb$, $^{206}Pb/^{204}Pb$, respectively, after Galer & Abouchami (1998).

All Pb isotope data were corrected for:

1. Hg interference by subtraction of on-peak, gas-blank background measurements
2. instrumental mass fractionation using the exponential law and a $^{205}Tl/^{203}Tl$ value of 2.3889 (Galer & Abouchami, 1998)

Two certified reference materials (CRM) JG-2 and BHVO-2 were analysed along with the samples. The results agree with published values and previous results from this facility, and are given in Tables 4 and 5.

3.4.2. Sr and Nd

Sr and Nd separation:

On analysis of the trace element data it was noted that most of the dyke samples had extremely high Rb/Sr ratios. Rb/Sr ratio that are too large for normal correction of the isobaric interference of ^{87}Rb on ^{87}Sr will remain after routine Sr separation chemistry. This will impact the accuracy of the $^{87}Sr/^{86}Sr$ measurements of these samples, and negatively affect their age

correction and the errorchron. For this reason an extra step was added to the routine chemistry for additional removal of Rb before the usual Sr.Spec/Ln.Spec chemistry of Míková & Denková (2007) to quantitatively remove Rb while retaining Sr.

This step employed large (6.4 mm ID) PFA Teflon columns with a 185mm resin bed and a 125ml column reservoir, filled with pre-cleaned AG50W-X8 100-200mesh cation exchange resin. The columns were calibrated using an incompatible element-rich ocean island basalt sample passed through the column in 2.5M HCl with eluted acid solutions collected every 2-3ml. Elution intervals for Rb, Sr and REE were set so as to maximize recovery of Sr while quantitatively excluding Rb. The Sr and REE fractions were then evaporated to dryness, re-dissolved in 1.5ml of 2M HNO_3, ready for further routine processing following the method of Míková & Denková (2007).

Sr.Spec and Tru.Spec columns were conditioned with 2ml of 2M HNO_3. Sr.Spec columns were placed above the Tru.Spec columns, conditioned with 1ml 2M HNO_3 and the samples loaded. Strontium was retained in the upper column while the REE were retained in the lower, filled with the Tru.Spec resin. The racks were then separated and Sr collected in clean beakers after elution in water. The Sr fractions were dried down and cooled before addition of 2ml 0.2% HNO_3. The solutions were ready for analysis by the MC-ICP-MS after 20mins in the ultrasonic bath.

For Nd elution, Ln.Spec columns were conditioned before placement below the Tru.Spec columns retaining the REE. After washing the Tru.Spec columns with 3ml 0.05M HNO_3, the racks were separated. The Ln.Spec columns were washed with 1ml of HNO_3, followed by 7ml of 0.2M HCl and then washed with another 7ml of 0.2M HCl. After this step, the Nd was eluted with 7ml of 0.2M HCl into clean beakers. The Nd fraction was dried down, converted to nitrate and re-dissolved in 2ml 2% HNO_3. The solutions were ready for analyis on the MC-ICP-MS after 20minutes in the ultrasonic bath.

<u>Sr and Nd analysis:</u>

The samples were analysed for $^{87}Sr/^{86}Sr$ and $^{143}Nd/^{144}Nd$ compositions on a Nu Instruments NuPlasma HR multi-collector inductively coupled plasma mass spectrometer (MC-ICP-MS). The Strontium solutions were introduced using a micro-cyclonic spraychamber , while Nd solutions were introduced by a DSN-100 desolvating nebuliser. Each analysis took 10minutes and standards were run after every fifth sample. The standard used for $^{87}Sr/^{86}Sr$ analysis was NIST987 for which a reference value of 0.710255 was used. For $^{143}Nd/^{144}Nd$ analysis, the standard was JNdi-1 for which a reference value of 0.512115 was used.

All Sr isotope data were corrected for:

1. Rb interference using the measured signal for ^{85}Rb and the natural $^{85}Rb/^{87}Rb$ ratio = 2.593.
2. instrumental mass fractionation using the exponential law and a $^{86}Sr/^{88}Sr$ value of 0.1194

All Nd isotope data were corrected for:

3. Sm and Ce interference using the measured signal for ^{147}Sm and ^{140}Ce, and natural Sm and Ce isotope abundances
4. Instrumental mass fractionation using the exponential law and a $^{146}Nd/^{144}Nd$ value of 0.7219

$^{143}Nd/^{144}Nd$ analysis of BHVO-2 gave 0.512982 ±16 (2S, n=16) within error of the value from Weis et al. (2006) of 0.512984 ±11 and the long term UCT average of 0.512985 ±15 (2S, n=44). $^{143}Nd/^{144}Nd$ analysis of JG-2 gave 0.512243 ±28 (2S, n=16), within error of the range listed on GeoReM: 0.51221-0.51224. $^{87}Sr/^{86}Sr$ measured on BHVO-2 gave an average of 0.703469 (2S, n=17) within the range of Weis et al. (2006) of 0.703479 ±20 and the long term average at UCT of 0.703479 ±22 (2S, n=47)

Sr	ICP-MS	XRF
ST76	3.483	4
ST203	7.324	5
ST212	2.401	2
ST133	125.4	140
ST138	154	159
ST241	501	514
ST264	298.9	316

Table 3: Strontium analysed via XRF and ICP-MS have similar concentrations and the ICP-MS data can be used for further analysis and interpretation.

JG-2	Measured value	Published value (Tanimizu & Ishikawa, 2006)
$^{208}Pb/^{204}Pb$	39.0422 (± 0.0034) 38.9829 (±0.0024)	39.0335
$^{207}Pb/^{204}Pb$	15.6483 (±0.0009) 15.6345 (±0.0008)	15.6470
$^{206}Pb/^{204}Pb$	18.6121 (±0.0010) 18.6050 (±0.0007)	18.6157

Table 4: Measured and published Pb isotope ratios for CRM JG-2 after normalisation of the values from Tanimizu & Ishikawa (2006) to the reference values for NIST SRM981 used in this study.

BHVO-2	Measured value	Published, reference values
$^{208}Pb/^{204}Pb$	38.2355 (± 0.0025) 38.2461 (±0.0026)	38.2367 (± 0.0182); Weis et al, 2006. 37.992-38.294; GEOREM 38.2237 (± 0.0483); Long term UCT (n=11)
$^{207}Pb/^{204}Pb$	15.5428 (±0.0009) 15.5301 (±0.0010)	15.5334 (± 0.0094); Weis et al, 2006. 15.457-15.558; GEOREM 15.5337 (± 0.0139); Long term UCT average (n=11)
$^{206}Pb/^{204}Pb$	18.5896 (±0.0010) 18.6532 (±0.0010)	18.6474 (± 0.0242); Weis et al, 2006. 18.514-18.687; GEOREM 18.6306; Long term UCT average (n=11)

Table 5: Measured and published or reference Pb isotope ratios for CRM BHVO-2

3.5. Stable Isotopes

3.5.1. Oxygen Isotopes

Oxygen isotopes for this study were determined on quartz and aegirine aggregates using the laser fluorination method described by Harris & Vogeli (2010). This method is preferable for analysis of mineral separates. The cleaned, 2-3mg chips were placed in 10 of the 12 sample holes of a nickel sample holder. The remaining two were filled with 2-3mg chips of the internal standard MONGT.

After loading, the Ni sample holder was placed in an oven at 110°C for at least one hour following which the samples were transferred to the reaction chamber. The samples were exposed to two rounds of BrF_5 pre-fluorination. The first, a 30s exposure to 10Kpa BrF_5 (to avoid the formation of any HF that may cloud the BaF2 window), was then pumped out, while the second was left overnight in the sample chamber.

Each sample was reacted in the presence of approximately 10kPa BrF_5 to liberate the oxygen (as O_2 gas). Blanks were run at the start of each day to ensure that all oxygen liberated was from the sample. The blank pressure was typically < 1/200 of the sample volume of a 1 mg sample and thus negligible. The 12 samples thus extracted were analysed off-line.

All O-isotope ratios were measured off-line using a Finnegan DeltaXP mass spectrometer housed in the Department of Archaeology at UCT, in dual inlet mode, and all data are reported in the familiar δ notation, where $\delta^{18}O = (R_{sample}/R_{standard}-1)*1000$; R is the measured $^{18}O/^{16}O$ ratio and SMOW is the standard. Oxygen isotope ratios were measured on O_2 gas and the isotope composition of the O_2 reference gas was determined by converting an aliquot of O_2 to CO_2 using the carbon convertor on the conventional extraction line. This value was used to calculate raw (delta) values of each sample relative to the SMOW scale. MONGT was calibrated against the UWG-2 garnet standard of Valley et al. (1995) using the current laser system and has a $\delta^{18}O$ value of 5.38‰, assuming a δO^{18} value of 5.80 for UWG-2. The $\delta^{18}O$ value of 5.38‰ for MONGT was used to normalise the raw data to the SMOW scale (Harris & Vogeli 2010).

Whole rock $\delta^{18}O$ and $\delta^{18}O$ of mineral separates (feldspar and nepheline) for selected peralkaline granites, nepheline syenites and gneisses from the original study are given in table 4 of Harris & Grantham (1993). Oxygen isotopes ratios were obtained by conventional methods using ClF_3 as an oxidising reagent following the method of Harris & Erlank (1992).

4. Results

A total of 18 dykes were selected for the study of major elements in this thesis. In addition 5 samples for which thin sections and whole rock data were available from the initial study (pre 1993) were added to make a total of 23 dyke samples. Of these a subset of 19 (13 from Group 1 and 6 from Group 2) were chosen for further trace element and radiogenic isotopic analysis. In addition to the dykes, 3 nepheline syenites and 5 country rock gneisses were analysed for trace elements and radiogenic isotopes for later comparison. The nepheline syenites were previously analysed for major elements by Harris and Grantham (1993) while the gneisses were analysed as part of an unpublished honours thesis (Maisela 2012).

4.1. Mineral Chemistry

Pyroxene

A subset of 9 dykes with the most euhedral aegirines were analysed by electron microprobe to determine the composition of the pyroxenes and the unknown zirconium silicates. Recalculation of the pyroxene compositions in *Appendix A* following the method of Droop (1987), shows that all the analysed pyroxenes are sodic and predominantly end-member aegirine except in two samples (ST226 and ST248) where the pyroxene is aegirine-augite.

The ternary diagram shown in Figure 27 highlights that exchange between Na and Ca is the cause of most of the variation in the cation content of the aegirines. There appears to be no systematic variation between the Na content of aegirines from different samples or petrographic groups.

The microprobe data for aegirines from all 9 samples showed a range in Na cations per formula unit (based on 6 oxygens) of 0.745 – 1.039. The aegirines in sample ST226 and ST248 contain the lowest number of Na cations per formula unit (on average 0.791pfu in ST226 and 0.828pfu in ST248) and from the pyroxene calculation (Appendix A) can be seen to be aegirine-augite rather than pure aegirine. An average value for each element in the pyroxenes was calculated to show if there was any inter-element correlation between the samples. Most samples contain similar amounts of Na cations per formula unit with increasing Si^{4+} except for the two samples, ST226 and ST248, already mentioned. These two samples also tend to have a higher proportion of Ca and lower Total Fe than the other samples with ST226 also containing the most Ti^{4+} cations. This agrees well with the petrography and the pyroxene calculation of Droop (1987) that shows these pyroxenes to be aegirine-augite. Sample ST226 is also host to the sodium-titanium silicate, narsarsukite ($Na_2(Ti,Fe^{3+})Si_4(O,F)_{11}$),which may also explain the lower than average Na content of its pyroxenes. In the plots of Figure 29 it can be seen that Na shows an inverse correlation with Ca. Based on the recalculation scheme of Droop (1987) the proportion of Fe^{3+} cations with increasing proportion of Si^{4+} cations in aegirine is on average between 0.9 and 1.1 with two exceptions, ST226 and ST248. This is shown graphically in Figure 29b. This is due to

the 1:1 ratio between Na and Fe^{3+} cations in aegirine and the presence of aegirine-augite in ST226 and ST248. No correlation is visible for Ti^{4+} vs Si^{4+} (Fig.29c) while total Fe vs Ti^{4+} shows an inverse correlation. The aegirine in Sample ST226 has the highest Ti^{4+} which together with the presence of narsarsukite in this sample suggests that the magma from which these dykes crystallised was enriched in Ti^{4+} relative to the other dyke samples but this is not obvious from the major element analysis in Table 10.

It was noted from the petrography that the coarse-grained aegirines showed evidence for at least two episodes of crystallisation. Cores and rims of 3 samples were analysed (ST217, FL1 and STFL1A) to determine if there was any chemical variation between the zones. No systematic difference was observed for the elements analysed as can be seen in Figure 27 and Table 6. Layering was also observed in some samples (Figure 30). In these samples the layering was defined by interstitial aegirine in a granite matrix or phenocrystic aegirine in a granite matrix. The aegirines in the two layers were analysed in ST217. Aegirines that appear as phenocrysts tend to have lower Si^{4+} cation contents than the interstitial aegirines and also have a higher Na^{+} cation content. The variations are quite small though (generally <0.03 formula units) so can be ruled out as showing any meaningful variation.

Amphibole was not analysed under the electron microprobe as no pure amphibole crystals were identified in any of the samples. Amphibole was only seen to exist as intergrowths with aegirine and these intergrowths were observed to only exist as fine-grained minerals that comprised the matrix material as explained in the petrography of Chapter 2.

Unusual Minerals

Eudialyte: Eudialyte was first discovered in 1819 in nepheline syenite of the alkaline Ilimaussaq Complex, Greenland. It forms a complex group of Na-Ca-Zr silicates with 22 mineral species (Rastsvetaeva 2007). The IMA-accepted formula for the eudialyte group is $N_{15}[M(1)]_6[M(2)]_3[M(3)][(M4)]Z_3[Si_{24}O_{72}]O'X_2$ (Johnsen et al. 2003) where:

N = Na, Ca, K, Sr, REE, Ba, Mn, H_3O^+

M(1) = Ca, Mn, REE, Na, Sr, Fe
M(2) = Fe, Mn, Na, Zr, Ta, Ti, K, Ba, H_3O^+
M(3,4) = Si, Nb, Ti, W, Na

Z = Zr, Ti, Nb

O' = O, OH^-, H_2O

X = H_2O, Cl^-, F^-, OH^-, CO_3^{2-}, SO_4^{2-}, SiO_4^{4-}

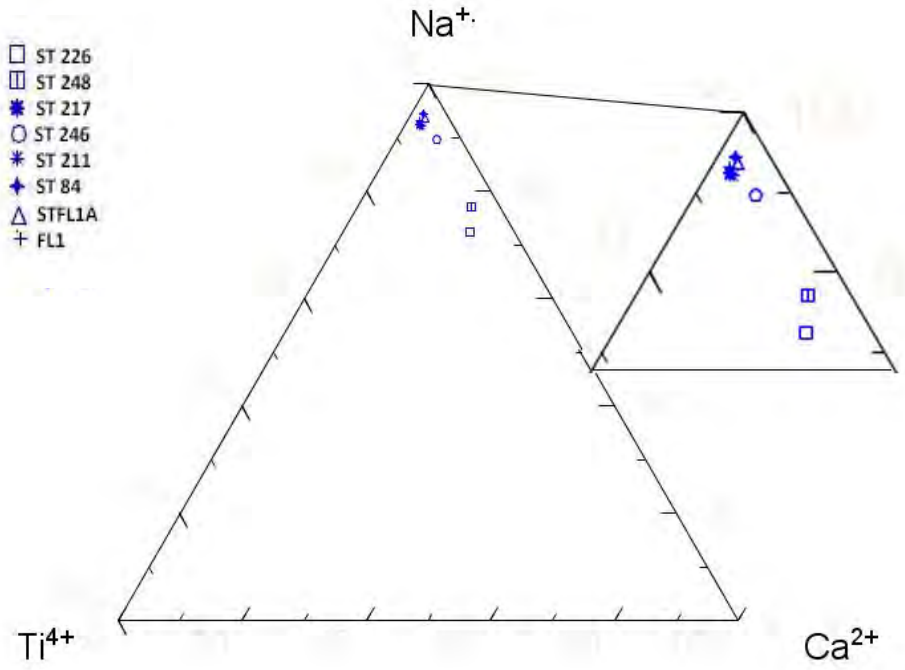

Figure 27: Ternary plot highlighting that most of the variation in major elements of the pyroxenes is as a result of Na^{+}, Ca^{2+} and Ti^{4+} exchange. Each symbol represents the average cation distribution in one sample. The Samples analysed were FL1, FL1A, ST84, ST211, ST217, ST226, ST246 and ST248. The last two, ST 246 and ST248 are from Group 2.

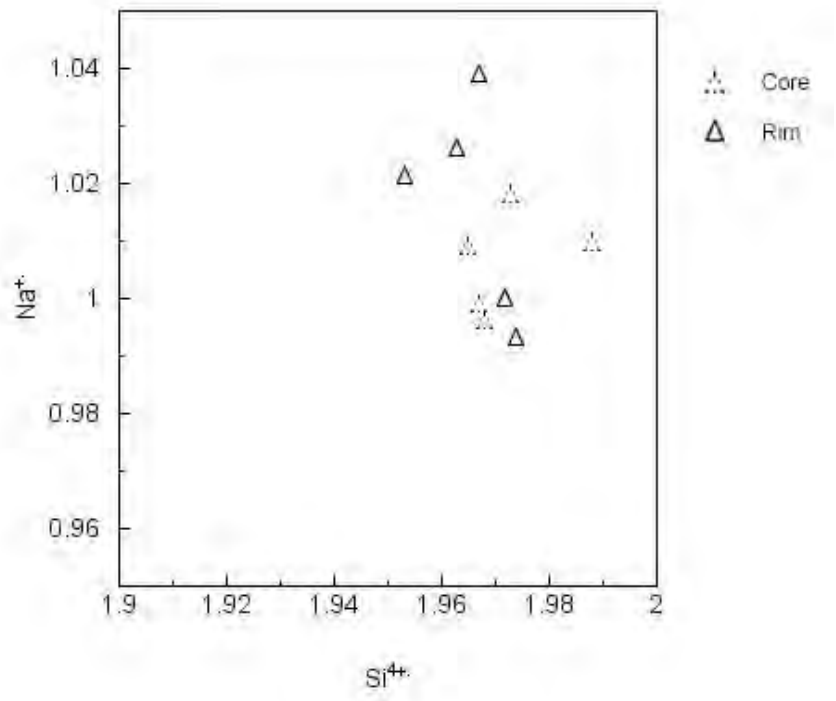

Figure 28: Na^{+} cations in cores (dashed triangles) and rims (solid triangles) of pyroxenes from 3 samples show very little variation in composition.

Eudialyte group minerals (EGM) are common in peralkaline igneous rocks that are silica undersaturated, e.g. syenites (Schilling et al. 2011), and are characteristic minerals of highly evolved, peralkaline mantle –derived magmas (Kogarko et al. 2010). EGM's are rarely found in peralkaline granites except as xenoliths in basaltic lavas at Ascension Island and within peralkaline dykes at Straumsvola (Harris 1983; Harris & Rickard 1987).

A peralkaline granite, ST38, from Straumsvola was collected by Harris and co-workers and found to contain REE-enriched eudialyte. This eudialyte and eudialyte from a peralkaline granite at Ascension Island was analysed by electron microprobe by Schilling et al. (2011). The average major and trace elemental compositions of these minerals and ST84 and ST246 of this study are shown in Table 7. Low totals for eudialyte measured on the electron microprobe at UCT, i.e. samples ST84 and ST246, result from an appropriate standard not being available to analyse the unusual Zr-silicates against. The analysis also included only the major elements unlike the data of Schilling et al. (2011) where trace and REE are included. By comparison with the data from Schilling et al. (2011) it can be seen that eudialytes analysed on the microprobe at UCT have much lower Na than that of ST38, the peralkaline granite from Straumsvola. While this may suggest a problem with the microprobe it is unlikely given the excellent totals calculated on aegirine grains analysed within the same run (Table 6). This suggests that eudialytes, particularly ST84, are low Na eudialyte that likely has its cation sites filled by REE e.g. Ce as seen in eudialyte from ST38 (Harris & Grantham (1993) and Table 7. Si, Mn, Zr and Ca in all Straumsvola samples are however, comparable with one another with Mn and Ca being on average higher in Straumsvola vs Ascension and the reverse for Fe.

Narsarsukite ($Na_2(Ti,Fe^{3+})Si_4(O,F)_{11}$): Narsarsukite is a rare silicate named after the Narsarsuk pegmatite of the Illimassauq Complex (Flink 1899). In samples ST211, ST226 and STFL1A, narsarsukite appears as acicular or blocky crystals in thin section (See Petrography, Ch2). Narsarsukite in ST211 is poikilitic and the most euhedral of all the crystals analysed. From Table 6 it can be seen that it has the highest proportion of Na^+ cations. Narsarsukite in ST226 and STFL1A have very low totals especially for Na, less than half that of ST211. In ST226 the narsarsukite is interstitial and skeletal and so the low totals may be a result of the beam diameter being greater than the narsarsukite phase and possibly also some interaction with the matrix. However in STFL1A the Na total is still low despite the more euhedral crystal shapes in this sample. This is likely due to the volatility of Na under the electron beam at high voltages.

Vlasovite ($Na_2ZrSi_4O_{11}$): Vlasovite is usually a late stage phase in nepheline syenites and syenite pegmatites. It was first discovered in the Lovozero Massif of the Kola Peninsula in Russia (Tikhonenkova & Kazakova 1961). It has however, also been noted in the peralkaline granite xenoliths at Ascension Island in the Atlantic Ocean (Harris 1983). At Straumsvola vlasovite is seen in sample FL1 as an interstitial, anhedral mineral in the groundmass growing near to aegirine (See Petrography, Ch 2). Two analyses were made by electron microprobe. Cation analysis in Table 8 confirms that the unknown mineral analysed by electron microprobe is indeed vlasovite despite the low totals. The poor totals are likely due to the poor crystal shapes

in thin section (e.g. FL1) and the instability of Na under the electron probe at high voltages (e.g. ST226) (Table 8). Vlasovite was also only observed in this one sample however, so there is no other sample to compare it with.

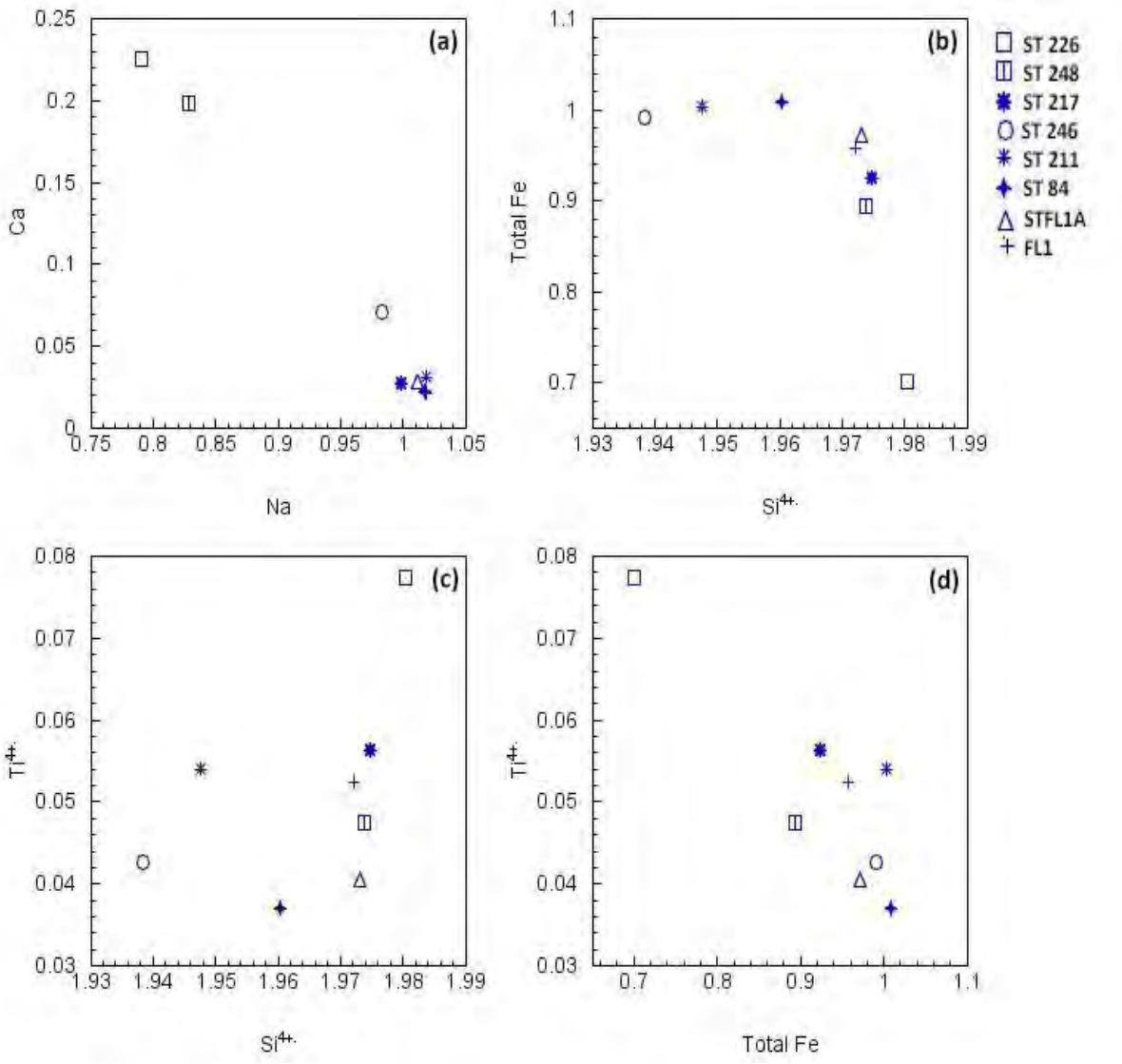

Figure 29: Cations of the major elements in aegirine. a) Ca^{2+} plotted against Na^{+} shows a strongly inverse correlation. b) Total Fe against Si^{4+} is generally constant except in 3 samples, ST 217, ST248 and the most Fe depleted, ST226, the narsarsukite bearing sample. c) There is no clear correlation between Ti^{4+} and Si^{4+} cations while an inverse correlation (d) exists between Ti^{4+} and Total Fe. ST226, ST248, ST217,ST211, ST84, STFL1A and FL1 = Group 1; ST246= Group 2

		SiO_2	TiO_2	Al_2O_3	Cr_2O3	FeO	MnO	MgO	CaO	Na_2O	K_2O	ZrO_2	Total
217	core	53.0	3.15	0.280	0.010	28.6	0.25	-	0.850	13.8	0.01	0.290	100
217	rim	53.0	2.39	0.310	0.020	29.5	0.24	-	0.790	13.8	0.01	0.370	100
217	core	53.0	2.61	0.360	0.030	29.0	0.24	0.00	0.750	13.9	-	0.370	100
217	rim	52.6	2.16	0.280	0.010	29.5	0.25	0.01	0.780	13.8	0.00	0.330	99.6
FL1	core	52.8	0.780	0.390	-	29.6	0.49	0.03	0.360	14.4	0.05	0.090	98.9
FL1	rim	53.4	1.79	0.330	0.030	29.7	0.20	0.02	0.440	14.2	0.01	0.410	101
FL1	core	52.1	3.00	0.290	0.020	28.2	0.19	0.01	0.810	13.8	0.02	0.490	98.9
FL1	rim	52.5	1.66	0.290	-	29.6	0.29	-	0.420	14.1	0.02	0.420	99.3
FL1A	rim	52.8	1.16	0.310	0.010	30.5	0.13	-	0.760	14.2	0.01	0.140	100
FL1A	core	52.4	1.42	0.290	-	28.8	0.31	0.05	0.510	13.7	0.01	0.090	97.5
		Si	Ti	Al	Cr	Fe^{3+}	Fe^{2+}	Mn	Mg	Ca	Na	K	
217	core	1.97	0.067	0.014	0.001	0.913	0.002	0.008	0.000	0.032	0.996	0.000	
217	rim	1.97	0.088	0.012	0.000	0.857	0.033	0.008	0.000	0.034	0.993	0.000	
217	core	1.97	0.061	0.012	0.000	0.932	-0.011	0.008	0.001	0.031	0.999	0.000	
217	rim	1.97	0.073	0.016	0.001	0.894	0.007	0.008	0.000	0.030	1.00	0.000	
FL1	core	1.97	0.085	0.013	0.001	0.897	-0.010	0.006	0.001	0.033	1.01	0.001	
FL1	rim	1.96	0.047	0.013	0.000	0.995	-0.070	0.009	0.000	0.017	1.03	0.001	
FL1	core	1.97	0.050	0.014	0.001	0.957	-0.038	0.006	0.001	0.018	1.02	0.000	
FL1	rim	1.97	0.022	0.017	0.000	1.05	-0.124	0.015	0.002	0.014	1.04	0.002	
FL1A	rim	1.96	0.032	0.014	0.000	1.04	-0.092	0.004	0.000	0.030	1.02	0.000	
FL1A	core	1.99	0.040	0.013	0.000	0.940	-0.025	0.010	0.003	0.021	1.01	0.000	

Table 6: Core and rim analyses of aegirine in 3 dyke samples shows no systematic variation when measured in either wt.% (top) or as cation proportions (bottom). Fe^{2+}/Fe^{3+} proportions calculated using the method of Droop (1987).

Sample		SiO_2	Na_2O	CaO	Al_2O_3	K_2O	FeO	MnO	ZrO_2	TiO_2	Cr_2O_3	MgO	Cl	HfO_2	Nb_2O_5	Nd_2O_3	Ce_2O_3	Y_2O_3	La_2O_3	SrO	Total
ST84	eud1	47.1	2.63	5.61	b.d.l.	0.245	1.06	8.44	9.59	0.172	b.d.l.	b.d.l.	N/A	N/A	N/A	N/A	N/A	N/A	N/A	N/A	74.8
ST84	eud1	45.8	3.92	5.79	0.02	0.262	0.98	8.71	9.58	0.164	b.d.l.	0.01	N/A	N/A	N/A	N/A	N/A	N/A	N/A	N/A	75.2
ST84	eud2	44.6	4.74	5.86	b.d.l.	0.336	0.78	9.08	9.17	0.182	0.06	b.d.l.	N/A	N/A	N/A	N/A	N/A	N/A	N/A	N/A	74.8
ST84	eud2	44.4	7.26	5.69	0.02	0.290	0.88	8.79	8.57	0.193	0.01	0.01	N/A	N/A	N/A	N/A	N/A	N/A	N/A	N/A	76.1
ST84	eud3	49.2	2.13	5.33	b.d.l.	0.211	1.29	7.93	9.43	0.181	0.03	b.d.l.	N/A	N/A	N/A	N/A	N/A	N/A	N/A	N/A	75.7
ST246	eud1	43.3	10.70	7.26	b.d.l.	0.181	2.61	6.44	7.48	0.726	0.02	0.01	N/A	N/A	N/A	N/A	N/A	N/A	N/A	N/A	78.7
ST246	eud1	47.5	10.23	7.27	b.d.l.	0.327	2.97	5.44	8.98	0.663	b.d.l.	b.d.l.	N/A	N/A	N/A	N/A	N/A	N/A	N/A	N/A	83.4
ST38	Eud	46.0	13.2	5.25	0.02	0.253	0.79	8.43	9.34	0.176	N/A	N/A	0.735	0.206	3.41	1.26	3.89	1.17	1.98	0.133	96.2
H30(1)	Eud	45.1	14.1	3.39	0.00	0.460	4.75	2.65	10.1	0.572	N/A	N/A	1.89	0.256	1.77	1.14	2.22	4.66	0.875	b.d.l.	94.0
	cations p.f.u based on 72 oxygens																				
		Si	**Na**	**Ca**	**Al**	**K**	**Fe**	**Mn**	**Zr**	**Ti**	**Cr**	**Mg**	**Cl**	**Hf**	**Nb**	**Nd**	**Ce**	**Y**	**La**	**Sr**	
ST84	eud1	28.1	3.05	3.59	0.00	0.187	0.53	4.27	2.79	0.077	0.00	0.00	N/A	N/A	N/A	N/A	N/A	N/A	N/A	N/A	
ST84	eud1	27.6	4.57	3.73	0.01	0.201	0.49	4.44	2.81	0.074	0.00	0.01	N/A	N/A	N/A	N/A	N/A	N/A	N/A	N/A	
ST84	eud2	27.2	5.61	3.83	0.00	0.262	0.40	4.69	2.73	0.084	0.03	0.00	N/A	N/A	N/A	N/A	N/A	N/A	N/A	N/A	
ST84	eud2	26.9	8.52	3.69	0.02	0.224	0.45	4.51	2.53	0.088	0.01	0.01	N/A	N/A	N/A	N/A	N/A	N/A	N/A	N/A	
ST84	eud3	28.7	2.41	3.33	0.00	0.156	0.63	3.91	2.68	0.079	0.01	0.00	N/A	N/A	N/A	N/A	N/A	N/A	N/A	N/A	
ST246	eud1	25.8	12.4	4.63	0.00	0.137	1.30	3.25	2.17	0.321	0.01	0.01	N/A	N/A	N/A	N/A	N/A	N/A	N/A	N/A	
ST246	eud1	26.4	11.0	4.32	0.00	0.231	1.38	2.56	2.43	0.277	0.00	0.00	N/A	N/A	N/A	N/A	N/A	N/A	N/A	N/A	
ST38	eud	25.5	14.2	3.12	0.01	0.179	0.368	3.96	2.53	0.073	N/A	N/A	0.691	0.033	0.855	0.250	0.791	0.346	0.406	0.040	
H30(1)	eud	25.5	15.5	2.05	b.d.l	0.332	2.25	1.27	2.77	0.243	N/A	N/A	1.809	0.041	0.453	0.232	0.461	1.403	0.183	b.d.l	

Table 7: Electron microprobe data showing cation proportions for eudialytes (eud) in ST84 and ST246(this study) and ST38 and H30-(1) from Straumsvola and Ascension Island, respectively (Schilling et al. 2011). Low totals for ST 84 and ST246 are observed due to an appropriate standard not being available for these unusual Zr-silicates. The average of 4 analyses for samples ST38 and H3O-(1) was used in this study.

	Narsarsukite						Vlasovite	
	ST211	**ST211**	**ST226**	**ST226**	**ST226**	**FL1A**	**FL1**	**FL1**
SiO_2	69.5	69.6	66.6	65.2	65.9	64.3	52.8	54.1
TiO_2	12.8	12.9	14.3	15.1	14.4	12.2	0.167	0.030
Al_2O_3	0.608	0.618	0.307	0.253	0.265	0.712	0.00	0.23
Cr_2O_3	-	-	-	0.00	0.01	-	0.00	0.01
FeO	4.59	4.13	3.64	2.92	3.06	4.85	0.03	0.04
MnO	0.123	0.042	0.077	0.064	0.051	0.255	0.034	0.00
MgO	-	-	0.130	0.172	0.173	0.002	0.00	0.00
CaO	0.015	0.016	0.009	0.00	0.01	0.026	0.016	0.013
Na_2O	13.2	13.0	4.81	5.36	5.46	5.50	9.00	10.1
K_2O	0.045	0.016	0.063	0.083	0.111	0.084	0.034	0.00
ZrO_2	0.616	0.776	0.110	0.410	0.447	1.31	26.2	27.0
Total	102	101	90.1	89.6	89.9	89.2	88.3	91.5
cations	based on 11 (O)							
Si	4.34	4.35	4.49	4.44	4.47	4.48	4.14	4.11
Ti	0.603	0.607	0.726	0.773	0.736	0.638	0.010	0.002
Al	0.045	0.046	0.024	0.020	0.021	0.058	0.000	0.021
Cr	0.000	0.000	0.000	0.000	0.000	0.000	0.000	0.001
Fe2+	0.240	0.216	0.205	0.166	0.173	0.283	0.002	0.003
Mn	0.006	0.002	0.004	0.004	0.003	0.015	0.002	0.000
Mg	0.000	0.000	0.013	0.017	0.017	0.000	0.000	0.000
Ca	0.001	0.001	0.001	0.000	0.000	0.002	0.001	0.001
Na	1.596	1.581	0.628	0.708	0.718	0.743	1.37	1.49
K	0.004	0.002	0.005	0.007	0.010	0.007	0.003	0.000
Zr	0.000	0.000	0.000	0.000	0.000	0.000	1.00	1.000
Total	6.83	6.81	6.09	6.13	6.15	6.23	6.53	6.63

Table 8: Electron microprobe analysis and cation proportions of two unusual silicates, narsarsukite ($Na_2(Ti,Fe^{3+})Si_4(O,F)_{11}$ and vlasovite ($Na_2ZrSi_4O_{11}$). Low totals are observed for most of the analyses and is likely due to interference with the matrix and the volatility of Na under the electron microprobe beam at high voltages.

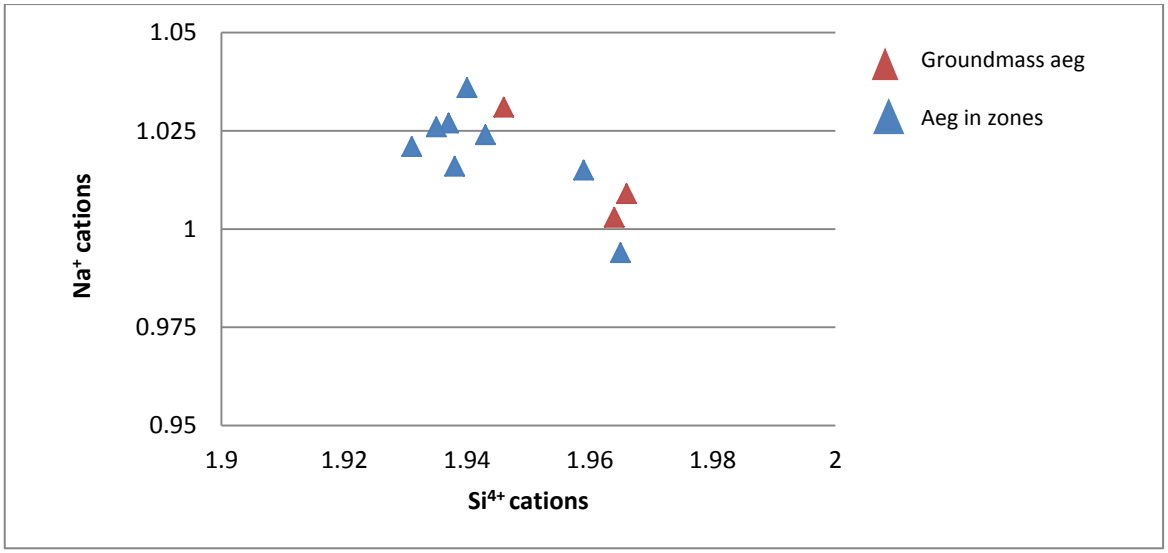

Figure 30: In thin section two types of aegirine are observed in ST211. Matrix aegirine (Groundmass aeg) that usually defines the layering AND euhedral aegirine phenocrysts that form isolated zones(Aeg in zones) are clearly visible. From the Na+ vs Si^{4+} cation content it can be seen that on average the aegirines in pods have higher Na+ and lower Si^{4+}content than the aegirines in the groundmass. However, the number of analyses (n= 11) and the variation was very small and is unlikely to be meaningful.

4.2 Major element geochemistry

Dykes:

All Group 1 samples have a SiO_2 content > 70 % with the exception of 3 samples, ST 226, ST88 and ST217, SiO_2= 68.41, 66.20 and 65.30 respectively (Table 9). These samples however appear to have experienced some fluid alteration as seen by the seritized feldspars and resorbed aegirines in thin section (ST217 and ST88). ST226 also has an unusual mineralogy and shows signs of aegirine replacement to amphibole. Group 2 samples show a range in SiO_2 from 67.99 to 74.69, overlapping that of Group 1.

Figure 31 shows that the dykes all plot in the top right-hand corner of the diagram and fall within two fields with increasing SiO_2: trachyte (syenite) and rhyolite (granite). Major elements as determined by XRF are shown in Table 10 with the Peralkalinity Index (PI) (Molecular ($Na_2O + K_2O$) /Al_2O_3) for each sample. PI for all dyke samples is>1 further illustrating the peralkalinity of all the dykes.

The analysed dykes are also all silica-oversaturated and peralkaline with *acmite* and *sodium metasilicate (ns)* in the norm (Table 9). The normative mineralogy of all the samples in the study is compared with SiO_2 in Figure 63 of the Discussion.

	Range	Average (wt.%)
SiO_2 (wt. %)	64.70 - 75.92	71.05
***acmite* (norm)**	1.91 - 9.32	6.68
***ns* (norm)**	0.59 - 2.7	1.69
if all Fe as Fe3+	0- 1.53	
if all Fe as Fe2+	1.67- 4.69	

Table 9: SiO_2 content and peralkalinity of the analysed dykes according to the CIPW Norm. It should be noted that regardless of the valence state of Fe (i.e. whether all as Fe^{3+} or Fe^{2+} or a mixture), the dykes are usually peralkaline with *ns (sodium metasilicate)* in the norm. Only when Total Fe contains only Fe^{3+} cations and the proportion of acmite in the norm is >9 wt.%, does the proportion of sodium metasilicate equal zero.

Major elements vs SiO_2 for the suite of dykes is shown in Figures 32 and 33. Most of the elements show a strongly negative correlation with SiO_2. SiO_2 vs Na_2O+K_2O shows this well with a Pearson's r value = - 0.92. In general it can be seen that Group 2 samples have lower total alkalis than Group 1 (Figure 32). No distinction between the petrographic groups is visible in any of the plots in Figure 32 and 33 but three Group 1 outliers (ST88, ST217 and ST226) are easily visible at the low silica end as the black dots with the highest total alkali content. Samples ST217 and ST226 were previously analysed via electron microprobe. ST217 contains matrix aegirine and aegirine phenocrysts that have undergone minor replacement to amphibole while ST226 has skeletal aegirine/amphibole and also contains narsarsukite. ST88 has aegirines that have been totally replaced by a Ca-rich amphibole (Richterite/Pargasite). This suggests that these outliers are formed as a result of alteration and/or aegirine replacement to amphibole. SiO_2 is negatively correlated with Na_2O, r= -0.94 while for K_2O the relationship is not very well defined with r= 0.52.

Al_2O_3 and Fe_2O_3 (total) show similar negative correlations with SiO_2, r = -0.84 and r= -0.48 respectively in Figure 32. For Fe_2O_3 vs SiO_2 two Group 1 outliers, ST88 and ST226, have lower Fe_2O_3 than the rest of the samples. As previously mentioned these samples show evidence for replacement of aegirine to amphibole. In general CaO decreases with increasing SiO_2 (r= -0.53). With the exception of the regular outliers (ST88, -216 and -217), SiO_2 decreases with increasing TiO_2 (Figure 33); the correlation co-efficient increasing from -0.43 to -0.79 when these outliers are removed. Group 2 samples have higher TiO_2 concentrations than Group 1 and also form a petrographic trend from high TiO_2, Group 2 to low TiO_2, Group 1. P_2O_5 is also present but in very low abundance (typically <0.1 wt%) and appears to be constant with increasing SiO_2 regardless of the group (r=-0.6). MnO also shows a slightly inverse correlation with SiO_2, r= -0.58 after the two low SiO_2 outliers are removed (previously r=- 0.36). Loss on Ignition(LOI) is generally below 0.5wt% indicating that these samples were not affected by hydrothermal alteration. However,

the Group 2 samples (open circles) do on average have higher LOI than the Group 1 suggesting that if the samples experienced fluid alteration it had a greater effect on the Group 2 samples.

Overall the data show an increase in SiO_2 from Group 2 to Group 1. Based on the major elements vs. SiO_2 the two petrographic groups do not appear to form separate groupings but are continuous from low SiO_2 to high SiO_2 hence no further comparison with petrographic groupings will be made. The Group 1 outliers (ST88, ST216 and ST217) are easily visible at the low SiO_2 end of the Al_2O_3, Fe_2O_3 and CaO plots in Figures 32 and 33.

Nepheline Syenite:

Table 11 shows the major element geochemistry of a nepheline syenite collected from each of the zones identified by Harris & Grantham (1993) at Straumsvola and surrounding nunataks i.e. massive outer zone, layered inner zone and mafic zone. SiO_2 and K_2O appear to decrease from the outer zone inwards, while CaO and MgO show the reverse relationship. Since only one sample has been analysed from each rock type, no further observations will be discussed here.

Gneiss:

The gneisses were selected based on their proximity to the contact zone with the nepheline syenite at Straumsvola. With the exception of ST181, the only gneiss not from Straumsvola, there appears to be a decrease in SiO_2, MgO and CaO with increasing distance from the contact zone. ST181 and ST 241 have the highest Na_2O concentrations, which is in agreement with them representing the most fenitised samples.

4.3 Trace elements

Trace element data for the samples of this study are shown in Table 12. Trace elements will be used in this study to determine any fractionation trends are evident in the suite of dykes. Incompatible element ratios are also useful in identifying fractionation trends in evolved magmas especially where linear trends are evident. Plots of selected trace elements vs SiO_2 and inter-trace element variations (e.g. Zr) for the 19 dykes in the study are shown in Figure 34 and 35. Most of the correlations are not well defined except where zirconium is plotted against Nb or Y. The diagrams show graphically the large difference in concentration of Rb and Sr, and of Rb/Sr, which is an important consideration for the determination of the radiogenic isotopes (see Chapter 3, Methods).

Rb concentration remains relatively constant with increasing SiO_2 ($r= 0.28$) (Figure 34b). The samples all have high Rb contents (>200 ppm) except for two samples, ST38 and ST226 which have Rb concentrations <150 ppm. There appears to be a negative correlation between Sr and SiO_2, $r= -0.63$ but the samples form two groups, one at low Sr and another at high Sr rather than a strong trend (Figure 34c). Generally the samples have very low Sr concentrations (<140

ppm) with the majority below 50ppm. The three samples that have Sr concentrations >100 ppm are all group 2 quartz syenites (ST113, ST246 and ST268).

Sample	FL 1	ST 75	ST FL1B	ST 228	ST FL1A	FL 2	ST 211	ST 84	ST 147	ST 203	ST 113	ST 246	ST 226	ST 268	ST 88	ST 217	ST 216	*ST 76*	*ST 38*	*ST 60*	*ST 144*
Group	**1**	**1**	**1**	**1**	**1**	**1**	**1**	**1**	**1**	**2**	**2**	**2**	**2**	**2**	**2**	**2**	**2**	***2***	***1***	***2***	***2***
	Vlas.		Nars.		Nars	Vlas.		Eud.					Nars					*Nars.*	*Eud*		
SiO_2	75.02	74.48	74.39	74.34	73.60	73.50	72.09	71.22	70.64	71.87	69.75	68.04	67.99	67.65	65.91	65.01	64.25	*74.69*	*71.85*	*69.63*	*67.99*
TiO_2	0.16	0.18	0.13	0.17	0.13	0.16	0.21	0.16	0.17	0.25	0.33	0.30	0.10	0.29	0.08	0.33	0.27	*0.19*	*0.21*	*0.19*	*0.27*
Al_2O_3	11.26	11.08	11.46	11.04	11.47	11.07	11.37	12.09	11.56	11.77	12.11	12.61	16.65	12.40	16.15	14.88	14.98	*11.44*	*12.28*	*13.98*	*13.78*
Fe_2O_3	3.09	3.69	3.24	3.48	3.29	3.73	4.63	4.62	5.05	4.73	5.74	5.49	1.24	5.52	3.62	5.52	6.06	*3.57*	*4.65*	*4.61*	*5.01*
MnO	0.04	0.07	0.02	0.10	0.02	0.04	0.13	0.07	0.17	0.13	0.07	0.19	0.02	0.20	0.03	0.12	0.14	*0.09*	*0.06*	*0.13*	*0.09*
MgO	0.06	0.03	0.05	0.03	0.07	0.04	0.04	0.10	0.05	0.06	0.04	0.03	0.07	0.00	0.03	0.07	0.02	*0.01*	*0.00*	*0.03*	*0.04*
CaO	0.32	0.08	0.26	0.05	0.25	0.37	0.38	0.38	0.39	0.32	0.09	1.14	0.22	1.44	0.46	0.55	0.65	*0.22*	*0.46*	*0.43*	*0.62*
Na2O	5.04	5.51	5.13	5.47	5.77	5.52	5.67	6.85	6.59	5.47	6.13	6.72	6.96	6.73	7.42	7.74	7.75	*5.45*	*6.02*	*6.36*	*7.53*
K2O	4.61	4.25	4.64	4.55	4.95	4.67	4.57	3.76	4.25	4.49	5.01	4.82	6.09	4.72	5.83	5.13	4.90	*4.34*	*4.46*	*4.64*	*4.66*
P_2O_5	0.04	0.04	0.04	0.05	0.04	0.04	0.05	0.04	0.04	0.05	0.06	0.06	0.04	0.06	0.04	0.21	0.27	*0.00*	*0.00*	*0.00*	*0.01*
SO_3	0.01	0.02	0.01	0.02	0.02	0.02	0.02	0.00	0.02	0.01	0.01	0.01	0.00	0.01	0.02	0.00	0.02				
Cr_2O_3	0.00	0.00	0.00	0.00	0.00	0.00	0.00	0.00	0.00	0.00	0.00	0.00	0.00	0.00	0.01	0.00	0.00				
NiO	0.01	0.01	0.01	0.01	0.01	0.01	0.01	0.01	0.01	0.01	0.03	0.01	0.01	0.01	0.01	0.01	0.01				
H_2O-	0.03	0.04	0.03	0.03	0.04	0.05	0.04	0.04	0.02	0.06	0.13	0.09	0.05	0.06	0.04	0.06	0.12				
LOI	0.18	0.06	0.10	0.06	0.10	0.14	0.16	0.17	0.16	0.19	0.27	0.38	0.10	0.43	0.07	0.12	0.31				
Total	99.87	99.55	99.51	99.39	99.76	99.35	99.37	99.51	99.13	99.41	99.77	99.89	99.55	99.52	99.71	99.74	99.77	*100.00*	*99.99*	*100.00*	*100.00*
P.I.	1.18	1.23	1.17	1.26	1.3	1.28	1.26	1.17	1.34	1.18	1.28	1.29	1.08	1.31	1.15	1.23	1.21	1.19	1.2	1.11	1.26

Table 10: Major elements(wt.%) of the dykes analysed by XRF .The samples in italics were analysed prior to this study by Harris & Grantham (1993). The blank cells therefore represent elements that were not analysed in the original study. All analyses conducted at the University of Cape Town. Group refers to petrographic Groups 1 and 2 as identified in Chapter 2. Also shown are the samples the unusual minerals: vlas (ovite); nars(arsukite) and eud(dalyite) occur in. P.I. = Peralkalinity Index: If [molecular(Na+K)/molecular Al] >1, the dyke is peralkaline. LOI: Loss On Ignition.

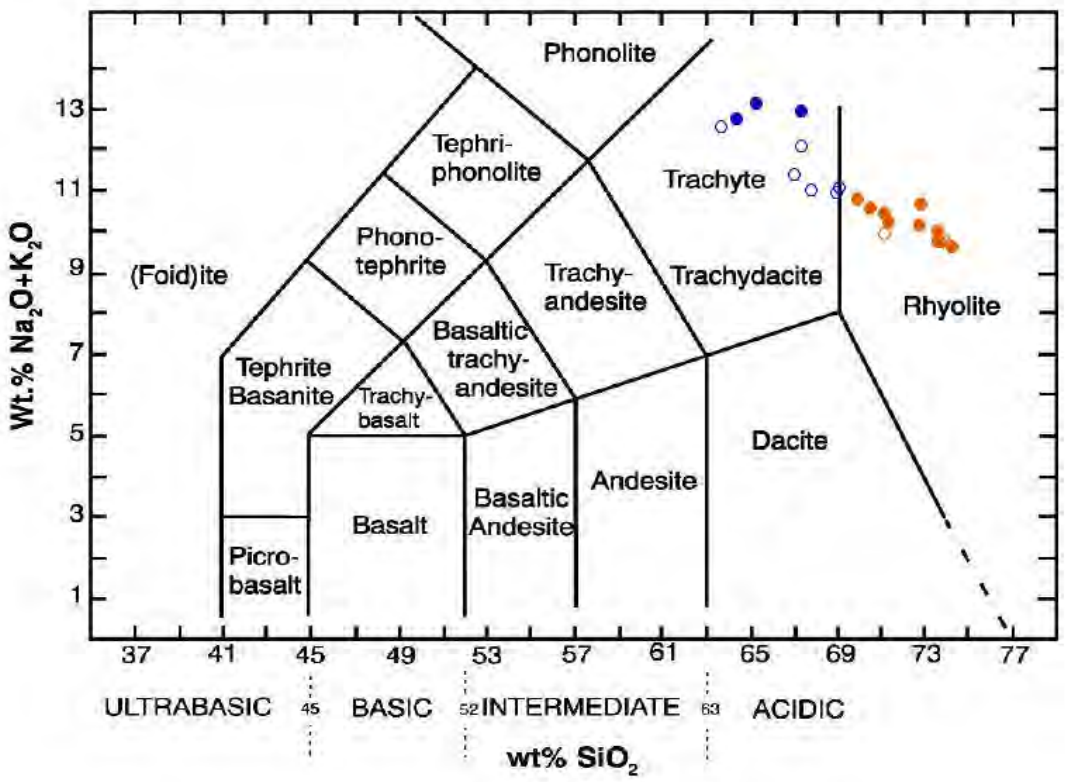

Figure 31: Total-Alkali-Silica diagram showing the major petrographic groups; Group 1= filled circles and Group2 = unfilled circles. Diagram also shows that the dykes range from trachyte(blue)/syenite to rhyolite(orange)/granite after the classification scheme of (Le Maitre 2002).

Sample	ST 71	ST 133	ST 138	ST 181	ST 241	ST 242	ST 264	ST 254
Locality	Storjeon	Straumsvola	Straumsvola	Joungane	Straumsvola	Straumsvola	Straumsvola	Straumsvola
SiO_2	58.01	51.59	47.32	70.72	54.22	56.32	69.65	75.97
TiO_2	0.50	0.26	1.01	0.26	0.86	0.81	0.5	0.2
Al_2O_3	20.83	19.64	13.66	14.69	14.6	18.23	15.42	13.67
Fe_2O_3	4.15	7.86	11.76	2.04	10.47	8.95	3.68	1.67
MnO	0.16	0.33	0.42	0.04	0.17	0.15	0.04	0.01
MgO	0.67	1.01	8.01	0.80	5.85	3.48	1.17	0.56
CaO	1.18	3.75	6.99	2.66	7.78	6.92	3.71	1.61
Na_2O	7.84	11.08	7.11	7.49	5.7	3.72	4.68	5.86
K_2O	6.47	4.26	3.43	1.18	1.23	1.97	1.37	0.57
P_2O_5	0.20	0.22	0.30	0.12	0.17	0.36	0.14	0.05
Total	100.01	100.00	100.01	100.00	101.05	100.91	100.36	100.17

Table 11: Major element geochemistry of the nepheline syenites and gneisses used in this study. Nepheline syenites: ST 71 - Storgeon, outer zone nepheline syenite; ST 133 - Straumsvola, layered zone nepheline syenite; ST 138- Straumsvola, mafic marker. Gneiss: ST 181 – Joungane, fenitised gneiss; ST 241 – Straumsvola, fenitised gneiss at the contact with nepheline syenite; ST 242 – Straumsvola, gneiss 7m from contact zone; ST264 – Straumsvola, fenitised gneiss 400m from contact zone; ST254 – Straumsvola, gneiss 2000m from contact

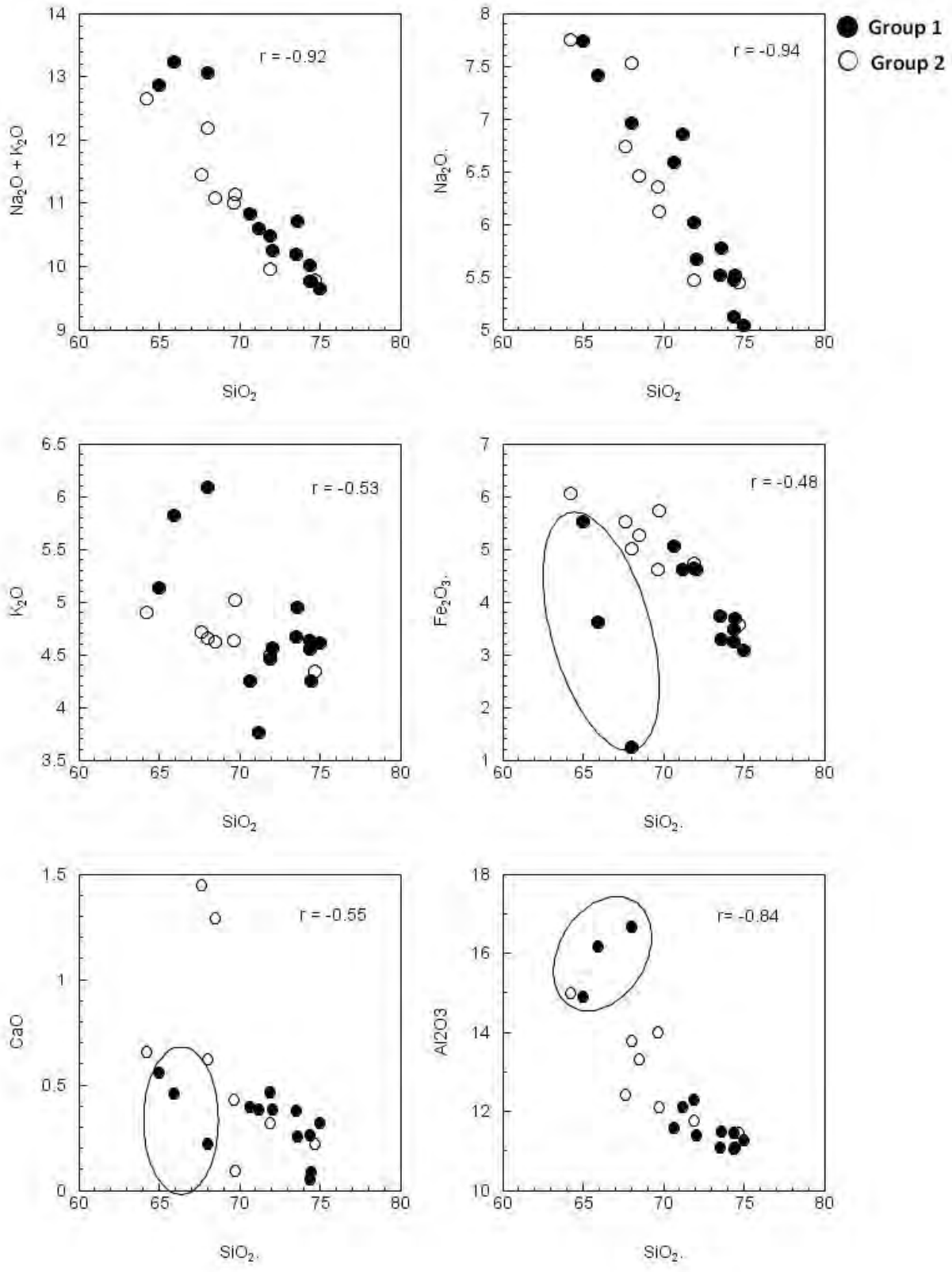

Figure 32: Major elements vs SiO_2 (wt.%). Correlation co-efficients are shown in the top right corner. The three Group 1 outliers, ST88, ST217 and ST226, are outlined in the black ellipses (see text).

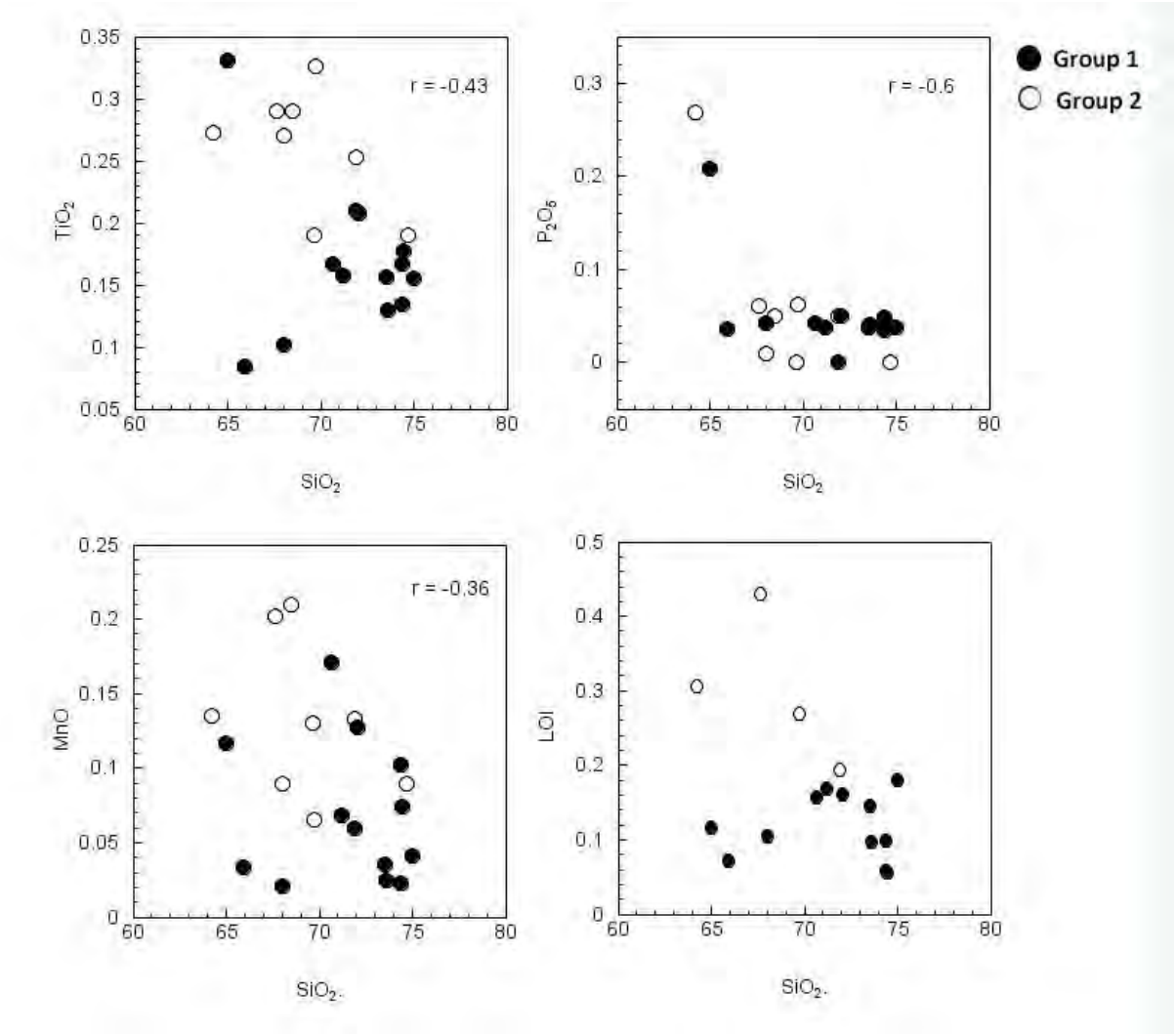

Figure 33: Major elements (wt%) and Loss on Ignition (LOI) vs SiO_2. Correlation co-efficients are shown in the top right corner.

Zr plotted against SiO_2 also shows a poor correlation (r= 0.36) but a range in concentration from <100 ppm to >1000 ppm (Figure 34d). There is no correlation with the petrographic groupings, despite Group 1 samples having a higher proportion of minerals with Zr-silicates. Y shows a very poor correlation with SiO_2, r= 0.13 (Figure 34e), with Group 1 samples on average having higher Y concentrations than Group 2. It also shows a wide range in concentration from 0-200 ppm. Nb also shows a poor correlation with increasing SiO_2, r= -0.02. There does appear to be a difference in concentration between the two petrographic groups however, with Group 2 samples having higher Nb concentrations than Group 1 i.e. Nb >110 ppm except for one Group 1 sample. Li ranges from 0 to 150 ppm with most of the samples falling below 50ppm. There is no significant correlation (r=-0.29) and no difference between the two groups. Zn displays a wide range in concentration with increasing SiO_2 from 45 ppm up to 300 ppm with a weakly negative correlation, r=-0.22 (Figure 35a).

Inter-element ratios e.g. between Sr and Rb show a very poor correlation, r= -0.04 (Figure 35b). Three Group 2 samples (ST113, ST246 and ST268) show higher than average Sr concentrations. The high Sr concentration may be the result of a Sr-enriched alteration fluid, which is supported by the presence of seritised feldspars in two samples, ST113 and ST246. In addition these samples all have higher than average CaO concentrations. Sr might then be substituting for Ca in these samples. Nb and Y, two incompatible trace elements were plotted and compared with Zr to determine if they behave similarly with evolution of the dyke suite (Figure 35e, f). A positive trend is observed for both Nb/Zr and Y/Zr with correlation co-efficients of 0.68 and 0.69, respectively. From the plots it can be seen that at low values, the elements behave almost linearly suggesting a fractional crystallisation trend but as Zr content increases to >1000ppm the pattern becomes slightly parabolic to higher Nb and Y. Two outliers ST203 and ST38 are observed at the high Zr end (Zr~1300 ppm) and two at the low Zr end, ST113 and ST216. ST38 is a Group 1 sample that contains eudialyte and explains the high Zr content. ST203 is a group 2 sample that has no phenocryst phases. This suggests this sample crystallised from a Zr-enriched magma. ST113 and ST216 have been outliers in previous plots (see above) and so can be ignored. With the outliers removed, the correlation between the variables becomes almost linear with r = 0.88 for Nb/Zr and r =0.94 for Y/Zr. Rb plotted against Zr also shows little correlation. There does appear to be a petrographic grouping of Group2 samples at the high Zr end and Group1 at the low Zr end (Figure 35c-e).

Overall, Rb concentration in the dykes ranges from 120 ppm to 304 ppm. The nepheline syenites have a range of 176-190 ppm and the gneisses have Rb concentrations from 19-51 ppm. Rb concentration is therefore highest in the dykes and lowest in the gneisses. The nepheline syenites and gneisses show a wide range in Sr concentration that is in general higher than the dykes and shows the reverse pattern to Rb, being lowest in the dykes and highest in the gneiss. A plot of Rb vs Sr in 34a shows this relationship quite clearly with the dykes generally falling at low Rb concentration and the gneisses and syenites at high Rb and moderate Sr concentrations.

	Li	Ni	Cu	Zn	Rb	Sr	Rb/Sr	Y	Zr	Nb	Zr/Nb	Ba	La	Ce	Ce/Y	Pr
Dykes																
ST75	11.8	3.48	4.00	167	268	6.90	38.8	59.4	778	96.0	8.10	5.04	111	230	3.87	24.7
ST84	4.80	1.34	4.01	158	267	25.5	10.5	13.7	291	31.4	9.26	2.15	20.3	38.8	2.83	4.35
ST88	2.00	0.93	2.63	46	230	6.34	36.2	2.60	129	7.13	18.11	10.6	5.90	11.7	4.52	1.31
ST113	11.2	3.33	6.39	136	211	11.9	17.7	62.2	634	288	2.20	106	25.3	91.7	1.48	6.59
ST147	69.6	1.55	2.96	262	270	8.32	32.5	42.4	234	38.0	6.16	3.84	64.9	110	2.59	11.9
ST203	66.1	2.09	3.61	238	304	7.32	41.5	89.7	1296	208	6.23	28.0	206	376	4.19	43.1
ST211	117	1.29	3.60	278	294	7.31	40.2	137	908	194	4.68	6.16	184	376	2.74	39.4
ST216	143	0.75	2.83	305	274	129	2.12	30.0	304	135	2.25	24.3	188	347	11.6	35.2
ST217	31.3	0.60	3.30	222	291	53.7	5.42	34.6	410	73.5	5.58	18.9	105	206	5.94	23.5
ST226	3.00	3.36	4.88	50	120	7.27	16.5	3.1	70.7	21.3	3.32	28.0	5.93	11.8	3.79	1.20
ST246	17.0	0.67	2.39	238	221	101	2.19	153	922	172	5.38	26.4	826	1583	10.4	164
ST268	18.7	0.54	3.44	231	233	105	2.23	91.7	863	173	5.01	16.5	319	530	5.78	51.7
FL1	3.00	1.32	2.21	93.0	286	17.4	16.5	39.8	663	105	6.33	5.12	54.2	119	3.00	13.7
FL2	2.60	3.36	4.53	79.5	251	13.5	18.6	14.3	242	7.05	34.38	2.05	11.0	21.0	1.47	3.15
STFL1A	2.20	2.90	2.98	54	266	11.2	23.8	9.82	188	12.4	15.17	2.70	11.0	23.1	2.35	3.01
STFL1B	2.10	< d.l.	2.51	52.7	267	11.6	23.0	8.90	198	9.41	21.07	1.87	8.46	17.6	1.97	2.30
ST212	76.4	< d.l.	1.82	220	304	2.40	126	76.4	1020	133.8	7.62	3.46	110	227	2.97	25.6
ST76	76.8	< d.l.	2.28	221	301	3.48	86.5	97.1	996	101.2	9.84	3.37	134	268	2.75	30.2
ST228	17.9	2.13	2.74	232	276	4.41	62.7	52.5	821	120	6.84	4.32	108	252	4.81	23.8
Gneiss																
ST264	43.8	2.54	12.4	42.9	33.9	299	0.11	13.0	16.8	10.1	1.66	330	31.9	61.2	4.69	6.69
ST254	11.0	8.61	23.2	16.5	18.8	506	0.04	11.5	56.5	9.50	5.95	121	39.7	79.0	6.88	8.35
ST241	4.64	66.6	38.9	88.0	34.3	501	0.07	19.2	28.4	10.5	2.71	514	20.1	40.8	2.12	4.81
ST242	41.1	< d.l.	27.8	82.9	50.8	991	0.05	15.6	10.9	9.76	1.11	795	35.3	64.9	4.17	7.16
ST181	6.76	1.02	6.12	44.6	27.6	617	0.04	10.3	86.0	12.8	6.72	402	39.3	74.3	7.20	8.02
Nepheline Syenite																
ST71	17.2	< d.l.	7.39	80.1	195	479	0.41	12.6	153	59.6	2.57	638	50.2	95.8	7.58	10.1
ST133	27.2	< d.l.	4.07	115	176	125	1.40	23.6	697	114	6.13	47.5	69.5	149	6.30	15.5
ST138	36.2	< d.l.	9.06	314	190	154	1.23	21.5	793	156	5.10	30.6	94.7	205	9.56	22.7

Table 12a: Trace element concentrations of the dyke samples and a subset of nepheline syenite and country rock gneisses analysed for the study. Gneisses ordered from furthest from the contact with the nepheline syenite except ST 181, which is from Joungane.

	Nd	Sm	Eu	Tb	Gd	Dy	Ho	Er	Tm	Yb	Lu	Hf	Ta	Pb	Th	U
Dykes																
ST75	89.3	17.4	0.74	2.09	14.4	12.2	2.06	5.47	0.87	6.92	1.16	18.0	4.90	21.3	20.7	4.64
ST84	15.6	2.99	0.179	0.369	2.49	2.32	0.461	1.33	0.205	1.57	0.283	8.59	2.71	36.3	2.55	0.621
ST88	4.65	0.825	0.055	0.086	0.556	0.534	0.104	0.323	0.053	0.518	0.102	3.72	0.401	0.926	1.64	0.206
ST113	24.6	5.93	0.465	1.38	5.94	11.7	2.55	7.41	1.04	7.64	1.17	17.9	11.4	22.3	71.8	11.1
ST147	45.0	8.39	0.492	0.998	7.40	5.85	1.07	2.83	0.414	3.24	0.615	4.97	2.13	11.1	4.43	1.59
ST203	147	25	1.11	2.66	19.0	16.4	3.11	9.64	1.54	11.1	1.64	32.1	10.6	45.3	30.9	8.4
ST211	139	26	1.16	3.49	21.9	24.6	5.09	15.20	2.10	12.8	1.71	22.2	11.0	28.9	28.7	8.16
ST216	121	19.6	1.13	1.40	11.9	7.25	1.25	4.07	0.952	9.65	2.03	7.76	6.44	31.5	33.1	4.29
ST217	87.9	18.4	1.03	1.78	13.9	9.41	1.48	3.99	0.688	6.18	1.22	10.4	2.89	7.74	6.80	1.37
ST226	3.88	0.736	0.086	0.089	0.556	0.56	0.114	0.378	0.079	0.628	0.102	2.11	0.831	7.56	2.59	0.545
ST228	84.4	16.8	0.697	2.09	13.9	11.6	1.87	4.83	0.783	6.64	1.12	19.9	6.29	25.3	21.3	5.66
ST246	537	73.9	5.58	5.74	44.1	32.6	5.65	14.6	1.95	11.7	1.58	22.4	7.92	42.8	30.6	4.69
ST268	166	23.2	1.66	2.63	16.6	17.4	3.58	11.0	1.63	10.9	1.56	20.6	8.47	48	21.3	3.21
FL1	51.2	10.2	0.494	1.24	8.64	7.63	1.42	3.77	0.474	3.08	0.472	18.8	7.98	25.3	6.04	3.58
FL2	14	2.98	0.131	0.343	2.89	1.96	0.349	0.89	0.128	1.09	0.227	7.82	0.517	1.42	0.535	0.159
STFL1A	12.1	2.50	0.107	0.28	2.17	1.56	0.283	0.732	0.103	0.788	0.144	5.94	0.609	2.07	1.21	0.306
ST212	93.8	18.2	0.729	2.18	14.3	13.4	2.72	8.54	1.38	9.54	1.40	24.4	7.86	36.3	23.0	5.92
ST76	109	21.6	0.978	3.02	19.7	17.7	3.18	8.70	1.26	8.79	1.28	25.2	4.73	48.5	19.1	5.51
STFL1B	9.54	2.12	0.089	0.251	1.92	1.41	0.256	0.68	0.096	0.751	0.14	6.34	0.537	1.33	0.935	0.305
Gneiss																
ST264	24.0	4.11	1.31	0.43	3.06	2.48	0.468	1.25	0.167	0.992	0.143	0.489	0.72	10.8	1.74	0.238
ST254	28.5	4.72	1.05	0.442	3.37	2.39	0.41	1.08	0.145	0.978	0.141	1.87	0.583	21.6	9.44	1.43
ST241	18.9	3.85	1.11	0.573	3.72	3.62	0.708	2.00		1.84	0.28	0.988	0.821	8.51	3.98	0.902
ST242	27.4	4.77	1.49	0.523	3.90	3.04	0.573	1.57	0.225	1.40	0.203	0.423	0.64	11.2	6.34	0.573
ST181	28.6	4.92	1.35	0.451	3.67	2.35	0.388	0.943	0.124	0.807	0.117	2.15	0.549	12.5	7.39	0.584
Nepheline Syenite																
ST71	32.9	4.71	1.15	0.469	3.36	2.63	0.498	1.35	0.204	1.32	0.199	3.58	3.32	7.88	5.43	0.928
ST133	49.8	7.47	1.33	0.764	4.96	4.48	0.88	2.69	0.46	3.85	0.685	16.1	5.4	4.60	10.2	2.91
ST138	75.2	11.2	1.86	0.989	6.91	5.48	0.969	2.75	0.461	3.95	0.728	17.9	6.57	3.71	6.46	1.01

Table 12b: Trace element abundance cont. from Table 12a.

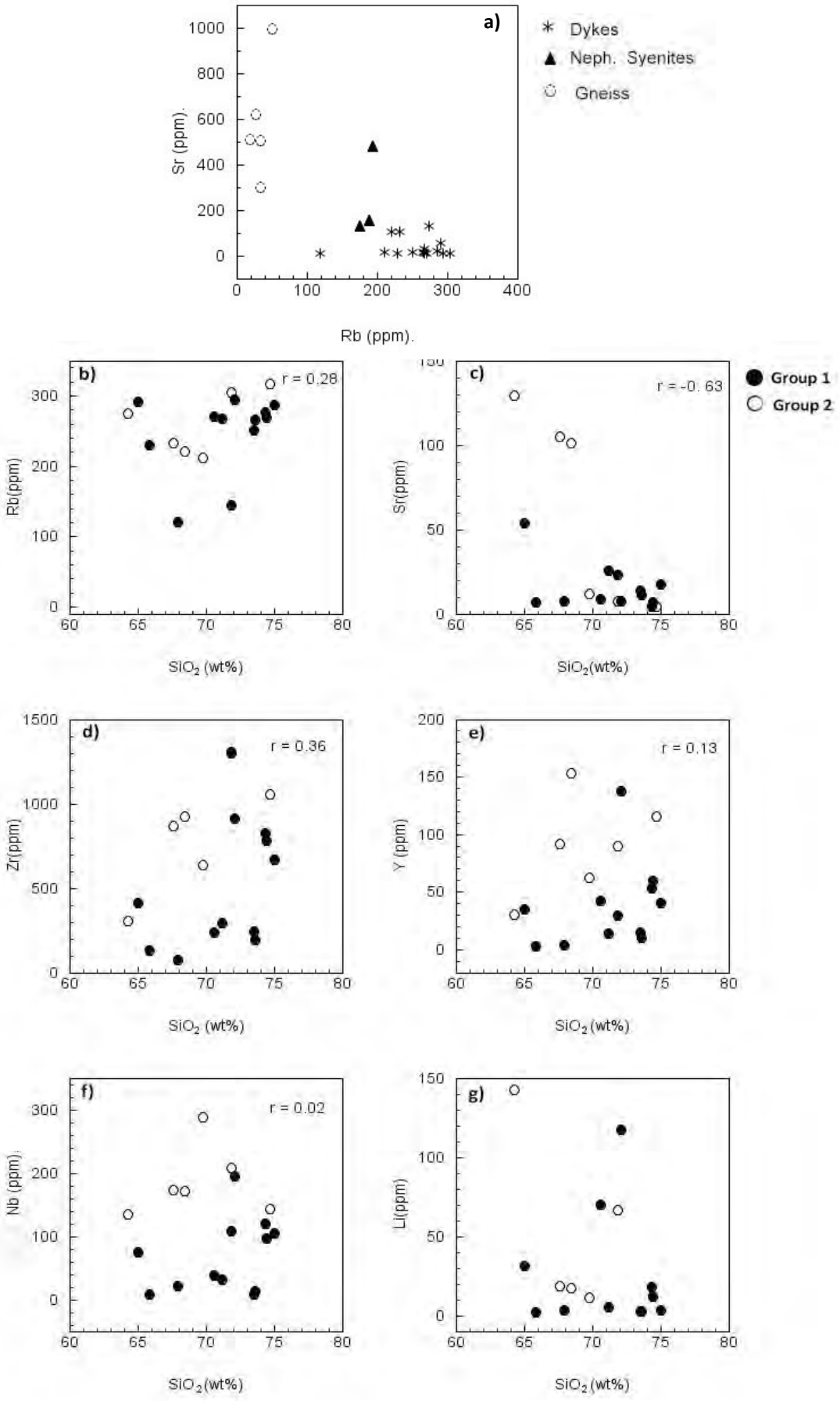

Figure 34: Trace elements. a)Sr vs Rb of all the samples analysed. The gneisses have very low Rb concentrations while the dykes have very low Sr and high Rb concentrations. b-g) Trace element variation with SiO_2 (wt.%) in the dykes. Correlation co-efficients are shown in the top right corner.

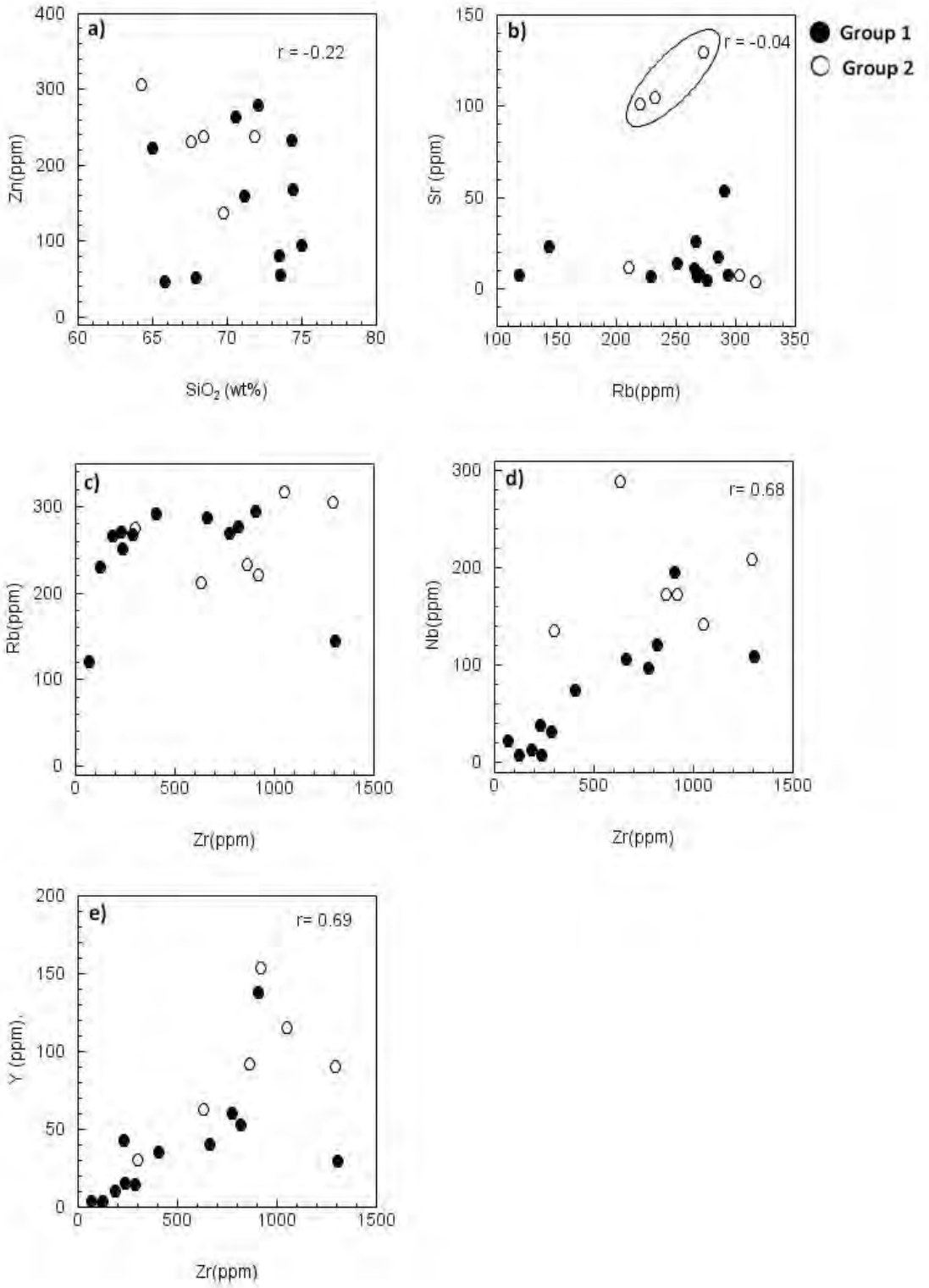

Figure 35: Trace element variation between SiO_2, Rb and Zr. Outliers highlighted in black ellipses (see text).

4.3.1 Rare Earth Elements

Similarity in REE patterns often suggests derivation from similar sources. At Straumsvola these sources are the country rock gneiss or the nepheline syenite. The concentration of certain REE can also provide information about the characteristics of the source from which it was derived. REE plots for the dykes normalised to chondrite values are shown in Figure 36. There is a large spread in the REE data from very low concentrations to extreme enrichment and up to two orders of magnitude difference within the light rare earth elements (LREE). All the samples are enriched in the LREE and exhibit steep La-Sm profiles that become flat/slightly upturned for the elements between Gd-Lu. A strong Europium anomaly is seen in all the samples suggestive of plagioclase fractionation at some stage in the magma's evolution. The open squares are dykes of trachytic/microsyenite composition that generally span the upper i.e. enriched portion of the plot. The lower i.e. less enriched portion of the REE plot contains the rhyolitic/microgranite dykes (crosses). The enriched nature of the dykes may be the result of a heavy rare earth element (HREE) enriched phase that is yet to fractionate. The REE profile for a eudialyte in ST38, the peralkaline granite of Harris & Grantham (1993), is included in Figure 36 and highlights the extreme REE enrichment, at least one order of magnitude greater than the most enriched dyke sample in this study. Overall the REE profiles between eudialyte and the dykes are very similar including having a pronounced Eu anomaly. Eudialyte with its enriched composition might therefore be the phase hosting the HREE and causing the upturn in the REE plots of some of the dyke samples.

Schilling et al. (2011) found that a Eu anomaly is only found in EGM's that are derived from an observed/ assumed alkali basaltic parental melt. All the peralkaline dykes in this study show a Eu anomaly and given the results of (Schilling et al. 2011) may indicate that the dykes are derived from an alkali basaltic parent. Other possibilities include partial melting of a source with a Eu anomaly or metasomatism by a fluid with a Eu anomaly. These possibilities will be evaluated in the next chapter.

The REE patterns of the dykes are compared with those of the nepheline syenites and surrounding country rock gneisses in Figures 37 and 38. The nepheline syenites in Figure 37 are from the nunataks Straumsvola (ST133 and ST138- black squares) and Storjeon (ST71- red square). The trends lie midway between the least and most enriched dykes and generally have a negative slope showing LREE enrichment. However, two of the nepheline syenites, ST138 and ST133, show the upturned HREE pattern seen in the dykes. These nepheline syenites are from the layered zone (ST133) and the base of the mafic zone (ijolite) that unconformably overlies the layered zone (ST138) at Straumsvola. The gneisses (half-filled circles) form a trend that lies midway between the dykes with the most and least enriched REE patterns (Figure 38). No europium anomaly is observed while the overall pattern shows LREE enrichment and HREE depletion. Two gneisses, ST241 and ST242, are from the contact zone of the nepheline syenite and country rock. They show a slight enrichment of the HREE relative to the other gneiss samples.

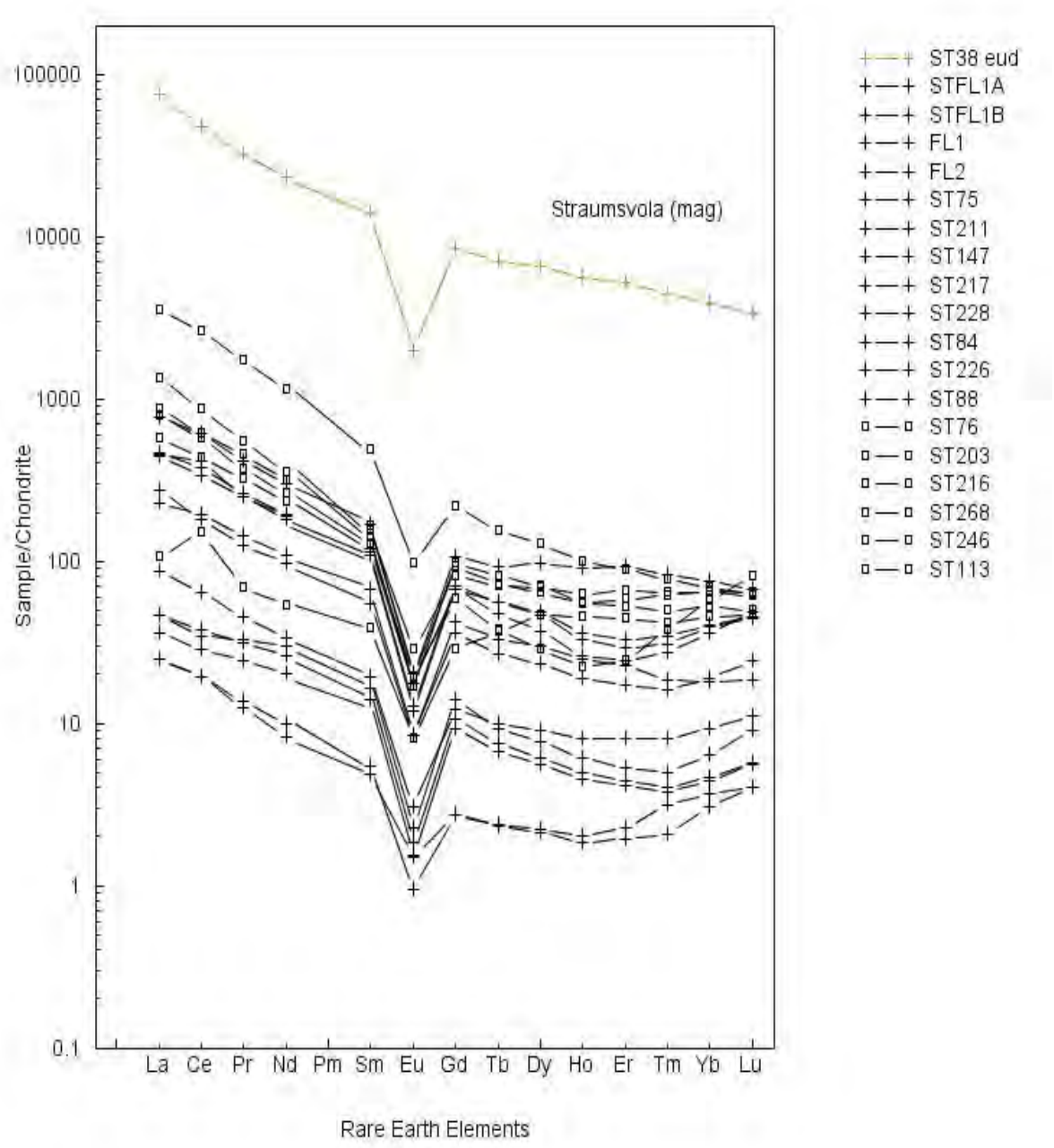

Figure 36: REE plot of the peralkaline dykes normalised to chondrite. Microsyenite dykes (squares) generally fill the upper portion of the graph at higher REE concentrations while the more evolved granitic dykes (crosses) tend to have lower REE concentrations and fill the lower part of the diagram. A wide range in REE concentations over 3 orders of magnitiude is observed. ST226 and ST88 plot at the lowest REE concentrations but are known to be outliers in most variation diagrams. Extreme REE concentration in eudialyte in ST38 (data extracted from Schilling et.al (2011)) is also shown. (Mag)= magmatic eudialyte i.e. not from a vug. It can be seen that the dykes and eudialyte in ST38 show a pronounced Eu anomaly and very similar REE profiles.

.

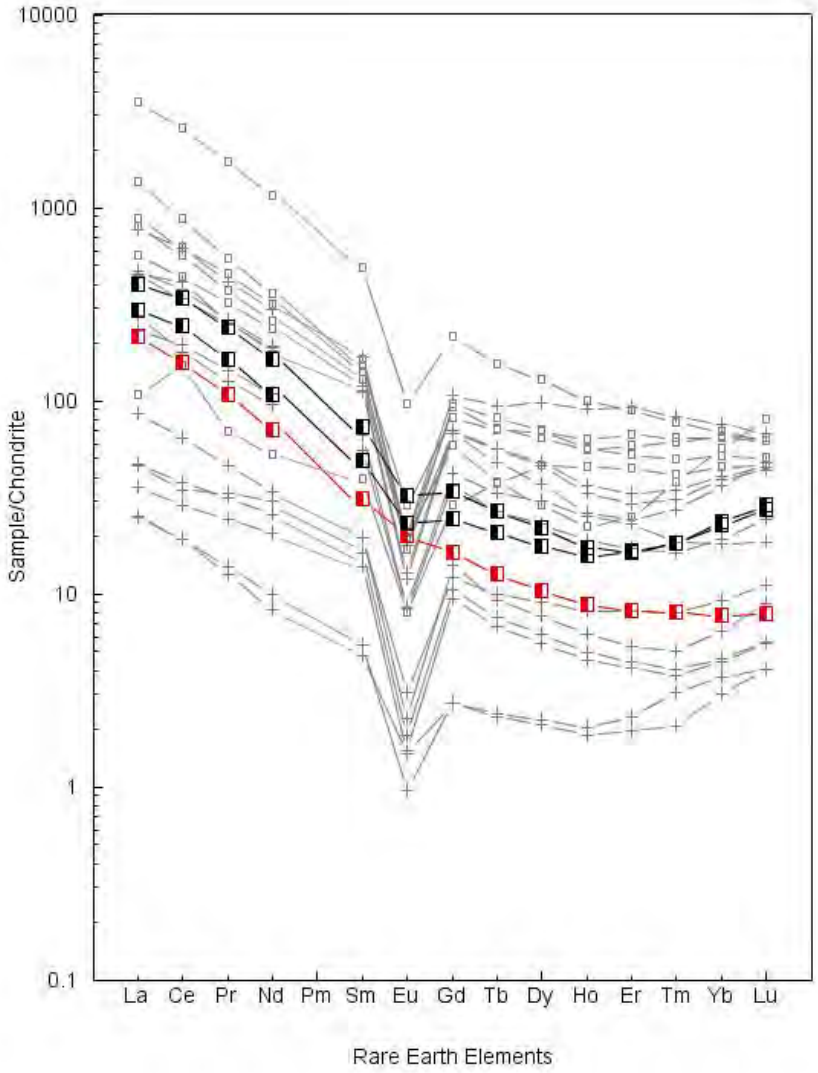

Figure 37: REE pattern of the dykes (grey) and the nepheline syenite plutons. ST 71 (red square) is from the outer zone at Storjeon and shows a negative slope while ST133 and ST138 from the layered zone, show LREE and the unusual HREE enrichment seen in some of the dyke samples (black squares).

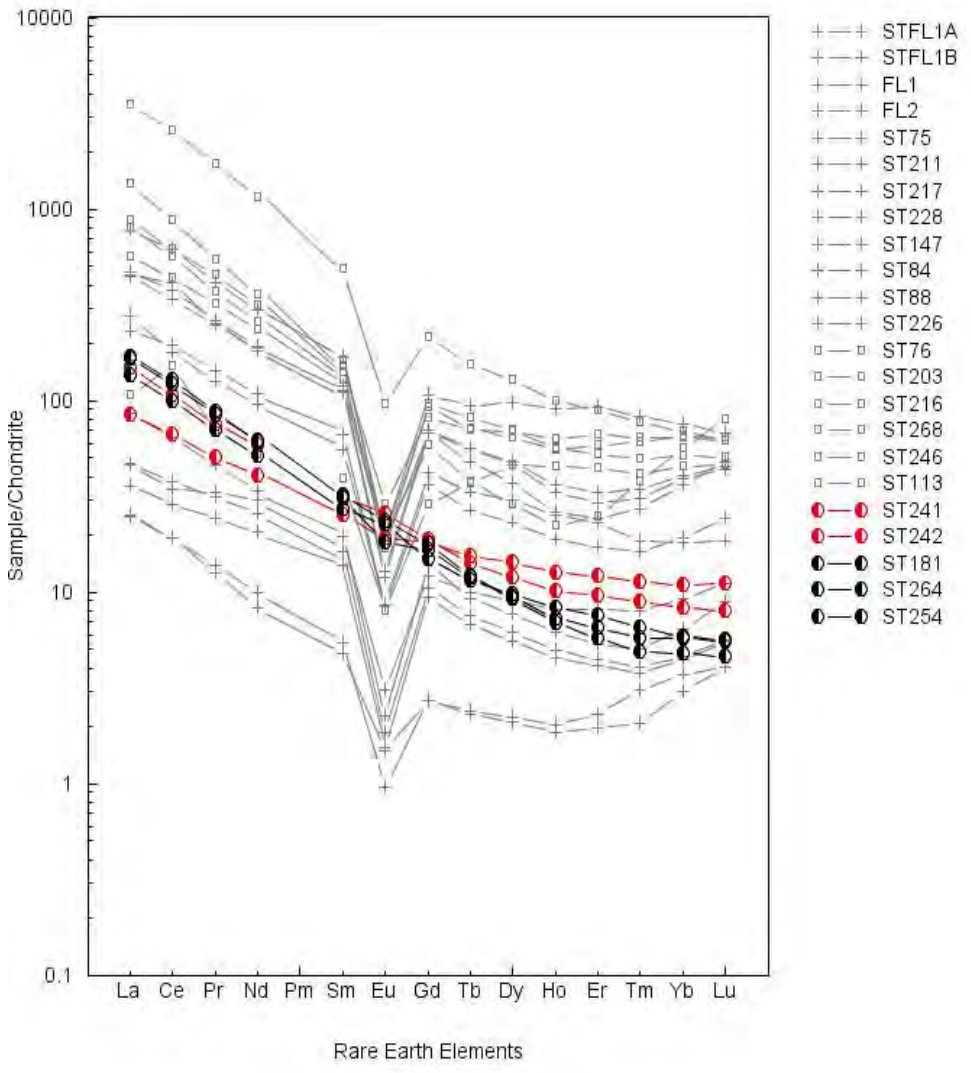

Figure 38: REE patterns of the dykes (grey) compared to 5 country rock gneisses (black circles). The gneisses lie midway in the suite of dykes and are generally LREE enriched and have a gentle negative slope with moderate HREE depletion.Gneisses from the contact zone (red) are slightly HREE relative to the other gneisses (black)

4.4 Isotopes

4.4.1 Oxygen Isotopes

Oxygen isotopes can be useful in constraining the source from which a melt was derived. Mafic melts tend to have lower oxygen isotope ratios vs more felsic melts and are interpreted in very general terms to reflect derivation from mantle or crustal sources respectively.

The oxygen isotope data used in this study is from 3 sources. Whole rock oxygen isotopes for the dykes, syenites and country rock gneisses were obtained from Harris & Grantham (1993) and Maisela (2012). Data on mineral separates are from Maisela (2012), Harris & Grantham (1993) and this study. Mineral separates (quartz and aegirine) from 9 fresh dyke samples were analysed. A summary of the data is provided in Table 13. All data are reported in the familiar δ notation, where $\delta^{18}O = (R_{sample}/R_{standard}-1)*1000$ and $R = {}^{18}O/{}^{16}O$, and SMOW is the standard.

The dykes show a narrow range in $\delta^{18}O$ quartz values from 8.4 to 9.2‰ with an average value of 8.6‰. These values are much higher than those expected from mantle derived crustal magmas (average 5.5-7‰; Eiler 2001) and suggest that there has been a significant amount of crustal input. Oxygen isotopes on quartz separates in the surrounding gneisses are also higher than those of a mantle derived magma but are not as high as those observed for the dykes. Quartz $\delta^{18}O$ in the gneisses ranges from 7.3 to 8.4‰ with an average value of 7.7‰.

Whole rock $\delta^{18}O$ ratios for the nepheline syenites show the lowest values ranging from 5.2-6.4‰, consistent with their being mantle-derived (Harris & Grantham 1993). The dykes show a constant range in whole rock $\delta^{18}O$ values between 7.2 and 7.4‰ while the gneisses are more variable ranging from 6.9 to 8.7‰. The dykes therefore fall within the range of the surrounding country rock gneisses. $\delta^{18}O$ was also calculated for aegirine in the dyke samples. These show a narrow range from 4.8 to 5.4‰.

Table 13: $\delta^{18}O$ values of mineral separates (quartz and aegirine) and whole rock powders.

	Sample	SiO_2	Whole rock $\delta^{18}O$	Quartz $\delta^{18}O$	Aegirine $\delta^{18}O$
Dykes	ST-FL1-A	73.9		8.5	5.1
	ST-FL1-B	74.9		9.2	5.0
	FLOAT-1	75.3		8.4	5.0
	FLOAT-2	74.1		8.7	5.2
	ST-75	74.9		8.4	5.4
	ST-76	74.7	7.3	8.5	
	ST-84	71.7		8.9	4.8
	ST-147	71.4			5.1
	ST-212		7.4	8.9	
	ST-228	74.9		8.4	5.1
	ST-38	71.9	7.2		5.2
	ST-144	68.0	7.2		
Gneiss	ST181	70.7	7.6	7.4	
	ST241	54.2	6.9	8.4	
	ST242	56.3	6.9	7.4	
	ST264	69.7	7.1	7.6	
	ST254	76.0	8.7	7.3	
Nepheline syenite	ST71	58.0	6.2		
	ST133	51.6	6.4		
	ST138	47.3	5.2		

***Whole rock data obtained by standard methods on a conventional line. All values relative to SMOW.**

4.5 Radiogenic Isotopes

A total of 27 Samples (19 dykes, 3 syenites and 5 gneisses) were selected for radiogenic isotopic analysis. The isotopic systems analysed were Sr, Nd and Pb. Sr and Nd are complementary isotopic systems that are useful individually and in tandem in discriminating between melts derived in different geologic settings. Pb isotopes are useful in constraining the mantle source from which a melt is derived. Measured and calculated isotope ratios for the aforementioned systems are shown in Appendix B. A summary of the values used to construct the isochrons and comparative plots are shown in Tables 14 and 15.

The equations used to calculate the $^{87}Rb/^{86}Sr$ ratio from Sr and Rb concentrations (ppm) and the measured $^{87}Sr/^{86}Sr$ ratio (obtained by MC-ICP-MS) is shown below. Equations for determining the $^{147}Sm/^{144}Nd$ ratio following the same method is also given:

$$\frac{^{87}Rb}{^{86}Sr} = \left(\frac{Rb}{Sr}\right)\left[2.6939 + 0.2832\frac{^{87}Sr}{^{86}Sr}\right]$$

$$\frac{^{147}Sm}{^{144}Nd} = \left(\frac{Sm}{Nd}\right)\left[0.53151 + 0.14252\frac{^{143}Nd}{^{144}Nd}\right]$$

The equations used to calculate the age-corrected initial $^{87}Sr/^{86}Sr$ and $^{143}Nd/^{144}Nd$ ratios are as follows (where λ= decay constant, t= age and x_0= initial ratio of the isotopic system being analysed):

$$\frac{^{87}Sr}{^{86}Sr} = \left(\frac{^{87}Sr}{^{86}Sr}\right)_0 + \frac{^{87}Rb}{^{86}Sr}(e^{\lambda t} - 1)$$

$$\frac{^{143}Nd}{^{144}Nd} = \left(\frac{^{143}Nd}{^{144}Nd}\right)_0 + \frac{^{147}Sm}{^{144}Nd}(e^{\lambda t} - 1)$$

The values of ε_{Sr} and ε_{Nd} were calculated using the equations below:

$$\varepsilon_{Nd} = 10^4 * \frac{(^{143}Nd/^{144}Nd)_{sample}}{(^{143}Nd/^{144}Nd)_{CHUR} - ((^{147}Sm/^{144}Nd)_{CHUR} * (e^{(EA*6.54*10\text{-}6)}-1))} - 1$$

$$\varepsilon_{Sr} = 10^4 * \frac{(^{87}Sr/^{86}Sr)_{sample}}{((^{87}Sr/^{86}Sr)_{BE} - (^{87}Rb/^{86}Sr)_{BE} * (e^{(EA*1.42*10\text{-}5)}-1))} - 1$$

$^{143}Nd/^{144}Nd_{CHUR}$: Present day $^{143}Nd/^{144}Nd$ ratio (i.e. 0.51264 *) of an undifferentiated Chondrite Uniform Reservoir (CHUR) (as measured in chondrites) and assumed to represent the undifferentiated Bulk Earth.

$^{147}Sm/^{144}Nd_{CHUR}$: Present day $^{147}Sm/^{144}Nd$ ratio (i.e. 0.1967*) of undifferentiated CHUR.

$(^{87}Sr/^{86}Sr)_{BE}$: Present day $^{87}Sr/^{86}Sr$ ratio (i.e. 0.705*) of the bulk earth
$(^{87}Rb/^{86}Sr)_{BE}$: Present day $^{87}Rb/^{86}Sr$ ratio (i.e. 0.09*) of the bulk earth
EA: Estimated age e.g. 170Ma
* All values for present day CHUR and Bulk Earth ratios taken from White (2007).

The measured initial ratios for each sample are shown in Tables 14 and 15. The following discussion summarises the key results of Table 14 with the aid of Figure 40. The measured $^{87}Sr/^{86}Sr$ ratios in the dykes range from 0.71960 to 1.54501. The range observed for the nepheline syenites is 0.71291 to 0.71524 while that for the gneisses is 0.70904 to 0.75347. The average measured $^{87}Sr/^{86}Sr$ ratio is therefore highest in the dykes. This is largely due to three samples that have $^{87}Sr/^{86}Sr$ ratios >1.100000, without these the range has a maximum $^{87}Sr/^{86}Sr$ = 1.001517.

Based on a Rb-Sr whole-rock isochron age of 170 ±4 Ma for the Straumsvola Complex (Grantham et al. 1988) and the Rb-Sr isochron calculated for the dykes in this study, 171 Ma ± 4.4 Ma (and discussed in the next chapter), the estimated age for the dykes and nepheline syenites was chosen as 171Ma. The same age was used to determine the isotope ratio of the gneisses at the time of the nepheline syenite intrusion. As can be seen from Table 14 the samples with the highest $^{87}Rb/^{86}Sr$ ratios, ST76, ST228 and ST212 all have very large errors associated with the calculation and very large Rb/Sr ratios (due to low Sr concentrations). Figure 39 shows the calculated $^{87}Rb/^{86}Sr$ ratio vs Sr concentration.

The initial $^{87}Sr/^{86}Sr$ ratios for the dykes (see next chapter) is 0.7075; 0.70537 – 0.71005 in the nepheline syenites and 0.70868 – 0.75320 in the gneisses. From this it can be seen that the initial $^{87}Sr/^{86}Sr$ ratios are highest in the gneisses, while the dykes overlap the range observed in the nepheline syenites.

Measured $^{143}Nd/^{144}Nd$ ratios by MC-ICP-MS in the dykes ranged from 0.51187 to 0.51236. The range observed for the nepheline syenites is 0.51189 to 0.51236 and in the gneisses is 0.51067 to 0.51181, Table 15. The estimated age of the dykes (171 Ma) as discussed above was used to calculate the initial $^{143}Nd/^{144}Nd$ ratio.

The calculated initial $^{143}Nd/^{144}Nd$ ratios at 171 Ma in the dykes showed a very narrow range from 0.511739 to 0.512033. In the nepheline syenites the range falls between 0.511753 and 0.512259 while in the gneisses the range is between 0.510910 and 0.511667. ε_{Nd} was also calculated for the suite of samples from the equations given earlier. The errors associated with most of the calculated ε_{Nd} values were very low.

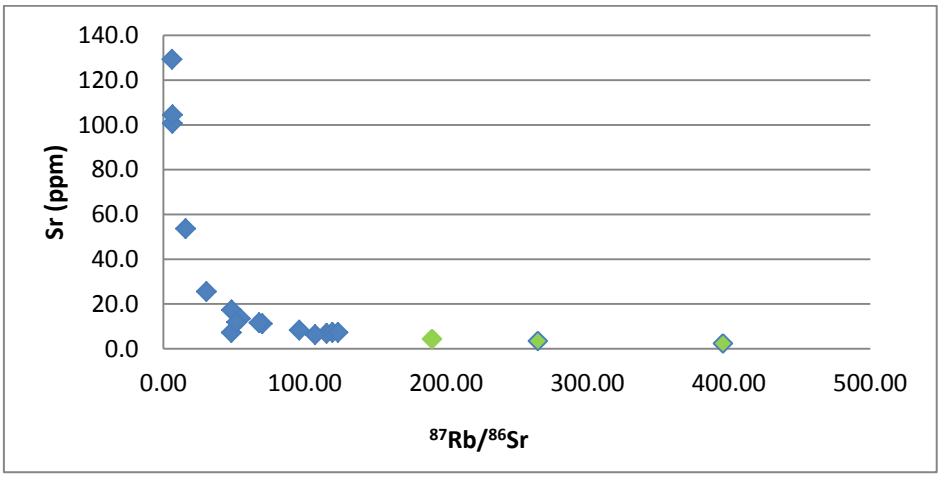

Figure 39: Plot of Sr vs $^{87}Rb/^{86}Sr$ for the dykes. The samples shown in green and have very large $^{87}Rb/^{86}Sr$ ratios as a result of very low Sr concentrations.

4.5.1 Comparison with other elements:

A plot of initial $^{143}Nd/^{144}Nd$ vs SiO_2 in Figure 40a shows three groupings of samples with increasing SiO_2. At low SiO_2 and initial $^{143}Nd/^{144}Nd$ >0.51800 are the nepheline syenites from the layered zone and the two gneisses from the contact zone. The dykes fall at constant $^{143}Nd/^{144}Nd$ ~0.51900 and SiO_2 in the range 64-75wt.% while the gneisses more than 400m from the contact zone, that form the third group, fall at similar SiO_2 but lower initial $^{143}Nd/^{144}Nd$ (<0.51100). No correlation is observed when Zr is plotted against initial $^{143}Nd/^{144}Nd$ as in Figure 40b but it can be seen that nepheline syenite ST133 plots within the range observed for the dykes while the gneisses tend to plot at low Zr concentrations and lower initial $^{143}Nd/^{144}Nd$.

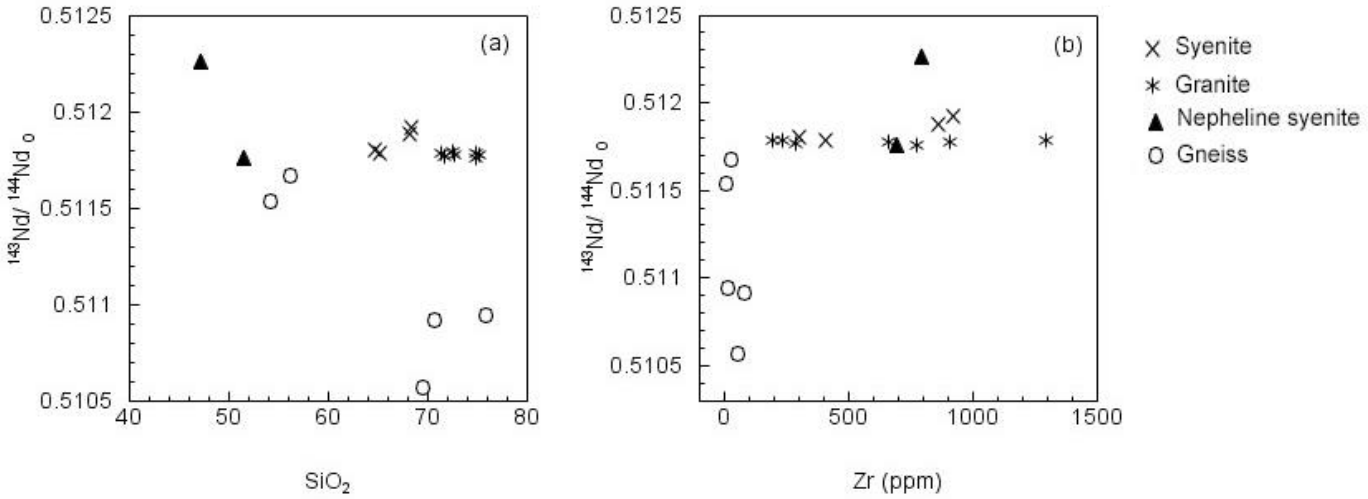

Figure 40: a) Nepheline syenites and dykes tend to overlap in initial $^{143}Nd/^{144}Nd$ and are less evolved than the gneisses except for two gneisses, ST241 and ST242, which are from the contact zone. b) No correlation between Zr and $^{143}Nd/^{144}Nd$ is observed but the gneisses form a distinct group to more evolved Nd.

Dykes	Rb	%RSD	Final %RSD	Sr	%RSD	Final %RSD	Rb/Sr	$^{87}Sr/^{86}Sr$	±2σ internal	$^{87}Rb/^{86}Sr$	±2σ	$^{87}Sr/^{86}Sr$ (171 Ma)	±2σ
STFL-1A	266	0.471	1.5	11.2	0.886	1.5	24	0.881708	0.000018	70.0	2.97		
FL1B	267	0.434	1.5	11.6	1.078	1.5	23	0.871963	0.000017	67.7	2.87		
FL1	286	0.245	1.5	17.4	0.61	1.5	16	0.822846	0.000018	48.2	2.05		
FL2	251	0.300	1.5	13.5	0.633	1.5	19	0.841198	0.000015	54.4	2.31		
ST75	268	0.296	1.5	6.90	0.634	1.5	39	0.993819	0.000015	116	4.90		
ST147	270	0.210	1.5	8.32	1.021	1.5	32	0.944372	0.000015	96.2	4.08		
ST211	294	0.638	1.5	7.31	0.994	1.5	40	0.997161	0.000019	120	5.07		
ST217	291	0.222	1.5	53.7	0.351	1.5	5	0.747102	0.000012	15.7	0.67		
ST84	267	0.277	1.5	25.5	0.194	1.5	10	0.777809	0.000012	30.5	1.29		
ST226	120	0.346	1.5	7.27	0.606	1.5	36	0.830892	0.000018	48.2	4.55	**0.7075**	**0.0032**
ST88	230	0.165	1.5	6.34	0.575	1.5	42	0.956208	0.000019	107	5.24		
ST203	304	0.325	1.5	7.32	0.799	1.5	2	1.001517	0.000017	124	0.260		
ST216	274	0.140	1.5	129	0.461	1.5	18	0.725744	0.000014	6.14	2.20		
ST113	211	0.363	1.5	11.9	0.352	1.5	2	0.835119	0.000017	51.9	0.269		
ST246	221	0.298	1.5	101	0.85	1.5	2	0.719599	0.000012	6.35	0.274		
ST268	233	0.167	1.5	105	0.401	1.5	16	0.721448	0.000012	6.46	2.04		
ST-76	301	0.004	1.5	3.48	1.204	1.5	87	1.300065	0.000016	265	11.2		
ST228	276	0.168	1.5	4.41	0.726	1.5	63	1.196014	0.000021	190	8.06		
ST212	304	0.531	1.5	2.40	1.536	1.5	126	1.545008	0.000022	396	16.8		
Nepheline Syenite													
ST-71	195	0.607		479	0.438			0.712906	0.000016	1.17	0.02	0.710050	5.88E-05
ST133	176	0.833		125	0.749			0.715240	0.000013	4.06	0.10	0.705373	2.34E-04
ST138	190	0.842		154	0.991			0.714759	0.000012	3.57	0.10	0.706085	2.38E-04
Gneiss													
ST181	27.6	0.607		617	0.695			0.713064	0.000009	0.130	0.002	0.712749	1.48E-05
STS242	50.8	1.11		991	0.428			0.709039	0.000013	0.148	0.004	0.708678	2.16E-05
ST241	34.3	1.45		501	0.909			0.711056	0.000011	0.198	0.007	0.710574	2.75E-05
ST254	18.79	0.397		506	1.917			0.753465	0.000012	0.108	0.004	0.753202	2.23E-05
ST264	33.93	1.11		299	0.31			0.715054	0.000011	0.329	0.008	0.714255	2.93E-05

Table 14: Radiogenic isotope data for all the samples in the Rb-Sr system. %RSD= Percent Relative Standard Deviation; Final %RSD = Analytical uncertainty used to calculate the Rb-Sr isochron in Ch5; ±2σ= 2 sigma standard deviation from the mean. The initial $^{87}Sr/^{86}Sr$ ratio for the granite and syenite dykes determined using the isochron method and discussed in Chapter 5 = 0.7075 ± 0.0032.

	Nd	%RSD	Sm	%RSD	$^{143}Nd/^{144}Nd$	±2σ internal	$^{147}Sm/^{144}Nd$	±2σ	$^{143}Nd/^{144}Nd$ (171Ma)	±2σ	εNd (171 Ma)	±2σ
Dykes												
STFL-1A	12.1	0.788	2.5	1.70	0.511922	0.000028	0.125008	0.004694	0.511782	3.99E-05	-12.4	0.65
STFL1B	9.54	0.717	2.12	0.797	0.512074	0.000033	0.134099	0.002875	0.511925	1.27E-05	-9.6	0.71
FL1	51.2	0.117	10.2	0.741	0.511907	0.000011	0.120478	0.001808	0.511772	2.24E-05	-12.6	0.25
FL2	14	0.291	2.98	1.65	0.511898	0.000026	0.128538	0.004297	0.511754	3.82E-05	-12.9	0.60
ST75	89.3	0.666	17.4	0.624	0.511888	0.000008	0.117808	0.002150	0.511756	1.92E-05	-12.9	0.20
ST147	45	0.296	8.39	0.933	0.511908	0.000015	0.112549	0.002203	0.511782	2.57E-05	-12.4	0.34
ST211	139	0.251	26	0.217	0.511897	0.000008	0.113112	0.000751	0.511770	1.87E-05	-12.6	0.17
ST217	87.9	0.355	18.4	1.21	0.511922	0.00001	0.126164	0.003187	0.511780	2.20E-05	-12.4	0.26
ST84	15.6	0.678	2.99	0.939	0.511892	0.000017	0.115523	0.002676	0.511763	2.80E-05	-12.8	0.39
ST88	4.65	2.080	0.825	2.47	0.511924	0.000044	0.107303	0.003574	0.511804	6.59E-05	-12.0	1.15
ST226	3.88	0.951	0.736	1.24	0.512162	0.000055	0.114574	0.006932	0.512033	5.42E-05	-7.5	1.01
ST203	147	0.330	25	0.197	0.511899	0.000009	0.102768	0.000790	0.511784	1.88E-05	-12.4	0.19
ST216	121	0.351	19.6	0.946	0.511906	0.000009	0.097945	0.001977	0.511797	1.83E-05	-12.1	0.22
ST113	24.6	0.208	5.93	1.56	0.511948	0.000017	0.145455	0.004587	0.511785	3.08E-05	-12.3	0.43
ST246	537	0.967	73.9	0.803	0.512007	0.000011	0.083087	0.002089	0.511914	1.89E-05	-9.8	0.26
ST268	166	0.733	23.2	0.582	0.511971	0.000011	0.084805	0.001587	0.511877	1.91E-05	-10.6	0.25
ST-76	109	0.433	21.6	0.230	0.511887	0.000009	0.119582	0.001173	0.511753	2.04E-05	-13.0	0.20
ST228	84.4	0.504	16.8	0.899	0.511874	0.000012	0.120339	0.002481	0.511739	2.34E-05	-13.2	0.288
ST212	93.8	0.433	18.2	0.932	0.511879	0.000011	0.117466	0.002414	0.511747	2.22E-05	-13.1	0.267
Nepheline Syenite												
ST-71	32.9	0.347	4.71	2.09	0.512356	0.000014	0.086579	0.003662	0.512259	2.22E-05	-3.1	0.4
ST133	109	0.592	21.6	0.651	0.511887	0.00001	0.119582	0.002104	0.511753	2.14E-05	-13.0	0.2
ST138	49.8	0.943	7.47	1.22	0.512359	0.000011	0.090585	0.002796	0.512258	1.96E-05	-3.1	0.3
Gneiss												
ST181	28.6	0.892	4.92	0.541	0.511027	0.000009	0.103962	0.002169	0.510910	1.85E-05	-29.4	0.22
STS242	27.4	0.624	4.77	0.658	0.511647	0.000010	0.105383	0.001911	0.511529	1.96E-05	-17.4	0.23
ST241	18.9	0.726	3.85	0.240	0.511805	0.000017	0.123091	0.001882	0.511667	2.91E-05	-14.7	0.38
ST254	28.5	0.911	4.72	0.888	0.510674	0.000018	0.100287	0.002552	0.510562	2.75E-05	-36.2	0.41
ST264	24	0.788	4.11	1.75	0.511051	0.000012	0.103469	0.003972	0.510936	2.20E-05	-28.9	0.32

Table15: Radiogenic isotope data for all the samples in the Sm-Nd system. Abbreviations the same as in Table 14. ST 88 and ST226 have higher measured RSD's on the Sm concentration than the average for these samples. These measurements were not included in the inter-element plots in Figure 40. ST 88, is known to be a highly altered sample that is an outlier in most comparison plots.

	Pb (ppm)	$^{208}Pb/^{204}Pb$	±2σ	$^{207}Pb/^{204}Pb$	±2σ	$^{206}Pb/^{204}Pb$	±2σ
Dykes							
STFL1A	2.07	38.0564	0.0030	15.4569	0.0010	17.5352	0.0010
STFL1B	1.33	38.0791	0.0025	15.4577	0.0009	17.6091	0.0009
FL1	25.3	38.2394	0.0030	15.4395	0.0010	17.4600	0.0010
FL2	1.42	38.4393	0.0044	15.5398	0.0015	17.9740	0.0017
ST75	21.3	38.3584	0.3380	15.4305	0.0011	17.4777	0.0010
ST147	11.1	37.8525	0.0030	15.3512	0.0010	17.1543	0.0009
ST211	28.9	38.2787	0.0034	15.4319	0.0011	17.5385	0.0011
ST217	7.74	38.3295	0.0035	15.4436	0.0010	17.6040	0.0011
ST84	36.3	37.6071	0.0030	15.3326	0.0011	16.9245	0.0010
ST88	0.926	38.8699	0.0038	15.5455	0.0014	18.0593	0.0015
ST226	7.56	38.1016	0.0034	15.4986	0.0011	17.7439	0.0011
ST203	45.3	38.1690	0.0039	15.4254	0.0013	17.4065	0.0013
ST216	31.5	38.3833	0.0037	15.4336	0.0012	17.4424	0.0011
ST113	22.3	38.8510	0.0030	15.5277	0.0009	18.2557	0.0009
ST246	42.8	38.2353	0.0033	15.4570	0.0010	17.5692	0.0011
ST268	48	38.2171	0.0036	15.4394	0.0011	17.4094	0.0012
ST76	48.5	38.0251	0.0026	15.4194	0.0008	17.3037	0.0009
ST228	25.3	38.2748	0.0040	15.4329	0.0012	17.5017	0.0012
ST212	36.3	38.2085	0.0035	15.4283	0.0011	17.3797	0.0009
Neph.Syenite							
ST71	7.88	38.3948	0.0026	15.5166	0.0010	17.8314	0.0009
ST133	4.60	39.1453	0.0033	15.5634	0.0012	18.6838	0.0012
ST138	3.71	38.9519	0.0034	15.5411	0.0012	18.1703	0.0014
Gneiss							
ST181	12.5	39.2295	0.0026	15.5329	0.0010	17.4906	0.0010
ST241	8.51	38.5167	0.0024	15.6308	0.0009	18.5469	0.0010
ST242	11.2	38.5513	0.0033	15.6096	0.0012	18.2368	0.0012
ST264	10.8	38.7723	0.0033	14.9223	0.0010	15.1546	0.0010
ST254	21.6	38.2951	0.0033	15.7273	0.0012	18.2613	0.0013

Table 16: Pb concentration and isotopic ratios obtained by ICP-MS and MC-ICP-MS at UCT for all samples of this study. The Pb data were not age corrected to avoid overcorrection of the Pb isotope ratios given the young age of the dykes and the relative mobility of Pb vs U and Th.

4.5.2 Comparison with other isotopes: Pb

All the samples (dykes, syenites and gneisses) were analysed for $^{208}Pb/^{204}Pb$, $^{207}Pb/^{204}Pb$ and $^{206}Pb/^{204}Pb$ ratios and the results shown in Table 16. $^{208}Pb/^{204}Pb$ ratios in the dykes range from 37.6071 to 38.8699. In the nepheline syenites the range is from 38.3948 to 39.1453 and the gneisses from 38.2951 to 39.2295. $^{207}Pb/^{204}Pb$ shows a small range in the dykes from 15.3512 to 15.5455. In the nepheline syenites, the range is 15.5166 to 15.5634 while in the gneisses it is 14.9223 to 15.7273. $^{206}Pb/^{204}Pb$ has a range of 16.9245 to 18.0593 in the dykes, 17.8314 to 18.6838 in the nepheline syenites and a large range (15.1546 to 18.5469) in the gneisses. On a $^{207}Pb/^{204}Pb$ vs $^{206}Pb/^{204}Pb$ plot, the suite of samples generally show a linear, positive correlation from the dykes at low $^{207}Pb/^{204}Pb$ and $^{206}Pb/^{204}Pb$ ratios (Figure 41) through the syenites and then the gneisses at high $^{207}Pb/^{204}Pb$ and $^{206}Pb/^{204}Pb$. One gneiss, ST264, plots at the low $^{207}Pb/^{204}Pb$ and $^{206}Pb/^{204}Pb$ end. $^{208}Pb/^{204}Pb$ vs $^{206}Pb/^{204}Pb$ shows a similar trend to the previous plot except the range in $^{208}Pb/^{204}Pb$ is wider. The gneisses show the most variability with two samples lying off the general array. These samples, ST181 and ST264, are >400m from the contact zone but are not the furthest away. ST254, which is furthest away falls on the general data array.

The 'outlier' gneisses in Figure 41c are furthest from the contact with the nepheline syenite. ε_{Nd} vs $^{206}Pb/^{204}Pb$ shows again that most of the samples (dykes, nepheline syenites and two gneiss samples) cluster together, here it is not around one value but rather the cluster forms above ε_{Nd} values > -12. The outliers at more negative ε_{Nd} are once again the gneisses furthest from the contact with the nepheline syenites attesting to their crustal nature. However, overall there appears to be no real correlation between Pb and Sr or Pb and Nd for the samples of this study.

That the dykes and nepheline syenites plot together in most variation diagrams suggests that they are related and are possibly derived from a similar source. In addition, in most of the plots, two gneisses, ST 241 and ST242, cluster with the dykes and nepheline syenites. These samples are at the contact zone of the nepheline syenite intrusion and therefore suggest they were affected by intrusion of the nepheline syenite.

** The dykes in this study are young and the age correction is not large. Any age correction runs the risk of overcorrecting for growth of radiogenic Pb because of the relative mobility of Pb compare to the parent isotopes of U and Th. Thus there is no guarantee that age correcting the data would give the correct initial Pb-isotope ratios. Hence the Pb data in this study were not age corrected to 171Ma as was done for Sm-Nd."*

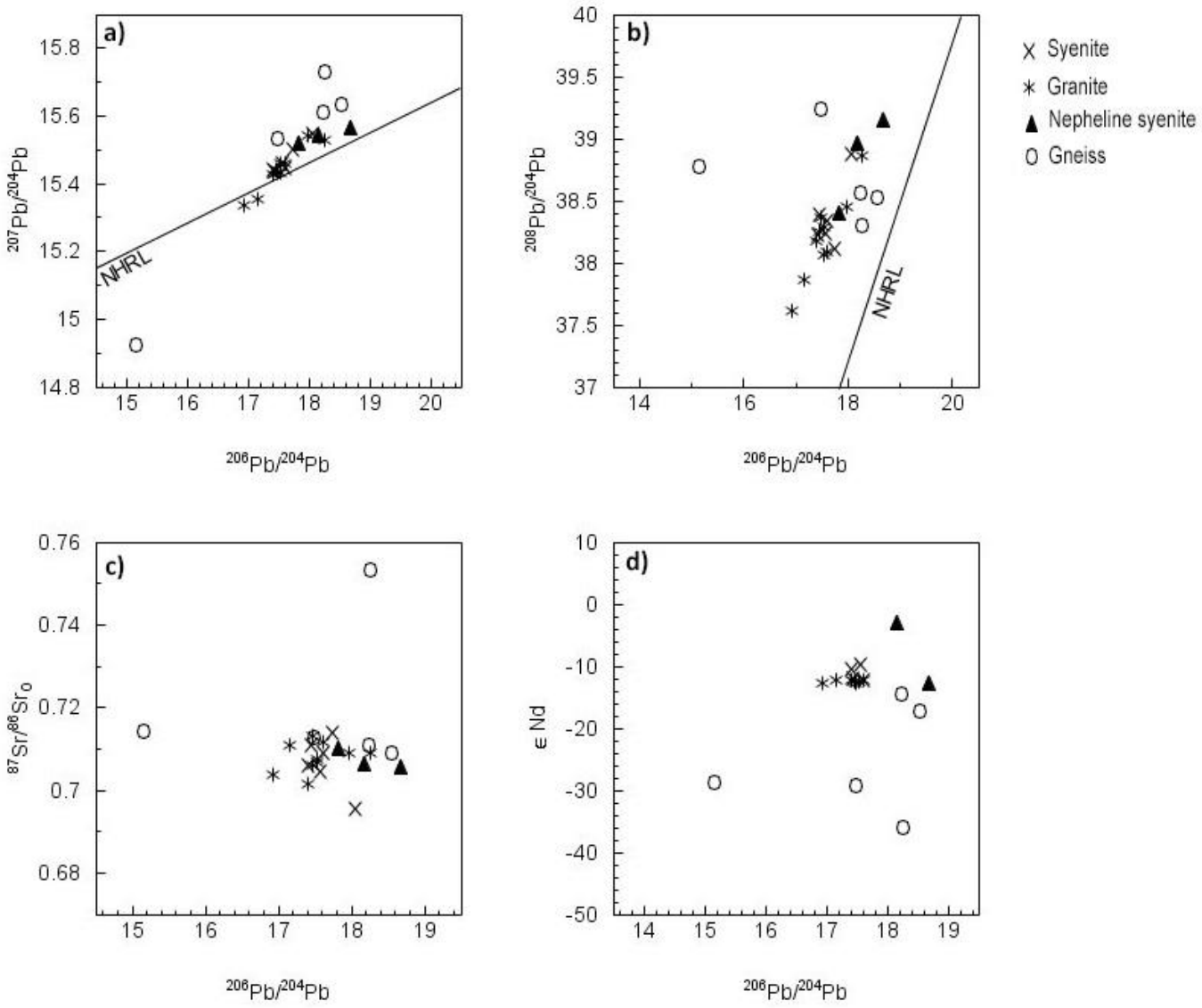

Figure 41: Pb isotopes plotted against one another, initial $^{87}Sr/^{86}Sr$ and ε_{Nd}. a) $^{207}Pb/^{204}Pb$ vs $^{206}Pb/^{204}Pb$ shows a positive correlation with the dykes being the least radiogenic and the gneisses the most strongly radiogenic except for ones gneiss, ST 264. This gneiss and two dykes, ST 147 and ST84 are the only samples that plot below the Northern Hemisphere Reference Line (NHRL). b) $^{208}Pb/^{204}Pb$ vs $^{206}Pb/^{204}Pb$ shows similar trends to the previous graph for all the samples except that all the samples now plot above the NHRL. c) Two gneisses, ST254 and ST264, do not fall within the cluster of samples to more radiogenic $^{206}Pb/^{204}Pb$. These samples are furthest from the contact zone. d) The two gneisses from the contact zone fall within the cluster of the dykes and nepheline syenites and suggest they were affected by intrusion of the nepheline syenite.

5. Discussion

The peralkaline dykes of the Straumsvola Complex have been shown in the previous chapters to be silica-oversaturated, peralkaline and extremely fresh. Trace element and REE plots in the previous chapter (Figures 35-38) highlight enrichment of the incompatible elements: Zr, Y, Nb and the REE in the some of the dykes in addition to the relatively high concentrations of Rb (>100ppm) overall. Given the peralkaline nature of the dykes, their enriched compositions and their formation in what is likely a rift-related i.e. anorogenic setting, the dykes can be classified as A-type by the original definition of Loiselle & Wones (1979) and as outlined in the Introduction to this study. The definition of A-type remains controversial due to its occurrence in a variety of environments (including other planets) and their variable chemistry e.g. strongly alkaline or aluminous (Bonin 2010). A-type granites rarely represent crustal melts alone given their high magma temperatures (>900°C) and isotopic signatures suggestive of a mantle component (Bonin 2007; C. Frost & Frost 2011). Two of the more favoured mechanisms include: 1) Differentiation of transitional basalts (C. Frost & Frost 2011) or mantle-derived mafic magmas and 2) Mantle-derived basaltic magmas variably contaminated by the crust. Most models however, favour a degree of crustal contamination in the petrogenesis of A-type magmas, with the mantle as a source of mafic magma that either interacts with the crust or plays a secondary role as a heat source to induce melting of the crust (Bonin, 2010).

At Straumsvola, silica-oversaturated dykes are known to intrude the nepheline syenite, quartz syenite and alkali basalts of the complex. While the association of silica under- and oversaturated magma types is unexpected (given the thermal divide at low pressure in the Q-Al-Ne-Ks system) it is not unique to the Straumsvola complex nor is it uncommon. The association of these magma types however, remains poorly understood given that the magmas often appear to be co-genetic and has led most authors to conclude that there is a significant crustal component in their evolution (Foland et al. 1993; Marks et al. 2003) . The evidence for crustal contamination in the genesis of the Straumsvola dyke magmas must therefore be examined.

This chapter will investigate the extent to which the data presented in this study can be used to assess the evidence for crustal contamination and the role, if any, of the mantle in the generation of these peralkaline dykes. Comparison with the nearby Sistefjell alkaline pluton will also aid in the development of petrogenetic a model for the Straumsvola Complex. The model should account for the petrogenesis of the dyke magma in its local context, how it came to be peralkaline and the presence of the unusual silicates.

5.1. Major element variation

On a Total-Alkali-Silica diagram the dykes show a negative correlation (r=-0.83) from low to high SiO_2 (See chapter 4, Figure 31). The trend suggests that Total alkali content decreases almost linearly as the dyke magma evolves to higher SiO_2, which is in part due to the constant sum effect. Nonetheless, this is expected in systems where a mineral/minerals are fractionating out of the main assemblage. The dykes are therefore likely showing a fractionation or assimilation process that will be investigated in this chapter.

The dominant minerals present in the dykes of this study are quartz, feldspar and aegirine (which is present either as phenocrysts or as interstitial aegirine/amphibole crystals in the groundmass). The average compositions of aegirine and feldspar were used to determine if the trend seen on the TAS diagram (Figure 31) could be explained by removal of these phases. The average aegirine composition was calculated by averaging all the aegirine data obtained by electron microprobe. The feldspar composition was more complicated to obtain as all of the feldspars are exsolved to various degrees, which makes the bulk composition difficult to estimate. To estimate the amount of K_2O and Na_2O in the feldspars, the average normative proportion of albite: orthoclase for the suite of dykes was calculated. The elemental analysis of the feldspar end members albite and orthoclase as given in Deer et al. (2001) (pg 414-415) was then used to determine the concentration of the major elements in a feldspar with the normative composition Ab_{57}:Or_{43} . The result of these calculations is shown in Table 18 where K_2O and Na_2O were calculated as 6.72 and 6.71wt.% respectively. SiO_2 and Al_2O_3 were calculated in the same way and were calculated as 65.79 and 20.00 wt.% respectively.

The composition of the average feldspar and aegirine was then used to evaluate if the major element variation of the dyke suite could be explained by fractionation of these major phases. A regression analysis was performed on each major element of the dataset with SiO_2, producing a trend line through the data. A line joining the average composition of feldspar and aegirine was constructed and by the lever rule, the intersection of this trend line through the aegirine-feldspar join was used to determine the relative proportion of each fractionating mineral for the element of interest. It can be seen from Figures 42-45 that fractionation of the major phases, feldspar and aegirine, can account for the variation in the major elements of the suite. Two samples, ST88 and ST 226, are outliers in these graphs but are known from previous analyses to be outliers and are not considered further. For SiO_2 vs Total-Alkali-Silica (Figure 42), the model shows that the variation is consistent with fractionation of feldspar and aegirine in the proportions 90:10, respectively suggesting that fractionation of these phases is driving the residual magma toward a more evolved composition. Na_2O and K_2O were then plotted separately against SiO_2 in Figures 43 and 44. For Na_2O, feldspar and aegirine appear to fractionate in the proportion 76:24, respectively. A similar ratio of 70:30 for K_2O vs SiO_2 is observed. Lastly, Fe_2O_3 vs SiO_2 suggests that fractionation of feldspar and aegirine in the proportions 84:16 could account for the change in Fe_2O_3 as the system evolves. Given the above results, it appears that feldspar fractionation plays a more important role than aegirine in the evolution of the dyke

suite. This is supported by the petrography where aegirine phenocrysts appear to crystallise very late. However, most of the Fe_2O_3 is contained in aegirine which also means that some aegirine must be fractionating along with feldspar. Overall the predicted trends evolve to a quartz and together with the major element results of Chapter 4, support fractional crystallisation as a mechanism to explain the evolution of the dyke magma.

A further test of fractional crystallisation was made using a least-squares regression. The model used the average feldspar and aegirine compositions calculated above and the primitive trachyte, ST144 and evolved granite, ST75. Table 17 shows that removal of 60% of an assemblage of feldspar and aegirine in the proportion 80:20 produces a granite with a composition very similar to ST75. It is notable from the calculation that no addition of quartz is required to produce the evolved granite. The model also confirms the aforementioned findings that aegirine and feldspar fractionation are responsible for most of the major element variation in the dyke suite.

	%		SiO_2	TiO_2	Al_2O_3	FeO	MnO	MgO	CaO	Na_2O	K_2O
evolved rock:											
ST75	**40**	0.40	74.91	0.18	11.14	3.34	0.07	0.03	0.08	5.55	4.28
Quartz	0.0	0.00	100.00	0.00	0.00	0.00	0.00	0.00	0.00	0.00	0.00
Aeg	11.6	0.12	52.53	1.90	0.33	28.42	0.31	0.48	1.82	13.26	0.01
Fsp	48.5	0.48	66.19	0.00	19.04	0.55	0.00	0.00	0.00	6.05	7.51
		1									
calculated			68.01	0.29	13.71	4.89	0.07	0.07	0.25	6.68	5.34
Primitive rock:											
ST144			67.99	0.27	13.78	4.51	0.09	0.04	0.62	7.53	4.66
Sum of squares	1.49	residuals	-0.02	-0.02	0.07	-0.39	0.02	-0.03	0.37	0.85	-0.68

Table 17: Least squares regression modelling of evolved granite (ST75) shows that it can be produced by 60% fractional crystallisation of primitive trachyte, ST 144 by removal of the phases aegirine and feldspar in the proportions 20:80, respectively. This agrees well with the major element variations discussed earlier. The model was tested using an Excel spreadsheet and the Solver add-in for Excel, 2010.

Albite in the norm		**37%**	**57%**		
Orthoclase in the norm		**27%**	**43%**		
			100%		
	Orthoclase (DHZ)	**Norm. orthoclase X pure orthoclase**	Sanidine (DHZ)	**Norm. albite X pure albite**	**Sum**
SiO_2	63.66	27.37	67.39	38.41	**65.79**
TiO_2	0	0.00	0.00	0.00	**0.00**
Al_20_3	19.54	8.40	20.35	11.60	**20.00**
fe_20_3	0.10	0.04	0.00	0.52	**0.04**
FeO	0	0.00	0.00	0.00	**0.00**
MgO	0	0.00	0.00	0.00	**0.00**
BaO	0	0.00	0.00	0.00	**0.00**
CaO	0.50	0.22	1.07	0.61	**0.82**
Na_2O	0.80	0.34	11.19	6.38	**6.72**
K_2O	15.6	6.71	0.00	0.00	**6.71**

Deer, Howie and Zussman (2001), pg 414- 415

	analysis wt %	cations	atoms	*based on Ca, Na, K ratios only	
SiO_2	65.79	Si	2.95		
TiO_2	0.00	Ti	0.00		
Al_2O_3	20.00	Al	1.06	Si+Ti+Al+Fe3=	
Cr_2O_3	0.00	Cr	0.00	ideal =	4.00
Fe_20_3	0.04	Fe^{3+}	0.00		4
FeO	0.00	Fe^{2+}	0.00	Ca+Na+K=	
MnO	0.00	Mn	0.00	ideal =	1.01
MgO	0.00	Mg	0.00		1
BaO	0.82	Ca	0.04		
CaO	0.00	Ba	0.00		
Na_2O	6.71	Na	0.58		
K_2O	6.72	K	0.38		
Total	99.36				

Table 18: Calculation of the average feldspar composition of the dykes based on the proportion of albite and orthoclase in the norm. An average feldspar composition is required given that all the feldspars are affected by exsolution. The normative proportion was multiplied against the concentration of Na_2O, K_2O and the other major elements in pure albite and orthoclase respectively from Deer et al (2001) (DHZ). The sum of these produced the concentrations of the major elements of a feldspar with the average normative composition in the suite of Straumsvola dykes.

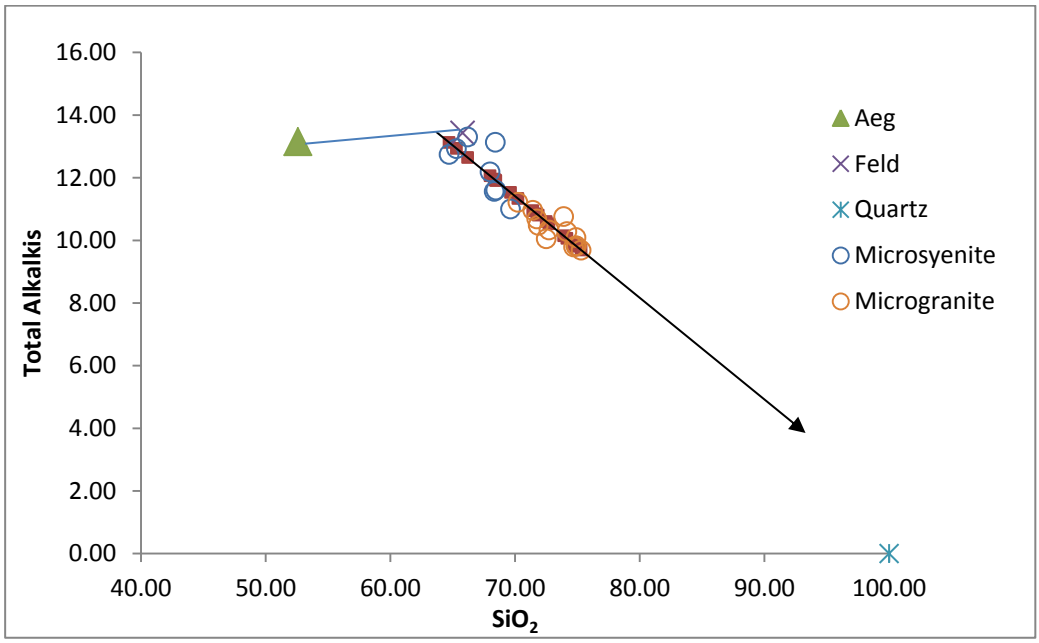

Figure 42: Total-alkali vs SiO_2 diagram showing that the variation in major elements can be explained by fractionation of the major phases present in the dykes namely: Aegirine(green triangle) and feldspar (purple cross). Aegirine to feldspar fractionation is 10:90. Two microsyenite samples, ST88 and ST226 plot off the general trend but have been observed to be outliers in most analyses. Aeg: Average Straumsvola aegirine, Feld: Normative feldspar as calculated in Table 18. In Figures 42-45 a regression analysis performed in Excel, produced the black line and red squares that define the trend. The alkali-feldspar join (light blue line) was constructed manually.

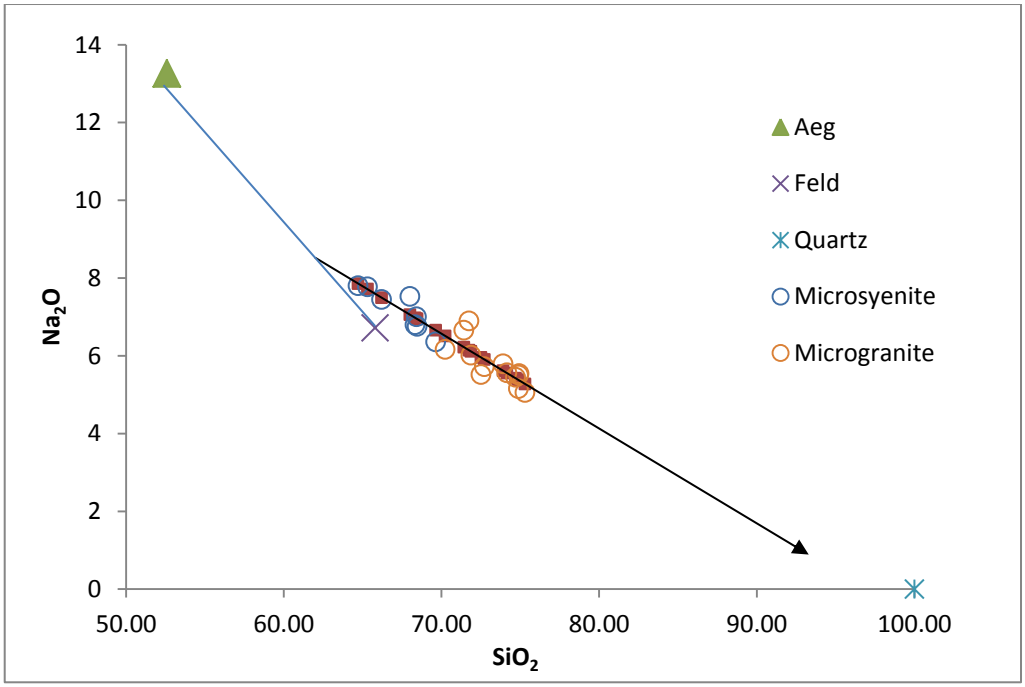

Figure 43: On a Na vs SiO_2 plot, the proportion that the two main phases, aegirine and feldspar, could fractionate is 24:76 respectively.

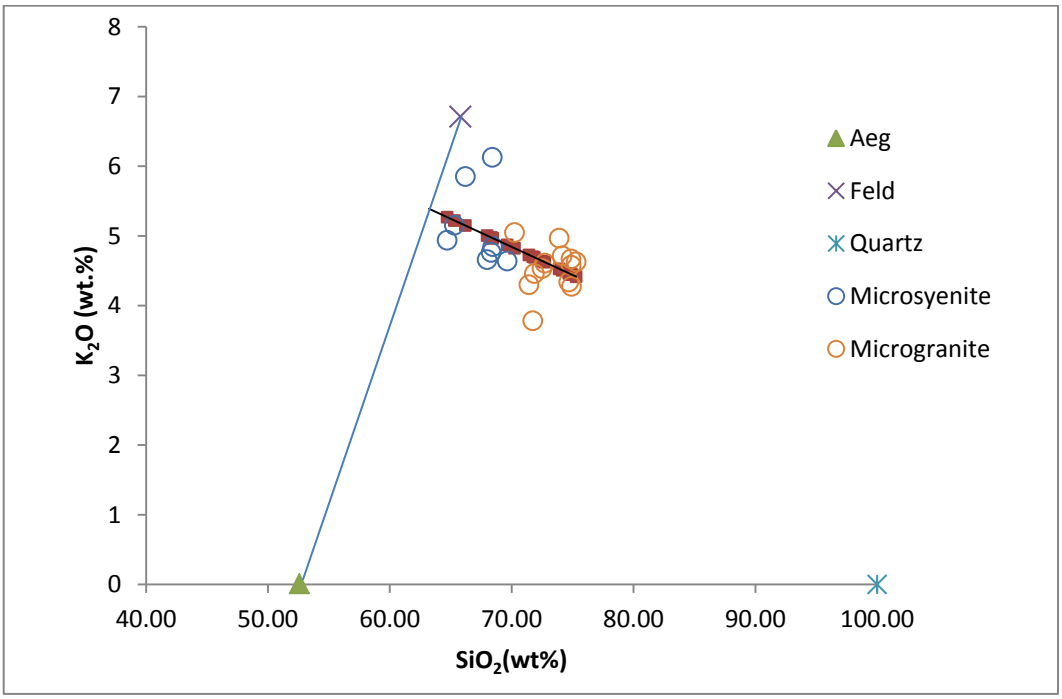

Figure 44: In this diagram the proportion of aegirine to feldspar that could account for the observed variation with SiO_2 is 30:70. Two of the trachyte samples, ST 88 and ST226, plot off the general trend and were not included in the construction of the trend line.

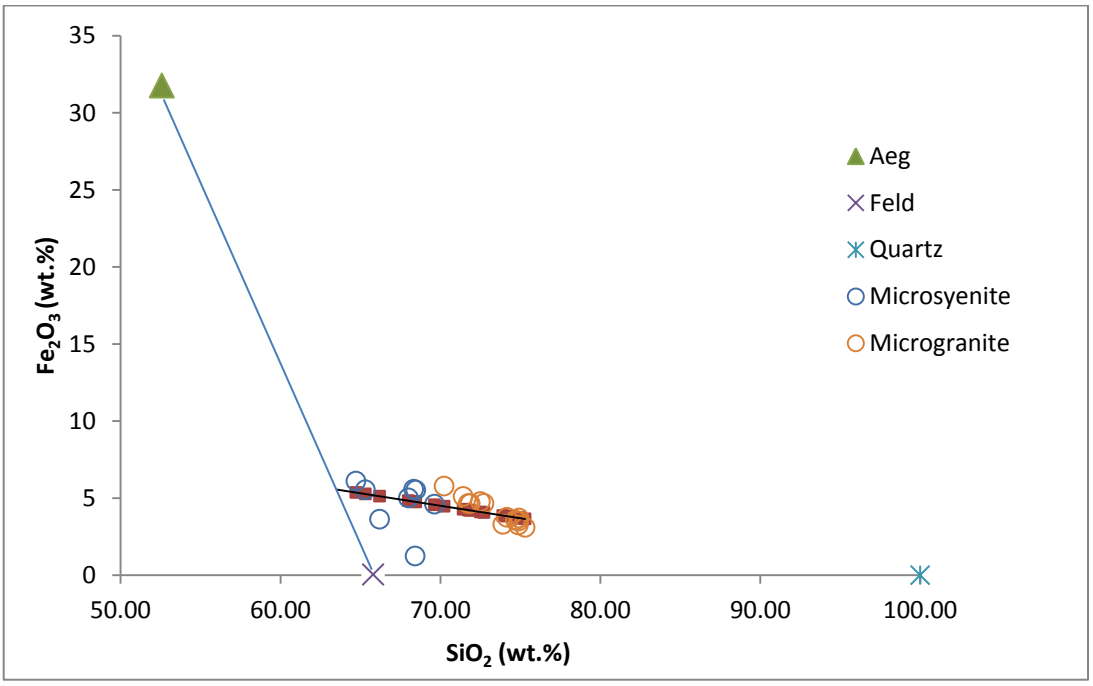

Figure 45: Fe_2O_3 vs SiO_2 shows that fractionation of aegirine and feldspar can produce the changes observed in Fe_2O_3 concentration for the suite of samples. The ratio of aegirine to feldspar is 16:84. Again ST226 and ST88 plot off the general trend and are excluded from the trend line analysis.

5.2. Trace elements

5.2.1. Trace element variation in the dykes

Fractional crystallisation was tested in the previous section using a least-squares approach to model the major elements. It was shown that an evolved rock with a similar composition to ST75 (a strongly peralkaline granite) could be produced from a primitive quartz syenite (ST144) by fractionation of the major phases aegirine and feldspar. If this model is correct then it should be possible to reproduce the observed trace element abundance in the evolved or primitive rock using the proportions calculated in the major element model and by calculating the bulk distribution co-efficient for each rock. The result of this calculation is shown in Table 19. Distribution co-efficients for feldspar in peralkaline trachytes was obtained from the GERM database while those for aegirine were averaged from augite in two quartz syenites from Marks et al. (2004)as no data for aegirine was available on the GERM database. Trace element abundances were modelled using the Rayleigh fractionation equation:

$$\frac{Cl}{Co} = F^{(Di-1)}$$

where:
Co= trace element abundance in the original rock
Cl = trace element abundance in the final rock
Di= Sum of the distribution co-efficients for the element of interest in the major phases
F = Fraction of crystals removed

Table 19 shows that the observed and calculated trace element abundances of the incompatible trace elements (Sr, Ba, Rb, Zr, Y and Nb) agree quite well, despite the calculated abundances being greater than those observed in all instances. The largest difference is observed for Zr which is ~400ppm greater in the calculated rock than actually observed in ST75. This is surprising considering that overall the Straumsvola granites are enriched in Zr, with at least half of the samples having Zr concentrations >300ppm. It has been shown that a few of the dykes contain a Zr-enriched phase (e.g. eudialyte or vlasovite).The effect of these unusual silicates on the composition of the evolving magma will therefore be assessed in the next section.

The Rb concentration is also much lower in granite, ST75 than is predicted by the calculation and is only 3ppm higher than the primitive trachyte, ST144. Marks et al. (2004) noted that "There is a considerable mismatch between calculated melt and whole-rock data for various elements, i.e., Zr, Hf and the HREE, when melt compositions are calculated from $NaFe^{3+}$-rich aegirine–augites and aegirines." They suggested the reasons for these variations were: (1) The evolution of the melt might not be expressed with a single partition co-efficient as the crystallisation history may actually be quite complex. (2) Published distribution co-efficients for alkaline- peralkaline systems do not adequately describe fractionation processes. (3) Whole

rocks do not reflect the melt composition. For the Straumsvola dykes, the petrography shows that the dykes are very fine grained and are likely a close approximation of the final melt composition. It was also shown in the previous section that there are only two major phases fractionating and controlling the chemical evolution of the dyke suite as a whole. We can thus conclude that the likely reason for the differences between the observed and calculated concentrations of the trace elements (according to Marks et al. (2004)) is poor constraints on the distribution co-efficients of elements in strongly alkaline systems. However, the calculation may also suggest that fractional crystallisation is not the only mechanism driving the changes in composition of the peralkaline dykes. This interpretation is supported by the observation in Chapter 4 that there is little variation in the trace element abundances including the incompatible elements (Zr, Rb, Nb) with increasing SiO_2, which is unexpected for an evolving granitic magma. In addition when the incompatible elements Y and Nb are plotted against Zr (Figure 46) they produce non-linear trends that would not be expected in systems undergoing closed system fractional crystallisation. However, when Nb and Ce are plotted against Y (Figure 47), near linear trends (r= 0.73 and 0.8 respectively) are observed suggesting that Zr is responsible for the non-linear array and is therefore not always behaving as an incompatible element as the magma evolves. Zr concentration in these magmas is likely controlled by some other process, most likely the crystallisation of Zr-enriched minerals as the dykes evolve to higher SiO_2.

From the above discussion we can deduce that aegirine and feldspar fractionation depletes the residual magma in the major elements Na, K and Fe but enriches the residual magma in Zr and the incompatible elements (Figures 46 and 47)). These elements most likely behave as incompatible elements until they are taken up by Zr-enriched phases eudialyte, dalyite and vlasovite, at a very late stage in the evolution of the suite.

5.2.2. The effect of the unusual silicates on the composition of the dyke magma

The data of Schilling et al. (2011) presented in Table 7, Chapter 4 shows that eudialyte in oversaturated peralkaline granites is highly enriched in the REE (on average 11% of the total elemental concentration). This is understood to be a result of REE substitution for Ca in eudialyte that has crystallised from Ca-deficient oversaturated peralkaline liquids i.e. the plagioclase effect (Bowen 1945; Harris & Rickard 1987). REE substitution into a late-stage mineral will therefore affect the trace element budget of the residual magma. Similarly Zr is strongly concentrated in eudialyte and the effect of this on the whole rock trace element abundance needs to be evaluated. Table 20 adapted from Schilling et al. (2011) shows the concentration of the REE and Zr in eudialyte from ST38, the peralkaline granite at Straumsvola. It can be seen that while the overall concentration of each trace element in eudialyte is very high (>1wt%) the overall concentration in the whole rock is much less than 1wt% thus the trace element concentration of the whole rock may be strongly controlled by the presence of a small percent of eudialyte. To evaluate this effect a calculation was performed on ST38 using the data of Schilling et al. (2011) (Table 20). It assumes that 100% ZrO_2 in the whole rock (WR) resides in eudialyte (given that zircon does not crystallise in peralkaline melts (Watson 1979)). Based on the number of cations per formula unit

(c.p.f.u) of Zr and the combined REE (Nb, Nd, Ce, Y and La) in eudialyte of ST38, 2.53 and 2.65 c.p.f.u. respectively (Table 7, Chapter 4), it can be deduced that the ratio of the REE and Zr is 1:1. This means that if the Zr concentration in ST38 is due to eudialyte crystallisation only, the REE should have concentrations that are in proportion to this. Table 20 shows the calculated concentrations of the REE in ST38 (if 100% Zr in whole rock ST38 is attributable to eudialyte crystallisation) vs the observed concentrations in ST38 (Harris & Grantham, 1993). The calculation shows that 6.91wt% Zr in average eudialyte, is equivalent to 1.90wt% Zr in whole rock ST38. When this factor is applied to the concentration of the REE in average eudialyte, to determine the calculated concentration of the REE in whole rock ST38, the calculated concentrations are an order of magnitude larger than the observed concentrations (Table 20). The calculation therefore suggests that the proportion of ZrO_2 due to eudialyte crystallisation was overestimated (i.e. not 100%) and hence that it partitions into other phases as well most likely vlasovite, dalyite and aegirine/amphibole.

Overall, zirconium concentration in the suite of dykes show mostly enriched but highly variable values between 70ppm and 1305ppm. There is a poor correlation of Zr with increasing SiO_2 (r=0.26) and little relation exists between the crystallisation of Zr-enriched minerals (eudialyte and vlasovite) and the Zr, SiO_2, total alkalis(TAS) or Ca content of the magma (Figure 46). The only constraint for the presence of these unusual silicates seems to be that the dyke magma must have a SiO_2 content >69wt% i.e. must be granitic and this also suggests that crystallisation of the unusual Zr-silicates occurs at a late stage when the magma is more evolved. It should also be noted that some of the samples with very high Zr concentrations were not associated with samples that showed Zr-bearing minerals e.g. ST 226 and ST76 (which contain narsarsukite, the Na-Ti, etc silicate). Other Zr-bearing phases must therefore exist but perhaps due to the size of the thin section vs the whole rock, they were not observed. Another alternative is that dalyite is present in these samples (as in ST38 and ST39) but given the very fine-grain size of the matrix it may have been misidentified as quartz. Dalyite is known to fluoresce under cathodoluminescence (CL) but due to time constraints the thin sections could not be tested via this method for the presence of dalyite. Finally Zr might also be present in aegirine, although in very low abundance (ZrO_2<0.5wt%) as can be seen in the microprobe analysis of ST217 in Table 6 of Chapter 4.

To conclude, trace element abundances of the samples tested by the least squares model, confirms that the dykes are consistent with a fractional crystallisation model based on the major elements. However, the calculations also suggest that there is another process causing the concentration of the trace elements tested to be lower than expected. Zr was particularly affected and it was shown to not always behave as an incompatible element in the dykes. Rather it was taken up by the rare Zr-silicates eudialyte, dalyite and vlasovite and possibly also aegirine/amphibole. The late stage nature of these silicates may therefore explain the lower than expected concentrations of the REE. It does not, however, explain the lower Sr, Ba and Rb concentrations observed in ST75 and suggests that an additional process is affecting the dykes or that there is considerable uncertainty in the model.

Variables		ST144 (obs)	ST75 (obs)	ST75 (calc)	D_{Aeg}	D_{Afld}	Bulk D
F= 0.6	**Sr**	27	**6.9**	**15.8**	1.0	2.3	2.1
Aeg*= 20	**Ba**	4	**5.0**	**7.6**	2.8	3.4	3.3
Fdsp*= 80	**Rb**	265	**268.1**	**357.7**	0.8	0.3	0.4
	Y	43	**59.4**	**63.5**	1.2	0.0	0.2
	Zr	710	**778**	**1087.3**	0.8	0.0	0.2
	Nb	72	**96.0**	**119**	0.1	0.0	0.0

Table 19: Observed (obs) vs calculated (calc) trace element abundances for the evolved granite, ST75, using the Rayleigh fractionation equation. Distribution co-efficients for aegirine (aeg)were obtained from the average of two aegirines in quartz syenite from Marks et al. (2004) while those for feldspar (Fdsp) were obtained from the GERM reference database. F = Fraction of crystals removed. Aeg*/Fdsp*= Normalised proportion of aegirine/feldspar from the major element regression model in Table 17.

	ZrO_2 (wt%)		Ce_2O_3 (wt%)	Y_2O_3 (wt%)	Nb_2O_5 (wt%)	La_2O_3 (wt%)	Nd_2O_3 (wt%)	
ST38_EGM1	9.03		4.13	1.12	3.7	2.22	1.2	
ST38_EGM2	9.47		3.79	1.08	3.06	1.91	1.29	
ST38_EGM3	9.32		3.92	1.06	3.62	1.93	1.28	
ST38_EGM4	9.53		3.73	1.43	3.25	1.87	1.28	
average	**9.34**		**3.89**	**1.17**	3.41	1.98	1.26	
C.F.	0.740		0.854	0.787	0.699	0.853	0.857	
wt%	**Zr**		**Ce**	**Y**	**Nb**	**La**	**Nd**	
elemental eud wt%	**6.910**		3.324	0.922	2.382	1.690	1.082	
$ST38_{WR}$	**0.131**							
REE sum								**9.401**
WR C.F.	=(0.131/6.910)*100	**1.90%**						
WR calculated								**0.17862**
WR observed			0.0072	0.0061	0.0108	0.0038	0.0031	**0.03104**

Table 20: The average concentration of Zr and the REE in 4 ST 38 eudialytes(Eud) (as measured by Schilling et al. (2011)) is compared to the overall concentration in whole rock (WR), ST38 (the peralkaline granite of Harris & Grantham. (1993)) to determine whether the concentration of these elements in whole rock, ST38, can be explained by eudialyte crystallisation alone. An oxide conversion factor (C.F) was applied to each element to convert the oxides to elemental concentration in wt%. The concentration of Zr in eudialyte was then taken to represent 100% of the Zr concentration in whole rock ST38 and found to represent 1.90 wt% of ST38. This value represents the whole rock(WR) conversion factor which was applied to the total REE concentration(REE sum) assuming a 1:1 ratio between Zr and the REE. This gave the calculated REE concentration in whole rock ST 38 (WR calculated). The results are compared with the observed concentrations in ST38 (whole rock observed) and it can be seen that the calculated concentration is an order of magnitude larger than the observed. Therefore not all Zr in ST38 can be explained by eudialyte crystallisation alone.

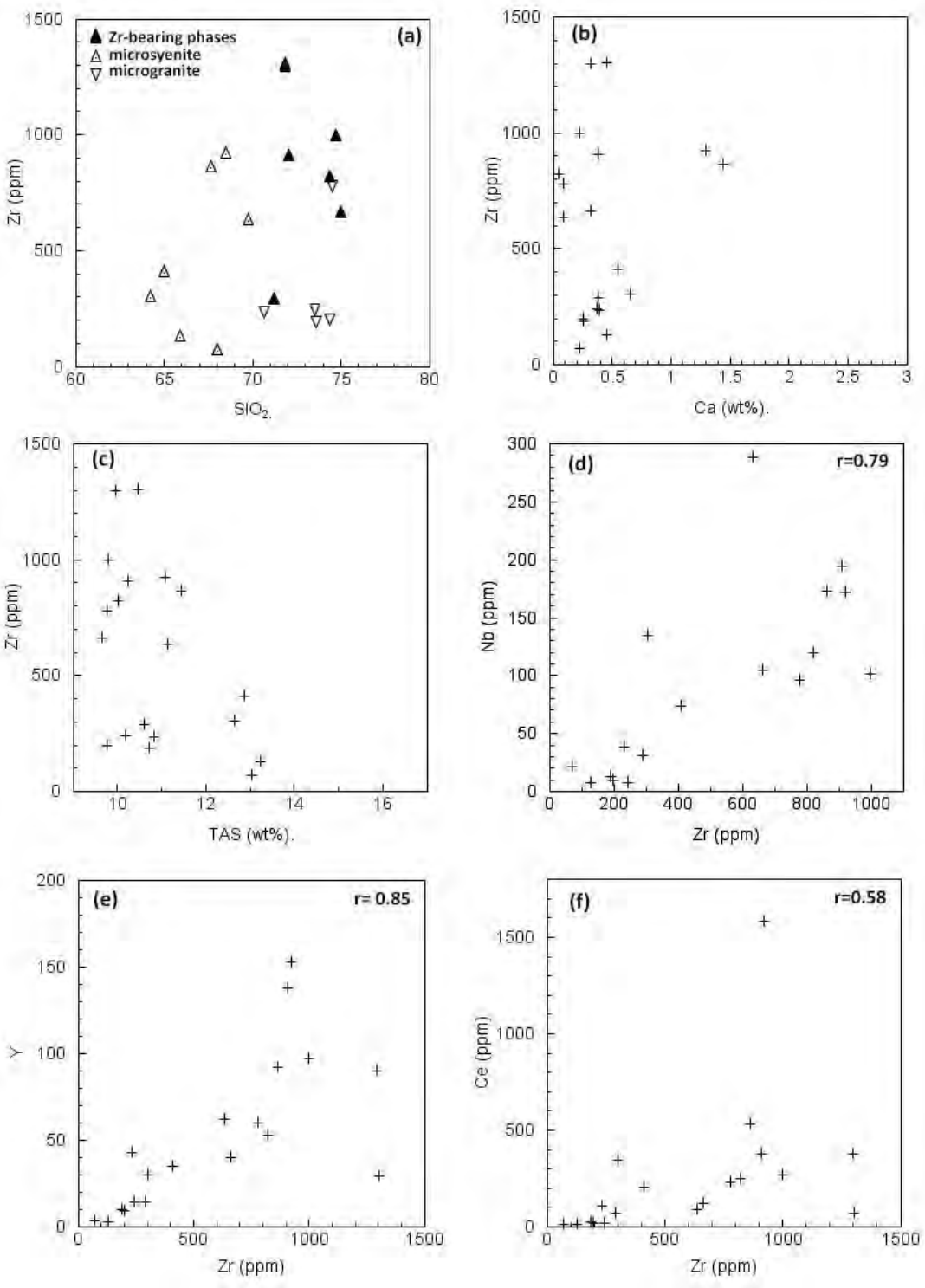

Figure 46: a) Zr-bearing phases are only observed in dykes with a granitic composition. There is poor correlation between Zr and the major elements, Ca (b) or K+Na (TAS) in (c). (d-f) Zr vs the incompatible elements Nb, Ce and Y show positive correlations but non-linear patterns at high concentration.

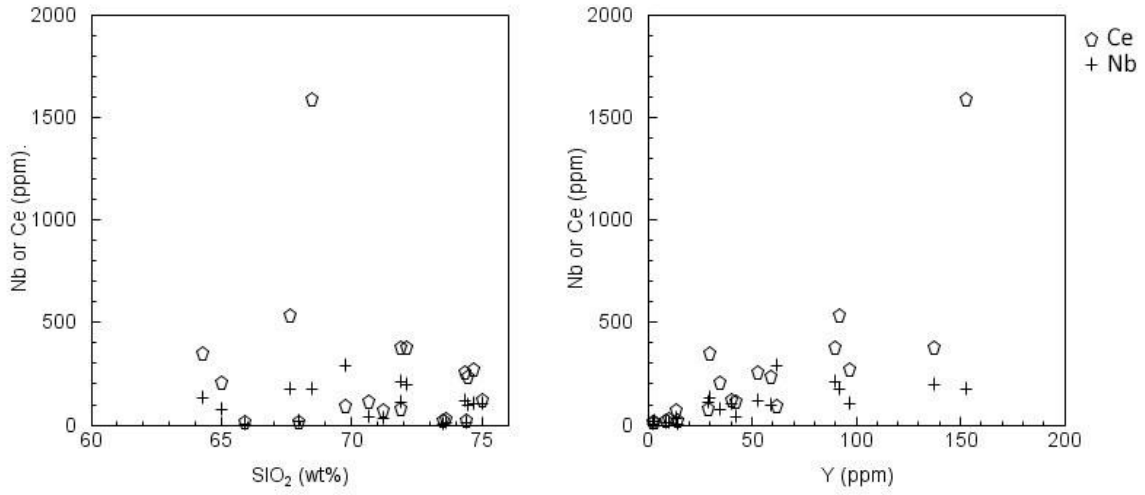

Figure 47: a) Nb and Ce show little correlation with SiO_2. b) Nb and Ce both show positive correlations with Y, r= 0.73(Nb) and 0.8 (Ce), respectively

5.3. The REE

Whole rock REE profiles for the suite of dykes shows an interesting association between the least evolved and most evolved dykes. The least evolved dykes have the highest REE concentrations decreasing as the dykes evolve to higher SiO_2. Four granites have REE concentrations well below the average for the suite of dykes. They are FL2, STFL1A, STFL1B and ST84, which also contain at least one unusual mineral: eudialyte (in ST84) or vlasovite. It is unusual that ST84, the eudialyte-bearing granite, forms part of this group and it is likely due to undersampling of the eudialyte rich portion of the rock than this representing the true pattern. These samples define a new group of dykes that will be discussed further throughout this chapter and referred to as the granite outliers. An upturn of the HREE was also identified as a common feature of the REE profiles for the Straumsvola dykes. In the previous chapter this was suggested to indicate that a HREE-enriched mineral is yet to fractionate out of the magma. This mineral is most likely eudialyte, which is known to concentrate REE in Ca-deficient magmas (Harris & Rickard (1987)). Zircon can also concentrate HREE but it is known from the petrography to be absent in these rocks.

REE profiles for the Straumsvola nepheline syenites in the previous chapter showed that nepheline syenites from the layered, inner zone have the same REE pattern as the majority of the dykes including the upturned HREE pattern. This suggests that the Straumsvola dykes and nepheline syenite magmas are related. This relationship will be evaluated further using the radiogenic isotope data later in this chapter. In addition when the outlier dykes are not considered, it can be seen in the REE plot of Figure 48 that fractional crystallisation of a phonolite magma that has crossed the thermal divide could produce all of the Straumsvola peralkaline microsyenites and the majority of the microgranite dykes.

The gneisses are an unlikely source of the dyke magma due to the lack of alkalis and a Eu anomaly (observed in all the dyke samples) but they are suitable as a crustal contaminant. The gneisses of the contact zone tend to show the HREE- enriched pattern observed in the granites and nepheline syenites (ST 241, Figure 37) and are thus likely inheriting this signature from the intruding nepheline syenite.

5.3.1. The significance of eudialyte

Late stage, magmatic eudialyte is common in the peralkaline granite dykes at Straumsvola (samples: ST38, ST39, ST84 and ST246), but is unusual in granites elsewhere in the world. The only other locality where eudialyte has been found in peralkaline granite is at Ascension Island, a composite volcano in the South Atlantic Ocean (Harris 1983).

The island is almost completely igneous composed mostly of basaltic lavas, pyroclastics and associated plutonic inclusions that include peralkaline granite blocks (Harris 1983). The granite blocks are mineralogically very similar to those at Straumsvola composed predominantly of quartz, feldspar (90%) and mafic minerals aegirine and arvedsonite (Harris 1983). Texturally however, the granite at Ascension is much coarser-grained (Harris 1983) while at Straumsvola the dykes have a very fine-grained matrix. At both localities eudialyte is seen to grow near and along aegirine grains as a product of late-stage crystallisation. Other rare accessories (dalyite and vlasovite) are also present within the Ascension granites (Harris 1983).

A Chondrite normalised whole rock REE profile for the eudialyte-bearing, Ascension Island granite is shown with the Straumsvola dykes and the REE profile of eudialyte from a peralkaline granite at Straumsvola (after Schilling et al. (2011) (Figure 48). As noted previously eudialyte is extremely enriched in the LREE and on average has REE concentrations 2 orders of magnitude greater than the whole rock. The whole rock REE plot for the Ascension Island granite lies within the range of the Straumsvola dyke suite but within the less evolved i.e. microsyenitic portion of the diagram. It should be noted here that Sheppard & Harris (1985) showed that the least evolved lavas (basalt and hawaiite)of Ascension Island were able to produce the eudialyte granite magma by fractional crystallisation at low pressures (Sheppard & Harris 1985). Since Ascension Island has experienced no crustal contamination it thus also represents the granitic end-member of a fractional crystallisation trend of a mantle-derived magma. This suggests that the process that drives the dykes of the Straumsvola Complex to higher SiO_2 also lowers the REE concentration. It is known that the Straumsvola Complex was intruded into basement gneisses and so crustal input is suspected. This may also explain why the incompatible elements especially Rb show poor correlations with SiO_2.

Given the similarities in the whole rock REE patterns for Straumsvola and Ascension, it is possible that the least evolved Straumsvola dykes could have been produced from a mantle-derived parental magma that underwent extensive fractional crystallisation. However, some crustal input is required to account for the most evolved granites especially the granite outliers.

A strong Eu anomaly in eudialyte, as seen in the Straumsvola eudialyte, was interpreted by Schilling et al. (2011) to represent derivation from an alkali-basaltic parent. While the parental magma to the Straumsvola dykes may be alkali-basalt, the oxygen isotope ratios are far too high to represent purely mantle-derived melts (see next section). The results of this study hence show that Eu anomalies in eudialyte from peralkaline granites are not only produced by pure fractional crystallisation of mantle-derived magmas.

5.4. Oxygen Isotope constraints on magmatic evolution at Straumsvola

The range in $\delta^{18}O$ quartz of the mineral separates is narrow between 8.36‰ and 9.15‰ (Figure 49) with only the granite outliers having quartz $\delta^{18}O$ values >8.6‰ (with the exception of STFL1A and ST212*). There is no observable correlation between the $\delta^{18}O$ of quartz separates and the whole rock SiO_2 and Fe_2O_3 contents (Figure 49) other than the data clustering in narrow bands at SiO_2: 74-76wt% and Fe_2O_3 :3-4wt%, (r= -0.38). In all plots the granite outlier samples form a separate grouping at high quartz $\delta^{18}O$. A plot of Zr vs quartz $\delta^{18}O$ shows these outlier samples to have low Zr concentration <200ppm while the majority of samples have Zr concentrations >600ppm (Figure 50). Quartz $\delta^{18}O$ vs. Rb shows a less striking difference but does show a granite outlier group with constant Rb concentration ~255ppm vs. the remainder of samples that have Rb concentrations ranging between 250 and 300ppm. Sr shows the reverse pattern with the granite outliers having constant but higher Sr than the majority of samples. The data is consistent with a late stage fluid that has remobilised the trace elements Zr, Rb and Sr of the granite outlier dykes and crystallised quartz with the highest $\delta^{18}O$ ratios observed in this study.

Overall, the relatively narrow range in quartz $\delta^{18}O$ values of the mineral separates (8.36‰ - 9.15‰) is indicative of closed system behaviour and a common origin for all of the dykes. A key point is that the quartz $\delta^{18}O$ values of the dykes are all > 8‰. This is much higher than would be expected for a mantle derived magma that has undergone closed system fractional crystallisation. This is shown graphically in Figure 51 where the peralkaline Straumsvola granites are compared with the mantle-derived Ascension Island peralkaline granites (quartz $\delta^{18}O$= 7.2‰) after the data of Sheppard & Harris (1985).

**ST212 is described by C. Harris as a granite sill in field notes. This sample was previously analysed by XRF in 1993 but only a powder remained for analysis in this study in 2013. There is no thin section or whole rock available to determine if it contains any unusual silicates hence it is not included as a granite outlier dyke despite having a quartz $\delta^{18}O$ ratio> 8.6‰.*

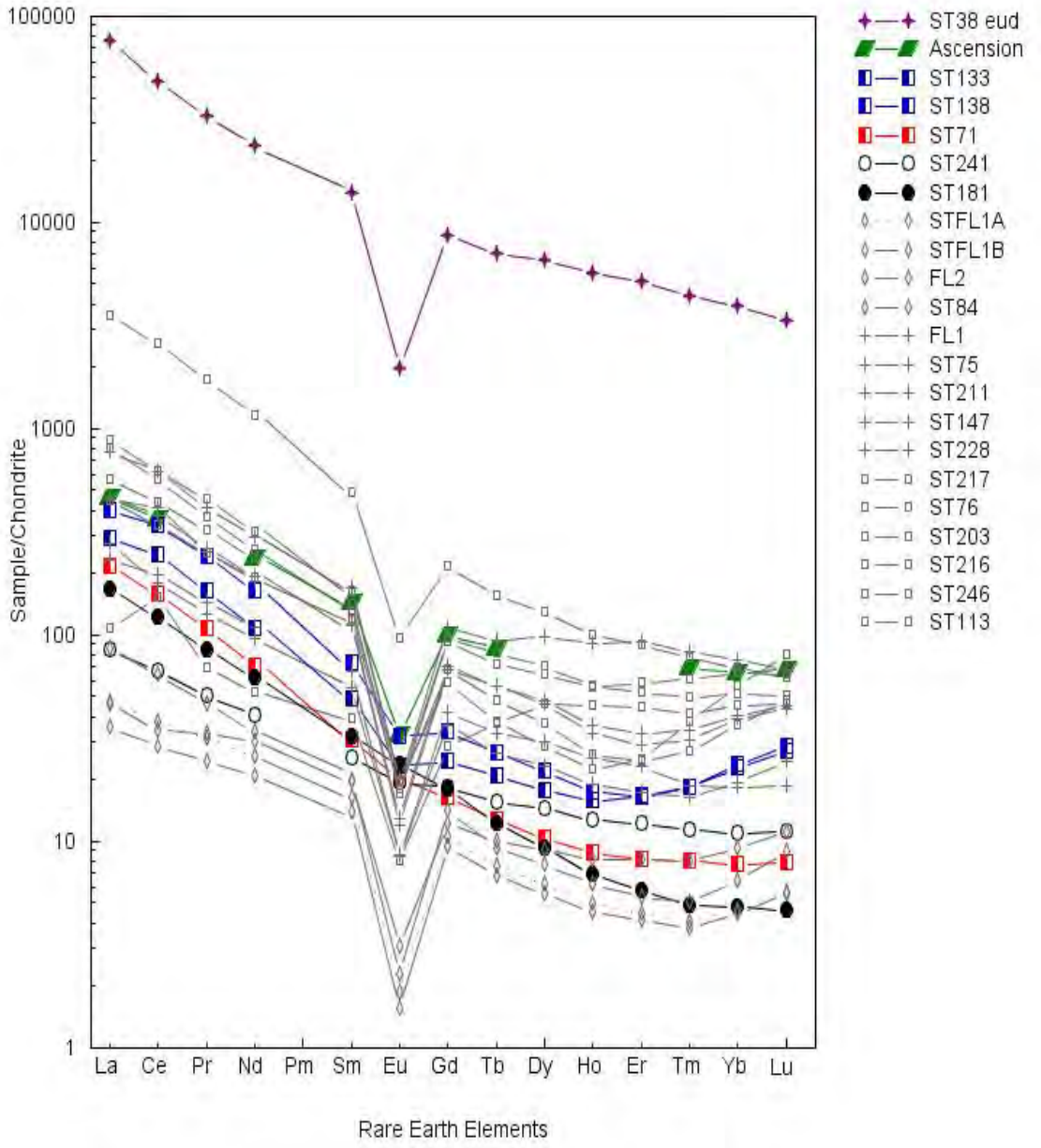

Figure 48: Chondrite-normalised REE plots for the Straumsvola dykes, ST38 eudialyte and Ascension Island granite. Straumsvola magmatic eudialyte, ST38, is shown at the top and is extremely enriched. The whole rock REE profile for the Ascension peralkaline, eudialyte-granite is shown in green. Data for the Middle- to Heavy REE is unavailable for this sample. Rock types in the Straumsvola Complex are: Straumsvola nepheline syenites (blue); the outer zone nepheline syenite at Storgeon (red); a contact zone gneiss (open black circle), regional gneiss (filled black circle) and peralkaline dykes (grey). Four samples: FL2, STFL1A/B and ST84 form outliers at the lowest REE concentration (grey diamonds).

Aegirine separates from the same samples were also measured for their $\delta^{18}O$ value. They show a narrow range from 4.80 to 5.15‰ and can be seen plotted against quartz $\delta^{18}O$ in Figure 52. Also shown on this diagram are lines of constant difference between quartz and aegirine with temperatures calculated from the fractionation equations of Zhao & Zheng (2003) The dykes concentrate around a ΔQtz-Aeg fractionation factor of 3.5 which corresponds to a temperature of formation estimated at 500°C. These temperatures are generally considered to be sub-solidus for this magma composition and suggests that aegirine in these dykes did not crystallise at magmatic temperatures. Rather is it likely that they have experienced some post crystallisation re-equilibration. This agrees with the petrography that shows aegirines with poikilitic cores suggestive of sub solidus crystallisation. The granite outliers are once again visible at quartz $\delta^{18}O$>8.6‰ . These samples while generally clustering with the majority of samples can be seen to plot just off the trend and are indicative of even lower temperature equilibration possibly as a result of the passage of an alteration fluid.

At Straumsvola the only exposed crustal rocks are the country rock gneisses. Whole rock $\delta^{18}O$ values for the gneisses of Dronning Maud Land is shown in Figure 53. The majority of the samples have whole rock $\delta^{18}O$ values between 7 and 9‰, with an average value of 7.3‰ (Johnstone, 2000). This is indistinguishable from the dykes which also have an average $\delta^{18}O$ whole rock = 7.3‰. Quartz separates from the country rock gneisses have an average $\delta^{18}O$ of 7.6‰, this value for the gneisses is 1‰ lower than the average quartz $\delta^{18}O$ of the dykes (8.64‰). However the quartz $\delta^{18}O$ of the dykes is not the $\delta^{18}O$ of the magma the dykes would have crystallised from. The magma $\delta^{18}O$ value can be estimated from the Δquartz-rhyolite value of Zhao & Zheng (2003) and Bindeman (2008). These $\Delta^{18}O_{\text{quartz-rhyolite}}$ are 0.77‰ and 0.4‰ respectively and averages out to $\Delta^{18}O_{\text{quartz-rhyolite}}$=0.6‰. The average Straumsvola dyke magma would then have a $\delta^{18}O_{\text{melt}}$= 8.04‰, which is 0.7‰ higher than the average whole rock $\delta^{18}O$ of the regional gneisses. It should also be noted that the dykes selected for oxygen isotopic analysis are all granitic in composition and therefore the most evolved. It can be assumed then that the quartz syenites would have quartz $\delta^{18}O$ values ~8‰ (assuming they are related to the granites by fractional crystallisation). In this case, the syenites would have crystallised from a melt with a $\delta^{18}O_{\text{melt}}$= 7.4‰ which is very comparable with the whole rock $\delta^{18}O$ of the country rock gneiss ($\delta^{18}O$ =7.3‰).

When the oxygen isotope ratios of the granites, gneisses and nepheline syenites of this study are compared it becomes clear that the granites have the highest oxygen isotope ratios, much higher than even the regional gneisses. Only one gneiss, ST241 from the contact zone, has a quartz $\delta^{18}O$ ratio that is similar to the granites ($\delta^{18}O$= 8.4‰) (Table 10), which suggests that the oxygen isotope signature of the dykes is related to the local gneisses and is in agreement with the whole rock data for the regional gneisses. The cause of the high $\delta^{18}O$ values i.e. $\delta^{18}O$ >8.7‰ in a few of the granites is more difficult to explain and in the absence of other evidence must be related to fractional crystallisation of a small portion of the very last granite magma. This last magma is likely the 'granite outlier' magma identified in the REE plots as these dykes all have $\delta^{18}O$ values >8.6‰ (except for STFL1A, $\delta^{18}O$=8.4‰ and ST212) . That these dykes have also

crystallised at least one unusual silicate is suggestive of a magma in which conditions were only favourable for vlasovite and narsarsukite crystallisation once the magma had evolved sufficiently i.e. SiO_2 >69wt%. Zircon is known to be unstable in peralkaline magmas (Watson 1979) and so the Zr-silicate, vlasovite, crystallises as the very last products of the highly evolved FL1 and FL2 magmas. It is unclear why STFL1A and STFL1B crystallise narsarsukite over vlasovite or eudialyte but another peralkaline granite, ST76, has a Zr concentration >900ppm and also crystallises narsarsukite and no other Zr-silicate phases. It seems therefore that the presence of these late stage silicates is highly dependent on the conditions of the individual magmas from which they crystallise.

5.5. Radiogenic Isotopes

In the previous chapter comparison plots of the radiogenic isotopes revealed that the nepheline syenites and peralkaline dykes overlap in ε_{Nd} and form positive trends on Pb isotope plots. A petrogenetic relationship between the dykes and nepheline syenites is therefore suspected. The gneisses of the contact zone (ST241 and ST242) also show similarities in their isotopic ratios with the dykes and nepheline syenites and suggest that they were affected by intrusion of the nepheline syenite. In addition gneisses further from the contact zone at 171 Ma have an average initial $^{87}Sr/^{86}Sr$ ratio = 0.726736 (n=3), much higher than the average for the contact zone gneisses, initial $^{87}Sr/^{86}Sr$ = 0.709626 (n=2). Homogenisation of the Sr isotopic composition by the intruding nepheline syenite would require extensive remobilisation of Rb possibly via an aqueous fluid. Intrusion of the nepheline syenite could potentially produce the heat necessary to create such a fluid. Petrographically there is evidence to suggest that an alteration fluid exists. It is evident that the pyroxenes in the gneisses close to the contact zone have been fenitised by a Na-rich alteration fluid (Harris & Grantham, 1993). This is visible as green rims on pyroxene as seen in Chapter 2 and replacement to aegirine. The alteration fluid appears to have affected a zone >500m from the contact zone as replacement to Na-rich pyroxene is still observed in the gneisses even at these distances. Initial $^{143}Nd/^{144}Nd$ isotopic ratios at 171Ma of the fenitised gneisses at the contact zone are on average = 0.511598 while the average for the surrounding country rocks is <0.510803 (n=3). There is a clear division of initial $^{143}Nd/^{144}Nd$ on the comparison plots in Chapter 4, which also shows the overlap in the initial $^{143}Nd/^{144}Nd$ of a nepheline syenite and contact zone gneiss, ST241. This together with the similarities in initial $^{87}Sr/^{86}Sr$ between the contact zone gneisses and the nepheline syenites confirms that the nepheline syenite intrusion provided the heat to circulate an alteration fluid and is also likely the source of the alteration fluid.

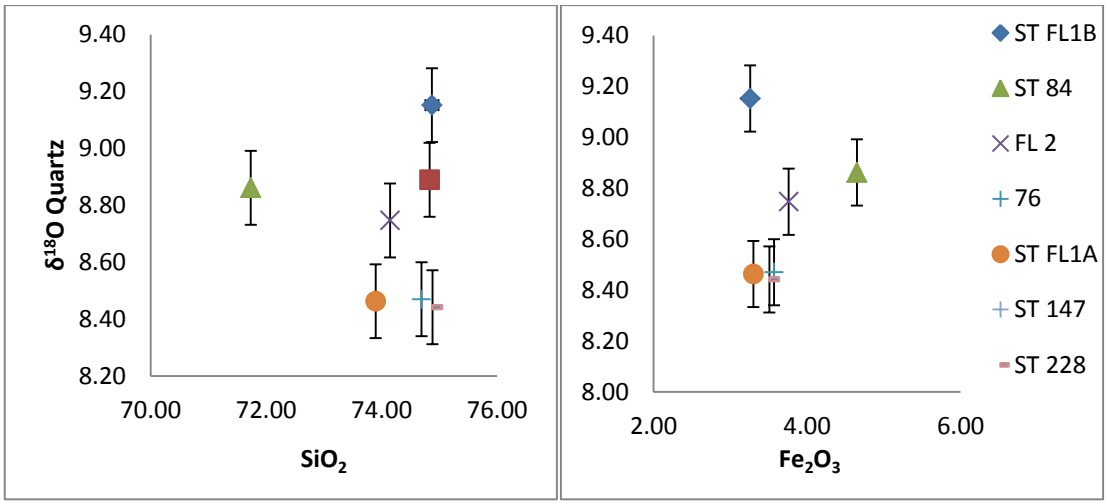

Figure 49: $\delta^{18}O$ of quartz separates vs SiO_2 and Fe_2O_3. Error bars are equal to the long term average error on the MON-GT garnet standard of 0.13‰

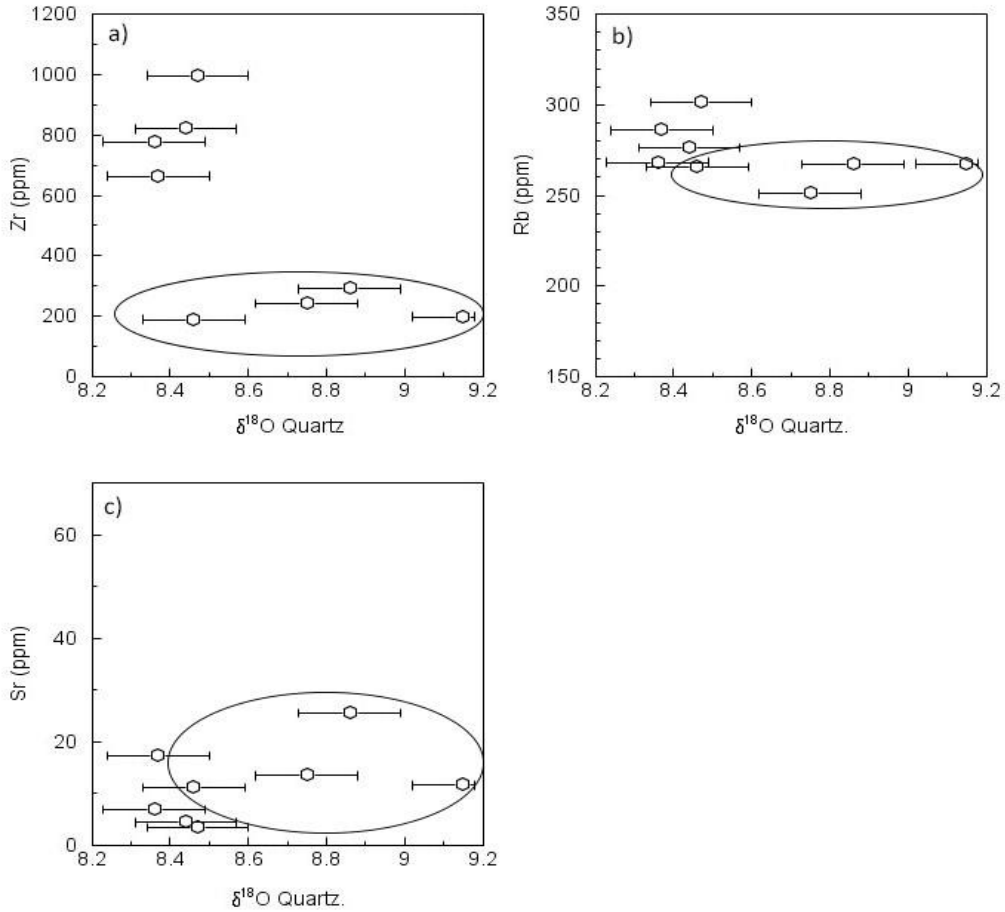

Figure 50: (a-c)Zr, Rb and Sr vs $\delta^{18}O$ Quartz. The samples with lower Zr, Rb and Sr concentrations are known to be the granite outliers (grey ellipses). Error bars are equal to the long term average error on the MON-GT garnet standard of 0.13‰

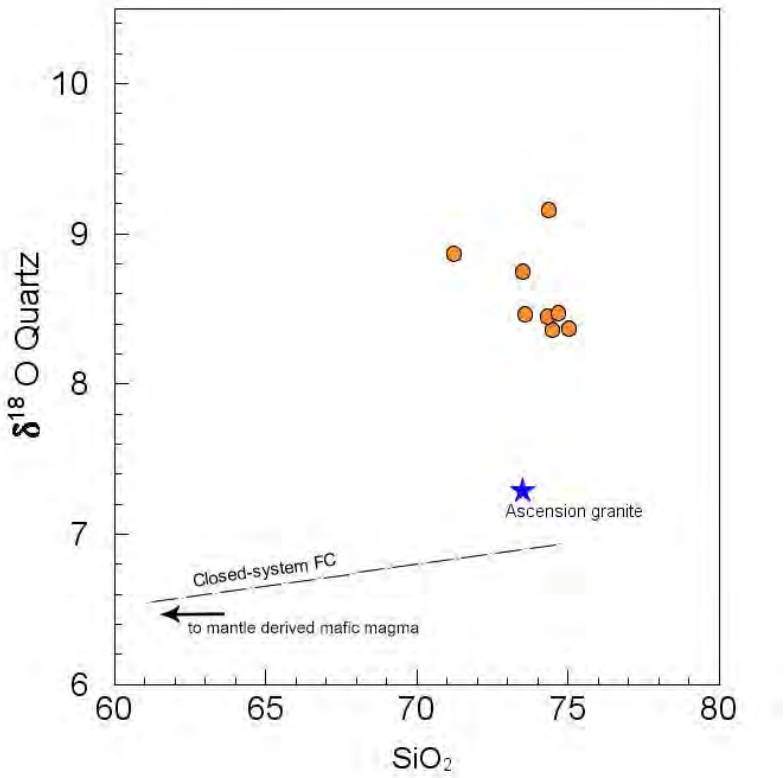

Figure 51: Quartz $\delta^{18}O$ vs SiO_2 showing closed-system fractional crystallisation of the mantle-derived Ascension Island magmas. Highlighted in blue is the average quartz $\delta^{18}O$ of Ascension peralkaline granite. The Straumsvola granites (orange) plot to more positive $\delta^{18}O$ values. Figure modified from Sheppard & Harris(1985)

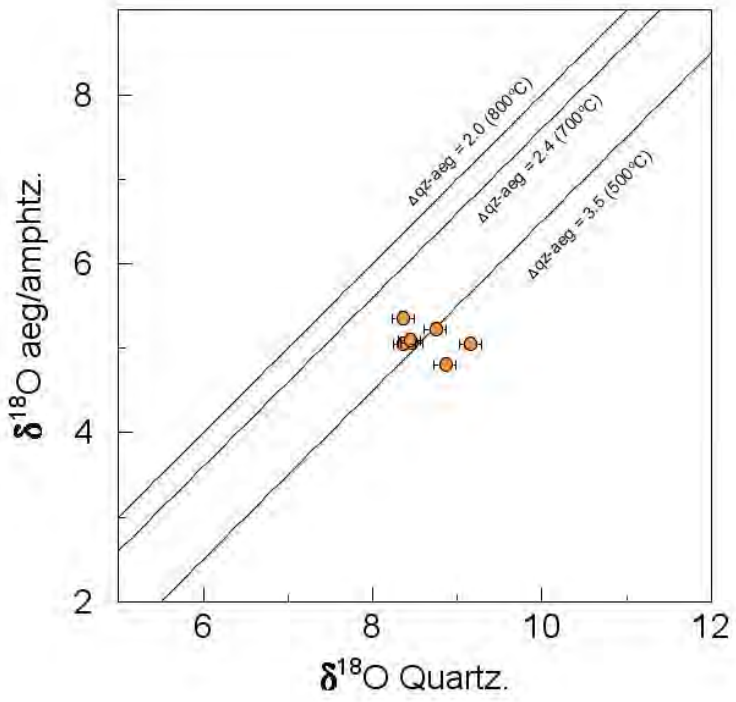

Figure 52: Quartz $\delta^{18}O$ vs. aegirine $\delta^{18}O$ of the Straumsvola granites. Lines of constant temperature are calculated using the fractionation equations of Zhao & Zheng (2003). The dyke samples fall closest to the fractionation trend representing aegirine crystallisation temperatures of 500C. A few of the dyke samples to higher $\delta^{18}O$ fall off the trend and equilibrated at even lower temperatures. These samples are all granite outliers.

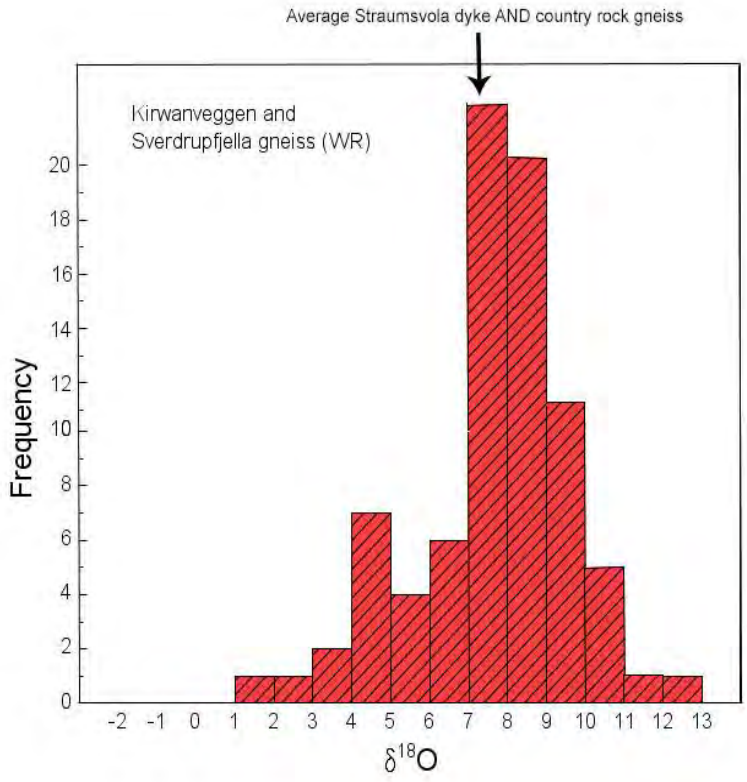

Figure 53: Whole rock $\delta^{18}O$ values for the gneisses of Dronning Maud Land. The majority of samples tend toward whole rock $\delta^{18}O$ values between 7 and 9‰, with an average value of 7.3‰ (Johnstone (2000)- unpublished data). Figure adapted from Johnstone (2001), unpublished MSc Thesis.

A Rb-Sr isochron for the suite of dykes (excluding outliers identified in Chapter 4) based on the data presented in Table 14, Chapter 4 is shown in Figures 54 and 55. Using the program *Isoplot 4.1* (Ludwig 2003) a line of best fit through the data was constructed that took the errors associated with each ratio into account. The error on the $^{87}Rb/^{86}Sr$ ratio was calculated assuming the maximum accepted analytical errors for routine quadrupole ICP-MS i.e. $2\sigma = 3\%$. The percent relative standard deviation of the measured trace element concentration data was hence adjusted for this ('Final RSD' Table 14, Chapter 4). The maximum error was applied as the samples had not been specifically selected for age-dating and given that the majority of samples had very low Sr concentrations resulting in very large Rb/Sr ratios. However, despite this the slope of the best fit line calculated by Isoplot gave an age of 171 ±4.4 Ma. This age matches that of a late stage phonolite dyke identified by Curtis et al. 2008 that produced a whole rock $^{40}Ar/^{39}Ar$ =170.93±1.67 Ma. The errors on the line of best fit were approximated using a Mean Square Weighted Deviation (MSWD) and calculated to be 18. This is quite high but is to be expected given that the samples were not prepared specifically for dating. The data points themselves (with the exception of three points) plot on or very close to the predicted isochron so it can be said that the samples were likely derived from the same magma which had an initial ratio equal to the y-intercept of Figure 54b i.e. = 0.70750 ±0.0032. This value is higher than would be expected from a purely mantle-derived magma and suggests there has been some input from the

crust, but it should be noted that the error in the initial ratio is large. The samples that do not plot on the isochron had very high $^{87}Rb/^{86}Sr$ ratios (Figure 54) which is likely due to the error on low Sr concentrations being greater than the error based on counting statistics.

Figure 55 is an inset of Figure 54b in which the gneisses and nepheline syenites (at 171Ma) are also plotted with the Rb-Sr isochron calculated for the dykes. The gneisses plot at the least radiogenic Sr values but around the initial $^{87}Sr/^{86}Sr$ ratio calculated for the suite of dykes. The nepheline syenites plot to slightly higher $^{87}Sr/^{86}Sr$ values than the gneisses and can be seen to plot along the same isochron as the dykes. This may suggest that they are derived from a similar source as the dykes but given that at least one nepheline syenite sample plots near the initial $^{87/86}Sr$ ratio calculated for the dykes, the nepheline syenites could potentially also be the source of the dyke magma.

A similar isochron was calculated for the dykes in the Sm-Nd system and shown in Figure 56. Two populations become evident in this figure; a group with higher $^{143}Nd/^{144}Nd$ and another (that contains the majority of samples) at lower $^{143}Nd/^{144}Nd$. The lack of correlation is due to the young age of these rocks (~170Ma) which in the Sm-Nd system have had very little time to produce Nd by radioactive decay of Sm, t½ = 106Ga. This is further evidenced by the irrational age = -46 ±360 Ma calculated by *Isoplot 4.1*. The calculated initial $^{143}Nd/^{144}Nd$ ratio for the dykes suite is 0.51197±0.00028, which is very similar to the initial ratios calculated for the individual dyke samples but given the poor correlation cannot represent the true initial ratio of the original magma. The two populations suggest derivation from different magmas but on consideration of the samples that define the enriched portion it was found that the samples to lower initial $^{143}Nd/^{144}Nd$ are all Group 2 quartz syenites that have experienced some alteration, while the samples with the highest $^{143}Nd/^{144}Nd$ are ST226 and STFL1B, which contain narsarsukite and vlasovite, respectively and have been outliers in other graphs. Therefore the samples that fall within the high $^{143}Nd/^{144}Nd$ portion are not representative of the dykes. The dykes that define the lower $^{143}Nd/^{144}Nd$ portion are host to the majority of the samples and thus reflect the true isotopic characteristics of the suite, which have an initial $^{143/144}Nd$ ratio ~0.51190.

The $^{143}Nd/^{144}Nd$ vs $^{147}Sm/^{144}Nd$ ratios of the dyke samples in Figure 56 are compared with the gneisses and nepheline syenites in Figure 57. It can be seen that one nepheline syenite, ST 133, plots within the area of the majority of the dykes to lower ratios while another two nepheline syenites plot to higher ratios. The gneisses have the lowest ratios and plot to the most unradiogenic values consistent with their being continental crust. Gneiss samples, ST 241 and ST 242 however, plot closest to the dykes and nepheline syenite and have the highest $^{143}Nd/^{144}Nd$ ratios of the gneisses. This supports the suggestion that the gneisses have been affected by intrusion of the nepheline syenite.

The REE plots and radiogenic isotope data are ambiguous as to the source of the granite dyke magma with both the nepheline syenite and country rock gneisses as possible parental melts. The dykes tend to plot with the nepheline syenites in most diagrams but oxygen isotope data are consistent with the dykes being derived by melting of the gneisses. The gneisses at the

very least must be responsible for the elevated quartz $\delta^{18}O$ of the Straumsvola dykes, which are on average 2‰ higher than the mantle- derived Ascension Island granites.

The origin of the dykes can be further evaluated using the plot of ε_{Nd} vs initial $^{86}Sr/^{87}Sr$ ratios (Figure 58). None of the data (Straumsvola granite dyke, nepheline syenite or gneiss) plot in the upper left, depleted mantle portion of the diagram. Nepheline syenite, ST138, is the most primitive sample in this dataset (ε_{Nd} = -2) and therefore is assumed to be the closest in composition to the original magma. The strongly negative ε_{Nd} (=-12) and enriched initial $^{87}Sr/^{86}Sr$ ratios (at 171Ma) of the Straumsvola dyke is consistent with the presence of a crustal component. Nepheline syenite, ST133 from the layered zone, has εNd values similar to the dykes (ε_{Nd} =-10) but lies midway between the regional gneisses and ST138. It may thus represent a nepheline syenite that has already experienced some crustal contamination. This interpretation is supported by the isotopic composition of the contact zone gneisses, which plot directly below the layered zone syenite to lower values of ε_{Nd}. The remainder of the gneisses have even lower ε_{Nd} and enriched $^{87}Sr/^{86}Sr$ values characteristic of continental crust. Since the dykes lie midway between the most primitive nepheline syenite and the regional gneisses, the exact nature of the source is difficult to constrain. Both the nepheline syenite and gneiss are probably involved in the genesis of the dyke magma at Straumsvola.

The initial $^{87}Sr/^{86}Sr$ ratios of the gneisses is constant with distance from the contact zone (Figure 59) and suggests that the gneisses have indeed experienced remobilisation of Sr as a result of the nepheline syenite intrusion at least up to 500m from the contact with the nepheline syenite. This is consistent with the presence of an alteration fluid. Nd is less obviously affected (Figure 59b) as it is not affected by fluids to the same extent as Rb and Sr. Hence only the gneisses at the contact zone show any effect of alteration in the initial $^{143}Nd/^{144}Nd$ ratio.

Most of the data shown above is consistent with the nepheline syenite from the mafic zone representing the most primitive mantle-like magma while that from the layered zone has been affected by some interaction with the crust. The most likely contaminant is the regional gneisses given their low ε_{Nd} values and given that the gneisses at the contact zone overlap in initial $^{143}Nd/^{144}Nd$ with the layered zone nepheline syenite. Nepheline syenite, ST133, has ε_{Nd} and initial $^{87}Sr/^{86}Sr$ ratios that overlap with the dykes providing a possible source for the dyke magma. However, it still requires a mechanism to cross the thermal divide.

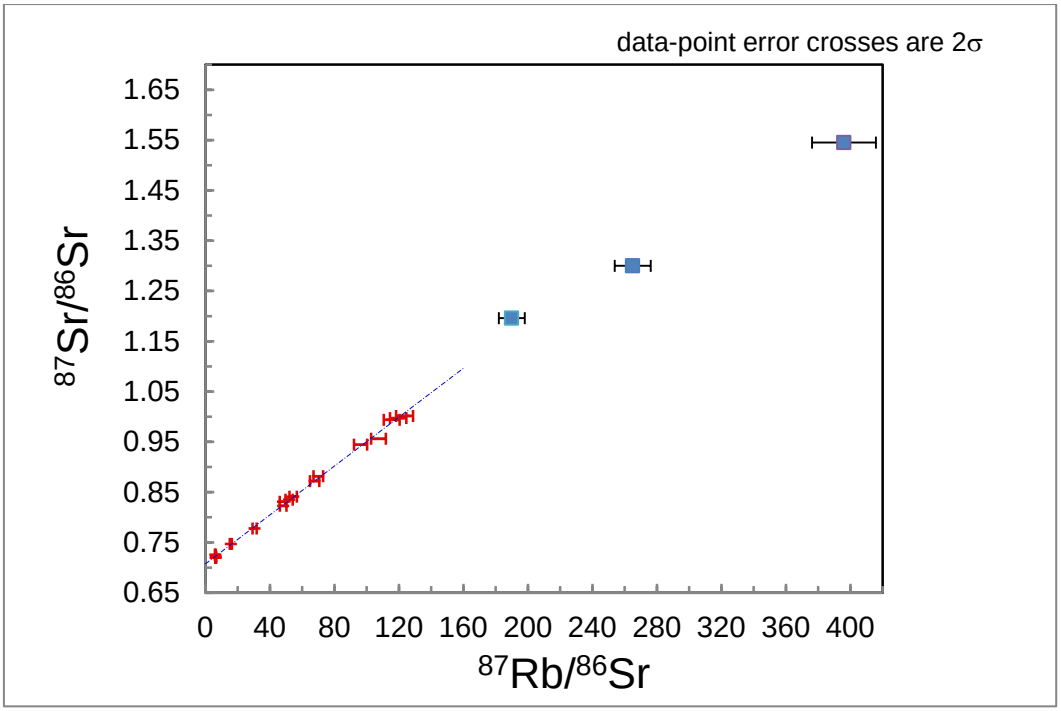

Figure 54 a: Rb-Sr isochron for the Straumsvola dykes. The isochron was calculated using *Isoplot 4.1*. Three of the dykes (blue squares) have very high $^{87}Rb/^{86}Sr$ ratios and do not fall on the isochron.

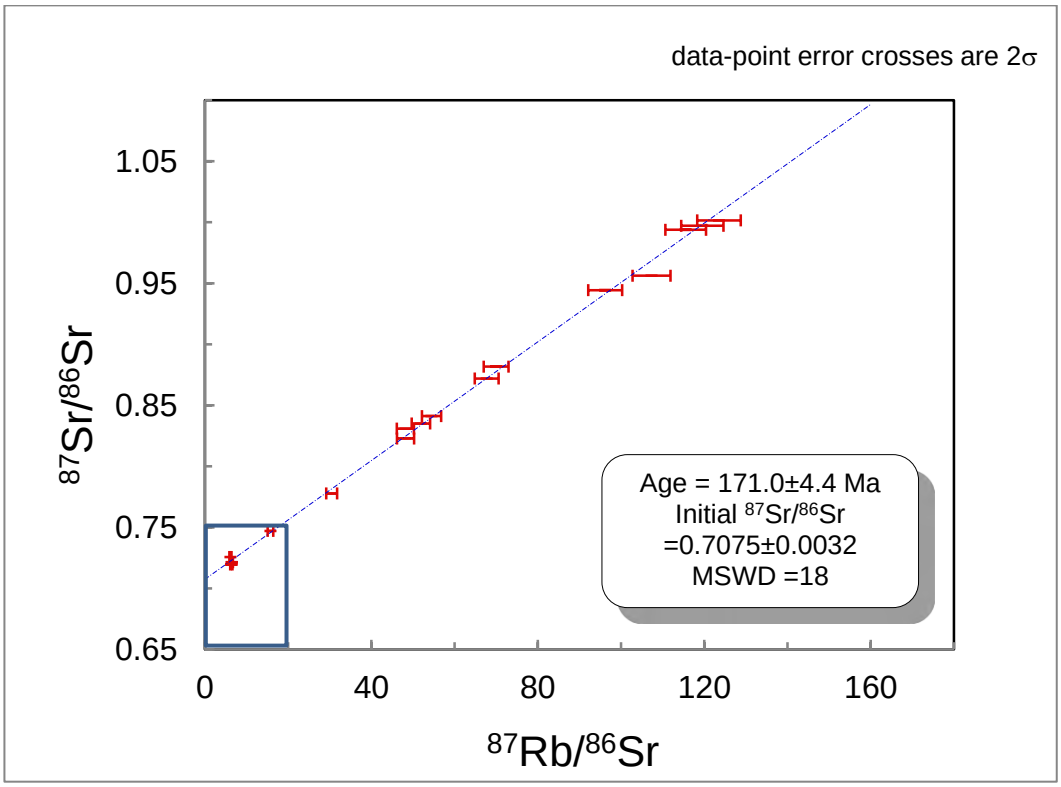

Figure 54b: Rb-Sr isochron for the Straumsvola dykes with $^{87}Rb/^{86}Sr$ <150. The data all plot on the isochron calculated using *Isoplot 4.1*. The blue inset is reproduced in Figure 55c.

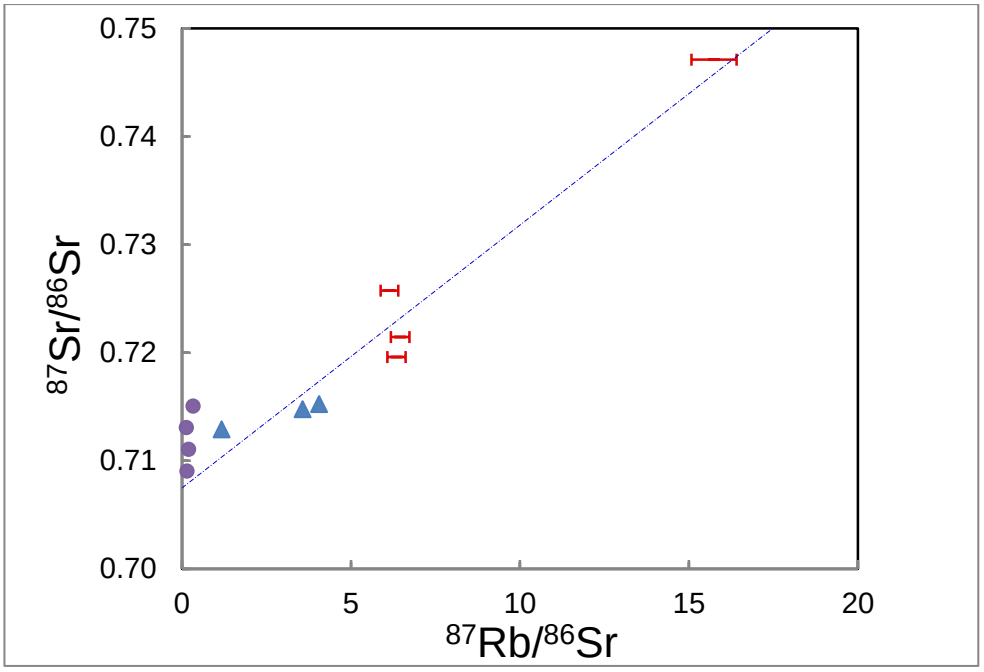

Figure 55: Inset from Figure 54b with the nepheline syenites (blue triangles) and the gneisses (purple circles) superimposed on the Rb-Sr isochron of the dykes (red). The gneisses and nepheline syenite plot to low $^{87}Rb/^{86}Sr$ and have low initial $^{87}Sr/^{86}Sr$ ratios. They also have initial $^{87}Sr/^{86}Sr$ ratios (at 171Ma) very similar to the initial $^{87}Sr/^{86}Sr$ ratio of the original dyke magma as calculated by *Isoplot* and are hence both possible sources.

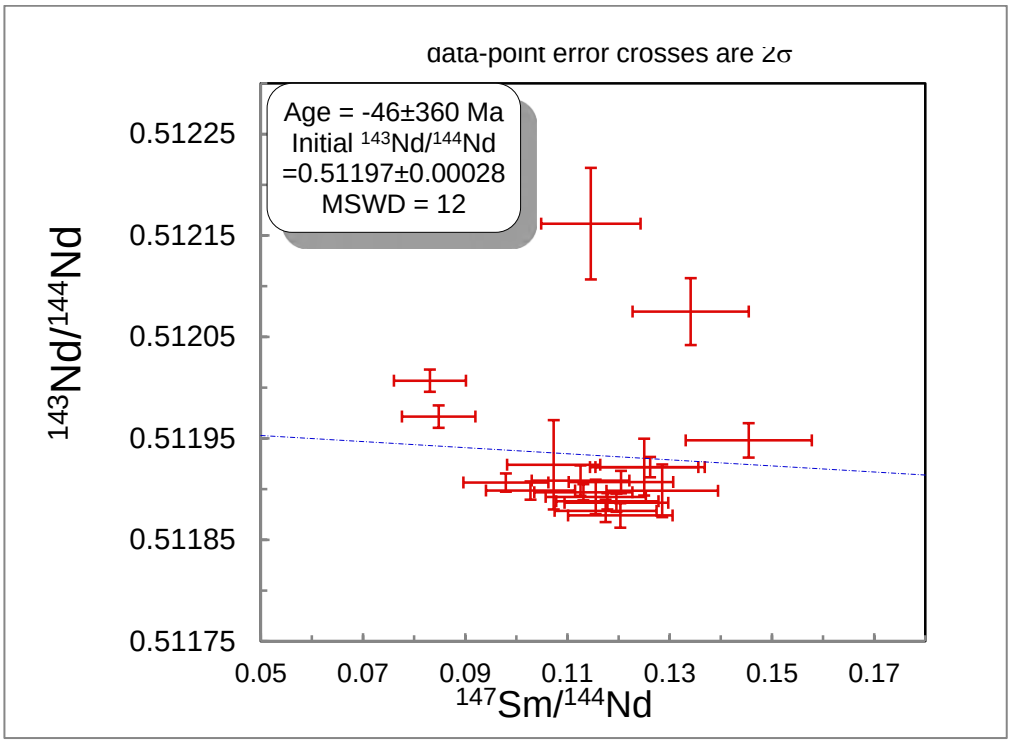

Figure 56: $^{143}Nd/^{144}Nd$ vs $^{147}Sm/^{144}Nd$ ratios of the dykes. The dykes do not plot on an isochron and therefore the age and initial ratio of the dyke suite as determined by *Isoplot 4.1* is not relevant. Two groups, high and low $^{143}Nd/^{144}Nd$, are visible but are related to the dyke samples that fall in these portions (see text). The majority of the samples have an initial $^{143}/^{144}Nd$ ratio ~0.51190. The two samples with the most enriched compositions are ST226 and STFL1B, which have each crystallised at least one Zr-silicate and plot in the 'enriched portion' at the highest initial $^{143}Nd/^{144}Nd$.

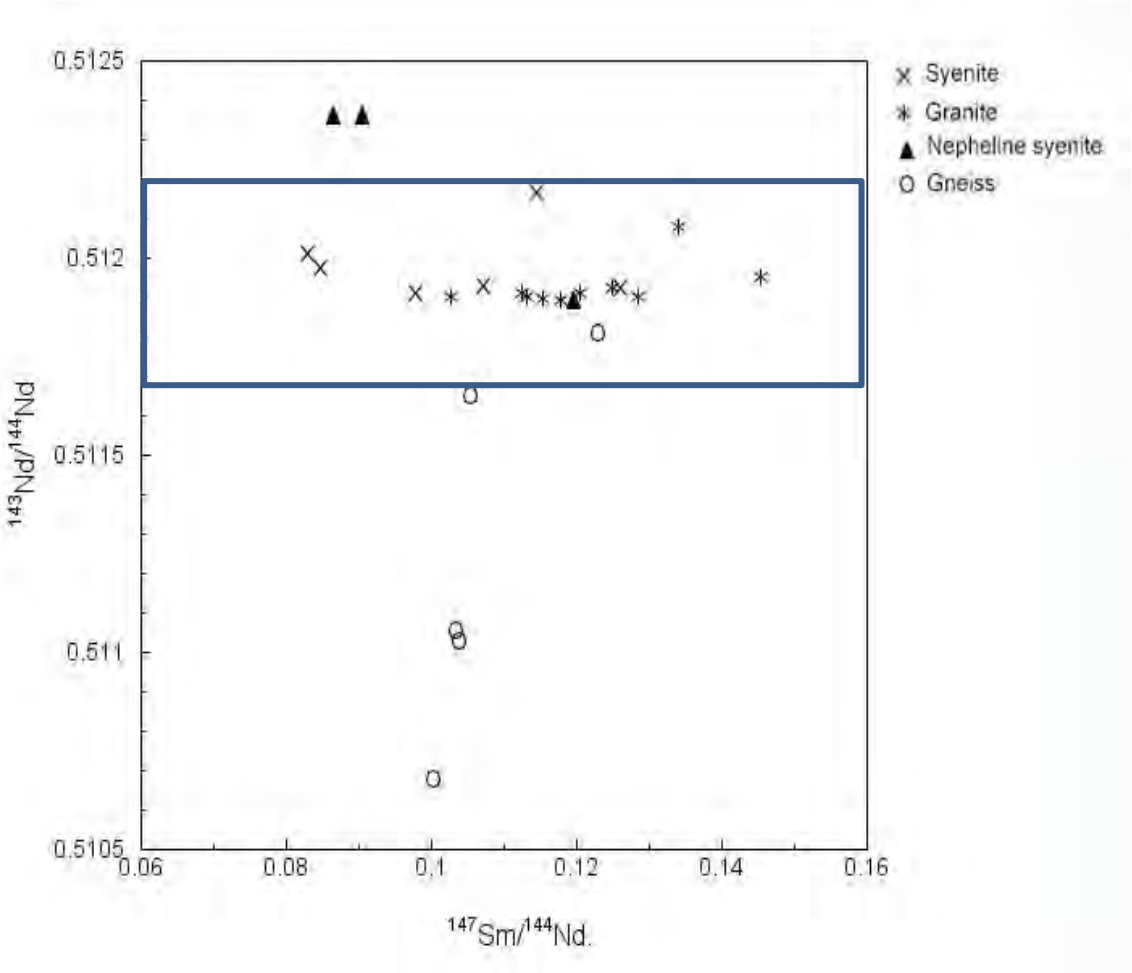

Figure 57: Plot of measured $^{143/144}$Nd vs ^{147}Sm/^{144}Nd for the dykes, gneisses and nepheline syenites in the study. The blue inset represents the range in ^{147}Sm/^{144}Nd shown in Figure 55.The gneisses are the least radiogenic with only the contact zone gneisses plotting close to the dykes. They thus represent the crustal end members for the rocks of this study, becoming less radiogenic with distance from the contact zone. One Nepheline syenite, ST 133, plots with the dykes while two others have higher ^{143}Nd/^{144}Nd forming the most primitive magmas in the suite. The dykes lie midway between the primitive nepheline syenites and crustal gneisses with the least evolved samples (trachytes) also generally having lower ^{147}Sm/^{144}Nd ratios.

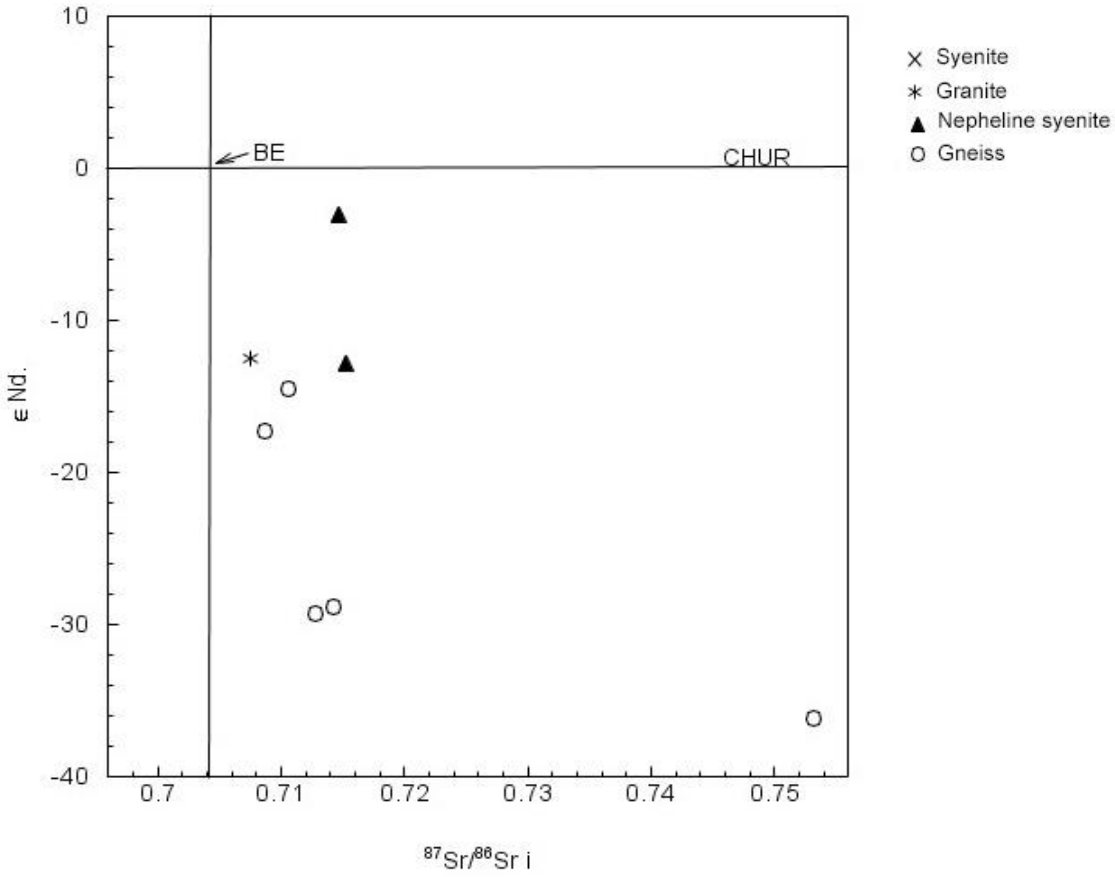

Figure 58: ε_{Nd} vs initial $^{87}Sr/^{86}Sr$ at 171Ma. A Straumsvola dyke with an initial $^{87}Sr/^{86}Sr = 0.7075$ (from the isochron) and the average εNd (=-12) is shown with the nepheline syenites and gneisses relative to the Bulk Silicate Earth (BSE) and a Chondrite Uniform Reservoir (CHUR). None of the samples have $\varepsilon Nd > 0$ indicating that none are direct melts of MORB-type magmas while one nepheline syenite, ST138, has $\varepsilon Nd = -3$ and represents the most primitive sample in this study.

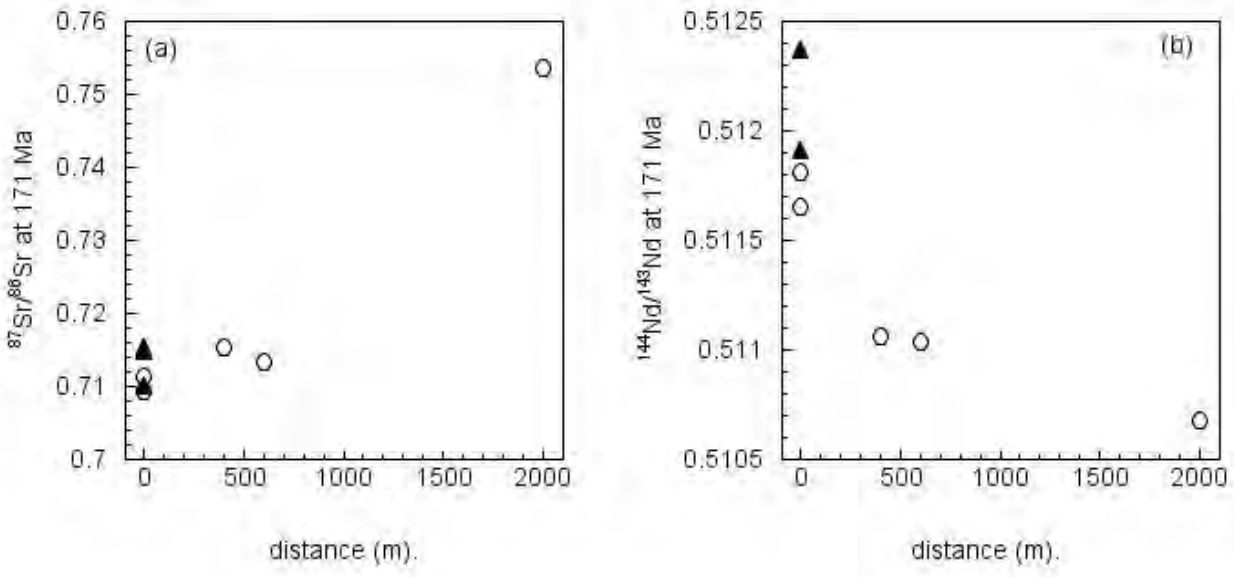

Figure 59: The initial ratios of the gneisses for both Sr(a) and Nd(b) increase and decrease respectively with distance from the contact with the nepheline syenite. Sr remobilisation is evident for the dyke samples up to 500m.

5.5.1. Pb Isotopes

In general the concentration of Pb in the nepheline syenites is < 8ppm while the gneisses and dykes have higher concentrations with two dykes containing 48ppm Pb (Table 16, Chapter 4). The Pb data for this study was compared with that from Heinonen et al (2010), who looked at the isotopic composition of mafic dykes from Vestfjella, WDML Antarctica to determine the mantle origins of the Karoo LIP in Southern Africa and Antarctica.

The following comparison plots were adapted from the figures presented in Heinonen (2010). The fields identified by Heinonen et al. (2010) as possible mantle sources include: South-west Indian Ridge Mid Ocean Ridge Basalt (MORB), Depleted Mantle, Gondwana Subcontinental Lithospheric Mantle and a broad field of Karoo CFB's with a lithosphere-signature. It is important to indicate here that the Pb data of Heinonen et al. (2010) was age –corrected to180 Ma unlike the data presented in this study. However, as explained in Chapter 4, the young age of the dykes makes it unlikely that there will be a significant change in the Pb isotope ratios. Nevertheless the Pb data of Heinonen et al. (2010) is used in this study only to highlight the potential mantle reservoirs from which the Straumsvola dykes could have been derived. The boundaries of these sources are also likely subject to large errors so the Straumsvola dykes are only analysed here in the broadest sense to see if there are any common features between the dykes and any of the mantle sources identified by Heinonen et al. (2010).

Figure 60 is a comparison plot of ε_{Nd} vs $^{206}Pb/^{204}Pb$ modified from Heinonen et al.(2010). The dykes plot within an area represented by Gondwana Subcontinental Lithospheric Mantle indicating that they are affected by much deeper lithosphere than originally thought in this study and may suggest that the gneisses are not the only possible source of crustal contaminant. The gneisses further from the contact zone do however, have more negative ε_{Nd} and remain a possible source for the dyke magma. The two nepheline syenites from Straumsvola have more radiogenic Pb but fall outside of any field identified by Heinonen et al. (2010). ST138 from the mafic zone, plots near the end-member of a fractional crystallisation trend identified by Heinonen et al. (2010) that tracks a depleted Vestfjella ferropicrite from the depleted mantle to the lower crust (Red outline in Figure 60).This agrees well with the mafic nature of ST138 and its primitive isotopic signature, and supports the interpretation of Harris & Grantham (1993) that ST138 is a separate intrusion to the Straumsvola nepheline syenite magmas at Straumsvola. The contact zone gneisses plot near the layered zone nepheline syenite in ε_{Nd} but share the same $^{206}Pb/^{204}Pb$ ratios as the rest of the gneisses. We can infer from this that the Pb isotopic composition of the gneisses has been unaffected by intrusion of the nepheline syenite.

A plot of $^{207}Pb/^{204}Pb$ vs $^{206}Pb/^{204}Pb$ as in Figure 61 shows a positive data array from the dykes through the nepheline syenites and the gneisses as seen in the previous chapter. The majority of the dykes and nepheline syenites, ST71 (outer zone) and ST138 (mafic zone), fall in the field for SW Indian Ridge MORB. This would imply derivation of the dykes from a depleted

mantle source. Nepheline syenite, ST133, plots just outside of any field for mantle with a lithosphere-signature but is known from its ε_{Nd} to be crustally contaminated. The contact zone gneisses plot at the edge of the field for SW Indian Ridge MORB and appear to form an endmember at enriched $^{207}Pb/^{204}Pb$ and $^{206}Pb/^{204}Pb$.

Figure 62, a $^{208}Pb/^{204}Pb$ vs $^{206}Pb/^{204}Pb$ plot for all the samples of this study, shows a similar positive array as the previous $^{207}Pb/^{204}Pb$ vs $^{206}Pb/^{204}Pb$ plot. The majority of the dykes and one nepheline syenite now fall within the field for mantle-derived Karoo CFB's that have interacted with the lithosphere while the other two nepheline syenites, a few of the dykes and the majority of the gneisses fall outside of any field identified by Heinonen et al. (2010).

The data presented above seem to suggest that all the dykes in this study and at least one nepheline syenite share isotopic characteristics of mantle-derived Karoo CFB's that have interacted with a proposed Karoo lithosphere. The dykes show a compositional and isotopic trend from higher to lower Pb as the suite evolves from syenite to granite. It remains unclear on the basis of the Pb isotopic data presented here whether the source is derived from the country rock gneiss or the nepheline syenite or a combination of the two. However, the gneissic samples that fall nearest the dykes in all plots are from the contact zone and have been affected by intrusion of the nepheline syenite. The Pb data might hence support a mechanism in which both the nepheline syenite and the gneiss play a role in the genesis of the dyke magma. One gneiss sample, ST264, is an outlier in all the Pb plots. Given that it is not the furthest sample from the contact zone it has likely experienced some contamination during the analytical process and will therefore not be considered further.

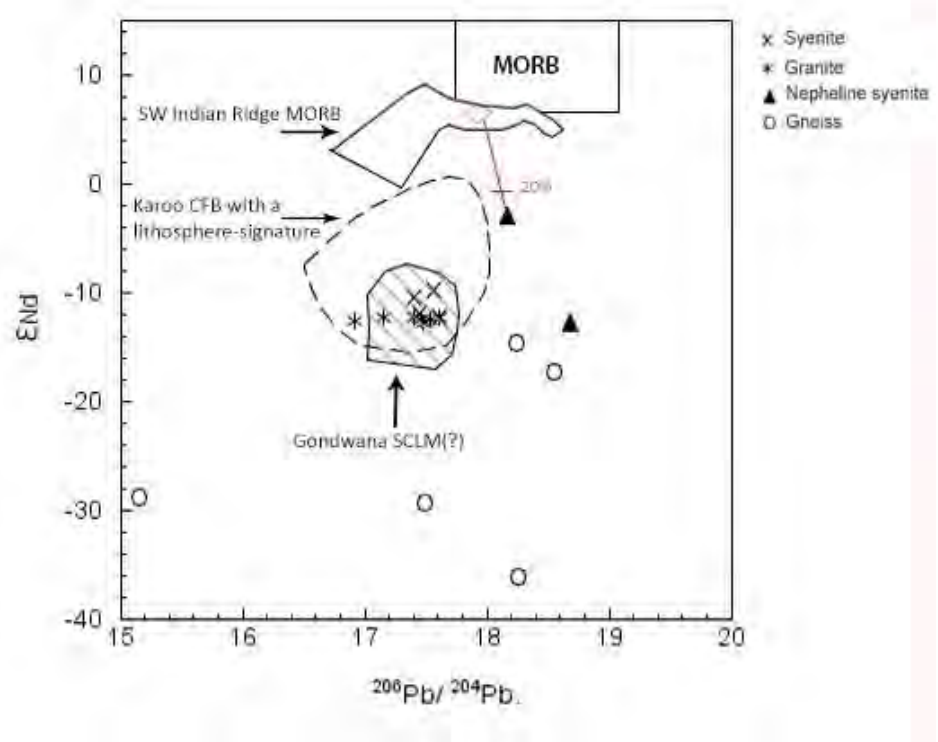

Figure 60: Microsyenites and granites of the study fall within the fields identified by Heinonen et al. (2010) of Karoo CFBs with a lithosphere-signature but also Gondwana Subcontinental Lithospheric Mantle. ST138 from the mafic zone plots near the endmember of a Vestfjella basalt fractional crystallisation trend identified by Heinonen et al.(2010) that interacts with the lower crust (highlighted in red) and confirms it is the most primitive sample in this dataset. The gneisses and nepheline syenites have very similar Pb ratios overall.

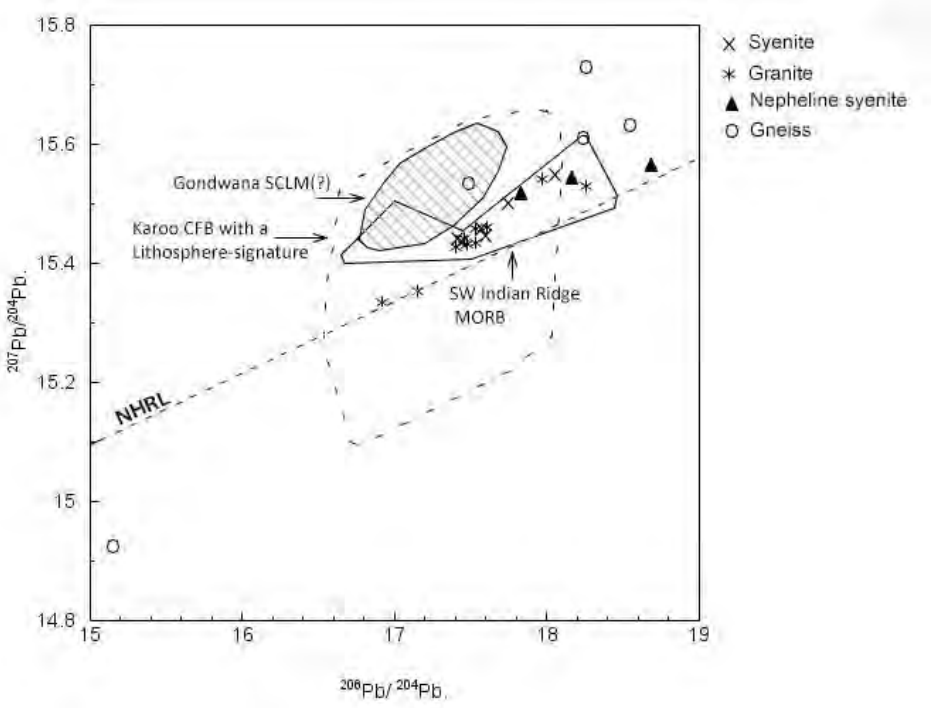

Figure 61: The majority of the dyke samples plot in the field for mantle with SW Indian Ridge MORB characterisitcs and more generally within the field of Karoo CFB's with a lithosphere-signature.

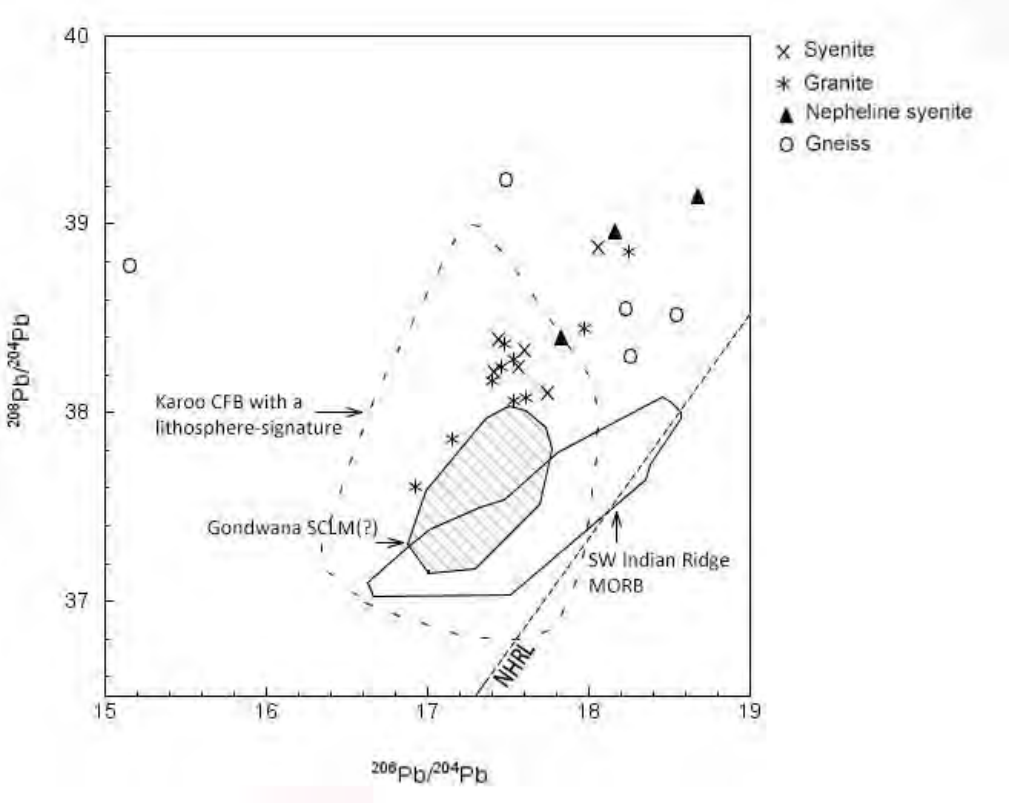

Figure 62: Most of the dyke samples plot within the field of Karoo CFB's with a lithosphere-signature. The gneisses and Straumsvola nepheline syenites remain outside any field identified by Heinonen et al. (2010).

5.6. Towards a final synthesis

One of the questions that needs to be addressed in this study is how the dykes came to be peralkaline. Figure 62 is a TAS vs SiO_2 diagram for the suite of dykes, the nepheline syenites and the gneisses. The dykes form an array that extends from the critical plane of silica saturation at high total alkalis to evolved granites with low total alkali content. This has previously been attributed to fractional crystallisation of alkali feldspar and aegirine as the system evolves. Some Group 2 samples plot on the divide and suggest that these samples were derived from a magma that was just qtz-normative. As expected the nepheline syenites plot to the left of the SiO_2 saturation plane and define an array that becomes enriched in alkali feldspar as the system evolves. While the dykes cannot have evolved from the nepheline syenite by closed system fractional crystallisation, it is clear that if a phonolite magma derived from the nepheline syenite at high total alkalis was able to cross the thermal divide, that its first magma would have the composition of the least evolved, alkali-rich Straumsvola trachytes. If this is the case, a mechanism to cross the thermal divide at low pressure must still be established. The gneisses have the lowest total alkali content of all the samples and show a wide variation. Even so a low volume partial melt of these fenitised gneisses could produce an alkali enriched melt that with fractional crystallisation could produce the peralkaline granites.

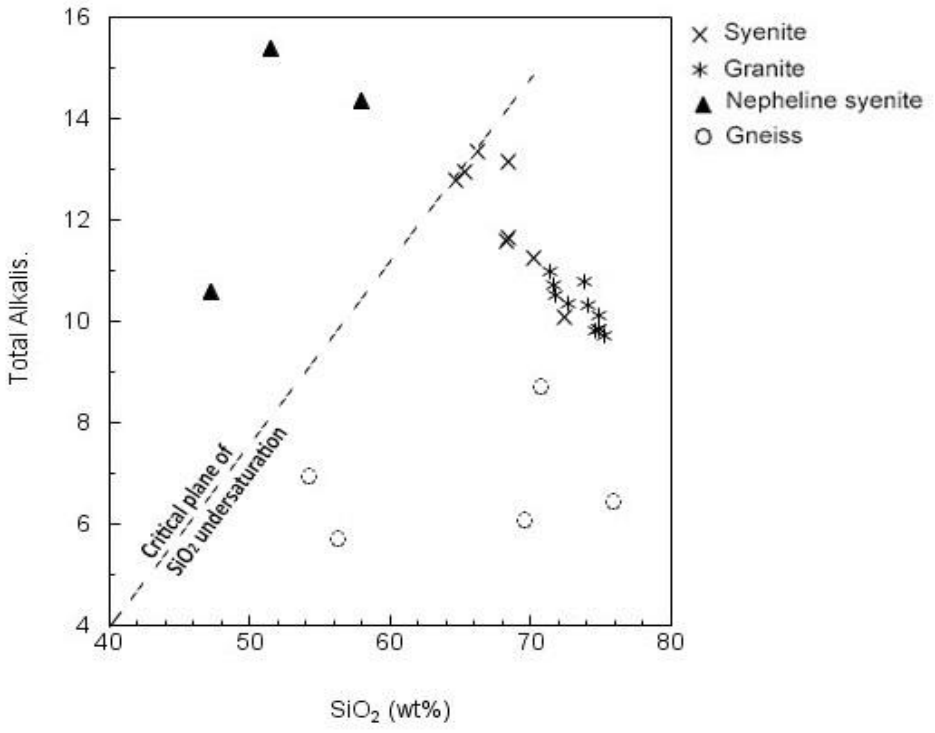

Figure 63: TAS vs SiO_2 for all the samples. The gneisses have generally low total alkali contents. The nepheline syenites have much higher total alkali contents than even the granites but are chemically constrained at low pressures by a thermal divide (Critical plane of SiO_2 undersaturation).

5.7. Comparison with other Mesozoic plutons

The Sistefjell syenite to the south of the Straumsvola group of nunataks is the only other Mesozoic (173Ma) alkaline pluton in WDML, Antarctica (Harris et al. 2002). It is a 10km wide syenite intruded by dykes and sills of a more evolved composition. While the major element geochemistry of the suite can be explained by fractional crystallisation, rocks of the Sistefjell syenite complex also have ε_{Nd} values consistent with extensive crustal contamination. Crustal contamination by the regional Sverdrupfjella gneisses appears to have affected only the syenite magma while the more evolved intrusions show evidence for contamination by the low $\delta^{18}O$ Sistenup lavas. Harris et al. (2002) concluded that the Sistefjell syenite was produced by fractional crystallisation of an originally mantle-derived magma that underwent crustal contamination by the silica-rich gneisses and unusual Sistefjell lavas.

The variation in incompatible trace element ratios is shown in Figure 64 for the Sistefjell and Straumsvola plutons and related intrusions. With the exception of two quartz syenites (ST113 and ST246) and one microgranite (ST226), the Straumsvola dykes fall within a narrow range of La/Nb ratios between 0.5 - 2 and Zr/Nb ratios <10. Dykes with large Zr/Nb (>10) are all granite outlier dykes that plot with the Sistefjell lavas. These samples were also shown in the previous chapter to have been affected by an alteration fluid so it is unlikely that they share any real petrogenetic relationship with the low $\delta^{18}O$ Sistefjell lavas. The remaining microgranite dykes share similar incompatible element ratios with the Sistefjell syenites while the Straumsvola syenite dykes share similarities with the Sistefjell quartz porphyries and microgranite. The data do appear to suggest overall that the Sistefjell and Straumsvola plutons and associated intrusions were derived from similar magmas. The plutons and associated intrusions also have relatively low Zr/Nb ratios (<10), a feature characteristic of rift zone magmas. The implication is that these magmas are forming in an active rift environment possibly with the involvement of a mantle plume such as that inferred for the region of the Jutulstraumen during the Mesozoic.

Figure 65 shows the major rock types of the Sistefjell pluton plotted with the Straumsvola samples for ε_{Nd} against initial $^{87}Sr/^{86}Sr$. The Sistefjell samples have ε_{Nd} values >-5 and a range in initial $^{87/86}Sr$ (0.70500- 0.75500), the most primitive being the low $\delta^{18}O$ country rock Sistefjell lavas. Nepheline syenite, ST138, the most primitive Straumsvola sample overlaps with the Sistefjell dykes in ε_{Nd} and with a Sistefjell syenite at low $^{87}Sr/^{86}Sr$ and implies mantle-derivation for all the Sistefjell samples and ST138. The range in $^{87}Sr/^{86}Sr$ of the Sistefjell samples can also be seen to overlap with the range observed for the Straumsvola gneisses and suggests that crustal contamination by the regional gneisses has affected the associated intrusions. This is in disagreement with its low ε_{Nd}, which has been interpreted by Harris et al. (2002) to result from extensive crustal contamination by the low $\delta^{18}O$ Sistefjell lavas. The data are consistent with the Sistefjell microgranite dykes having experienced at least two stages of crustal contamination, the

first by the gneisses presumably in the lower crust, followed by contamination by the Sistenup lavas in the upper crust, which is in agreement with the findings of Harris et al. (2002).

Calculated quartz (and nepheline) magma $\delta^{18}O$ plotted against initial $^{87}Sr/^{86}Sr$ for the Sistefjell and Straumsvola samples is shown in Figure 66a. A quartz fractionation factor between mineral and magma of 0.6‰ was assumed for the Straumsvola dyke. For nepheline-magma, a fractionation factor of 0.4‰ was assumed, based on the calculation of Zhao & Zheng for nepheline in nephelinite of 0.44‰. For the purposes of this study the exact mineral-melt fractionation factors are not important as it does not change the overall picture of the oxygen isotopic data i.e. the high $\delta^{18}O$ dyke magma and mantle-signatured nepheline syenites and Sistefjell lavas, and is merely to allow comparison between the under- and oversaturated magmas of this study.

There is a clear distinction in magma $\delta^{18}O$ between the Straumsvola nepheline syenite and Sistefjell basalt lavas at low $\delta^{18}O$ (<6‰), and the associated felsic magmas at higher $\delta^{18}O$ (>6.5‰). This is expected given the mafic rocks are known to be mantle derived (Harris & Grantham 1993; Harris et al. 2002). Even within the felsic magmas however, there is a distinction between the Sistefjell and Straumsvola magmas, the former having higher initial $^{87}Sr/^{86}Sr$ and plotting to lower magma $\delta^{18}O$. The high $^{87}Sr/^{86}Sr$ ratios (>0.75000) of the Sistefjell dykes is interesting though as this could not have been an effect of the Sistefjell lavas which have average initial $^{87}Sr/^{86}Sr = 0.70460$. These samples plot with one Straumsvola gneiss, ST254,that is furthest from the contact with the Straumsvola nepheline syenite and confirms that the evolved Sistefjell intrusives have experienced contamination by the surrounding gneisses. If the effect of the 'granite bias' in oxygen isotope sample selection of the Straumsvola dykes is accounted for, the Sistefjell intrusives, and Straumsvola syenite dykes would likely overlap in magma $\delta^{18}O$. This would again suggest derivation from a similar magma as was suggested by the incompatible element ratios. The majority of the Straumsvola gneisses overlap in magma $\delta^{18}O$ with a Straumsvola dyke that has an initial ratio = 0.7075 (based on the isochron calculated in Isoplot) and could imply that the gneisses are responsible for the enriched $\delta^{18}O$ of the Straumsvola dykes.

Whole rock $\delta^{18}O$ vs. ε_{Nd} is shown in Figure 66b. The samples with the highest whole rock $\delta^{18}O$ values are the gneisses furthest from the contact zone, the Sistefjell syenite and the Straumsvola dykes**. The Sistefjell syenite is thought to have interacted with the gneissic lower crust and given the similarities between the two plutons highlighted in the previous section, confirms that the Straumsvola dykes are inheriting their crustal signature from the gneisses. Straumsvola nepheline syenite, ST133 overlaps in ε_{Nd} and whole rock $\delta^{18}O$ with the gneisses of the contact zone, supporting the hypothesis that the local gneisses are responsible for crustal contamination of at least the layered zone nepheline syenite magma.

The Straumsvola and Sistefjell plutons and associated intrusions show evidence for derivation from a similar source magma. This was seen in the plots of incompatible trace element ratios, ε_{Nd}, initial $^{87}Sr/^{86}Sr$ vs. magma and whole rock $\delta^{18}O$. This can be explained if their genesis

is related to tectonism i.e. in an active rift as inferred from the incompatible element ratios. Oxygen isotope data suggest the Straumsvola dykes could be derived from a Sistefjell-type magma by fractional crystallisation while the syenites themselves were likely derived from even more primitive magmas possibly similar to the nepheline syenite magma at Straumsvola.

One major difference between the evolved dykes at Straumsvola and that of Sistefjell is that at Sistefjell the dykes only intrude the gneisses and not the pluton itself whereas the reverse is true at Straumsvola. This will be discussed further in the model presented in Chapter 7.

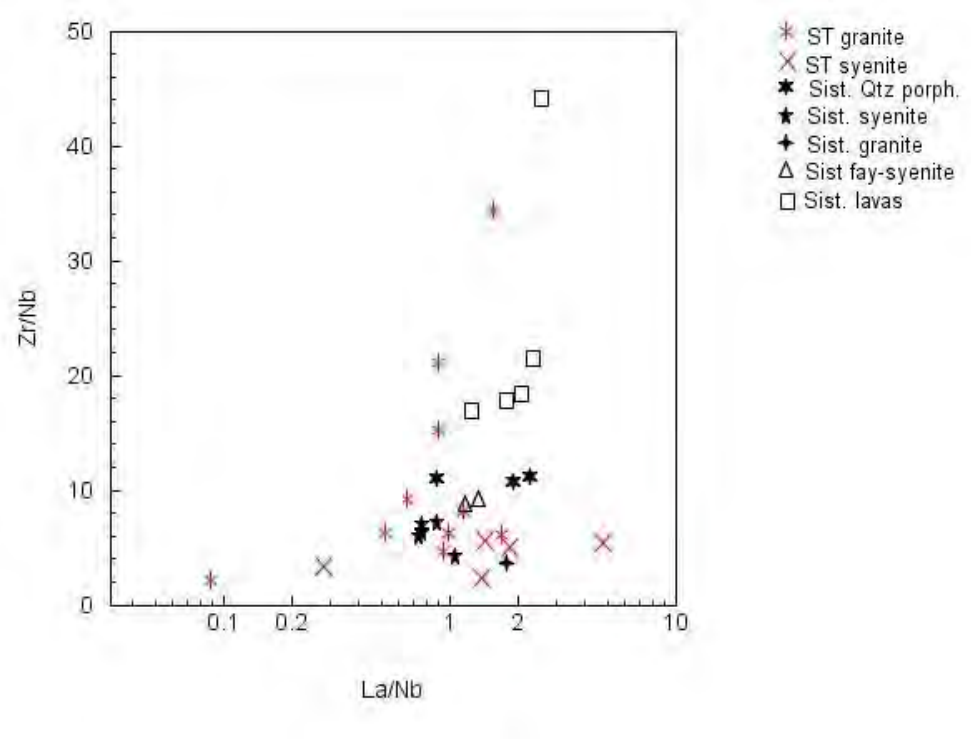

Figure 64: Comparison of the incompatible element ratios of the only other Mesozoic alkaline pluton, Sistefjell with the Straumsvola dykes. The Straumsvola microgranites overlap with the Sistefjell syenites and fayalite syenites. The dykes that fall to high Zr/Nb ratios are the granite outliers identified earlier that are Nb-depleted rather than Zr-enriched.

***The Straumsvola dykes shown in Figure 66b (ST 76 and ST212) were removed in Chapter 4 due to large errors in the Rb/Sr ratio but they are the only samples for which both whole rock oxygen isotope analyses (Harris & Grantham (1993)) and ε_{Nd} (this study) are available. However, their values are consistent with the rest of the Straumsvola dykes.*

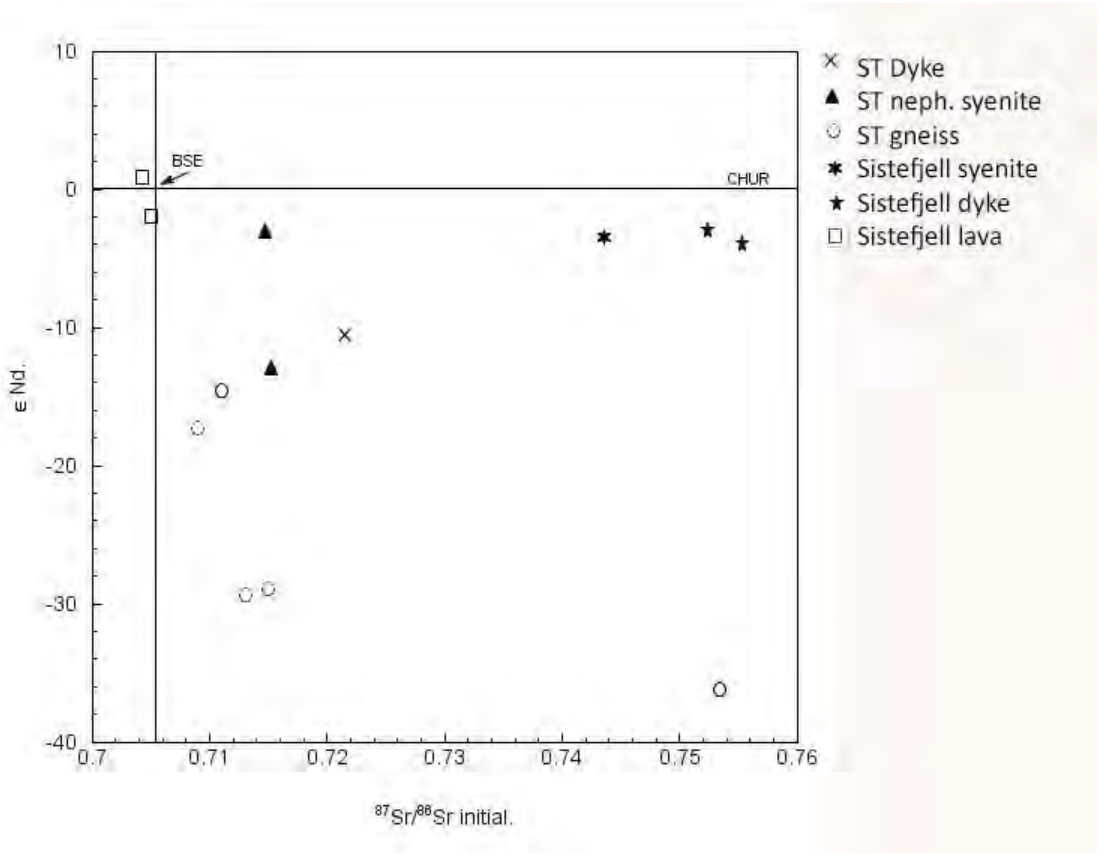

Figure 65: The major lithologies of the Sistefjell Complex can be seen to plot to less enriched ε_{Nd} and reflects interaction with the low $\delta^{18}O$ Sistefjell lavas (squares) i.e. the country rock to the Sistefjell syenite. A range in initial $^{87}Sr/^{86}Sr$ is observed for the Sistefjell syenite and an associated microsyenite dyke that overlaps the range in $^{87}Sr/^{86}Sr$ of the Straumsvola gneisses i.e. the regional Sverdrupfjella gneisses. ST= Straumsvola. The Straumsvola granites are represented by a single point using the initial $^{87}Sr/^{86}Sr$= 0.7075 determined from the isochron and average granite εNd=-12

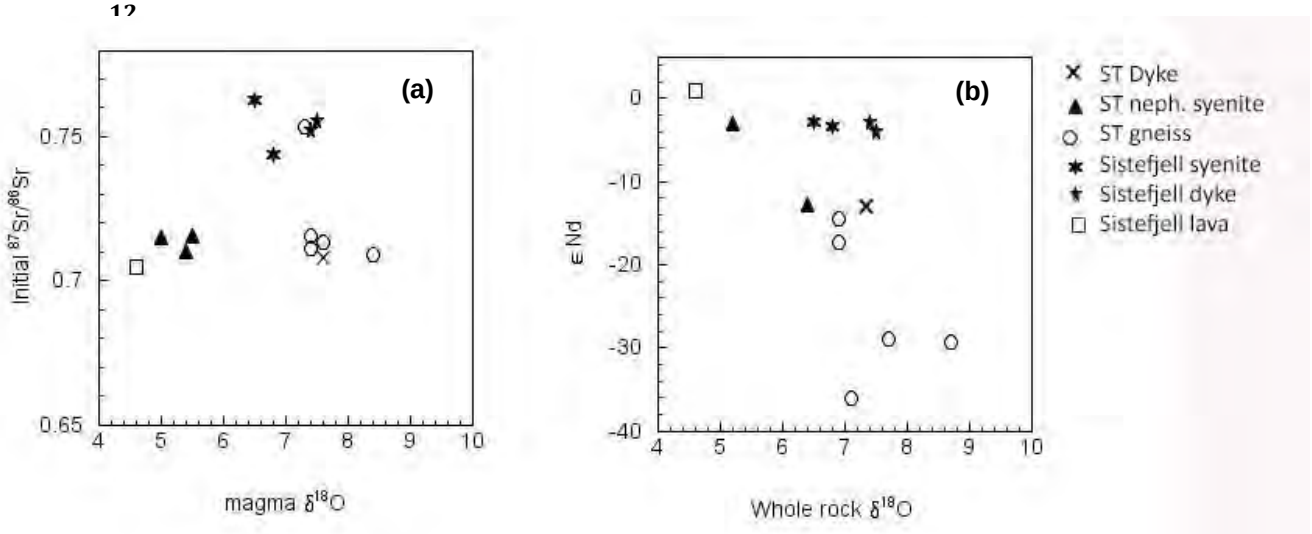

Figure 66: a) The syenite and associated rocks of the Sistefjell pluton all have magma $\delta^{18}O$ values that overlap with the regional Straumsvola gneisses. Only one Straumsvola granite is plotted using the initial $^{87}Sr/^{86}Sr$ ratio= 0.7075 (from the isochron calculated using Isoplot) and the average $\delta^{18}O$ value. It can be seen to have lower initial $^{87}Sr/^{86}Sr$ ratios than both the gneisses and Sistefjell rocks. b) The Sistefjell syenite and related intrusions have εNd values equal to ST138, the most primitive Straumsvola sample but whole rock $\delta^{18}O$ that is much higher. Average Straumsvola granite, the Sistefjell syenites and the gneisses further from the contact zone have the highest whole rock $\delta^{18}O$ while a Sistefjell lava is the most primitive sample in the dataset.

6.1. Petrography

- The dykes are extremely fresh, very fine-grained and can be subdivided into two major classes: aegirine phenocryst-rich(Group 1) and phenocryst poor (Group 2). In general Group 1 dykes tend to be granites while Group 2 dykes are quartz syenites.
- Aegirine phenocrysts are perfectly euhedral in outline but poikilitic in their cores and only observed in the granites. These textures indicate a two-stage crystallization history for aegirine in the most evolved samples. There is no evidence of resorption suggestive of a magma that was in chemical equilibrium throughout aegirine crystallization.
- An alkali-enriched alteration fluid is proposed to have fenitised the surrounding gneisses causing Na-enrichment of pyroxene rims.
- Other notable unusual minerals included a few Zr-Silicates namely: eudialyte, vlasovite and dalyite as well as Ti-rich narsarsukite. The presence of these minerals attests to the strongly peralkaline and highly incompatible element enriched melts that they crystallised from. These minerals are commonly associated with undersaturated alkaline complexes but are clearly late-stage magmatic products in these dykes. Their presence agrees with the hypothesis that a fluid enriched in alkalis affected the dykes quite late in their evolution, combining with SiO_2 and Zr to crystallise the zirconium silicates.

6.2. Major and trace element geochemistry

- The samples fall into two geochemical classes: syenites and granites.
- All of the dykes in the study have a Peralkalinity Index >1, which accounts for the abundance of aegirine in the dykes.
- Major element modelling using a least squares regression showed that the dyke suite is broadly consistent with fractional crystallisation of alkali feldspar and aegirine in the ratio 80:20 respectively.
- Trace element modelling of 6 incompatible elements also showed a case for fractional crystallisation but overestimation of the concentrations by the calculation suggested that an additional mechanism is required to explain the data. This was supported by the lack of correlation between the incompatible elements (especially Zr) with increasing SiO_2, unexpected in a system undergoing closed system fractional crystallisation.
- The effect of eudialyte crystallisation on the trace element budget was also considered. It was found that Zr was compatible in a number of other phases including vlasovite, dalyite and even aegirine/amphibole. Eudialyte and other unusual silicate crystallisation could not however, explain the lower than expected Sr, Ba and Rb trace element concentrations.

6.2.1. REE

- REE concentration in the dykes decreased as the SiO_2 concentration increased so that the most evolved dykes were the least REE enriched.
- A group of granite outliers at the lowest REE concentrations were also host to a few of the unusual silicates namely vlasovite and narsarsukite.

- The majority of the dykes had similar REE patterns to the nepheline syenites including an enrichment in the HREE. The gneisses of the contact zone, however, also showed similar REE patterns to the nepheline syenites and so could not be excluded as possible sources.

6.3. Oxygen isotopes

- The dykes selected for oxygen isotope analysis were all granites and found to have $\delta^{18}O$ values between 8.36‰ - 9.15‰. The granite outliers accounted for the samples with the highest ratios ($\delta^{18}O$ >8.6‰).
- These values are much greater than would be expected from an evolved mantle-derived magma e.g. Ascension Island granite ($\delta^{18}O$= 7.2‰). A crustal component is therefore suspected.
- Assimilation and fractional crystallisation of the regional gneisses could produce the average $\delta^{18}O$ seen in the Straumsvola dykes but only one gneiss from the contact zone has a $\delta^{18}O$ quartz value similar to the granite outlier dykes.
- Aegirine $\delta^{18}O$ vs quartz $\delta^{18}O$ shows that most of the aegirines crystallised at around 500°C well below the solidus for a magma of this composition and suggests post-crystallisation re-equilibration. The granite outlier dykes fall to even lower temperatures of equilibration and is consistent with the presence of an alteration fluid in the very late stages of crystallisation.
- Oxygen isotopes plotted against the incompatible elements reveals that the Zr, Sr and Rb concentrations of the granite outlier samples are all similar (i.e. Zr=200ppm; Rb=260ppm and Sr=20ppm) and is in agreement with interaction of the granite magma with an alteration fluid.

6.4. Radiogenic isotopes

- Rb-Sr isochron for the dykes produced an age of 171Ma±4.4 Ma, within the accepted age for the Straumsvola pluton of 170±4 Ma (Grantham et al. (1988)). The age implies the dykes are synchronous with emplacement of the pluton but this must be considered with caution given the Ar-Ar age of 178.45±1.52 Ma of a mafic dyke intrusive into the pluton that defines the minimum age of the pluton (Curtis et al. 2008).
- The nepheline syenites have initial $^{87}Sr/^{86}Sr$ ratios equal to the initial ratio for the suite of dykes i.e. 0.70750 ±0.0032 and could thus be a potential source. This value is higher than would be expected from a mantle-derived magma and implies that the nepheline syenites may have experienced some crustal contamination. The contact zone gneisses are the likely contaminant as they overlap with the nepheline syenites in comparison plots throughout this study.
- Overall the dykes become more radiogenic with increasing SiO_2 and show overwhelmingly crustal signatures (ε_{Nd}=-12).
- The isochron calculated for Sm-Nd is very poor owing to the young age of the dykes.

- An enriched and less enriched group of dykes was observed with the majority falling in the less enriched group. The enriched group, however, was found to be an artefact of two granite outlier dyke samples and so the initial $^{143}Nd/^{144}Nd$ ratio for the dykes was calculated to be = 0.51190.
- A plot of ε_{Nd} vs initial $^{87}Sr/^{86}Sr$ at 171 Ma showed that none of the samples were directly sampled from MORB-type magma. Nepheline syenite, ST138, was found to be the most primitive sample in the dataset (ε_{Nd} = -2) while nepheline syenite, ST133, was likely crustally contaminated (ε_{Nd} =-10). The regional gneisses plot to the most negative ε_{Nd} as expected for continental crust. The dykes lie midway between the primitive nepheline syenite and gneisses so a source is difficult to constrain and might suggest that there is a contribution from both.
- When initial $^{87}Sr/^{86}Sr$ ratios of the gneisses at 171Ma was plotted with distance from the intrusion, it could be seen that the Sr ratios were homogenised up to 500m from the contact, which is consistent with the presence of an alteration fluid acting on the gneisses as a result of the nepheline syenite intrusion.
- The dykes evolve from more enriched to less enriched Pb as the suite evolves from syenite to granite.
- Mantle signatures similar to Karoo CFB and Gondwana SCLM for the suite of dykes was revealed by the Pb isotope data of Heinonen et al. (2010)
- The Pb data overall is consistent with a combination of both the gneiss and nepheline syenite involved in the genesis of the Straumsvola dykes as with Sm-Nd.

6.4.1. Comparison with the Sistefjell Syenite

- All the data point to the two plutons and associated intrusions showing similar petrogenesis and derivation from a very similar source. A tectonic setting in an active-rift environment with the involvement of a mantle-plume would provide primary magmas of the correct composition to produce the Straumsvola and Sistefjell syenites by a process broadly consistent with fractional crystallisation.

7. Model for the petrogenesis of the Straumsvola dykes

Much of the evidence presented so far suggests that the oversaturated dyke magmas are related to or derived from the undersaturated nepheline syenite magma at Straumsvola. The principal ways in which an oversaturated magma can co-exist with an undersaturated magma is through:

1) High and low pressure melting of the mantle. Melting of the mantle at high pressures produces alkali basalt while at low pressures, basalt of tholeiitic composition is expected. These melts after extensive fractional crystallisation could produce an oversaturated (quartz normative) and undersaturated (nepheline normative) melt, respectively (Tuttle & Bowen 1958).

2) Assimilation of felsic crust by an undersaturated magma (e.g. Foland et al. (2003) and Frost & Frost (2010))

3) Partial melting of fenitised country rock gneiss and fractional crystallisation in the presence of an undersaturated magma (e.g. Martin (2006))

Only Model 2 requires interaction with the nepheline syenite magma. The nepheline syenite requires assimilation of felsic crust to produce a magma that can cross the thermal divide that exists at low pressures in the Nepheline-Albite-Quartz-Kalsilite system. This quartz-normative melt after extensive fractional crystallisation could produce a granite. Models 1 and 3 require no interaction with the nepheline syenite to produce the oversaturated melt with which it co-exists.

The data presented in this study however, show a close association between the nepheline syenites (especially ST133), the dykes and the gneisses of the contact zone, which could be broadly explained by a process such as that of Model 2. The high $\delta^{18}O$ values of the granites is evidence for a strong crustal component in the petrogenesis of these dykes so Model 1 involving melting of a mantle source can be discarded as a mechanism to produce the dykes at Straumsvola. While melting of the upper crust and fractional crystallisation could produce granite dykes as required for Model 3, it would not produce peralkaline granite dykes unless the gneiss was previously enriched by alkalis. The gneisses, particularly at the contact zone do show evidence for sodic metasomatism and so could potentially be the source of the Straumsvola dyke magma. Martin (2006) inferred that fenitisation of the lower and upper crust should be expected in areas of extension where mantle-derived magmas are accompanied by alkaline fluid phases (either H_20 or $C0_2$ rich) during their ascent into the upper crust. Martin (2006) further states that the alkaline fluids fenitise the crust enriching them in alkalis, which also predisposes the crust to partial or complete melting that ultimately results in the formation of A-type granite magmas of metaluminous or peralkaline character in extensional environments.

In addition to the above, there are a few other important considerations to take into account when trying to construct a model for the petrogenesis of these dykes:

Firstly, Harris & Grantham (1993) note that the felsic, Straumsvola dykes are only seen to intrude the nepheline syenite pluton and not the surrounding gneisses. The model therefore needs to address this especially given the presence of numerous dykes that could act as conduits for later magmas.

Secondly, comparison of the Straumsvola pluton and associated intrusions with that of the Sistefjell complex to the south has shown the remarkable similarities in age, tectonic setting and petrogenesis between these two plutons. The Sistefjell syenite is understood to be a crustally-contaminated mantle-derived magma with associated intrusions that can be broadly explained by fractional crystallisation. The evolved intrusions include microgranite and are known to only intrude the country rocks and not the pluton itself unlike at Straumsvola. At Sistefjell this is likely due to the fact that the associated intrusions are evolving outward into the upper crust away from the syenite. If the Straumsvola magmas were generated by the same process, the evolved dykes would have to have been generated from a syenite magma produced by fractional crystallisation of a crustally contaminated mantle-derived magma. At Straumsvola there is no syenite pluton, only syenite dykes implying that the overall magma produced in this process is of low volume. This implies that interaction of crustal or magmatic melts was not extensive. The fact that the resultant syenite-granite suite does not emplace into the gneiss is consistent with the crust in the region of the Straumsvola pluton being cold and the dykes are in effect quenched before they can intrude.

The source of the nepheline syenite at Straumsvola also needs to be established in order to create a petrogenetic model for the Complex. Harris & Grantham (1993) proposed this source was mantle- derived based on the low $\delta^{18}O$ values of nepheline separates ($\delta^{18}O$ = 5.1- 6.4‰) and its calculated whole rock $\delta^{18}O$ ($\delta^{18}O$ = 5.2- 6.4‰). Alkali-basalt dykes are present within the Straumsvola Complex and form a younger alkaline swarm of mafic intrusives into the nepheline syenites at Straumsvola and Tvora. Extensive fractional crystallisation of an alkali basalt will produce a ne-normative magma so these dykes are the most obvious choice for the parental magma to the nepheline syenite pluton at Straumsvola. Ar-Ar dating by Curtis et al (2008) shows the age of these dykes to be 175-178Ma, which also constrains the minimum age of the pluton to 178Ma. It is unlikely then that the nepheline syenite is derived from these alkali basalts but based on aeromagnetic and AMS fabrics, a mafic body underlies the Straumsvola pluton which is likely the source of both the alkali basalt dykes and the nepheline syenite pluton (Curtis et al. 2008; Riley et al. 2009; Ferraccioli et al. 2005). ST 138, the nepheline syenite from the mafic zone is the most primitive sample in this study and might represent an undifferentiated product of fractional crystallisation of the alkali basalt dykes while ST133 from the layered zone shows evidence for interaction with the regional gneiss.

7.1. Proposed model

The nepheline syenite at Straumsvola was produced by extensive fractional crystallisation of a mantle-derived alkali basalt. It was then emplaced into the mid to upper crust of the regional Sverdrupfjella gneisses as a result of rifting related to the onset of Gondwana break-up. During emplacement the pluton was crustally contaminated by the gneisses but as it cooled, a magmatic fluid enriched in alkalis exsolved leading to local metasomatism of the surrounding gneisses producing the alkali-metasomatised gneisses of the contact zone. Fenitisation of the gneisses can be observed petrographically and geochemically in the gneisses up to 500m from the contact between the nepheline syenite and country rock gneiss. A small volume of alkali-metasomatised gneiss was subsequently partially melted to produce a strongly peralkaline syenite melt with enriched $\delta^{18}O$. This low volume melt then underwent fractional crystallisation as it cooled to produce the peralkaline granites. However, this melt owing to its low volume was quenched before it could intrude outwards into the colder regional gneisses and instead intruded into the parental nepheline syenite as a system of dykes. It is further suggested that the alkali-enriched alteration fluid (responsible for metasomatismof the gneisses) came into contact with the last remaining dyke magma that had now evolved to a high $\delta^{18}O$ microgranite. This is consistent with equilibration of aegirine and quartz at sub-solidus temperatures around 500°C. This low temperature fluid mixed with and further enriched the dyke magma in alkalis resulting in the crystallisation of euhedral aegirine around earlier-formed aegirine and groundmass minerals: quartz and feldspar (as observed for the majority of the granite dykes). Peralkaline granites formed by this process are consistent with the granite outlier dykes of the study that show even lower $\delta^{18}O$ equilibration temperatures and trace element concentrations that within the group are similar but very different to the majority of the dykes in the study. These granite outliers are also host to at least one unusual Zr-silicate. An alteration fluid interacting with the very last dyke magma is fully consistent with the formation of these late stage silicates especially in samples STFL1A and STFL1B where vlasovite crystallises due to the instability of zircon in strongly peralkaline magmas. The heat required to partially melt the gneiss was likely provided by the upwelling of mantle material as a consequence of rifting related to the initial stages of Gondwana breakup. This is supported by the presence of alkali basalt dykes that are known to intrude the nepheline syenite and country rock gneisses and are only found within the Straumsvola Complex. Gravity and aeromagnetic studies are also in support of a large mafic body underlying the Straumsvola pluton (Ferraccioli et al. 2005; Curtis et al. 2008). The heat generated within this active rift environment may also explain the lateral extent of the alteration fluid up to 500m from the contact zone.

While the model presented above explains the majority of the data it is still peculiar that isotopically the dykes share many characteristics of the nepheline syenite. For instance the nepheline syenites share a common initial ratio for the source magma of $^{87}Sr/^{86}Sr= 0.70750$. They also overlap in ε_{Nd} and while this is likely due to crustal contamination of the nepheline syenite prior to formation of the dykes, the similarities could also suggest that the dykes are in fact

derived from the nepheline syenite magma itself. This phonolite magma would not require significant input of Si-rich crust to cross the thermal divide given that it was previously contaminated. The resultant magma would also be enriched in alkalis and be of syenite composition as for the model above. Indeed late stage phonolite dykes are present within the Straumsvola pluton(Curtis et al. 2008; Riley et al. 2009) that have similar affinities to the dykes presented in this study e.g. $\varepsilon Nd = -12$, $^{87}Sr/^{86}Sr \sim 0.709\text{-}0.724$. The only difficulty with this model is producing the enriched $\delta^{18}O$ values observed in the granite dykes as partial melting and assimilation of enough crust to increase the $\delta^{18}O$ by such a low temperature melt is unlikely. Hence the model presented above (Model 3) is favoured for the petrogenesis of the peralkaline dykes at Straumsvola. This model is also in good agreement with the findings of Martin (2006) that most A-type granite magmas are produced by partial or complete melting of country rock previously fenitised by alkali-enriched fluids associated with a mantle-derived magma.

Similarities between the Sistefjell and Straumsvola complexes also make the favoured model more difficult to reconcile given the strong evidence for crustal contamination and fractional crystallisation at Sistefjell. It must be kept in mind though that the related intrusions at Sistefjell were all derived from a voluminous qtz-normative syenite unlike at Straumsvola where the syenite and peralkaline granite magma together only account for 7% of the dyke suite and given that the dominant rock type at Straumsvola is ne-normative.

Interaction of mantle derived magmas with continental crust is the interpretation favoured by most workers to produce peralkaline granites worldwide e.g. Foland et al. (1993); Bonin (2007); Frost & Frost(2011b); Estrade et al. (2014); Marks et al. (2011), etc. These authors however, favour assimilation of felsic crust by the undersaturated magma to produce a quartz-normative magma that is co-genetic with the undersaturated one. However, at Straumsvola this appears to not be the case as the oversaturated peralkaline granite dyke magmas can most easily be explained by partial melting of metasomatised crustal rocks. In both cases, the mantle generally plays a role as a heat source to induce melting in the crust and is also the source of the undersaturated magma.

8. Concluding remarks

The alkaline plutons that define the Straumsvola complex are the nepheline syenites exposed at the Straumsvola and Storjeon nunataks. The plutons have been suggested to be rift-related and are known from aeromagnetic data to form gravity and magnetic anomalies that suggest they are underlain by significant mafic bodies. Curtis et al (2008) found that the regional dyke swarm in the vicinity of the Straumsvola Complex is composed of two dyke swarms of differing age and chemistry. They identified an older (206Ma), tholeiitic dyke swarm and a younger 175-178Ma alkaline swarm as well as a very late stage (171 Ma), low volume suite of phonolite and microgranite dykes that only intruded the nepheline syenite pluton. The presence of

oversaturated felsic dykes intruding an undersaturated complex that includes alkali basaltic dykes is therefore unexpected especially given the thermal divide that exists at low pressures between silica-under and -oversaturated phases (Bowen 1937).

The data presented in this study shows that the evolved peralkaline dykes of the Straumsvola Complex were produced by fractional crystallisation of aegirine and feldspar from a peralkaline syenite magma. This magma was produced by partial melting of an alkali-metasomatised gneiss along the contact area between the nepheline syenite and regional Sverdrupfjella gneiss. The parental magma to the nepheline syenite and mafic Straumsvola dyke swarm of Curtis et al. (2008) is likely the mafic body underlying the Straumsvola pluton as identified by Ferraccioli et al. (2007).

In comparison with the nearby Sistefjell alkaline pluton the Straumsvola Complex appear very similar but the Sistefjell pluton was contaminated by the regional Sverdrupfjella gneisses to a much greater extent than at Straumsvola resulting in a wider variety and greater volume of quartz-normative magmas. The generation of peralkaline dykes at Straumsvola is unusual because they are produced by partial melting and fractional crystallisation of the felsic crust rather than assimilation of this crust by an undersaturated magma followed by fractional crystallisation (as proposed by most authors). This study also highlights the role of an alteration fluid that not only metasomatised the gneiss enriching it in alkalis but then later mixed with the final products of fractional crystallisation to produce the high $\delta^{18}O$ peralkaline granites that is also host to some of the unusual silicates. The heat necessary to partially melt the gneissic crust is likely provided by the mantle-derived mafic body (parental to the alkali basalt and nepheline syenite) proposed by several authors to underlie the Straumsvola complex and indeed all of the Mesozoic alkaline plutons in WDML. The presence of these large bodies of mafic melt is consistent with rifting related to the onset of continental breakup between this part of Antarctica and Southern Africa during the Mesozoic. It is also consistent with the generation of granite rocks at Straumsvola, which required the heat from these mafic intrusions to create favourable conditions for partial melting.

References

Barton, J.M., Klemd, R., Allsopp, H.., Auret, S.., et al., 1987. The geology and geochronology of the Annandagstoppane granite. *Contributions to Mineralogy and Petrology*, 97(4), pp.488–496.

Bindeman, I., 2008. Oxygen Isotopes in Mantle and Crustal Magmas as Revealed by Single Crystal Analysis. *Reviews in Mineralogy and Geochemistry*, 69, pp.445–478.

Bonin, B., 2007. A-type granites and related rocks: Evolution of a concept, problems and prospects. *Lithos*, 97, pp.1–29.

Bowen, N., 1937. Recent high temperature research on silicates and it's significance in igneous geology. *American Journal of Science*, 33, pp.1–21.

Bowen, N.L., 1945. Phase equilibria bearing on the origin of and differentiation of alkaline rocks. *American Journal of Science*, 243(A), pp.75–89.

Chappell, B. & White, A., 1974. Two contrasting granite types. *Pacific Geology*, 8(2), pp.173–174.

Curtis, M.L., Riley, T.R., Owens, W.H., Leat, P.T., et al., 2008. The form, distribution and anisotropy of magnetic susceptibility of Jurassic dykes in H.U. Sverdrupfjella, Dronning Maud Land, Antarctica. Implications for dyke swarm emplacement. *Journal of Structural Geology*, 30(11), pp.1429–1447.

Deer, W.A., Howie, R. & Zussman, J., 2001. *The rock forming minerals*,

Droop, G.T, R., 1987. Droop, G. T. R. (1987). A general equation for estimating Fe3+ concentrations in ferromagnesian silicates and oxides from microprobe analyses, using stoichiometric criteria. *Mineralogical Magazine*, 51(361), pp.431–435.

Eiler, J.., 2001. Oxygen isotope variation of basaltic lavas and upper mantle rocks. *Stable isotope geochemistry*, 43, pp.319–364.

Estrade, G., Béziat, D., Salvi, S., Tiepolo, M., et al., 2014. Unusual evolution of silica-under- and -oversaturated alkaline rocks in the Cenozoic Ambohimirahavavy Complex (Madagascar): Mineralogical and geochemical evidence. *Lithos*, 206-207, pp.361–383.

Ferraccioli, F., Jones, P.C., Curtis, M.L., Leat, P.T., et al., 2005. Tectonic and magmatic patterns in the Jutulstraumen rift (?) region, East Antarctica, as imaged by high-resolution aeromagnetic data. *Earth, Planets and Space*, 57, pp.767–780.

Flink, G., 1899. On the minerals from Narsarsuk on the Firth of Tunugdliarfik in Southern Greenland. Part I. *Meddelelser om Grønland*, 1, pp.1–213.

Foland, K.., Landoll, J.., Henderson, C.M.. & Jianfeng, C., 1993. Formation of cogenetic quartz and nepheline syenites. *Geochimica et Cosmochimica Acta*, 57, pp.697–704.

Frindt, S., Trumbull, R.B. & Romer, R.L., 2004. Petrogenesis of the Gross Spitzkoppe topaz granite, central western Namibia: a geochemical and Nd–Sr–Pb isotope study. *Chemical Geology*, 206(1-2), pp.43–71.

Frost, C. & Frost, B., 2011. On ferroan (A-type) granitoids: Their compositional variability and modes of origin. *Journal of Petrology*, 52(0), pp.39–53.

Frost, C. & Frost, R., 2011. On ferroan (A-type) granitoids: Their compositional variability and modes of origin. *Journal of Petrology*, 52(1), pp.39–53.

Galer, S.J.. & Abouchami, W., 1998. Practical application of lead triple spiking for correction of instrumental mass discrimination. *Mineralogical Magazine*, 62(A), pp.491–492.

Grantham, G.H., Groenewald, P.B. & Hunter, D.., 1988. Geology of the northern HU Sverdrupfjella, western Dronning Maud Land and implications for Gondwana reconstructions. *South African Journal of Antarctic Research*, 18(1), pp.2–10.

Grantham, G.H. & Hunter, D.., 1991. *The timing and nature of faulting and jointing adjacent to the Pencksokket, western Dronning Maud Land, Antarctica*,

Grantham, G.H., Jackson, C., Moyes, a B., Groenewald, P.B., et al., 1995. The tectonothermal evolution of the Kirwanveggen-H . U . Sverdrupfjella areas , Dronning Maud Land , Antarctica. *Precambrian Research*, 75(1988), pp.209–229.

Groenewald, P.B., Grantham, G.H. & Watkeys, M.K., 1991. Geological evidence for a Proterozoic to Mesozoic link between southeastern Africa and Dronning Maud Land, Antarctica. *Journal of the Geological Society*, 148, pp.1115–1123.

Groenewald, P.B., Moyes, a. B., Grantham, G.H. & Krynauw, J.R., 1995. East Antarctic crustal evolution: geological constraints and modelling in western Dronning Maud Land. *Precambrian Research*, 75, pp.231–250.

Harris, C., 1982. An Occurrence of Rare-Earth-Rich Eudialyte from Ascension Island, South Atlantic. *Mineralogical Magazine*, 46(DECEMBER), pp.421–425.

Harris, C., 1983. The Petrology of Lavas and Associated Plutonic Inclusions of Ascension Island. *Journal of Petrology* , 24 , pp.424–470.

Harris, C. & Erlank, A., 1992. The production of large-volume, low-δ 18 O rhyolites during the rifting of Africa and Antarctica: the Lebombo Monocline, southern Africa. *Geochimica et Cosmochimica Acta*.

Harris, C. & Grantham, G.H., 1993. Geology and petrogenesis of the Straumsvola nepheline syenite complex, Dronning Maud Land, Antarctica.pdf. *Geological Magazine*, 130(4), pp.531–532.

Harris, C., Johnstone, W.P. & Phillips, D., 2002. Petrogenesis of the Mesozoic Sistefjell syenite intrusion, Dronning Maud Land, Antarctica and surrounding low-??18O lavas. *South African Journal of Geology*, 105, pp.205–226.

Harris, C. & Rickard, R., 1987. Rare-Earth rich eudialyte and dalyite from a peralkaline granite dyke at Straumsvola. Dronning Maud Land, Antarctica. *Canadian Mineralogist*, 25, pp.755–762.

Harris, C. & Vogeli, J., 2010. Oxygen isotope composition of garnet in the Peninsula Granite, Cape Granite Suite, South Africa: Constraints on melting and emplacement mechanisms. *South African Journal of Geology*, 113(1977), pp.401–412.

Harris, C., Watters, B.R. & Groenewald, P.B., 1991. Geochemistry of the Mesozoic regional basic dykes of Western Dronning Maud Land, Antarctica. *Contributions to Mineralogy and Petrology*, 107(1), pp.100–111.

Heinonen, J.S., Carlson, R.W. & Luttinen, A. V., 2010. Isotopic (Sr, Nd, Pb, and Os) composition of highly magnesian dikes of Vestfjella, western Dronning Maud Land, Antarctica: A key to the origins of the Jurassic Karoo large igneous province? *Chemical Geology*, 277(3-4), pp.227–244.

Jacobs, J., Thomas, R.. & Weber, K., 1993. Accretion and indentation tectonics at the southern edge of the Kaapvaal Craton during the Kibaran(Grenville) Orogeny. *Geology*, 21(3), pp.203–206.

Johnsen, O., Ferraris, G., Gault, R.., Grice, J.., et al., 2003. The nomenclature of eudialyte-group minerals. *The Canadian Mineralogist*, 41(3), pp.785–794.

Johnstone, W.P., 2001. *A stable isotope investigation into fluid-rock interaction during regional metamorphism in western dronning maud land, East Antarctica*.

Kogarko, L.N., Lahaye, Y. & Brey, G.P., 2010. Plume-related mantle source of super-large rare metal deposits from the Lovozero and Khibina massifs on the Kola Peninsula, Eastern part of Baltic Shield: Sr, Nd and Hf isotope systematics. *Mineralogy and Petrology*, 98, pp.197–208.

Loiselle, M.. & Wones, D., 1979. Characteristics and origin of anorogenic granites. *Geological Society of America, abstracts with programs*, p.468.

Ludwig, K., 2003. Isoplot 4.

Luttinen, a. V., Rämö, O.T. & Huhma, H., 1998. Neodymium and strontium isotopic and trace element composition of a Mesozoic CFB suite from Dronning Maud Land, Antarctica: Implications for lithosphere and asthenosphere contributions to Karoo magmatism. *Geochimica et Cosmochimica Acta*, 62(15), pp.2701–2714.

Maisela, K., 2012. *Fluid inclusion study of contact metasomatism at Straumsvola, Antarctica: An estimate of P-T conditions*.

Le Maitre, R.., 2002. *A Classification and Glossary of Terms. Recommendations of the International Union of Geological Sciences Subcommission on the Systematics of Igneous Rocks*,

Marks, M. a W., Hettmann, K., Schilling, J., Frost, B.R., et al., 2011. The mineralogical diversity of alkaline igneous rocks: Critical factors for thetransition from miaskitic to agpaitic phase assemblages. *Journal of Petrology*, 52(3), pp.439–455.

Marks, M., Halama, R., Wenzel, T. & Markl, G., 2004. Trace element variations in clinopyroxene and amphibole from alkaline to peralkaline syenites and granites: Implications for mineral-melt trace-element partitioning. *Chemical Geology*, 211, pp.185–215.

Marks, M., Vennemann, T., Siebel, W. & Markl, G., 2003. Quantification of Magmatic and Hydrothermal Processes in a Peralkaline Syenite–Alkali Granite Complex Based on Textures, Phase Equilibria, and Stable and Radiogenic Isotopes. *Journal of Petrology*, 44(7), pp.1247–1280.

Marschall, H.R., Hawkesworth, C.J. & Leat, P.T., 2013. Mesoproterozoic subduction under the eastern edge of the Kalahari-Grunehogna Craton preceding Rodinia assembly: The Ritscherflya detrital zircon record, Ahlmannryggen (Dronning Maud Land, Antarctica). *Precambrian Research*, 236, pp.31–4

Martin, A.K. & Hartnady, C.J.., 1986. Plate tectonic development of the south west Indian Ocean: A revised reconstruction of East Antarctica and Africa. *Journal of Geophysical Research*, 91.

Martin, R.F., 2006. A-type granites of crustal origin ultimately result from open-system fenitization-type reactions in an extensional environment. *Lithos*, 91(1-4), pp.125–136.

Míková, J. & Denková, P., 2007. Modified chromatographic separation scheme for Sr and Nd isotope analysis in geological silicate samples. *Journal of Geosciences*, 52, pp.221–226.

Norwegian Polar Institute, 2006. *Geological Map of H.U.Sverdrupfjella, Dronning Maud Land, Antarctica*,

Rastsvetaeva, R.K., 2007. Structural mineralogy of the eudialyte group: A review. *Crystallography Reports*, 52(1), pp.47–64.

Ravich, M.. & Solov'ev, D.., 1969. *Geology and petrology of the mountains of Central Queen Maud Land (Eastern Antarctica)*,

Riedel, S., Jacobs, J. & Jokat, W., 2013. Interpretation of new regional aeromagnetic data over Dronning Maud Land (East Antarctica). *Tectonophysics*, 585, pp.161–171.

Riley, T.R., Curtis, M.L., Leat, P.T. & Millar, I.L., 2009. The geochemistry of Middle Jurassic dykes associated with the Straumsvola À Tvora alkaline plutons , Dronning Maud Land , Antarctica and their association with the Karoo large igneous province. *Mineralogical Magazine*, 73(April), pp.205–226.

Riley, T.R., Leat, P.T., Curtis, M.L., Millar, I.L., et al., 2005. Early-middle Jurassic dolerite dykes from western Dronning Maud Land (Antarctica): Identifying mantle sources in the Karoo large igneous province. *Journal of Petrology*, 46(7), pp.1489–1524.

le Roex, A.., Spath, A. & Zartman, R.., 2001. lithospheric thickness beneath the southern Kenya Rift: implications from basalt geochemistry. *Contributions to Mineralogy and Petrology*, 142(1), pp.89–106.

Le Roex, A.P., 1985. Geochemistry, Mineralogy and Magmatic Evolution of the Basaltic and Trachytic Lavas from Gough Island, South Atlantic. *Journal of Petrology*, 26(1), pp.149–186.

Rousseau, R.., Willis, J.. & Duncan, A.., 1996. Practical XRF calibration proecedures for major and trace elements. *X-ray Spectometry*, 25(4), pp.179–189.

Schilling, J., Wu, F.-Y., McCammon, C., Wenzel, T., et al., 2011. The compositional variability of eudialyte-group minerals. *Mineralogical Magazine*, 75(February), pp.87–115.

Sheppard, S.M.F. & Harris, C., 1985. Hydrogen and oxygen isotope geochemistry of Ascension Island lavas and granites: variation with crystal fractionation and interaction with sea water. *Contributions to Mineralogy and Petrology*, 91, pp.74–81.

Tanimizu, M. & Ishikawa, T., 2006. Development of rapid and precise Pb isotopic analytical techniques using MC-IPMS and new results for GSJ rock reference samples. *Geochemical Journal*, 40(2), p.121.

Tikhonenkova, R.. & Kazakova, M.., 1961. Vlasovite, a new zirconium silicate from the Lovozero Massif. *Doklady Akademie Nouk, S.S.S.R*, 4, pp.944–946.

Tuttle, O.. & Bowen, N.., 1958. Origin of granite in the light of experimental studies in the system NaAlSi3O8-KAlSi308-SiO2-H2O. *Geological Society of America*, 74, pp.1–146.

Watson, E.., 1979. Zircon saturation in felsic liquids: experimental results and applications to trace element geochemistry. *Contributions to Mineralogy and Petrology*, 70, pp.407–419.

Weis, D., Kieffer, B., Maerschalk, C., Barling, J., et al., 2006. High-precision isotopic characterization of USGS reference materials by TIMS and MC-ICP-MS. *Geochemistry, Geophysics, Geosystems*, 7(8)

White, B. (Cornell), 2007. U-Th decay series dating.

Willis, J.. & Duncan, A.., 2008. *Understanding XRF Spectometry*,

de Wit, M., Jeffery, M., Bergh, H. & Nicolaysen, L., 1988. *Geological map of sectors of Gondwana reconstructed to their dispositions C.150Ma*,

Wolmarans, L.G.. & Kent, L.., 1982. *Geological Investigations in western Dronning Maud Land, Antarctica: A synthesis.*,

Zhao, Z.-F. & Zheng, Y.-F., 2003. Calculation of oxygen isotope fractionation in magmatic rocks. *Chemical Geology*, 193, pp.59–80.

Appendix

Appendix A:

Table A: Pyroxene calculation after the method of Droop, G.T (1987). The pyroxenes were analysed by electron microprobe at UCT. All pyroxenes are sodic and end-member aegirine or aegirine-augite.

	FL1	FL1	FL1	FL1	FL1	FL1	FL1	FL1	FL1	FL1	FL1	FL1	FL1
SiO_2	53.37	53.41	52.81	53.16	52.21	52.09	52.45	52.47	52.31	52.27	52.82	52.75	52.45
TiO_2	1.75	1.79	0.78	1.75	1.38	3.00	1.66	1.66	1.61	1.18	2.51	3.43	1.34
Al_2O_3	0.29	0.33	0.39	0.34	0.30	0.29	0.29	0.27	0.25	0.31	0.26	0.31	0.27
Cr_2O_3	0.00	0.03	0.00	0.00	0.00	0.02	0.00	0.01	0.01	0.00	0.00	0.00	0.00
FeO	27.64	29.74	29.56	29.08	29.79	28.12	29.56	29.55	29.59	28.96	28.95	28.00	30.20
MnO	0.21	0.20	0.49	0.20	0.23	0.19	0.29	0.22	0.19	0.22	0.21	0.23	0.14
MgO	0.01	0.02	0.03	0.05	0.01	0.01	0.00	0.00	0.00	0.01	0.00	0.01	0.01
CaO	0.43	0.44	0.36	0.44	0.57	0.81	0.42	0.58	0.59	0.34	0.78	0.67	0.36
Na_2O	14.09	14.21	14.38	13.89	13.98	13.80	14.14	14.18	14.04	13.80	13.87	13.94	14.17
K_2O	0.00	0.01	0.05	0.01	0.01	0.02	0.02	0.01	0.00	0.00	0.01	0.01	0.01
Total	98.02	100.59	98.93	99.25	98.77	98.85	99.25	99.39	98.99	97.18	99.83	99.68	99.18
Mol. Props.													
SiO_2	0.89	0.89	0.88	0.89	0.87	0.87	0.87	0.87	0.87	0.87	0.88	0.88	0.87
TiO_2	0.02	0.02	0.01	0.02	0.02	0.04	0.02	0.02	0.02	0.02	0.03	0.04	0.02
Al_2O_3	0.00	0.00	0.00	0.00	0.00	0.00	0.00	0.00	0.00	0.00	0.00	0.00	0.00
Cr_2O_3	0.00	0.00	0.00	0.00	0.00	0.00	0.00	0.00	0.00	0.00	0.00	0.00	0.00
FeO	0.39	0.41	0.41	0.41	0.42	0.39	0.41	0.41	0.41	0.40	0.40	0.39	0.42
MnO	0.00	0.00	0.01	0.00	0.00	0.00	0.00	0.00	0.00	0.00	0.00	0.00	0.00
MgO	0.00	0.00	0.00	0.00	0.00	0.00	0.00	0.00	0.00	0.00	0.00	0.00	0.00
CaO	0.01	0.01	0.01	0.01	0.01	0.01	0.01	0.01	0.01	0.01	0.01	0.01	0.01
Na_2O	0.23	0.23	0.23	0.22	0.23	0.22	0.23	0.23	0.23	0.22	0.22	0.23	0.23
K_2O	0.00	0.00	0.00	0.00	0.00	0.00	0.00	0.00	0.00	0.00	0.00	0.00	0.00
Total	1.54	1.57	1.55	1.55	1.54	1.54	1.55	1.55	1.55	1.52	1.56	1.55	1.55
Oxygen prop.													
SiO_2	1.78	1.78	1.76	1.77	1.74	1.73	1.75	1.75	1.74	1.74	1.76	1.76	1.75
TiO_2	0.04	0.05	0.02	0.04	0.04	0.08	0.04	0.04	0.04	0.03	0.06	0.09	0.03
Al_2O_3	0.01	0.01	0.01	0.01	0.01	0.01	0.01	0.01	0.01	0.01	0.01	0.01	0.01
Cr_2O_3	0.00	0.00	0.00	0.00	0.00	0.00	0.00	0.00	0.00	0.00	0.00	0.00	0.00
FeO	0.39	0.41	0.41	0.41	0.42	0.39	0.41	0.41	0.41	0.40	0.40	0.39	0.42
MnO	0.00	0.00	0.01	0.00	0.00	0.00	0.00	0.00	0.00	0.00	0.00	0.00	0.00
MgO	0.00	0.00	0.00	0.00	0.00	0.00	0.00	0.00	0.00	0.00	0.00	0.00	0.00
CaO	0.01	0.01	0.01	0.01	0.01	0.01	0.01	0.01	0.01	0.01	0.01	0.01	0.01

Na_2O	0.23	0.23	0.23	0.22	0.23	0.22	0.23	0.23	0.23	0.22	0.22	0.23	0.23
K_2O	0.00	0.00	0.00	0.00	0.00	0.00	0.00	0.00	0.00	0.00	0.00	0.00	0.00
Total	2.45	2.49	2.45	2.46	2.44	2.45	2.45	2.45	2.44	2.41	2.47	2.48	2.45
Norm. factor	2.45	2.41	2.45	2.44	2.46	2.45	2.45	2.45	2.46	2.49	2.43	2.42	2.45
Formula	6(O)	6(O)	6(O)	6(O)	6(O)	6(O)	6(O)	6(O)	6(O)	6(O)	6(O)	6(O)	6(O)
Si	2.17	2.14	2.16	2.15	2.14	2.12	2.14	2.14	2.14	2.16	2.13	2.12	2.14
Ti	0.05	0.05	0.02	0.05	0.04	0.09	0.05	0.05	0.05	0.04	0.08	0.10	0.04
Al	0.01	0.02	0.02	0.02	0.01	0.01	0.01	0.01	0.01	0.02	0.01	0.02	0.01
Cr	0.00	0.00	0.00	0.00	0.00	0.00	0.00	0.00	0.00	0.00	0.00	0.00	0.00
Fe++	0.94	1.00	1.01	0.99	1.02	0.96	1.01	1.01	1.01	1.00	0.98	0.94	1.03
Mn	0.01	0.01	0.02	0.01	0.01	0.01	0.01	0.01	0.01	0.01	0.01	0.01	0.01
Mg	0.00	0.00	0.00	0.00	0.00	0.00	0.00	0.00	0.00	0.00	0.00	0.00	0.00
Ca	0.02	0.02	0.02	0.02	0.03	0.04	0.02	0.03	0.03	0.02	0.03	0.03	0.02
Na	1.11	1.11	1.14	1.09	1.11	1.09	1.12	1.12	1.11	1.11	1.09	1.09	1.12
K	0.00	0.00	0.00	0.00	0.00	0.00	0.00	0.00	0.00	0.00	0.00	0.00	0.00
Total	4.32	4.35	4.38	4.33	4.37	4.32	4.36	4.36	4.36	4.35	4.33	4.31	4.37
Oxides (corr.)													
SiO_2	53.37	53.41	52.81	53.16	52.21	52.09	52.45	52.47	52.31	52.27	52.82	52.75	52.45
TiO_2	1.75	1.79	0.78	1.75	1.38	3.00	1.66	1.66	1.61	1.18	2.51	3.43	1.34
Al_2O_3	0.29	0.33	0.39	0.34	0.30	0.29	0.29	0.27	0.25	0.31	0.26	0.31	0.27
Cr_2O_3	0.00	0.03	0.00	0.00	0.00	0.02	0.00	0.01	0.01	0.00	0.00	0.00	0.00
Fe_2O_3	31.52	34.43	37.28	32.49	35.49	31.60	35.33	35.65	35.17	33.42	32.31	30.67	36.26
FeO	-0.72	-1.24	-3.99	-0.16	-2.14	-0.31	-2.23	-2.53	-2.05	-1.12	-0.12	0.40	-2.43
MnO	0.21	0.20	0.49	0.20	0.23	0.19	0.29	0.22	0.19	0.22	0.21	0.23	0.14
MgO	0.01	0.02	0.03	0.05	0.01	0.01	0.00	0.00	0.00	0.01	0.00	0.01	0.01
CaO	0.43	0.44	0.36	0.44	0.57	0.81	0.42	0.58	0.59	0.34	0.78	0.67	0.36
Na_2O	14.09	14.21	14.38	13.89	13.98	13.80	14.14	14.18	14.04	13.80	13.87	13.94	14.17
K_2O	0.00	0.01	0.05	0.01	0.01	0.02	0.02	0.01	0.00	0.00	0.01	0.01	0.01
total	100.95	103.63	102.58	102.18	102.02	101.52	102.37	102.52	102.12	100.44	102.64	102.41	102.58
Formula (corr.)	6(O)	6(O)	6(O)	6(O)	6(O)	6(O)	6(O)	6(O)	6(O)	6(O)	6(O)	6(O)	6(O)
Si	2.01	1.97	1.97	1.99	1.96	1.97	1.96	1.96	1.96	1.99	1.97	1.97	1.96
Ti	0.05	0.05	0.02	0.05	0.04	0.09	0.05	0.05	0.05	0.03	0.07	0.10	0.04
Al	0.01	0.01	0.02	0.02	0.01	0.01	0.01	0.01	0.01	0.01	0.01	0.01	0.01
Cr	0.00	0.00	0.00	0.00	0.00	0.00	0.00	0.00	0.00	0.00	0.00	0.00	0.00
Fe3+	0.89	0.96	1.05	0.92	1.00	0.90	1.00	1.00	0.99	0.96	0.91	0.86	1.02
Fe2+	-0.02	-0.04	-0.12	-0.01	-0.07	-0.01	-0.07	-0.08	-0.06	-0.04	0.00	0.01	-0.08
Mn	0.01	0.01	0.02	0.01	0.01	0.01	0.01	0.01	0.01	0.01	0.01	0.01	0.01
Mg	0.00	0.00	0.00	0.00	0.00	0.00	0.00	0.00	0.00	0.00	0.00	0.00	0.00

Ca	0.02	0.02	0.01	0.02	0.02	0.03	0.02	0.02	0.02	0.01	0.03	0.03	0.01
Na	1.03	1.02	1.04	1.01	1.02	1.01	1.03	1.03	1.02	1.02	1.00	1.01	1.03
K	0.00	0.00	0.00	0.00	0.00	0.00	0.00	0.00	0.00	0.00	0.00	0.00	0.00
Total	4.00	4.00	4.00	4.00	4.00	4.00	4.00	4.00	4.00	4.00	4.00	4.00	4.00
Mg/(Mg+Fe2)	-0.02	-0.03	-0.02	-1.47	-0.01	-0.05	0.00	0.00	0.00	-0.02	0.00	0.05	-0.01
Fe2/(Fetot)	-0.03	-0.04	-0.14	-0.01	-0.07	-0.01	-0.08	-0.09	-0.07	-0.04	0.00	0.01	-0.08
Al/(Al+Fe3+Cr)	0.01	0.02	0.02	0.02	0.01	0.01	0.01	0.01	0.01	0.01	0.01	0.02	0.01
Tri. plots													
En	-0.08	-0.06	-0.02	0.19	-0.01	0.02	0.00	0.00	0.00	-0.04	0.00	0.02	-0.01
Fs	4.55	1.96	1.15	-0.32	1.53	-0.42	1.32	1.42	1.58	1.70	-0.14	0.31	1.25
Wo	-3.47	-0.90	-0.13	1.13	-0.52	1.40	-0.32	-0.42	-0.58	-0.66	1.14	0.67	-0.24
Jd	0.02	0.02	0.02	0.02	0.01	0.01	0.01	0.01	0.01	0.02	0.01	0.02	0.01
Ac	1.02	1.00	1.02	0.99	1.01	1.00	1.01	1.02	1.01	1.00	0.99	0.99	1.02
Aug	-0.03	-0.02	-0.04	-0.01	-0.02	-0.01	-0.03	-0.03	-0.02	-0.02	0.00	-0.01	-0.03
Jd or Ac	0.01	0.02	0.02	0.02	0.01	0.01	0.01	0.01	0.01	0.01	0.01	0.02	0.01
A(+aqw)	1.03	0.63	-0.15	2.30	0.03	2.48	0.17	0.12	0.20	0.63	4.97	3.37	-0.05
C(+aqw)	-0.29	-0.49	-0.18	-1.03	-0.60	-1.64	-0.32	-0.42	-0.55	-0.37	-3.64	-1.34	-0.27
(FM)(+aqw)	0.26	0.86	1.32	-0.26	1.58	0.16	1.15	1.30	1.35	0.74	-0.33	-1.02	1.31
Mole fractions													
XSi (T)	1.01	0.99	0.98	1.00	0.98	0.98	0.98	0.98	0.98	1.00	0.99	0.99	0.98
XAl (T)	-0.01	0.01	0.02	0.01	0.02	0.02	0.02	0.02	0.02	0.01	0.01	0.02	0.02
XAl (M1)	0.03	-0.01	-0.02	0.01	-0.03	-0.02	-0.03	-0.03	-0.03	0.00	-0.02	-0.02	-0.03
XFe3 (M1)	0.89	0.96	1.05	0.92	1.00	0.90	1.00	1.00	0.99	0.96	0.91	0.86	1.02
XFe2 (M1)	0.05	0.01	-0.06	-0.03	-0.02	0.13	-0.02	-0.02	-0.01	0.01	-0.05	0.04	-0.03
XMg (M1)	0.00	0.00	0.00	0.02	0.00	-0.01	0.00	0.00	0.00	0.00	0.00	0.00	0.00
XFe2 (M2)	-0.07	-0.04	-0.06	0.03	-0.05	-0.13	-0.05	-0.06	-0.05	-0.04	0.05	-0.02	-0.05
XMg (M2)	0.00	0.00	0.00	-0.02	0.00	0.01	0.00	0.00	0.00	0.00	0.00	0.00	0.00
XCa (M2)	0.02	0.02	0.01	0.02	0.02	0.03	0.02	0.02	0.02	0.01	0.03	0.03	0.01
XNa (M2)	1.03	1.02	1.04	1.01	1.02	1.01	1.03	1.03	1.02	1.02	1.00	1.01	1.03
augite													
diopside													
hedenbergite													
pigeonite													
enstatite													
ferrosilite													

aegirine													
jadeite													
aegirine-augite													
omphacite													
Sodic pyx:	sodic	sodic	sodic	sodic	sodic	sodic	sodic	sodic	sodic	sodic	sodic	sodic	sodic

	FL1	**211**	**211**	**211**	**211**	**211**	**211**	**211**	**211**	**211**	**211**	**211**	**246**	**246**
SiO_2	52.12	52.49	52.16	52.27	51.99	51.62	51.06	51.32	51.37	51.12	50.81	52.25	51.06	51.40
TiO_2	2.12	2.74	1.64	1.68	1.97	1.21	1.22	1.68	1.51	2.69	2.44	2.18	1.38	1.45
Al_2O_3	0.28	0.20	0.27	0.33	0.24	0.31	0.28	0.30	0.30	0.28	0.26	0.25	0.43	0.86
Cr_2O_3	0.00	0.00	0.01	0.00	0.00	0.00	0.00	0.02	0.00	0.02	0.03	0.00	0.00	0.02
FeO	29.23	28.38	29.76	29.72	29.50	30.41	29.87	29.70	30.00	28.79	29.11	29.30	28.40	29.37
MnO	0.26	0.27	0.15	0.19	0.19	0.19	0.12	0.19	0.22	0.22	0.23	0.20	0.65	0.39
MgO	0.00	0.00	0.02	0.00	0.00	0.00	0.00	0.01	0.00	0.00	0.00	0.00	0.04	0.03
CaO	0.67	1.04	0.75	0.78	0.86	0.52	0.56	0.73	0.75	0.90	0.80	0.71	2.14	1.94
Na_2O	13.82	13.90	14.25	13.77	13.56	14.03	14.06	14.04	14.04	13.83	13.86	13.96	12.98	13.36
K_2O	0.01	0.01	0.00	0.00	0.01	0.03	0.02	0.01	0.01	0.00	0.00	0.00	0.01	0.01
Total	98.96	99.44	99.24	98.87	98.48	98.50	97.41	98.15	98.38	98.30	97.95	99.15	98.47	98.89
Mol. Props.														
SiO_2	0.87	0.87	0.87	0.87	0.87	0.86	0.85	0.85	0.86	0.85	0.85	0.87	0.85	0.86
TiO_2	0.03	0.03	0.02	0.02	0.03	0.02	0.02	0.02	0.02	0.03	0.03	0.03	0.02	0.02
Al_2O_3	0.00	0.00	0.00	0.00	0.00	0.00	0.00	0.00	0.00	0.00	0.00	0.00	0.00	0.01
Cr_2O_3	0.00	0.00	0.00	0.00	0.00	0.00	0.00	0.00	0.00	0.00	0.00	0.00	0.00	0.00
FeO	0.41	0.40	0.41	0.41	0.41	0.42	0.42	0.41	0.42	0.40	0.41	0.41	0.40	0.41
MnO	0.00	0.00	0.00	0.00	0.00	0.00	0.00	0.00	0.00	0.00	0.00	0.00	0.01	0.01
MgO	0.00	0.00	0.00	0.00	0.00	0.00	0.00	0.00	0.00	0.00	0.00	0.00	0.00	0.00
CaO	0.01	0.02	0.01	0.01	0.02	0.01	0.01	0.01	0.01	0.02	0.01	0.01	0.04	0.04
Na_2O	0.22	0.22	0.23	0.22	0.22	0.23	0.23	0.23	0.23	0.22	0.22	0.23	0.21	0.22
K_2O	0.00	0.00	0.00	0.00	0.00	0.00	0.00	0.00	0.00	0.00	0.00	0.00	0.00	0.00
Total	1.54	1.55	1.55	1.55	1.54	1.54	1.52	1.53	1.54	1.53	1.53	1.55	1.52	1.55
Oxygen prop.														
SiO_2	1.74	1.75	1.74	1.74	1.73	1.72	1.70	1.71	1.71	1.70	1.69	1.74	1.70	1.71
TiO_2	0.05	0.07	0.04	0.04	0.05	0.03	0.03	0.04	0.04	0.07	0.06	0.06	0.04	0.04
Al_2O_3	0.01	0.01	0.01	0.01	0.01	0.01	0.01	0.01	0.01	0.01	0.01	0.01	0.01	0.03
Cr_2O_3	0.00	0.00	0.00	0.00	0.00	0.00	0.00	0.00	0.00	0.00	0.00	0.00	0.00	0.00
FeO	0.41	0.40	0.41	0.41	0.41	0.42	0.42	0.41	0.42	0.40	0.41	0.41	0.40	0.41
MnO	0.00	0.00	0.00	0.00	0.00	0.00	0.00	0.00	0.00	0.00	0.00	0.00	0.01	0.01

MgO	0.00	0.00	0.00	0.00	0.00	0.00	0.00	0.00	0.00	0.00	0.00	0.00	0.00	0.00
CaO	0.01	0.02	0.01	0.01	0.02	0.01	0.01	0.01	0.01	0.02	0.01	0.01	0.04	0.04
Na_2O	0.22	0.22	0.23	0.22	0.22	0.23	0.23	0.23	0.23	0.22	0.22	0.23	0.21	0.22
K_2O	0.00	0.00	0.00	0.00	0.00	0.00	0.00	0.00	0.00	0.00	0.00	0.00	0.00	0.00
Total	2.44	2.46	2.45	2.44	2.43	2.42	2.39	2.42	2.42	2.42	2.41	2.45	2.40	2.44
Norm. factor	2.46	2.44	2.45	2.46	2.47	2.48	2.51	2.48	2.48	2.48	2.49	2.45	2.50	2.46
Formula	6(O)	6(O)	6(O)	6(O)	6(O)	6(O)	6(O)	6(O)	6(O)	6(O)	6(O)	6(O)	6(O)	6(O)
Si	2.13	2.13	2.13	2.14	2.13	2.13	2.13	2.12	2.12	2.11	2.11	2.13	2.13	2.11
Ti	0.07	0.08	0.05	0.05	0.06	0.04	0.04	0.05	0.05	0.08	0.08	0.07	0.04	0.05
Al	0.01	0.01	0.01	0.02	0.01	0.02	0.01	0.01	0.01	0.01	0.01	0.01	0.02	0.04
Cr	0.00	0.00	0.00	0.00	0.00	0.00	0.00	0.00	0.00	0.00	0.00	0.00	0.00	0.00
Fe++	1.00	0.96	1.02	1.02	1.01	1.05	1.04	1.03	1.04	0.99	1.01	1.00	0.99	1.01
Mn	0.01	0.01	0.01	0.01	0.01	0.01	0.00	0.01	0.01	0.01	0.01	0.01	0.02	0.01
Mg	0.00	0.00	0.00	0.00	0.00	0.00	0.00	0.00	0.00	0.00	0.00	0.00	0.00	0.00
Ca	0.03	0.05	0.03	0.03	0.04	0.02	0.03	0.03	0.03	0.04	0.04	0.03	0.10	0.09
Na	1.10	1.09	1.13	1.09	1.08	1.12	1.14	1.13	1.13	1.11	1.12	1.10	1.05	1.06
K	0.00	0.00	0.00	0.00	0.00	0.00	0.00	0.00	0.00	0.00	0.00	0.00	0.00	0.00
Total	4.35	4.33	4.38	4.35	4.34	4.39	4.39	4.38	4.39	4.35	4.37	4.35	4.35	4.36
Oxides (corr.)														
SiO_2	52.12	52.49	52.16	52.27	51.99	51.62	51.06	51.32	51.37	51.12	50.81	52.25	51.06	51.40
TiO_2	2.12	2.74	1.64	1.68	1.97	1.21	1.22	1.68	1.51	2.69	2.44	2.18	1.38	1.45
Al_2O_3	0.28	0.20	0.27	0.33	0.24	0.31	0.28	0.30	0.30	0.28	0.26	0.25	0.43	0.86
Cr_2O_3	0.00	0.00	0.01	0.00	0.00	0.00	0.00	0.02	0.00	0.02	0.03	0.00	0.00	0.02
Fe2O3	33.58	32.48	36.82	34.17	33.07	37.33	37.55	36.80	37.26	34.18	35.22	34.13	33.11	35.03
FeO	-0.99	-0.85	-3.37	-1.03	-0.26	-3.18	-3.92	-3.41	-3.53	-1.96	-2.58	-1.41	-1.39	-2.15
MnO	0.26	0.27	0.15	0.19	0.19	0.19	0.12	0.19	0.22	0.22	0.23	0.20	0.65	0.39
MgO	0.00	0.00	0.02	0.00	0.00	0.00	0.00	0.01	0.00	0.00	0.00	0.00	0.04	0.03
CaO	0.67	1.04	0.75	0.78	0.86	0.52	0.56	0.73	0.75	0.90	0.80	0.71	2.14	1.94
Na_2O	13.82	13.90	14.25	13.77	13.56	14.03	14.06	14.04	14.04	13.83	13.86	13.96	12.98	13.36
K_2O	0.01	0.01	0.00	0.00	0.01	0.03	0.02	0.01	0.01	0.00	0.00	0.00	0.01	0.01
Total	101.87	102.28	102.70	102.16	101.63	102.05	100.94	101.68	101.93	101.28	101.07	102.27	100.41	102.34

Formula (corr.)	6(O)	6(O)	6(O)	6(O)	6(O)	6(O)	6(O)	6(O)	6(O)	6(O)	6(O)	6(O)	6(O)	6(O)
Si	1.96	1.97	1.95	1.96	1.97	1.94	1.94	1.94	1.94	1.94	1.93	1.96	1.96	1.93
Ti	0.06	0.08	0.05	0.05	0.06	0.03	0.04	0.05	0.04	0.08	0.07	0.06	0.04	0.04
Al	0.01	0.01	0.01	0.02	0.01	0.01	0.01	0.01	0.01	0.01	0.01	0.01	0.02	0.04
Cr	0.00	0.00	0.00	0.00	0.00	0.00	0.00	0.00	0.00	0.00	0.00	0.00	0.00	0.00
Fe3+	0.95	0.92	1.03	0.97	0.94	1.06	1.07	1.05	1.06	0.98	1.01	0.96	0.95	0.99
Fe2+	-0.03	-0.03	-0.11	-0.03	-0.01	-0.10	-0.13	-0.11	-0.11	-0.06	-0.08	-0.04	-0.05	-0.07
Mn	0.01	0.01	0.01	0.01	0.01	0.01	0.00	0.01	0.01	0.01	0.01	0.01	0.02	0.01
Mg	0.00	0.00	0.00	0.00	0.00	0.00	0.00	0.00	0.00	0.00	0.00	0.00	0.00	0.00
Ca	0.03	0.04	0.03	0.03	0.04	0.02	0.02	0.03	0.03	0.04	0.03	0.03	0.09	0.08
Na	1.01	1.01	1.03	1.00	0.99	1.02	1.04	1.03	1.03	1.02	1.02	1.02	0.96	0.97
K	0.00	0.00	0.00	0.00	0.00	0.00	0.00	0.00	0.00	0.00	0.00	0.00	0.00	0.00
Total	4.00	4.00	4.00	4.00	4.00	4.00	4.00	4.00	4.00	4.00	4.00	4.00	4.00	4.00
Mg/(Mg+Fe2)	0.00	0.00	-0.01	0.00	0.00	0.00	0.00	-0.01	0.00	0.00	0.00	0.00	-0.05	-0.03
Fe2/(Fetot)	-0.03	-0.03	-0.11	-0.04	-0.01	-0.11	-0.13	-0.12	-0.12	-0.07	-0.09	-0.05	-0.05	-0.07
Al/(Al+Fe3+Cr)	0.01	0.01	0.01	0.02	0.01	0.01	0.01	0.01	0.01	0.01	0.01	0.01	0.02	0.04
Tri. plots														
En	0.00	0.01	-0.01	0.00	0.00	0.00	0.00	-0.01	0.00	0.00	0.00	0.00	0.05	0.14
Fs	7.74	-1.75	1.42	38.14	-0.31	1.26	1.22	1.39	1.38	2.43	1.67	2.85	-0.99	-5.61
Wo	-6.74	2.75	-0.40	-37.14	1.31	-0.26	-0.22	-0.38	-0.38	-1.43	-0.67	-1.85	1.94	6.47
Jd	0.01	0.01	0.01	0.02	0.01	0.01	0.01	0.01	0.01	0.01	0.01	0.01	0.02	0.04
Ac	1.00	1.00	1.02	0.99	0.98	1.01	1.02	1.02	1.01	1.00	1.01	1.00	0.95	0.94
Aug	-0.01	-0.01	-0.03	0.00	0.01	-0.02	-0.04	-0.03	-0.03	-0.02	-0.02	-0.02	0.04	0.03
Jd or Ac	0.01	0.01	0.01	0.02	0.01	0.01	0.01	0.01	0.01	0.01	0.01	0.01	0.02	0.04
A(+aqw)	1.23	2.27	-0.12	1.85	-1.83	-0.48	-0.35	-0.28	-0.43	0.44	0.02	0.69	0.07	0.53
C(+aqw)	-1.49	-2.22	-0.48	-5.18	3.01	-0.42	-0.31	-0.53	-0.59	-1.13	-0.77	-0.97	1.23	1.49

(FM)(+aqw)	1.26	0.95	1.61	4.33	-0.18	1.89	1.66	1.81	2.01	1.69	1.75	1.28	-0.30	-1.02
Mole fractions														
XSi (T)	0.98	0.98	0.97	0.98	0.98	0.97	0.97	0.97	0.97	0.97	0.97	0.98	0.98	0.97
XAl (T)	0.02	0.02	0.03	0.02	0.02	0.03	0.03	0.03	0.03	0.03	0.03	0.02	0.02	0.03
XAl (M1)	-0.03	-0.03	-0.04	-0.02	-0.02	-0.04	-0.05	-0.05	-0.05	-0.05	-0.06	-0.03	-0.03	-0.03
XFe3 (M1)	0.95	0.92	1.03	0.97	0.94	1.06	1.07	1.05	1.06	0.98	1.01	0.96	0.95	0.99
XFe2 (M1)	0.02	0.05	-0.04	0.01	0.11	-0.05	-0.06	-0.05	-0.05	0.00	-0.02	0.01	0.07	0.00
XMg (M1)	0.00	0.00	0.00	0.00	0.00	0.00	0.00	0.00	0.00	0.00	0.00	0.00	0.00	0.00
XFe2 (M2)	-0.05	-0.08	-0.06	-0.04	-0.12	-0.05	-0.06	-0.06	-0.06	-0.06	-0.06	-0.05	-0.11	-0.07
XMg (M2)	0.00	0.00	0.00	0.00	0.00	0.00	0.00	0.00	0.00	0.00	0.00	0.00	0.01	0.00
XCa (M2)	0.03	0.04	0.03	0.03	0.04	0.02	0.02	0.03	0.03	0.04	0.03	0.03	0.09	0.08
XNa (M2)	1.01	1.01	1.03	1.00	0.99	1.02	1.04	1.03	1.03	1.02	1.02	1.02	0.96	0.97
augite														
diopside														
hedenbergite														
pigeonite														
enstatite														
ferrosilite														
aegirine					aegirine								aegirine	aegirine
jadeite														
aegirine-augite														
omphacite														
Sodic pyx:	sodic	sodic	sodic	sodic	sodic	sodic	sodic	sodic	sodic	sodic	sodic	sodic	sodic	sodic

	246	**246**	**246**	**246**	**84**	**84**	**84**	**84**	**84**	**84**	**84**	**84**	**84**	**84**
SiO_2	51.94	51.41	51.78	51.69	53.51	53.06	53.43	53.75	53.02	53.10	53.22	53.14	53.31	53.14
TiO_2	1.37	1.51	0.96	2.34	1.20	1.18	1.38	1.16	2.06	1.57	1.80	0.76	1.29	1.01
Al_2O_3	1.00	0.78	0.72	0.32	0.31	0.34	0.28	0.30	0.37	0.36	0.32	0.32	0.37	0.37
Cr_2O_3	0.00	0.01	0.00	0.01	0.02	0.00	0.00	0.02	0.08	0.00	0.00	0.00	0.00	0.01
FeO	29.20	29.26	29.66	28.74	30.72	31.16	30.37	30.41	29.82	30.61	30.35	30.98	30.28	31.05
MnO	0.54	0.40	0.54	0.73	0.12	0.17	0.22	0.16	0.18	0.16	0.15	0.44	0.12	0.17
MgO	0.05	0.07	0.04	0.04	0.00	0.05	0.05	0.03	0.01	0.01	0.02	0.07	0.00	0.00
CaO	1.74	1.63	1.18	1.85	0.64	0.52	0.56	0.61	0.50	0.60	0.65	0.34	0.66	0.55
Na_2O	13.44	13.59	14.05	13.46	14.18	14.15	14.31	14.41	14.42	14.23	14.13	14.50	14.36	14.05
K_2O	0.01	0.02	0.00	0.00	0.01	0.00	0.01	0.00	0.00	0.00	0.00	0.03	0.01	0.00
Total	99.33	98.79	98.97	99.70	100.88	100.67	100.88	101.00	100.54	100.81	100.97	100.63	100.55	100.51
Mol. Props.														
SiO_2	0.86	0.86	0.86	0.86	0.89	0.88	0.89	0.90	0.88	0.88	0.89	0.88	0.89	0.88
TiO_2	0.02	0.02	0.01	0.03	0.02	0.02	0.02	0.01	0.03	0.02	0.02	0.01	0.02	0.01
Al_2O_3	0.01	0.01	0.01	0.00	0.00	0.00	0.00	0.00	0.00	0.00	0.00	0.00	0.00	0.00
Cr_2O_3	0.00	0.00	0.00	0.00	0.00	0.00	0.00	0.00	0.00	0.00	0.00	0.00	0.00	0.00
FeO	0.41	0.41	0.41	0.40	0.43	0.43	0.42	0.42	0.42	0.43	0.42	0.43	0.42	0.43
MnO	0.01	0.01	0.01	0.01	0.00	0.00	0.00	0.00	0.00	0.00	0.00	0.01	0.00	0.00
MgO	0.00	0.00	0.00	0.00	0.00	0.00	0.00	0.00	0.00	0.00	0.00	0.00	0.00	0.00
CaO	0.03	0.03	0.02	0.03	0.01	0.01	0.01	0.01	0.01	0.01	0.01	0.01	0.01	0.01
Na_2O	0.22	0.22	0.23	0.22	0.23	0.23	0.23	0.23	0.23	0.23	0.23	0.23	0.23	0.23
K_2O	0.00	0.00	0.00	0.00	0.00	0.00	0.00	0.00	0.00	0.00	0.00	0.00	0.00	0.00
Total	1.56	1.55	1.55	1.55	1.58	1.58	1.58	1.58	1.57	1.58	1.58	1.58	1.57	1.57
Oxygen prop.														
SiO_2	1.73	1.71	1.72	1.72	1.78	1.77	1.78	1.79	1.77	1.77	1.77	1.77	1.78	1.77
TiO_2	0.03	0.04	0.02	0.06	0.03	0.03	0.04	0.03	0.05	0.04	0.05	0.02	0.03	0.03
Al_2O_3	0.03	0.02	0.02	0.01	0.01	0.01	0.01	0.01	0.01	0.01	0.01	0.01	0.01	0.01
Cr_2O_3	0.00	0.00	0.00	0.00	0.00	0.00	0.00	0.00	0.00	0.00	0.00	0.00	0.00	0.00
FeO	0.41	0.41	0.41	0.40	0.43	0.43	0.42	0.42	0.42	0.43	0.42	0.43	0.42	0.43
MnO	0.01	0.01	0.01	0.01	0.00	0.00	0.00	0.00	0.00	0.00	0.00	0.01	0.00	0.00

MgO	0.00	0.00	0.00	0.00	0.00	0.00	0.00	0.00	0.00	0.00	0.00	0.00	0.00	0.00
CaO	0.03	0.03	0.02	0.03	0.01	0.01	0.01	0.01	0.01	0.01	0.01	0.01	0.01	0.01
Na_2O	0.22	0.22	0.23	0.22	0.23	0.23	0.23	0.23	0.23	0.23	0.23	0.23	0.23	0.23
K_2O	0.00	0.00	0.00	0.00	0.00	0.00	0.00	0.00	0.00	0.00	0.00	0.00	0.00	0.00
Total	2.46	2.44	2.44	2.45	2.49	2.48	2.49	2.50	2.49	2.49	2.49	2.48	2.49	2.48
Norm. factor	2.44	2.46	2.46	2.45	2.41	2.42	2.41	2.40	2.41	2.41	2.41	2.42	2.42	2.42
Formula	6(O)	6(O)	6(O)	6(O)	6(O)	6(O)	6(O)	6(O)	6(O)	6(O)	6(O)	6(O)	6(O)	6(O)
Si	2.11	2.11	2.12	2.11	2.15	2.14	2.14	2.15	2.13	2.13	2.13	2.14	2.14	2.14
Ti	0.04	0.05	0.03	0.07	0.04	0.04	0.04	0.04	0.06	0.05	0.05	0.02	0.04	0.03
Al	0.05	0.04	0.04	0.02	0.02	0.02	0.01	0.01	0.02	0.02	0.02	0.02	0.02	0.02
Cr	0.00	0.00	0.00	0.00	0.00	0.00	0.00	0.00	0.00	0.00	0.00	0.00	0.00	0.00
Fe++	0.99	1.00	1.02	0.98	1.03	1.05	1.02	1.02	1.00	1.03	1.02	1.05	1.02	1.05
Mn	0.02	0.01	0.02	0.03	0.00	0.01	0.01	0.01	0.01	0.01	0.01	0.02	0.00	0.01
Mg	0.00	0.00	0.00	0.00	0.00	0.00	0.00	0.00	0.00	0.00	0.00	0.00	0.00	0.00
Ca	0.08	0.07	0.05	0.08	0.03	0.02	0.02	0.03	0.02	0.03	0.03	0.02	0.03	0.02
Na	1.06	1.08	1.12	1.06	1.10	1.10	1.11	1.12	1.12	1.11	1.10	1.13	1.12	1.10
K	0.00	0.00	0.00	0.00	0.00	0.00	0.00	0.00	0.00	0.00	0.00	0.00	0.00	0.00
Total	4.35	4.37	4.39	4.35	4.36	4.37	4.37	4.37	4.36	4.37	4.35	4.39	4.37	4.37
Oxides (corr.)														
SiO_2	51.94	51.41	51.78	51.69	53.51	53.06	53.43	53.75	53.02	53.10	53.22	53.14	53.31	53.14
TiO_2	1.37	1.51	0.96	2.34	1.20	1.18	1.38	1.16	2.06	1.57	1.80	0.76	1.29	1.01
Al_2O_3	1.00	0.78	0.72	0.32	0.31	0.34	0.28	0.30	0.37	0.36	0.32	0.32	0.37	0.37
Cr_2O_3	0.00	0.01	0.00	0.01	0.02	0.00	0.00	0.02	0.08	0.00	0.00	0.00	0.00	0.01
Fe_2O_3	34.52	35.69	37.96	33.82	36.00	36.87	36.27	36.58	35.87	36.26	35.15	38.98	36.61	36.26
FeO	-1.87	-2.85	-4.50	-1.69	-1.67	-2.02	-2.27	-2.51	-2.46	-2.02	-1.28	-4.10	-2.66	-1.58
MnO	0.54	0.40	0.54	0.73	0.12	0.17	0.22	0.16	0.18	0.16	0.15	0.44	0.12	0.17
MgO	0.05	0.07	0.04	0.04	0.00	0.05	0.05	0.03	0.01	0.01	0.02	0.07	0.00	0.00
CaO	1.74	1.63	1.18	1.85	0.64	0.52	0.56	0.61	0.50	0.60	0.65	0.34	0.66	0.55
Na_2O	13.44	13.59	14.05	13.46	14.18	14.15	14.31	14.41	14.42	14.23	14.13	14.50	14.36	14.05
K_2O	0.01	0.02	0.00	0.00	0.01	0.00	0.01	0.00	0.00	0.00	0.00	0.03	0.01	0.00
total	102.74	102.26	102.74	102.58	104.33	104.32	104.23	104.51	104.06	104.28	104.16	104.48	104.07	103.98

Formula (corr.)	6(O)	6(O)	6(O)	6(O)	6(O)	6(O)	6(O)	6(O)	6(O)	6(O)	6(O)	6(O)	6(O)	6(O)
Si	1.94	1.93	1.93	1.94	1.97	1.95	1.96	1.97	1.95	1.95	1.96	1.95	1.96	1.96
Ti	0.04	0.04	0.03	0.07	0.03	0.03	0.04	0.03	0.06	0.04	0.05	0.02	0.04	0.03
Al	0.04	0.03	0.03	0.01	0.01	0.02	0.01	0.01	0.02	0.02	0.01	0.01	0.02	0.02
Cr	0.00	0.00	0.00	0.00	0.00	0.00	0.00	0.00	0.00	0.00	0.00	0.00	0.00	0.00
Fe3+	0.97	1.01	1.07	0.96	1.00	1.02	1.00	1.01	0.99	1.00	0.98	1.08	1.01	1.01
Fe2+	-0.06	-0.09	-0.14	-0.05	-0.05	-0.06	-0.07	-0.08	-0.08	-0.06	-0.04	-0.13	-0.08	-0.05
Mn	0.02	0.01	0.02	0.02	0.00	0.01	0.01	0.01	0.01	0.01	0.01	0.01	0.00	0.01
Mg	0.00	0.00	0.00	0.00	0.00	0.00	0.00	0.00	0.00	0.00	0.00	0.00	0.00	0.00
Ca	0.07	0.07	0.05	0.07	0.03	0.02	0.02	0.02	0.02	0.02	0.03	0.01	0.03	0.02
Na	0.97	0.99	1.02	0.98	1.01	1.01	1.02	1.02	1.03	1.02	1.01	1.03	1.02	1.01
K	0.00	0.00	0.00	0.00	0.00	0.00	0.00	0.00	0.00	0.00	0.00	0.00	0.00	0.00
Total	4.00	4.00	4.00	4.00	4.00	4.00	4.00	4.00	4.00	4.00	4.00	4.00	4.00	4.00
Mg/(Mg+Fe2)	-0.05	-0.04	-0.02	-0.05	0.00	-0.05	-0.04	-0.02	-0.01	-0.01	-0.03	-0.03	0.00	0.00
Fe2/(Fetot)	-0.06	-0.10	-0.15	-0.06	-0.05	-0.07	-0.08	-0.08	-0.08	-0.07	-0.04	-0.13	-0.09	-0.05
Al/(Al+Fe3+Cr)	0.04	0.03	0.03	0.02	0.01	0.01	0.01	0.01	0.02	0.02	0.01	0.01	0.02	0.02
Tri. plots														
En	0.19	-0.18	-0.03	0.10	0.00	-0.07	-0.06	-0.03	-0.01	-0.01	-0.10	-0.04	0.00	0.00
Fs	-4.17	4.41	1.55	-2.23	1.98	1.59	1.54	1.50	1.37	1.63	3.13	1.16	1.46	1.82
Wo	4.98	-3.22	-0.52	3.13	-0.98	-0.52	-0.49	-0.47	-0.36	-0.62	-2.04	-0.13	-0.46	-0.82
Jd	0.04	0.03	0.03	0.01	0.01	0.01	0.01	0.01	0.02	0.02	0.01	0.01	0.02	0.02
Ac	0.93	0.96	0.99	0.97	1.00	1.00	1.01	1.01	1.01	1.00	1.00	1.02	1.01	0.99
Aug	0.03	0.01	-0.02	0.02	-0.01	-0.01	-0.02	-0.02	-0.03	-0.02	-0.01	-0.03	-0.02	-0.01
Jd or Ac	0.04	0.03	0.03	0.02	0.01	0.01	0.01	0.01	0.02	0.02	0.01	0.01	0.02	0.02
A(+aqw)	0.40	1.39	-1.22	-0.12	0.02	-0.64	0.06	0.02	0.15	-0.08	0.56	-0.45	-0.06	-0.71
C(+aqw)	1.35	3.37	-1.43	1.76	-1.13	-0.99	-0.54	-0.51	-0.34	-0.77	-1.39	-0.21	-0.53	-1.75
(FM)(+aqw)	-0.75	-3.75	3.65	-0.65	2.11	2.62	1.49	1.49	1.19	1.85	1.83	1.65	1.58	3.46

Mole fractions														
XSi (T)	0.97	0.97	0.97	0.97	0.98	0.98	0.98	0.99	0.98	0.98	0.98	0.98	0.98	0.98
XAl (T)	0.03	0.04	0.03	0.03	0.02	0.02	0.02	0.02	0.02	0.02	0.02	0.03	0.02	0.02
XAl (M1)	-0.02	-0.04	-0.04	-0.05	-0.02	-0.03	-0.02	-0.02	-0.03	-0.03	-0.03	-0.04	-0.02	-0.02
XFe3 (M1)	0.97	1.01	1.07	0.96	1.00	1.02	1.00	1.01	0.99	1.00	0.98	1.08	1.01	1.01
XFe2 (M1)	0.01	-0.02	-0.07	0.05	-0.01	-0.03	-0.02	-0.03	-0.02	-0.02	0.00	-0.07	-0.03	-0.02
XMg (M1)	0.00	0.00	0.00	0.00	0.00	0.00	0.00	0.00	0.00	0.00	0.00	0.00	0.00	0.00
XFe2 (M2)	-0.07	-0.07	-0.07	-0.10	-0.04	-0.04	-0.05	-0.05	-0.05	-0.04	-0.04	-0.05	-0.05	-0.03
XMg (M2)	0.00	0.00	0.00	0.01	0.00	0.00	0.00	0.00	0.00	0.00	0.00	0.00	0.00	0.00
XCa (M2)	0.07	0.07	0.05	0.07	0.03	0.02	0.02	0.02	0.02	0.02	0.03	0.01	0.03	0.02
XNa (M2)	0.97	0.99	1.02	0.98	1.01	1.01	1.02	1.02	1.03	1.02	1.01	1.03	1.02	1.01
augite														
diopside														
hedenbergite														
pigeonite														
enstatite														
ferrosilite														
aegirine	aegirine	aegirine		aegirine										
jadeite	aegirine	aegirine		aegirine										
aegirine-augite														
omphacite														
Sodic pyx:	sodic	sodic	sodic	sodic	sodic	sodic	sodic	sodic	sodic	sodic	sodic	sodic	sodic	sodic

	84	**84**	**84**	**84**	**84**	**84**	**226**	**226**	**226**	**226**	**217**	**217**	**217**	**217**
SiO_2	53.16	53.16	53.16	52.57	53.29	52.95	54.10	53.82	53.99	53.89	53.00	53.02	52.59	52.98
TiO_2	1.58	1.11	1.06	1.46	1.12	1.37	2.38	2.41	3.16	3.24	2.39	3.15	2.16	2.61
Al_2O_3	0.32	0.31	0.34	0.24	0.32	0.32	0.28	0.27	0.25	0.22	0.31	0.28	0.28	0.36
Cr_2O_3	0.00	0.00	0.03	0.01	0.03	0.00	0.01	0.02	0.01	0.05	0.02	0.01	0.01	0.03
FeO	30.50	31.04	31.02	30.41	30.52	29.89	23.72	23.49	21.62	22.44	29.46	28.59	29.45	28.95
MnO	0.19	0.10	0.09	0.15	0.35	0.16	0.30	0.32	0.27	0.34	0.24	0.25	0.25	0.24
MgO	0.01	0.01	0.00	0.03	0.08	0.01	3.38	3.47	4.40	3.68	0.00	0.00	0.01	0.00
CaO	0.58	0.62	0.50	0.61	0.40	0.61	5.36	5.60	6.24	5.65	0.79	0.85	0.78	0.75
Na_2O	14.04	13.87	14.41	14.15	14.36	14.16	11.26	11.16	10.76	11.29	13.84	13.76	13.78	13.86
K_2O	0.00	0.01	0.00	0.00	0.00	0.01	0.00	0.01	0.00	0.00	0.01	0.01	0.00	0.00
Total	100.66	100.27	100.85	99.95	100.68	99.83	100.79	100.72	100.74	100.87	100.44	100.22	99.64	100.15
Mol. Props.														
SiO_2	0.89	0.89	0.89	0.88	0.89	0.88	0.90	0.90	0.90	0.90	0.88	0.88	0.88	0.88
TiO_2	0.02	0.01	0.01	0.02	0.01	0.02	0.03	0.03	0.04	0.04	0.03	0.04	0.03	0.03
Al_2O_3	0.00	0.00	0.00	0.00	0.00	0.00	0.00	0.00	0.00	0.00	0.00	0.00	0.00	0.00
Cr_2O_3	0.00	0.00	0.00	0.00	0.00	0.00	0.00	0.00	0.00	0.00	0.00	0.00	0.00	0.00
FeO	0.43	0.43	0.43	0.42	0.43	0.42	0.33	0.33	0.30	0.31	0.41	0.40	0.41	0.40
MnO	0.00	0.00	0.00	0.00	0.01	0.00	0.00	0.00	0.00	0.01	0.00	0.00	0.00	0.00
MgO	0.00	0.00	0.00	0.00	0.00	0.00	0.08	0.09	0.11	0.09	0.00	0.00	0.00	0.00
CaO	0.01	0.01	0.01	0.01	0.01	0.01	0.10	0.10	0.11	0.10	0.01	0.02	0.01	0.01
Na_2O	0.23	0.22	0.23	0.23	0.23	0.23	0.18	0.18	0.17	0.18	0.22	0.22	0.22	0.22
K_2O	0.00	0.00	0.00	0.00	0.00	0.00	0.00	0.00	0.00	0.00	0.00	0.00	0.00	0.00
Total	1.57	1.57	1.58	1.56	1.58	1.56	1.63	1.63	1.64	1.63	1.57	1.56	1.56	1.56
Oxygen prop.														
SiO_2	1.77	1.77	1.77	1.75	1.77	1.76	1.80	1.79	1.80	1.79	1.76	1.77	1.75	1.76
TiO_2	0.04	0.03	0.03	0.04	0.03	0.03	0.06	0.06	0.08	0.08	0.06	0.08	0.05	0.07
Al_2O_3	0.01	0.01	0.01	0.01	0.01	0.01	0.01	0.01	0.01	0.01	0.01	0.01	0.01	0.01
Cr_2O_3	0.00	0.00	0.00	0.00	0.00	0.00	0.00	0.00	0.00	0.00	0.00	0.00	0.00	0.00
FeO	0.43	0.43	0.43	0.42	0.43	0.42	0.33	0.33	0.30	0.31	0.41	0.40	0.41	0.40
MnO	0.00	0.00	0.00	0.00	0.01	0.00	0.00	0.00	0.00	0.01	0.00	0.00	0.00	0.00

MgO	0.00	0.00	0.00	0.00	0.00	0.00	0.08	0.09	0.11	0.09	0.00	0.00	0.00	0.00
CaO	0.01	0.01	0.01	0.01	0.01	0.01	0.10	0.10	0.11	0.10	0.01	0.02	0.01	0.01
Na_2O	0.23	0.22	0.23	0.23	0.23	0.23	0.18	0.18	0.17	0.18	0.22	0.22	0.22	0.22
K_2O	0.00	0.00	0.00	0.00	0.00	0.00	0.00	0.00	0.00	0.00	0.00	0.00	0.00	0.00
Total	2.48	2.48	2.48	2.46	2.48	2.46	2.56	2.56	2.58	2.57	2.49	2.49	2.46	2.48
Norm. factor	2.42	2.42	2.42	2.44	2.42	2.44	2.34	2.35	2.32	2.33	2.42	2.41	2.44	2.42
Formula														
Si	6(O)	6(O)	6(O)	6(O)	6(O)	6(O)	6(O)	6(O)	6(O)	6(O)	6(O)	6(O)	6(O)	6(O)
Ti	2.14	2.15	2.14	2.14	2.14	2.15	2.11	2.10	2.09	2.09	2.13	2.13	2.13	2.13
Al	0.05	0.03	0.03	0.05	0.03	0.04	0.07	0.07	0.09	0.10	0.07	0.10	0.07	0.08
Cr	0.02	0.02	0.02	0.01	0.02	0.02	0.01	0.01	0.01	0.01	0.02	0.01	0.01	0.02
Fe++	0.00	0.00	0.00	0.00	0.00	0.00	0.00	0.00	0.00	0.00	0.00	0.00	0.00	0.00
Mn	1.03	1.05	1.04	1.03	1.03	1.01	0.77	0.77	0.70	0.73	0.99	0.96	1.00	0.97
Mg	0.01	0.00	0.00	0.01	0.01	0.01	0.01	0.01	0.01	0.01	0.01	0.01	0.01	0.01
Ca	0.00	0.00	0.00	0.00	0.01	0.00	0.20	0.20	0.25	0.21	0.00	0.00	0.00	0.00
Na	0.03	0.03	0.02	0.03	0.02	0.03	0.22	0.23	0.26	0.24	0.03	0.04	0.03	0.03
K	1.10	1.09	1.12	1.11	1.12	1.11	0.85	0.85	0.81	0.85	1.08	1.07	1.08	1.08
Total	0.00	0.00	0.00	0.00	0.00	0.00	0.00	0.00	0.00	0.00	0.00	0.00	0.00	0.00
Oxides (corr.)	4.35	4.36	4.38	4.37	4.37	4.36	4.24	4.24	4.22	4.23	4.33	4.31	4.34	4.32
SiO_2														
TiO_2	53.16	53.16	53.16	52.57	53.29	52.95	54.10	53.82	53.99	53.89	53.00	53.02	52.59	52.98
Al_2O_3	1.58	1.11	1.06	1.46	1.12	1.37	2.38	2.41	3.16	3.24	2.39	3.15	2.16	2.61
Cr_2O_3	0.32	0.31	0.34	0.24	0.32	0.32	0.28	0.27	0.25	0.22	0.31	0.28	0.28	0.36
Fe_2O_3	0.00	0.00	0.03	0.01	0.03	0.00	0.01	0.02	0.01	0.05	0.02	0.01	0.01	0.03
FeO	35.10	35.24	37.85	36.47	37.09	35.54	24.79	24.91	22.48	23.98	32.66	30.59	33.11	31.93
MnO	-1.08	-0.67	-3.04	-2.41	-2.85	-2.09	1.42	1.07	1.39	0.86	0.07	1.06	-0.35	0.22
MgO	0.19	0.10	0.09	0.15	0.35	0.16	0.30	0.32	0.27	0.34	0.24	0.25	0.25	0.24
CaO	0.01	0.01	0.00	0.03	0.08	0.01	3.38	3.47	4.40	3.68	0.00	0.00	0.01	0.00
Na_2O	0.58	0.62	0.50	0.61	0.40	0.61	5.36	5.60	6.24	5.65	0.79	0.85	0.78	0.75
K_2O	14.04	13.87	14.41	14.15	14.36	14.16	11.26	11.16	10.76	11.29	13.84	13.76	13.78	13.86
total	0.00	0.01	0.00	0.00	0.00	0.01	0.00	0.01	0.00	0.00	0.01	0.01	0.00	0.00
	103.90	103.75	104.40	103.27	104.17	103.04	103.28	103.06	102.96	103.20	103.34	102.99	102.62	102.98

Formula (corr.)	6(O)	6(O)	6(O)	6(O)	6(O)	6(O)	6(O)	6(O)	6(O)	6(O)	6(O)	6(O)	6(O)	6(O)
Si	1.96	1.97	1.95	1.95	1.96	1.97	1.99	1.98	1.98	1.98	1.97	1.97	1.97	1.97
Ti	0.04	0.03	0.03	0.04	0.03	0.04	0.07	0.07	0.09	0.09	0.07	0.09	0.06	0.07
Al	0.01	0.01	0.02	0.01	0.01	0.01	0.01	0.01	0.01	0.01	0.01	0.01	0.01	0.02
Cr	0.00	0.00	0.00	0.00	0.00	0.00	0.00	0.00	0.00	0.00	0.00	0.00	0.00	0.00
Fe3+	0.98	0.98	1.05	1.02	1.03	0.99	0.69	0.69	0.62	0.66	0.91	0.86	0.93	0.89
Fe2+	-0.03	-0.02	-0.09	-0.08	-0.09	-0.07	0.04	0.03	0.04	0.03	0.00	0.03	-0.01	0.01
Mn	0.01	0.00	0.00	0.01	0.01	0.01	0.01	0.01	0.01	0.01	0.01	0.01	0.01	0.01
Mg	0.00	0.00	0.00	0.00	0.00	0.00	0.19	0.19	0.24	0.20	0.00	0.00	0.00	0.00
Ca	0.02	0.02	0.02	0.02	0.02	0.02	0.21	0.22	0.25	0.22	0.03	0.03	0.03	0.03
Na	1.01	1.00	1.03	1.02	1.02	1.02	0.80	0.80	0.77	0.80	1.00	0.99	1.00	1.00
K	0.00	0.00	0.00	0.00	0.00	0.00	0.00	0.00	0.00	0.00	0.00	0.00	0.00	0.00
Total	4.00	4.00	4.00	4.00	4.00	4.00	4.00	4.00	4.00	4.00	4.00	4.00	4.00	4.00
Mg/(Mg+Fe2)	-0.02	-0.03	0.00	-0.02	-0.05	-0.01	0.81	0.85	0.85	0.88	0.00	0.00	-0.08	0.02
Fe2/(Fetot)	-0.04	-0.02	-0.10	-0.08	-0.09	-0.07	0.06	0.05	0.06	0.04	0.00	0.04	-0.01	0.01
Al/(Al+Fe3+Cr)	0.01	0.01	0.01	0.01	0.01	0.01	0.02	0.02	0.02	0.01	0.02	0.01	0.01	0.02
Tri. plots														
En	-0.07	0.12	0.00	-0.03	-0.06	-0.01	0.42	0.43	0.46	0.45	0.00	0.00	0.04	0.00
Fs	3.37	-4.94	1.27	1.52	1.29	1.62	0.10	0.07	0.08	0.06	0.06	0.49	-0.51	0.19
Wo	-2.30	5.81	-0.27	-0.49	-0.23	-0.61	0.48	0.50	0.46	0.49	0.94	0.51	1.48	0.81
Jd	0.01	0.01	0.01	0.01	0.01	0.01	0.01	0.01	0.01	0.01	0.02	0.01	0.01	0.02
Ac	0.99	0.98	1.01	1.01	1.01	1.01	0.79	0.78	0.75	0.79	0.98	0.98	0.99	0.98
Aug	-0.01	0.00	-0.03	-0.02	-0.02	-0.02	0.20	0.20	0.24	0.20	0.00	0.01	0.00	0.00
Jd or Ac	0.01	0.01	0.01	0.01	0.01	0.01	0.02	0.02	0.02	0.01	0.02	0.01	0.01	0.02
A(+aqw)	0.67	-0.02	-0.33	-0.14	-0.18	0.15	-0.13	-0.12	-0.14	-0.16	-5.29	-4.62	-18.09	358.01
C(+aqw)	-1.92	3.41	-0.38	-0.62	-0.32	-0.59	0.53	0.54	0.52	0.56	4.82	2.55	20.56	-240.81
(FM)(+aqw)	2.25	-2.39	1.71	1.76	1.50	1.44	0.60	0.57	0.62	0.60	1.47	3.07	-1.47	-

														116.20
Mole fractions														
XSi (T)	0.98	0.99	0.98	0.98	0.98	0.98	0.99	0.99	0.99	0.99	0.98	0.99	0.98	0.99
XAl (T)	0.02	0.02	0.02	0.02	0.02	0.02	0.01	0.01	0.01	0.01	0.02	0.01	0.02	0.01
XAl (M1)	-0.02	-0.02	-0.03	-0.04	-0.03	-0.02	0.00	-0.01	-0.01	-0.02	-0.02	-0.01	-0.02	-0.01
XFe3 (M1)	0.98	0.98	1.05	1.02	1.03	0.99	0.69	0.69	0.62	0.66	0.91	0.86	0.93	0.89
XFe2 (M1)	0.00	0.01	-0.05	-0.03	-0.04	-0.02	0.05	0.04	0.04	0.03	0.01	0.06	0.14	0.02
XMg (M1)	0.00	0.00	0.00	0.00	0.00	0.00	0.20	0.20	0.25	0.22	0.00	0.00	-0.01	0.00
XFe2 (M2)	-0.04	-0.03	-0.05	-0.05	-0.05	-0.05	0.00	0.00	0.00	0.00	-0.01	-0.02	-0.15	-0.01
XMg (M2)	0.00	0.00	0.00	0.00	0.00	0.00	-0.01	-0.01	-0.01	-0.02	0.00	0.00	0.01	0.00
XCa (M2)	0.02	0.02	0.02	0.02	0.02	0.02	0.21	0.22	0.25	0.22	0.03	0.03	0.03	0.03
XNa (M2)	1.01	1.00	1.03	1.02	1.02	1.02	0.80	0.80	0.77	0.80	1.00	0.99	1.00	1.00
augite														
diopside														
hedenbergite														
pigeonite														
enstatite														
ferrosilite														
aegirine		aegirine					aegirine			aegirine	aegirine	aegirine	aegirine	
jadeite														
aegirine-augite	aegirine-augite							aegirine-augite	aegirine-augite					
omphacite														
Sodic pyx:	sodic	sodic	sodic	sodic	sodic	sodic	sodic	sodic	sodic	sodic	sodic	sodic	sodic	sodic

	217	**217**	**217**	**217**	**217**	**217**	**217**	**248**	**248**	**248**	**248**	**248**
SiO_2	53.00	53.15	53.50	52.75	53.20	53.35	53.07	53.53	52.09	51.79	52.10	51.81
TiO_2	1.07	0.98	0.63	2.01	3.55	2.04	1.39	2.47	2.16	1.32	1.63	1.19
Al_2O_3	0.28	0.26	0.40	0.24	0.31	0.28	0.30	0.28	0.31	0.31	0.25	0.29
Cr_2O_3	0.00	0.00	0.00	0.04	0.00	0.00	0.00	0.00	0.00	0.01	0.00	0.01
FeO	30.54	30.63	30.58	29.23	27.92	29.64	30.46	25.66	27.32	28.85	28.68	29.02
MnO	0.25	0.30	0.32	0.36	0.29	0.30	0.16	0.87	0.67	0.51	0.56	0.50
MgO	0.03	0.01	0.00	0.02	0.01	0.00	0.02	0.83	0.56	0.41	0.42	0.37
CaO	0.67	0.21	0.04	0.91	0.91	0.79	0.64	3.37	3.32	5.85	4.86	6.27
Na_2O	13.90	13.84	14.17	13.47	13.67	13.86	14.14	12.81	12.31	10.93	11.48	10.52
K_2O	0.00	0.00	0.00	0.01	0.00	0.00	0.00	0.00	0.00	0.00	0.02	0.01
Total	99.89	99.42	99.67	99.32	100.18	100.62	100.43	100.67	100.80	100.92	101.05	101.18
Mol. Props.												
SiO_2	0.88	0.89	0.89	0.88	0.89	0.89	0.88	0.89	0.87	0.86	0.87	0.86
TiO_2	0.01	0.01	0.01	0.03	0.04	0.03	0.02	0.03	0.03	0.02	0.02	0.01
Al_2O_3	0.00	0.00	0.00	0.00	0.00	0.00	0.00	0.00	0.00	0.00	0.00	0.00
Cr_2O_3	0.00	0.00	0.00	0.00	0.00	0.00	0.00	0.00	0.00	0.00	0.00	0.00
FeO	0.43	0.43	0.43	0.41	0.39	0.41	0.42	0.36	0.38	0.40	0.40	0.40
MnO	0.00	0.00	0.00	0.01	0.00	0.00	0.00	0.01	0.01	0.01	0.01	0.01
MgO	0.00	0.00	0.00	0.00	0.00	0.00	0.00	0.02	0.01	0.01	0.01	0.01
CaO	0.01	0.00	0.00	0.02	0.02	0.01	0.01	0.06	0.06	0.10	0.09	0.11
Na_2O	0.22	0.22	0.23	0.22	0.22	0.22	0.23	0.21	0.20	0.18	0.19	0.17
K_2O	0.00	0.00	0.00	0.00	0.00	0.00	0.00	0.00	0.00	0.00	0.00	0.00
Total	1.56	1.56	1.56	1.55	1.56	1.57	1.57	1.58	1.56	1.58	1.58	1.58
Oxygen prop.												
SiO_2	1.76	1.77	1.78	1.76	1.77	1.78	1.77	1.78	1.73	1.72	1.73	1.72
TiO_2	0.03	0.03	0.02	0.05	0.09	0.05	0.04	0.06	0.05	0.03	0.04	0.03
Al_2O_3	0.01	0.01	0.01	0.01	0.01	0.01	0.01	0.01	0.01	0.01	0.01	0.01
Cr_2O_3	0.00	0.00	0.00	0.00	0.00	0.00	0.00	0.00	0.00	0.00	0.00	0.00

FeO	0.43	0.43	0.43	0.41	0.39	0.41	0.42	0.36	0.38	0.40	0.40	0.40
MnO	0.00	0.00	0.00	0.01	0.00	0.00	0.00	0.01	0.01	0.01	0.01	0.01
MgO	0.00	0.00	0.00	0.00	0.00	0.00	0.00	0.02	0.01	0.01	0.01	0.01
CaO	0.01	0.00	0.00	0.02	0.02	0.01	0.01	0.06	0.06	0.10	0.09	0.11
Na_2O	0.22	0.22	0.23	0.22	0.22	0.22	0.23	0.21	0.20	0.18	0.19	0.17
K_2O	0.00	0.00	0.00	0.00	0.00	0.00	0.00	0.00	0.00	0.00	0.00	0.00
Total	2.47	2.46	2.47	2.46	2.50	2.49	2.48	2.51	2.46	2.47	2.47	2.46
Norm. factor	2.43	2.44	2.43	2.44	2.40	2.41	2.42	2.39	2.44	2.43	2.43	2.43
Formula	6(O)	6(O)	6(O)	6(O)	6(O)	6(O)	6(O)	6(O)	6(O)	6(O)	6(O)	6(O)
Si	2.15	2.16	2.17	2.14	2.13	2.14	2.14	2.13	2.12	2.10	2.11	2.10
Ti	0.03	0.03	0.02	0.06	0.11	0.06	0.04	0.07	0.07	0.04	0.05	0.04
Al	0.01	0.01	0.02	0.01	0.02	0.01	0.01	0.01	0.01	0.01	0.01	0.01
Cr	0.00	0.00	0.00	0.00	0.00	0.00	0.00	0.00	0.00	0.00	0.00	0.00
Fe++	1.04	1.04	1.04	0.99	0.93	0.99	1.03	0.85	0.93	0.98	0.97	0.98
Mn	0.01	0.01	0.01	0.01	0.01	0.01	0.01	0.03	0.02	0.02	0.02	0.02
Mg	0.00	0.00	0.00	0.00	0.00	0.00	0.00	0.05	0.03	0.02	0.03	0.02
Ca	0.03	0.01	0.00	0.04	0.04	0.03	0.03	0.14	0.14	0.25	0.21	0.27
Na	1.09	1.09	1.11	1.06	1.06	1.08	1.11	0.99	0.97	0.86	0.90	0.83
K	0.00	0.00	0.00	0.00	0.00	0.00	0.00	0.00	0.00	0.00	0.00	0.00
Total	4.36	4.35	4.36	4.32	4.29	4.33	4.36	4.28	4.30	4.28	4.29	4.27
Oxides (corr.)												
SiO_2	53.00	53.15	53.50	52.75	53.20	53.35	53.07	53.53	52.09	51.79	52.10	51.81
TiO_2	1.07	0.98	0.63	2.01	3.55	2.04	1.39	2.47	2.16	1.32	1.63	1.19
Al_2O_3	0.28	0.26	0.40	0.24	0.31	0.28	0.30	0.28	0.31	0.31	0.25	0.29
Cr_2O_3		0.00	0.00	0.00	0.04	0.00	0.00	0.00	0.00	0.00	0.01	0.00
Fe_2O_3	35.36	34.40	35.71	31.57	28.86	32.89	35.93	28.34	29.03	27.96	28.59	26.67
FeO	-1.28	-0.33	-1.55	0.83	1.95	0.05	-1.87	0.16	1.20	3.69	2.95	5.02
MnO	0.25	0.30	0.32	0.36	0.29	0.30	0.16	0.87	0.67	0.51	0.56	0.50
MgO	0.03	0.01	0.00	0.02	0.01	0.00	0.02	0.83	0.56	0.41	0.42	0.37
CaO	0.67	0.21	0.04	0.91	0.91	0.79	0.64	3.37	3.32	5.85	4.86	6.27
Na_2O	13.90	13.84	14.17	13.47	13.67	13.86	14.14	12.81	12.31	10.93	11.48	10.52

K_2O	0.00	0.00	0.00	0.01	0.00	0.00	0.00	0.00	0.00	0.00	0.02	0.01
total	103.28	102.83	103.21	102.21	102.75	103.55	103.78	102.65	101.66	102.79	102.84	102.66
Formula (corr.)	6(O)	6(O)	6(O)	6(O)	6(O)	6(O)	6(O)	6(O)	6(O)	6(O)	6(O)	6(O)
Si	1.97	1.98	1.99	1.98	1.98	1.98	1.96	1.99	1.97	1.96	1.96	1.97
Ti	0.03	0.03	0.02	0.06	0.10	0.06	0.04	0.07	0.06	0.04	0.05	0.03
Al	0.01	0.01	0.02	0.01	0.01	0.01	0.01	0.01	0.01	0.01	0.01	0.01
Cr	0.00	0.00	0.00	0.00	0.00	0.00	0.00	0.00	0.00	0.00	0.00	0.00
Fe3+	0.99	0.97	1.00	0.89	0.81	0.92	1.00	0.79	0.83	0.80	0.81	0.76
Fe2+	-0.04	-0.01	-0.05	0.03	0.06	0.00	-0.06	0.00	0.04	0.12	0.09	0.16
Mn	0.01	0.01	0.01	0.01	0.01	0.01	0.01	0.03	0.02	0.02	0.02	0.02
Mg	0.00	0.00	0.00	0.00	0.00	0.00	0.00	0.05	0.03	0.02	0.02	0.02
Ca	0.03	0.01	0.00	0.04	0.04	0.03	0.03	0.13	0.13	0.24	0.20	0.25
Na	1.00	1.00	1.02	0.98	0.99	1.00	1.01	0.92	0.90	0.80	0.84	0.77
K	0.00	0.00	0.00	0.00	0.00	0.00	0.00	0.00	0.00	0.00	0.00	0.00
Total	4.00	4.00	4.00	4.00	4.00	4.00	4.00	4.00	4.00	4.00	4.00	4.00
Mg/(Mg+Fe2)												
Fe2/(Fetot)	-0.04	-0.09	0.00	0.04	0.01	0.00	-0.02	0.90	0.46	0.17	0.20	0.12
Al/(Al+Fe3+Cr)	-0.04	-0.01	-0.05	0.03	0.07	0.00	-0.06	0.01	0.04	0.13	0.10	0.17
Tri. plots												
En	-0.13	-0.76	0.00	0.02	0.00	0.00	-0.04	0.25	0.16	0.06	0.07	0.05
Fs	3.46	9.52	1.03	0.41	0.62	0.04	1.85	0.03	0.19	0.31	0.30	0.37
Wo	-2.34	-7.76	-0.03	0.57	0.37	0.96	-0.81	0.73	0.66	0.63	0.63	0.59
Jd	0.01	0.01	0.02	0.01	0.02	0.01	0.01	0.01	0.01	0.01	0.01	0.01
Ac	0.99	0.99	1.00	0.97	0.97	0.98	1.00	0.91	0.89	0.79	0.83	0.76
Aug	0.00	0.00	-0.02	0.02	0.01	0.00	-0.01	0.08	0.10	0.20	0.16	0.23
Jd or Ac	0.01	0.01	0.02	0.01	0.02	0.01	0.01	0.01	0.02	0.02	0.01	0.02

A(+aqw)	0.03	3.33	0.07	-1.04	-3.38	-3.74	0.01	-0.39	-0.16	0.01	-0.03	0.00
C(+aqw)	-7.17	-2.35	-0.04	1.00	1.49	3.52	-0.95	0.88	0.69	0.60	0.61	0.56
(FM)(+aqw)	8.14	0.02	0.97	1.05	2.89	1.22	1.93	0.51	0.47	0.39	0.42	0.43
Mole fractions												
XSi (T)	0.99	0.99	0.99	0.99	0.99	0.99	0.98	1.00	0.98	0.98	0.98	0.98
XAl (T)	0.02	0.01	0.01	0.01	0.01	0.01	0.02	0.00	0.02	0.02	0.02	0.02
XAl (M1)	-0.02	0.00	0.00	-0.01	0.00	-0.01	-0.03	0.00	-0.02	-0.03	-0.03	-0.02
XFe3 (M1)	0.99	0.97	1.00	0.89	0.81	0.92	1.00	0.79	0.83	0.80	0.81	0.76
XFe2 (M1)	0.00	1.86	-0.02	0.04	0.08	0.01	-0.02	0.01	0.05	0.15	0.12	0.18
XMg (M1)	0.00	-0.15	0.00	0.00	0.00	0.00	0.00	0.08	0.04	0.03	0.03	0.02
XFe2 (M2)	-0.04	-1.87	-0.03	-0.01	-0.02	0.00	-0.04	0.00	-0.02	-0.03	-0.02	-0.02
XMg (M2)	0.00	0.15	0.00	0.00	0.00	0.00	0.00	-0.03	-0.01	-0.01	-0.01	0.00
XCa (M2)	0.03	0.01	0.00	0.04	0.04	0.03	0.03	0.13	0.13	0.24	0.20	0.25
XNa (M2)	1.00	1.00	1.02	0.98	0.99	1.00	1.01	0.92	0.90	0.80	0.84	0.77
augite												
diopside												
hedenbergite												
pigeonite												
enstatite												
ferrosilite												
aegirine												
jadeite												
aegirine-augite				aegirine	aegirine	aegirine		aegirine	aegirine	aegirine	aegirine	aegirine-augite
omphacite												
Sodic pyx	sodic	sodic	sodic	sodic	sodic	sodic	sodic	sodic	sodic	sodic	sodic	sodic

	248	**248**	**248**	**248**	**248**	**248**	**248**	**STFL1A**	**STFL1A**	**STFL1A**	**STFL1A**	**STFL1A**
SiO_2	52.00	52.63	52.25	51.86	51.79	52.48	52.38	52.39	52.77	52.35	53.00	52.87
TiO2	2.00	2.31	1.23	1.65	0.98	1.80	1.48	0.88	1.16	1.42	1.33	2.40
Al2O3	0.30	0.32	0.37	0.36	0.28	0.29	0.32	0.34	0.31	0.29	0.31	0.21
Cr2O3	0.00	0.00	0.00	0.03	0.00	0.01	0.01	0.01	0.01	0.00	0.00	0.00
FeO	28.16	27.84	28.66	28.54	28.82	28.35	28.45	29.66	30.52	28.81	29.92	28.82
MnO	0.57	0.70	0.52	0.48	0.65	0.57	0.61	0.18	0.13	0.31	0.19	0.22
MgO	0.43	0.42	0.39	0.47	0.44	0.43	0.45	0.01	0.00	0.05	0.02	0.01
CaO	4.23	3.48	5.98	4.64	6.91	4.08	4.95	0.51	0.76	0.51	0.64	1.11
Na2O	11.72	10.12	11.16	11.45	10.11	11.83	11.45	13.92	14.23	13.71	14.02	13.79
K2O	0.00	0.00	0.00	0.01	0.00	0.03	0.00	0.00	0.01	0.01	0.00	0.00
Total	101.44	101.57	101.70	101.83	101.95	102.08	102.21					
Mol. Props.												
SiO2	0.87	0.88	0.87	0.86	0.86	0.87	0.87	0.87	0.88	0.87	0.88	0.88
TiO2	0.03	0.03	0.02	0.02	0.01	0.02	0.02	0.01	0.01	0.02	0.02	0.03
Al2O3	0.00	0.00	0.00	0.00	0.00	0.00	0.00	0.00	0.00	0.00	0.00	0.00
Cr2O3	0.00	0.00	0.00	0.00	0.00	0.00	0.00	0.00	0.00	0.00	0.00	0.00
FeO	0.39	0.39	0.40	0.40	0.40	0.39	0.40	0.41	0.42	0.40	0.42	0.40
MnO	0.01	0.01	0.01	0.01	0.01	0.01	0.01	0.00	0.00	0.00	0.00	0.00
MgO	0.01	0.01	0.01	0.01	0.01	0.01	0.01	0.00	0.00	0.00	0.00	0.00
CaO	0.08	0.06	0.11	0.08	0.12	0.07	0.09	0.01	0.01	0.01	0.01	0.02
Na2O	0.19	0.16	0.18	0.18	0.16	0.19	0.18	0.22	0.23	0.22	0.23	0.22
K2O	0.00	0.00	0.00	0.00	0.00	0.00	0.00	0.00	0.00	0.00	0.00	0.00
Total	1.57	1.54	1.59	1.57	1.58	1.58	1.58	1.54	1.57	1.53	1.56	1.56
Oxygen prop.												
SiO2	1.73	1.75	1.74	1.73	1.72	1.75	1.74	1.74	1.76	1.74	1.76	1.76
TiO2	0.05	0.06	0.03	0.04	0.02	0.05	0.04	0.02	0.03	0.04	0.03	0.06
Al2O3	0.01	0.01	0.01	0.01	0.01	0.01	0.01	0.01	0.01	0.01	0.01	0.01
Cr2O3	0.00	0.00	0.00	0.00	0.00	0.00	0.00	0.00	0.00	0.00	0.00	0.00
FeO	0.39	0.39	0.40	0.40	0.40	0.39	0.40	0.41	0.42	0.40	0.42	0.40

MnO	0.01	0.01	0.01	0.01	0.01	0.01	0.01	0.00	0.00	0.00	0.00	0.00
MgO	0.01	0.01	0.01	0.01	0.01	0.01	0.01	0.00	0.00	0.00	0.00	0.00
CaO	0.08	0.06	0.11	0.08	0.12	0.07	0.09	0.01	0.01	0.01	0.01	0.02
Na2O	0.19	0.16	0.18	0.18	0.16	0.19	0.18	0.22	0.23	0.22	0.23	0.22
K2O	0.00	0.00	0.00	0.00	0.00	0.00	0.00	0.00	0.00	0.00	0.00	0.00
Total	2.46	2.45	2.48	2.46	2.46	2.48	2.48	2.43	2.46	2.42	2.46	2.47
Norm. factor	2.43	2.45	2.42	2.44	2.43	2.42	2.42	2.47	2.43	2.48	2.44	2.43
Formula												
Si	2.11	2.14	2.10	2.10	2.10	2.11	2.11	2.16	2.14	2.16	2.15	2.13
Ti	0.06	0.07	0.04	0.05	0.03	0.05	0.04	0.03	0.04	0.04	0.04	0.07
Al	0.01	0.02	0.02	0.02	0.01	0.01	0.02	0.02	0.01	0.01	0.01	0.01
Cr	0.00	0.00	0.00	0.00	0.00	0.00	0.00	0.00	0.00	0.00	0.00	0.00
Fe++	0.95	0.95	0.96	0.97	0.98	0.96	0.96	1.02	1.03	0.99	1.01	0.97
Mn	0.02	0.02	0.02	0.02	0.02	0.02	0.02	0.01	0.00	0.01	0.01	0.01
Mg	0.03	0.03	0.02	0.03	0.03	0.03	0.03	0.00	0.00	0.00	0.00	0.00
Ca	0.18	0.15	0.26	0.20	0.30	0.18	0.21	0.02	0.03	0.02	0.03	0.05
Na	0.92	0.80	0.87	0.90	0.79	0.92	0.89	1.11	1.12	1.10	1.10	1.08
K	0.00	0.00	0.00	0.00	0.00	0.00	0.00	0.00	0.00	0.00	0.00	0.00
Total	4.29	4.18	4.29	4.29	4.26	4.29	4.28	4.36	4.38	4.34	4.36	4.33
Oxides (corr.)												
SiO2	52.00	52.63	52.25	51.86	51.79	52.48	52.38	52.39	52.77	52.35	53.00	52.87
TiO2	2.00	2.31	1.23	1.65	0.98	1.80	1.48	0.88	1.16	1.42	1.33	2.40
Al2O3	0.30	0.32	0.37	0.36	0.28	0.29	0.32	0.34	0.31	0.29	0.31	0.21
Cr2O3	0.00	0.00	0.00	0.03	0.00	0.01	0.01	0.01	0.01	0.00	0.00	0.00
Fe2O3	28.10	17.41	28.58	28.27	25.77	28.32	28.16	35.15	37.20	32.89	34.92	32.28
FeO	2.87	12.18	2.94	3.10	5.63	2.87	3.11	-1.97	-2.96	-0.78	-1.51	-0.23
MnO	0.57	0.70	0.52	0.48	0.65	0.57	0.61	0.18	0.13	0.31	0.19	0.22

MgO	0.43	0.42	0.39	0.47	0.44	0.43	0.45	0.01	0.00	0.05	0.02	0.01
CaO	4.23	3.48	5.98	4.64	6.91	4.08	4.95	0.51	0.76	0.51	0.64	1.11
Na2O	11.72	10.12	11.16	11.45	10.11	11.83	11.45	13.92	14.23	13.71	14.02	13.79
K2O	0.00	0.00	0.00	0.01	0.00	0.03	0.00	0.00	0.01	0.01	0.00	0.00
Total	102.22	99.56	103.43	102.32	102.57	102.70	102.91	101.42	103.62	100.74	102.93	102.66
Formula (corr.)	6(O)	6(O)	6(O)	6(O)	6(O)	6(O)	6(O)					
Si	1.97	2.05	1.96	1.96	1.97	1.97	1.97	1.98	1.95	1.99	1.97	1.97
Ti	0.06	0.07	0.03	0.05	0.03	0.05	0.04	0.02	0.03	0.04	0.04	0.07
Al	0.01	0.01	0.02	0.02	0.01	0.01	0.01	0.02	0.01	0.01	0.01	0.01
Cr	0.00	0.00	0.00	0.00	0.00	0.00	0.00	0.00	0.00	0.00	0.00	0.00
Fe3+	0.80	0.51	0.81	0.81	0.74	0.80	0.80	1.00	1.04	0.94	0.98	0.91
Fe2+	0.09	0.40	0.09	0.10	0.18	0.09	0.10	-0.06	-0.09	-0.02	-0.05	-0.01
Mn	0.02	0.02	0.02	0.02	0.02	0.02	0.02	0.01	0.00	0.01	0.01	0.01
Mg	0.02	0.02	0.02	0.03	0.02	0.02	0.03	0.00	0.00	0.00	0.00	0.00
Ca	0.17	0.15	0.24	0.19	0.28	0.16	0.20	0.02	0.03	0.02	0.03	0.04
Na	0.86	0.77	0.81	0.84	0.75	0.86	0.83	1.02	1.02	1.01	1.01	1.00
K	0.00	0.00	0.00	0.00	0.00	0.00	0.00	0.00	0.00	0.00	0.00	0.00
Total	4.00	4.00	4.00	4.00	4.00	4.00	4.00	4.00	4.00	4.00	4.00	4.00
Mg/(Mg+Fe2)	0.21	0.06	0.19	0.21	0.12	0.21	0.20	-0.01	0.00	-0.14	-0.03	-0.08
Fe2/(Fetot)	0.10	0.44	0.10	0.11	0.20	0.10	0.11	-0.07	-0.10	-0.03	-0.05	-0.01
Al/(Al+Fe3+Cr)	0.02	0.03	0.02	0.02	0.02	0.02	0.02	0.01	0.01	0.01	0.01	0.01
Tri. plots												
En	0.09	0.04	0.06	0.08	0.05	0.09	0.08	-0.02	0.00	-2.49	-0.07	0.01
Fs	0.32	0.70	0.26	0.31	0.37	0.32	0.30	1.53	1.49	19.97	2.36	-0.19
Wo	0.60	0.26	0.68	0.60	0.58	0.59	0.62	-0.51	-0.49	-16.47	-1.29	1.17

Jd	0.01	0.02	0.02	0.02	0.01	0.01	0.01	0.02	0.01	0.01	0.01	0.01
Ac	0.85	0.74	0.80	0.82	0.73	0.85	0.82	1.00	1.01	1.00	1.00	0.99
Aug	0.14	0.23	0.19	0.16	0.25	0.14	0.17	-0.02	-0.02	-0.01	-0.01	0.00
Jd or Ac	0.02	0.03	0.02	0.02	0.02	0.02	0.02	0.01	0.01	0.01	0.01	0.01
A(+aqw)	-0.08	-0.25	0.02	-0.03	0.00	-0.09	-0.04	0.07	-0.33	1.45	0.42	-10.98
C(+aqw)	0.61	0.31	0.64	0.59	0.55	0.60	0.60	-0.55	-0.70	-1.05	-1.07	11.85
(FM)(+aqw)	0.47	0.95	0.35	0.44	0.44	0.49	0.43	1.49	2.03	0.60	1.65	0.13
Mole fractions												
XSi (T)	0.98	1.03	0.98	0.98	0.98	0.99	0.99	0.99	0.98	0.99	0.99	0.99
XAl (T)	0.02	-0.03	0.02	0.02	0.02	0.01	0.01	0.01	0.02	0.01	0.01	0.01
XAl (M1)	-0.02	0.07	-0.02	-0.02	-0.02	-0.01	-0.02	-0.01	-0.03	0.00	-0.01	-0.02
XFe3 (M1)	0.80	0.51	0.81	0.81	0.74	0.80	0.80	1.00	1.04	0.94	0.98	0.91
XFe2 (M1)	0.11	0.32	0.13	0.12	0.20	0.11	0.12	-0.02	-0.04	0.04	0.00	-0.60
XMg (M1)	0.03	0.02	0.03	0.03	0.03	0.03	0.03	0.00	0.00	0.00	0.00	0.04
XFe2 (M2)	-0.02	0.08	-0.04	-0.02	-0.02	-0.02	-0.02	-0.04	-0.05	-0.06	-0.04	0.60
XMg (M2)	-0.01	0.00	-0.01	-0.01	0.00	-0.01	-0.01	0.00	0.00	0.01	0.00	-0.04
XCa (M2)	0.17	0.15	0.24	0.19	0.28	0.16	0.20	0.02	0.03	0.02	0.03	0.04
XNa (M2)	0.86	0.77	0.81	0.84	0.75	0.86	0.83	1.02	1.02	1.01	1.01	1.00
augite												
diopside												
hedenbergite												
pigeonite												
enstatite												
ferrosilite												
aegirine	aegirine		aegirine	aegirine		aegirine	aegirine					
jadeite												
aegirine-augite		aegirine-augite			aegirine-augite							

omphacite							
undefined							
Sodic pyx:	sodic	sodic	sodic	sodic	sodic	sodic	sodic
Final name:	aegirine	aegirine-augite	aegirine	aegirine	aegirine-augite	aegirine	aegirine

Appendix B:

Sample	Rb	%RSD	Sr	%RSD	$^{87}Sr/^{86}Sr$	±2σ internal	^{88}Sr	^{87}Sr	^{86}Sr	^{84}Sr	Sr atomic weight
Syenite											
ST-71	194.5	0.607	479.2	0.438	0.712906	0.000016	0.82556	0.07027	0.09857	0.00560	87.61645
ST133	175.8	0.833	125.4	0.749	0.71524	0.000013	0.82537	0.07049	0.09855	0.00560	87.61628
ST138	189.8	0.842	154.0	0.991	0.714759	0.000012	0.82541	0.07044	0.09855	0.00560	87.61632
Dyke											
STFL1B	267.4	0.434	11.6	1.078	0.871963	0.000017	0.81281	0.08462	0.09705	0.00551	87.60552
STFL1A	265.7	0.471	11.2	0.886	0.881708	0.000018	0.81205	0.08549	0.09696	0.00551	87.60487
ST203	304.0	0.325	7.3	0.799	1.001517	0.000017	0.80272	0.09599	0.09584	0.00544	87.59687
ST211	293.8	0.638	7.3	0.994	0.997161	0.000019	0.80306	0.09561	0.09588	0.00545	87.59716
ST217	291.0	0.222	53.7	0.351	0.747102	0.000012	0.82279	0.07340	0.09824	0.00558	87.61407
ST226	119.6	0.346	7.3	0.606	0.830892	0.000018	0.81607	0.08096	0.09744	0.00553	87.60831
ST147	270.2	0.210	8.3	1.021	0.944372	0.000015	0.80714	0.09101	0.09637	0.00547	87.60066
ST113	210.7	0.363	11.9	0.352	0.835119	0.000017	0.81573	0.08134	0.09740	0.00553	87.60802
ST216	273.8	0.140	129.3	0.461	0.725744	0.000014	0.82452	0.07145	0.09845	0.00559	87.61555
ST75	268.1	0.296	6.9	0.634	0.993819	0.000015	0.80331	0.09532	0.09592	0.00545	87.59738
ST246	220.7	0.298	100.7	0.85	0.719599	0.000012	0.82501	0.07088	0.09851	0.00559	87.61598
ST268	232.9	0.167	104.5	0.401	0.721448	0.000012	0.82486	0.07105	0.09849	0.00559	87.61585
FL1	285.9	0.245	17.4	0.61	0.822846	0.000018	0.81671	0.08024	0.09751	0.00554	87.60886
FL2	251.0	0.300	13.5	0.633	0.841198	0.000015	0.81525	0.08188	0.09734	0.00553	87.60761
ST84	267.1	0.277	25.5	0.194	0.777809	0.000012	0.82031	0.07618	0.09794	0.00556	87.61195
ST88	229.8	0.165	6.3	0.575	0.956208	0.000019	0.80622	0.09205	0.09626	0.00547	87.59987
ST-76	301.4	0.004	3.5	1.204	1.300065	0.000016	0.78039	0.12114	0.09318	0.00529	87.57773
ST228	276.4	0.168	4.4	0.726	1.196014	0.000021	0.78803	0.11253	0.09409	0.00534	87.58428
ST212	303.6	0.531	2.4	1.536	1.545008	0.000022	0.76298	0.14075	0.09110	0.00517	87.56281
Gneiss											
ST181	27.6	0.607	616.5	0.695	0.713064	0.000009	0.82555	0.07029	0.09857	0.00560	87.61643
STS242	50.8	1.112	990.9	0.428	0.709039	0.000013	0.82587	0.06992	0.09861	0.00560	87.61672
ST241	34.3	1.454	501.0	0.909	0.711056	0.000011	0.82571	0.07010	0.09859	0.00560	87.61657
ST254	18.8	0.397	505.5	1.917	0.753465	0.000012	0.82227	0.07397	0.09818	0.00558	87.61363
ST264	33.9	1.105	298.9	0.31	0.715054	0.000011	0.82538	0.07047	0.09855	0.00560	87.61630

Table B 1: Measured and calculated Rb and Sr isotopic abundances in the Rb-Sr system as determined by quadrupole ICP-MS at the University of Cape Town, and associated alculations

Sample	$^{87}Rb/^{86}Sr$	±2σ	Ro	error	Ro max	Ro min	ƐSr	±2σ	ƐSr max	ƐSr min
Syenite										
ST-71	1.18	0.10	0.71005	5.88E-05	0.71011	0.70999	74.8	1.7	75.6	73.9
ST133	4.06	0.34	0.70537	2.34E-04	0.70561	0.70514	8.4	6.6	11.7	5.1
ST138	3.57	0.30	0.70608	2.38E-04	0.70632	0.70585	18.5	6.7	21.9	15.1
Dyke										
STFL1B	67.7	1.57	0.70738	3.84E-03	0.71122	0.70354	36.8	109.0	91.4	-17.7
STFL1A	70.0	1.40	0.71157	3.43E-03	0.71500	0.70814	96.3	97.4	145.0	47.6
ST203	124	2.13	0.70121	5.20E-03	0.70640	0.69601	-50.7	147.5	23.0	-124.5
ST211	120	2.82	0.70657	6.88E-03	0.71346	0.69969	25.4	195.3	123.1	-72.3
ST217	15.7	0.131	0.70883	3.30E-04	0.70916	0.70850	57.4	9.4	62.1	52.8
ST226	48.2	0.672	0.71378	1.65E-03	0.71543	0.71213	127.7	46.9	151.1	104.3
ST147	96.2	2.01	0.71054	4.89E-03	0.71543	0.70565	81.7	138.8	151.1	12.4
ST113	51.9	0.525	0.70894	1.29E-03	0.71023	0.70764	59.0	36.7	77.3	40.6
ST216	6.14	0.059	0.71082	1.58E-04	0.71098	0.71067	85.7	4.5	88.0	83.5
ST75	116	1.62	0.71295	3.95E-03	0.71689	0.70900	115.8	112.0	171.8	59.9
ST246	6.35	0.114	0.70417	2.90E-04	0.70446	0.70388	-8.7	8.2	-4.6	-12.8
ST268	6.46	0.056	0.70575	1.48E-04	0.70590	0.70560	13.8	4.2	15.9	11.7
FL1	48.2	0.633	0.70565	1.56E-03	0.70721	0.70409	12.3	44.2	34.4	-9.8
FL2	54.4	0.763	0.70883	1.87E-03	0.71070	0.70696	57.4	53.1	83.9	30.9
ST84	30.5	0.206	0.70375	5.13E-04	0.70427	0.70324	-14.6	14.6	-7.3	-21.9
ST88	107	1.28	0.69526	3.14E-03	0.69840	0.69212	-135.1	89.1	-90.6	-179.7
ST-76	265	6.38	0.65620	1.55E-02	0.67173	0.64068	-689.2	440.4	-469.0	-909.5
ST228	190	2.83	0.73416	6.90E-03	0.74107	0.72726	416.9	195.9	514.8	318.9
ST212	396	12.9	0.58287	3.13E-02	0.61416	0.55157	-1729.8	888.1	-1285.8	-2173.8
Gneiss										
ST181	0.130	0.00239	0.71275	1.48E-05	0.71276	0.71273	113.1	0.4	113.3	112.8
STS242	0.148	0.00354	0.70868	2.16E-05	0.70870	0.70866	55.3	0.6	55.6	55.0
ST241	0.198	0.00680	0.71057	2.75E-05	0.71060	0.71055	82.2	0.8	82.6	81.8
ST254	0.108	0.00423	0.75320	2.23E-05	0.75322	0.75318	687.0	0.6	687.4	686.7
ST264	0.329	0.00754	0.71426	2.93E-05	0.71428	0.71423	134.4	0.8	134.8	134.0

Table B 2: Calculated $^{87}Rb/^{86}Sr$ concentration, measured initial $^{87/86}Sr$ (Ro), ƐSr and 2σ error associated with ƐSr calculated using the 1σ measured trace element error.

Sample	Nd	%RSD	Sm	%RSD	$^{143}Nd/^{144}Nd$	±2σ internal	^{150}Nd	^{148}Nd	^{146}Nd	^{145}Nd	^{144}Nd	^{143}Nd	^{142}Nd	Nd atomic weight
Syenite														
ST-71	32.9	0.347	4.71	2.09	0.512355	0.000014	0.05637	0.05755	0.17186	0.08291	0.23793	0.12191	0.27147	144.24133
ST133	109	0.592	21.6	0.651	0.511886	0.00001	0.05638	0.05756	0.17188	0.08292	0.23796	0.12181	0.27150	144.24148
ST138	49.8	0.943	7.47	1.22	0.512359	0.000011	0.05637	0.05755	0.17186	0.08291	0.23793	0.12191	0.27147	144.24133
Dykes														
STFL1B	9.54	0.717	2.12	0.797	0.512075	0.000033	0.05637	0.05755	0.17187	0.08292	0.23795	0.12185	0.27149	144.24142
STFL1A	12.1	0.788	2.50	1.70	0.511921	0.000028	0.05638	0.05755	0.17188	0.08292	0.23796	0.12182	0.27150	144.24147
ST203	147	0.33	25.0	0.197	0.511898	0.000009	0.05638	0.05756	0.17188	0.08292	0.23796	0.12181	0.27150	144.24148
ST211	139	0.251	26.0	0.217	0.511896	0.000008	0.05638	0.05756	0.17188	0.08292	0.23796	0.12181	0.27150	144.24148
ST217	87.9	0.355	18.4	1.21	0.511921	0.00001	0.05638	0.05755	0.17188	0.08292	0.23796	0.12182	0.27150	144.24147
ST226	3.88	0.951	0.74	1.24	0.512161	0.000055	0.05637	0.05755	0.17187	0.08292	0.23795	0.12187	0.27148	144.24139
ST147	45.0	0.296	8.39	0.933	0.511908	0.000015	0.05638	0.05756	0.17188	0.08292	0.23796	0.12181	0.27150	144.24147
ST113	24.6	0.208	5.93	1.56	0.511948	0.000017	0.05637	0.05755	0.17187	0.08292	0.23796	0.12182	0.27149	144.24146
ST216	121	0.351	19.6	0.946	0.511906	0.000009	0.05638	0.05756	0.17188	0.08292	0.23796	0.12181	0.27150	144.24147
ST75	89.3	0.666	17.4	0.624	0.511888	0.000008	0.05638	0.05756	0.17188	0.08292	0.23796	0.12181	0.27150	144.24148
ST246	537	0.967	73.9	0.803	0.512006	0.000011	0.05637	0.05755	0.17187	0.08292	0.23795	0.12183	0.27149	144.24144
ST268	166	0.733	23.2	0.582	0.511971	0.000011	0.05637	0.05755	0.17187	0.08292	0.23796	0.12183	0.27149	144.24145
FL1	51.2	0.117	10.2	0.741	0.511906	0.000011	0.05638	0.05756	0.17188	0.08292	0.23796	0.12181	0.27150	144.24147
FL2	14	0.291	2.98	1.65	0.511898	0.000026	0.05638	0.05756	0.17188	0.08292	0.23796	0.12181	0.27150	144.24148
ST84	15.6	0.678	2.99	0.939	0.511892	0.000017	0.05638	0.05756	0.17188	0.08292	0.23796	0.12181	0.27150	144.24148
ST88	4.65	2.08	0.83	2.47	0.511924	0.000044	0.05638	0.05755	0.17187	0.08292	0.23796	0.12182	0.27150	144.24147
ST-76	109	0.433	21.6	0.23	0.511886	0.000009	0.05638	0.05756	0.17188	0.08292	0.23796	0.12181	0.27150	144.24148
ST228	84.4	0.504	16.8	0.899	0.511874	0.000012	0.05638	0.05756	0.17188	0.08292	0.23796	0.12181	0.27150	144.24148
ST212	93.8	0.433	18.2	0.932	0.511878	0.000011	0.05638	0.05756	0.17188	0.08292	0.23796	0.12181	0.27150	144.24148
Gneiss														
ST181	28.6	0.892	4.92	0.541	0.511026	0.000009	0.05639	0.05757	0.17191	0.08294	0.23801	0.12163	0.27155	144.24175
STS242	27.4	0.624	4.77	0.658	0.511646	0.000010	0.05638	0.05756	0.17189	0.08293	0.23797	0.12176	0.27151	144.24156
ST241	18.9	0.726	3.85	0.24	0.511804	0.000017	0.05638	0.05756	0.17188	0.08293	0.23797	0.12179	0.27150	144.24151
ST254	28.5	0.911	4.72	0.888	0.510674	0.000018	0.05639	0.05757	0.17193	0.08295	0.23803	0.12156	0.27158	144.24187
ST264	24.0	0.788	4.11	1.75	0.511051	0.000012	0.05639	0.05757	0.17191	0.08294	0.23801	0.12163	0.27155	144.24175

Table B 3: Measured and calculated isotopic abundances of Sm and Nd for rocks of the Straumsvola Complex.

Sample	$^{147}Sm/^{144}Nd$	±2σ error	Ro	error	Ro min	Ro min	ƐNd	±2σ error	ƐNd max	ƐNd min
Syenite										
ST-71	0.08658	0.00366	0.512259	1.81E-05	0.512241	0.512277	-3.11	0.353	-3.46	-2.75
ST133	0.11958	0.00210	0.511753	1.24E-05	0.51174	0.511765	-13	0.241	-13.2	-12.7
ST138	0.09058	0.00280	0.512258	1.41E-05	0.512244	0.512272	-3.12	0.276	-3.39	-2.84
Dykes										
STFL1B	0.13410	0.00288	0.511925	3.62E-05	0.511889	0.511962	-9.61	0.707	-10.3	-8.91
STFL1A	0.12501	0.00469	0.511782	3.33E-05	0.511749	0.511815	-12.4	0.649	-13.1	-11.8
ST203	0.10277	0.00079	0.511784	9.88E-06	0.511774	0.511793	-12.4	0.193	-12.6	-12.2
ST211	0.11311	0.00075	0.51177	8.84E-06	0.511761	0.511779	-12.6	0.173	-12.8	-12.5
ST217	0.12616	0.00319	0.51178	1.36E-05	0.511767	0.511794	-12.4	0.265	-12.7	-12.2
ST226	0.11457	0.00357	0.512033	5.9E-05	0.511974	0.512092	-7.50	1.151	-8.65	-6.35
ST147	0.11255	0.00220	0.511782	1.75E-05	0.511765	0.5118	-12.4	0.341	-12.7	-12.1
ST113	0.14545	0.00459	0.511785	2.21E-05	0.511763	0.511807	-12.4	0.432	-12.8	-11.9
ST216	0.09795	0.00198	0.511797	1.12E-05	0.511786	0.511808	-12.1	0.219	-12.3	-11.9
ST75	0.11781	0.00215	0.511756	1.04E-05	0.511746	0.511767	-12.9	0.203	-13.1	-12.7
ST246	0.08309	0.00209	0.511914	1.33E-05	0.511901	0.511927	-9.84	0.260	-10.1	-9.6
ST268	0.08480	0.00159	0.511877	1.28E-05	0.511864	0.511889	-10.6	0.249	-10.8	-10.3
FL1	0.12048	0.00181	0.511772	1.3E-05	0.511759	0.511785	-12.6	0.254	-12.9	-12.4
FL2	0.12854	0.00430	0.511754	3.08E-05	0.511724	0.511785	-13.0	0.601	-13.6	-12.4
ST84	0.11552	0.00268	0.511763	2E-05	0.511743	0.511783	-12.8	0.390	-13.2	-12.4
ST88	0.10730	0.00693	0.511804	5.18E-05	0.511752	0.511856	-12.0	1.010	-13.0	-11.0
ST-76	0.11958	0.00117	0.511753	1.03E-05	0.511742	0.511763	-13.0	0.201	-13.2	-12.8
ST228	0.12034	0.00248	0.511739	1.48E-05	0.511725	0.511754	-13.2	0.288	-13.5	-13.0
ST212	0.11747	0.00241	0.511747	1.37E-05	0.511733	0.511761	-13.1	0.267	-13.4	-12.8
Gneiss										
ST181	0.10396	0.00217	0.51091	1.1E-05	0.510899	0.510921	-29.4	0.216	-29.6	-29.2
STS242	0.10538	0.00191	0.511529	1.18E-05	0.511517	0.511541	-17.4	0.230	-17.6	-17.1
ST241	0.12309	0.00188	0.511667	1.95E-05	0.511647	0.511686	-14.7	0.381	-15.0	-14.3
ST254	0.10029	0.00255	0.510562	2.09E-05	0.510541	0.510583	-36.2	0.407	-36.6	-35.8
ST264	0.10347	0.00397	0.510936	1.66E-05	0.510919	0.510952	-28.9	0.325	-29.3	-28.6

Table B 4: Calculated $^{147}Sm/^{144}Nd$, initial $^{143/144}Nd$, error associated with the calculation and ƐNd and associated 2σ error.

Sample	$^{208/204}$Pb	±2σ internal	$^{207/204}$Pb	±2σ internal	$^{206/204}$Pb	±2σ internal
Syenite						
ST71	38.3948	0.0026	15.5166	0.0010	17.8314	0.0009
ST133	39.1453	0.0033	15.5634	0.0012	18.6838	0.0012
ST138	38.9519	0.0034	15.5411	0.0012	18.1703	0.0014
Dykes						
STFL1B	38.0791	0.0025	15.4577	0.0009	17.6091	0.0009
STFL1A	38.0564	0.0030	15.4569	0.0010	17.5352	0.0010
ST203	38.1690	0.0039	15.4254	0.0013	17.4065	0.0013
ST211	38.2787	0.0034	15.4319	0.0011	17.5385	0.0011
ST216	38.3833	0.0037	15.4336	0.0012	17.4424	0.0011
ST217	38.3295	0.0035	15.4436	0.0010	17.6040	0.0011
ST226	38.1016	0.0034	15.4986	0.0011	17.7439	0.0011
ST113	38.8510	0.0030	15.5277	0.0009	18.2557	0.0009
ST147	37.8525	0.0030	15.3512	0.0010	17.1543	0.0009
ST268	38.2171	0.0036	15.4394	0.0011	17.4094	0.0012
ST246	38.2353	0.0033	15.4570	0.0010	17.5692	0.0011
ST75	38.3584	0.3380	15.4305	0.0011	17.4777	0.0010
FL1	38.2394	0.0030	15.4395	0.0010	17.4600	0.0010
Float2	38.4393	0.0044	15.5398	0.0015	17.9740	0.0017
ST88	38.8699	0.0038	15.5455	0.0014	18.0593	0.0015
ST84	37.6071	0.0030	15.3326	0.0011	16.9245	0.0010
ST212	38.2085	0.0035	15.4283	0.0011	17.3797	0.0009
ST76	38.0251	0.0026	15.4194	0.0008	17.3037	0.0009
ST228	38.2748	0.0040	15.4329	0.0012	17.5017	0.0012
Gneiss						
ST181	39.2295	0.0026	15.5329	0.0010	17.4906	0.0010
ST241	38.5167	0.0024	15.6308	0.0009	18.5469	0.0010
ST242	38.5513	0.0033	15.6096	0.0012	18.2368	0.0012
ST264	38.7723	0.0033	14.9223	0.0010	15.1546	0.0010
ST254	38.2951	0.0033	15.7273	0.0012	18.2613	0.0013

Table B 5: Pb Isotope ratios as measured by LA-ICP-MS at the University of Cape Town. Accepted and measured values of international standards, JG-2 and BHV-O2 given in Chapter 3, Methods